Academic Press is an imprint of Elsevier
32 Jamestown Road, London NW1 7BY, UK
Radarweg 29, PO Box 211, 1000 AE Amsterdam, The Netherlands
225 Wyman Street, Waltham, MA 02451, USA
525 B Street, Suite 1900, San Diego, CA 92101-4495, USA

First edition 2012

Library of Congress Cataloging-in-Publication Data
A catalog record for this book is available from the Library of Congress

British Library Cataloguing in Publication Data
A catalogue record for this book is available from the British Library

ISBN: 978-0-12-396462-5
ISSN: 0898-8838

Printed and bound in USA

12 13 14 15 10 9 8 7 6 5 4 3 2 1

LIST OF CONTRIBUTORS

Michael T. Ashby
Department of Chemistry and Biochemistry, University of Oklahoma, Norman, Oklahoma, USA

Jaswir Basran
Department of Biochemistry, Henry Wellcome Building, University of Leicester, Leicester, United Kingdom

Damian E. Bikiel
Departamento de Química Inorgánica, Analítica y Química Física/INQUIMAE-CONICET, Buenos Aires, Argentina

Ariane Brausam
Department of Chemistry and Pharmacy, University of Erlangen-Nürnberg, Egerlandstr. 1, Erlangen, Germany

Ariela Burg
Chemical Engineering Department, Sami Shamoon College of Engineering, Beer-Sheva, Israel

Debabrata Chatterjee
Chemistry and Biomimetics Group, CSIR-Central Mechanical Engineering Research Institute, Durgapur, India

Sam P. de Visser
The Manchester Interdisciplinary Biocentre and the School of Chemical Engineering and Analytical Science, University of Manchester, Manchester, United Kingdom

Fabio Doctorovich
Departamento de Química Inorgánica, Analítica y Química Física/INQUIMAE-CONICET, Buenos Aires, Argentina

Igor Efimov
Department of Chemistry, University of Leicester, Leicester, United Kingdom

Miloš R. Filipović
Department of Chemistry and Pharmacy, University of Erlangen-Nürnberg, Egerlandstrasse 1, Erlangen, Germany

Sandeep Handa
Department of Chemistry, University of Leicester, Leicester, United Kingdom

Ivana Ivanović-Burmazović
Department of Chemistry and Pharmacy, University of Erlangen-Nürnberg, Egerlandstrasse 1, Erlangen, Germany

Marcelo A. Martí
Departamento de Química Inorgánica, Analítica y Química Física/INQUIMAE-CONICET, and Departamento de Química Biológica, Facultad de Ciencias Exactas y Naturales, Universidad de Buenos Aires, Ciudad Universitaria, Pab. II (1428), Buenos Aires, Argentina

Dan Meyerstein
Biological Chemistry Department, Ariel University Center of Samaria, Ariel, and Chemistry Department, Ben-Gurion University, Beer-Sheva, Israel

Christopher G. Mowat
EaStCHEM, School of Chemistry, University of Edinburgh, Edinburgh, United Kingdom

Juan Pellegrino
Departamento de Química Inorgánica, Analítica y Química Física/INQUIMAE-CONICET, Buenos Aires, Argentina

Emma Lloyd Raven
Department of Chemistry, University of Leicester, Leicester, United Kingdom

Sebastián A. Suárez
Departamento de Química Inorgánica, Analítica y Química Física/INQUIMAE-CONICET, Buenos Aires, Argentina

Sarah J. Thackray
EaStCHEM, School of Chemistry, University of Edinburgh, Edinburgh, United Kingdom

Rudi van Eldik
Department of Chemistry and Pharmacy, University of Erlangen-Nürnberg, Egerlandstr. 1, Erlangen, Germany

PREFACE

Volume 64 of *Advances in Inorganic Chemistry* is a thematic issue devoted to inorganic/bioinorganic reaction mechanisms, coedited by Ivana Ivanović-Burmazović from the University of Erlangen-Nürnberg, Germany. Understanding the mechanisms of inorganic/bioinorganic reactions is of fundamental importance in order to reveal the molecular nature of complex chemical and biochemical processes that could lead to the development of new pharmaceuticals and catalysts in a biomimetic way. The original idea for this thematic issue originates from the Inorganic Reaction Mechanism Group Meeting held at Kloster (Monastery) Banz, Germany, in January 2010, that was attended by 120 participants. This volume includes eight contributions highlighting the role of mechanistic studies in inorganic/bioinorganic chemistry. Interestingly, almost all mechanisms discussed in this volume are based on redox reactions, with a special emphasis on biological relevance and redox reactivity of small inorganic species on one side (such as oxygen, superoxide, nitric oxide, nitroxyl, and hypothiocyanate) and redox active metal centers (iron, manganese, ruthenium, and copper) on the other. We hope it will prove interesting and inspiring to researchers in this field.

The first chapter by Sam P. de Visser presents theoretical predictions of oxygen transfer reactions by Compound I of cytochrome P450 in aliphatic and aromatic hydroxylation, epoxidation, and sulfoxidation processes. This is followed by a chapter on heme dioxygenases, written by Emma Lloyd Raven and collaborators. The reactivity of manganese superoxide dismutase mimics toward superoxide and nitric oxide is covered in the following chapter by Ivana Ivanović-Burmazović and collaborators. In the fourth chapter, Fabio Doctorovich and collaborators present an account on azanone (HNO; also known as nitroxyl) interaction with (heme)-proteins and metalloporphyrins. In the subsequent chapter, Rudi van Eldik and collaborator report on advances in the mechanistic understanding of selected reactions of transition metal polyaminecarboxylate complexes. The kinetic and mechanistic impact of polyaminecarboxylate-ruthenium(III) complexes on the mosaic of bioinorganic reactions is covered by Debabrata

Chatterjee and collaborator in the sixth chapter. A short review on the chemistry of monovalent copper in aqueous solutions is presented in the seventh chapter by Dan Meyerstein and collaborator. The final chapter deals with a detailed review on hypothiocyanate written by Michael Ashby. These chapters present comprised overviews of recent developments in the understanding of inorganic/bioinorganic reaction mechanisms. The contributions come from the UK, Germany, Argentina, India, Israel, and the United States, and represent an international community of chemists working in this area.

We appreciate the constructive interaction we had with the authors of these chapters and thank them for their willingness to find time to contribute to this thematic issue. We trust that the readers in the inorganic/bioinorganic chemistry communities will find this volume informative and useful.

Rudi van Eldik and Ivana Ivanović-Burmazović
University of Erlangen-Nürnberg
November 2011

PREDICTIVE STUDIES OF OXYGEN ATOM TRANSFER REACTIONS BY COMPOUND I OF CYTOCHROME P450: ALIPHATIC AND AROMATIC HYDROXYLATION, EPOXIDATION, AND SULFOXIDATION

SAM P. DE VISSER

The Manchester Interdisciplinary Biocentre and the School of Chemical Engineering and Analytical Science, University of Manchester, Manchester, United Kingdom

ABSTRACT

This review overviews recent density functional theory studies accompanied by valence bond (VB) modeling of the reactivity patterns of Compound I of cytochrome P450 and taurine/α-ketoglutarate dioxygenase. These two enzymes both have a high-valent iron(IV)–oxo species as their active intermediate and are involved in oxygen atom transfer reactions to substrates including aliphatic hydroxylation, double-bond epoxidation, heteroatom oxidation (sulfoxidation), and aromatic hydroxylation. In recent years, a number of systematic studies on these four

INORGANIC/BIOINORGANIC REACTION MECHANISMS
VOLUME 64 ISSN 0898-8838 / DOI: 10.1016/B978-0-12-396462-5.00001-5

reaction mechanisms have been performed, and the barrier heights of the rate-determining steps in these reactions have been analyzed with VB models via curve-crossing diagrams. Those diagrams predict the overall mechanisms and explain the nature of the rate-determining step in the reaction through electron transfer processes. The computational models have gained insight into the fundamental factors that drive the reaction mechanisms and explain the differences between the various reaction processes.

Keywords: Nonheme enzymes; Heme enzymes; Hydroxylation; Epoxidation; Sulfoxidation; Iron–oxo; Valence bond theory; Density functional theory.

I. Background

Substrate hydroxylation is one of the most challenging catalytic reactions due to the strength of a C—H bond that has to be broken in the process. Nevertheless, nature has given us a range of different enzymes that catalyze this reaction efficiently. These enzymes typically have a transition metal center that binds and utilizes molecular oxygen and assists in the transfer of one (in monoxygenases) or both (in dioxygenases) oxygen atoms of molecular oxygen to a substrate. Usually in biological systems, the reaction takes place on an iron center that is either bound inside a heme group or located in a nonheme environment. In addition, binuclear and multinuclear metal oxidants are known in nature, but we will focus on mononuclear iron containing enzymes and biomimetics only here. In this review, we discuss recent advances in the understanding of substrate activation mechanisms on iron centers obtained through theoretical modeling of enzyme active sites and biomimetic complexes. These studies have provided explanations through thermodynamic cycles and valence bond (VB) modeling of the origin and nature of reaction barriers of the various oxidants. Moreover, the trends enable one to predict barrier heights of substrate activation.

The mononuclear iron containing enzymes involved in substrate hydroxylation reactions can roughly be divided into two classes: (i) the heme enzymes and (ii) the nonheme enzymes. Heme enzymes are a versatile group of enzymes that include heme monoxygenases, peroxidases, and catalases (*1*). The largest group of heme monoxygenases in the human body is the cytochromes P450 (P450s), which are involved in detoxification processes in

the liver, drug metabolism, and the biosynthesis of hormones (*2–5*). The P450s act as monoxygenases and activate aliphatic C—H bonds to form alcohols, convert C═C bonds into epoxides, but also react via sulfoxidation or N-dealkylation. The general reaction catalyzed by the P450s is given in Eq. (1) with RH a substrate.

$$RH + O_2 + 2H^+ + 2e^- \rightarrow ROH + H_2O \quad (1)$$

Nonheme oxygen-activating dioxygenases, by contrast, do not contain electron transfer proteins but utilize a co-substrate, usually α-ketoglutarate (αKG), to generate an active species that hydroxylates the substrate. These enzymes have important functions in biosystems ranging from DNA and RNA base repair to the biosynthesis of collagen in mammals and antibiotics in bacteria (*6–9*). As such a variety of different reactions are catalyzed by heme and nonheme enzymes ranging from, for example, oxidative cleavage of carbon—carbon bonds, monohydroxylation and dihydroxylation reactions. To understand the differences in chemical properties between heme and nonheme iron oxidants, extensive studies of biomimetic systems have been reported (*10–14*); these studies have given insight into the factors that influence the catalytic efficiency of the oxidant, such as the nature of the metal and its ligand environment.

Figure 1 displays extracts of the active site of two hydroxylases, namely cytochrome $P450_{BM3}$ ($P450_{BM3}$) and taurine/α-ketoglutarate dioxygenase (TauD) as examples of the two enzyme classes discussed here (*15,16*). In $P450_{BM3}$, the metal is part of a protoporphyrin IX macrocycle that binds as a tetradentate ligand, which leaves two binding sites of the metal free on opposing sites of the heme. These two binding sites are designated distal and axial and the ligands bound there are consequently assigned as the distal and axial ligand. The axial ligand is an amino acid side chain that links the metal-heme to the protein backbone. In the P450s, generally, a cysteinate ligand binds to iron (*17*), whereas in peroxidases and heme oxygenases, an imidazole group of a histidine side chain is the axial ligand, while in catalases a phenolate group of a tyrosinate residue is found in the axial position (*18*). The distal binding site in heme enzymes, therefore, is the variable binding position and is occupied by a water molecule in the resting state. This distal site also includes the binding pocket for the substrate (*N*-palmitoyl-glycine in $P450_{BM3}$), which does not bind directly to the metal but in its vicinity. In this particular isozyme, the substrate is held in position via several key hydrogen bonding

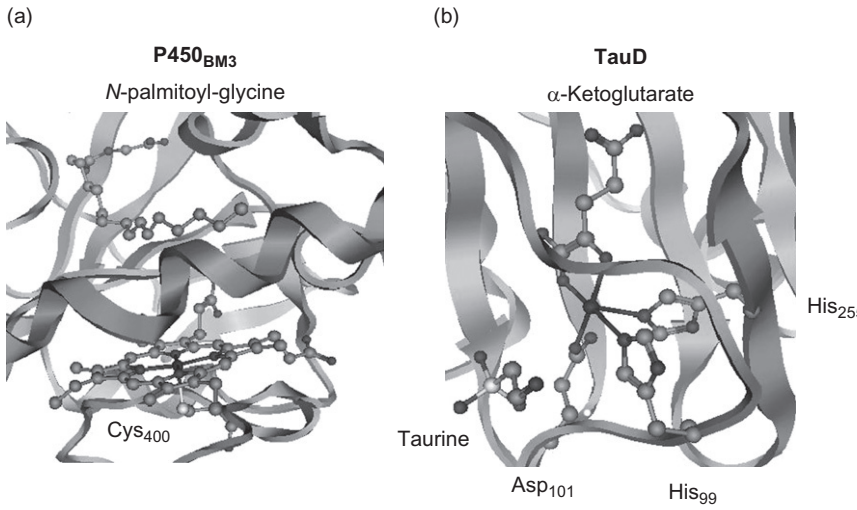

FIG. 1. Active site of $P450_{BM3}$ (a) and TauD (b) as taken from the 1JPZ and 1OS7 PDB files. Amino acids are labeled as in the PDB file.

interactions, which position the substrate into a specific orientation and thereby drive the regioselectivity of the reaction.

A. Catalytic Cycle of TauD Enzymes

The active site of TauD is shown in (b) of Fig. 1 as taken from the crystal structure of the substrates bound complex (*16*). Thus, the metal is bound to the protein via linkages with two histidines and one aspartic acid side chain via a 2His/1Asp structural motif. This motif is a common feature in nonheme iron containing dioxygenases, where these three ligands form a facial triad and keep three binding sites of the metal free (*19*). In the resting state of the enzyme, those three binding sites are occupied with water molecules, but binding of αKG displaces two of those opposite His_{99} and Asp_{101}. The last water ligand is replaced by molecular oxygen after substrate taurine binds into the binding pocket, which is the structure shown in Fig. 1b.

The catalytic cycle of TauD has been studied extensively (*20–22*) and is schematically depicted in Fig. 2 starting from the αKG-bound structure (**A**). When taurine enters the substrate binding pocket the last water ligand of the metal is released (structure **B**) prior to dioxygen binding (structure **C**). The terminal oxygen atom of the iron(III)–superoxo structure subsequently attacks the α-keto

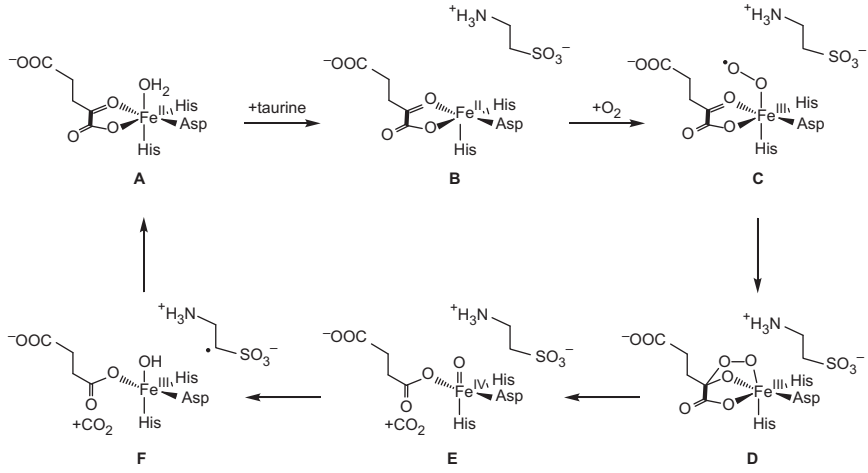

FIG. 2. Catalytic cycle of TauD.

position of αKG to form the bicyclic ring structure **D**. This structure has never been detected experimentally, but theoretical modeling has assigned it as an intermediate to the formation of an iron (IV)–oxo complex (*23,24*). In the ring structure, the C—C bond in αKG is weakened and decarboxylation leads to a peroxosuccinate complex (*23,24*), followed by O—O cleavage to form succinate and an iron(IV)–oxo complex (**E**). This iron(IV)–oxo complex has been characterized by Resonance Raman and rapid freeze–quench X-ray absorption spectroscopy (*25,26*). These studies identified a short Fe—O bond of 1.62±0.01Å characteristic for an iron(IV)–oxo intermediate (*26*). Resonance Raman spectroscopy studies measured the $^{16}O_2/^{18}O_2$ difference spectrum of TauD, which revealed isotope shifts corresponding to an iron(IV)–oxo species. Thus a downshift of an $\nu_{Fe=O}$ frequency from 821 to 787 cm^{-1} was measured due to isotopic substitution of O_2 (*25*). Density functional theory calculations confirmed this assignment and identified another peak in the difference spectrum at 859 cm^{-1} as originating from the OOC—C stretch vibration in the succinate group that also includes one ^{18}O atom originating from O_2 (*27*). The iron(IV)–oxo species is the oxidizing species in TauD enzymes that abstracts a hydrogen atom from taurine to form an iron(III)–hydroxo complex (**F**). Finally, rebound of the hydroxo group to taurine radical gives hydroxylated products, which are released to bring the system back into the resting state. Further evidence of an iron (IV)–oxo active species as active oxidant in the reaction mechanism came from kinetic isotope effect (KIE) studies on taurine versus

taurine-d_2 that determined a KIE of k_H/k_D=37 indicative of a rate-determining hydrogen abstraction step (*28*).

B. Catalytic Cycle of P450 Enzymes

Heme monoxygenases such as the P450s undergo a catalytic cycle that is very different from the one shown above for nonheme enzymes, like TauD. Figure 3 shows the catalytic cycle of P450 (*29–31*). Thus, in the resting state (structure **G**), a water

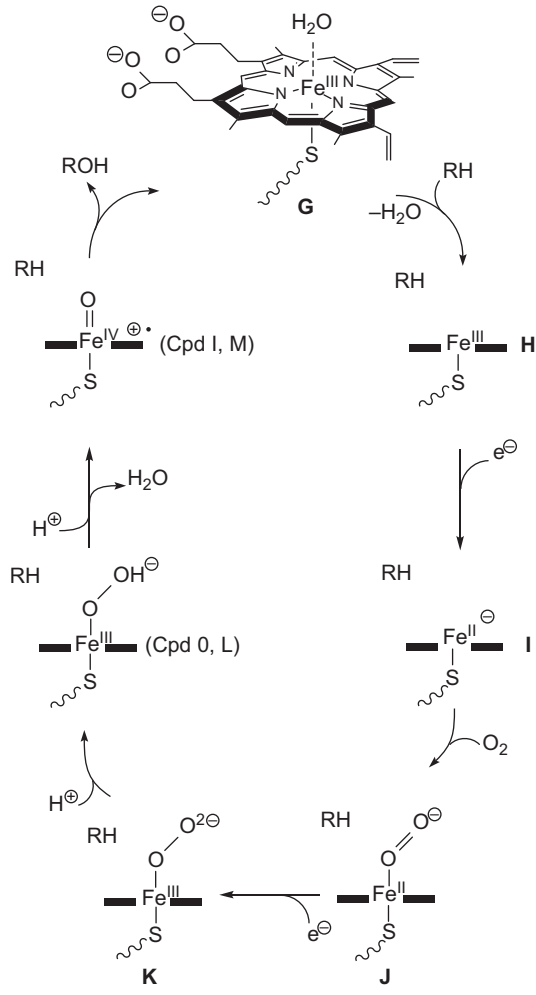

Fig. 3. Catalytic cycle of P450 enzymes.

molecule is bound in the distal position of the heme, but upon substrate binding in the binding pocket, this water molecule is released (structure **H**). Water release from the heme triggers a low-spin (doublet) to a high-spin (sextet) transition (*32*). Subsequently, the heme is reduced (structure **I**) and binds molecular oxygen (structure **J**). The next electron donation step is the rate-determining step in the catalytic cycle (*33*) and leads to the ferric–superoxo intermediate **K**. Thereafter, a proton transfer gives the ferric–hydroperoxo intermediate, also known as Compound 0 (Cpd 0). The latter has been characterized at low temperature with electron paramagnetic resonance/Electron-Nuclear DOuble Resonance, EPR/ENDOR (*34*), and resonance Raman spectroscopy (*35*) studies. A final proton transfer then leads to the iron(IV)–oxo heme cation radical active species (Compound I, Cpd I, **L**), which is the proposed oxidant that abstracts a hydrogen atom from the substrate (RH in Fig. 3) and rebounds the hydroxyl group to $R^{\bullet}$ to form hydroxylated products. Recent studies of Rittle and Green (*36*) characterized this intermediate using UV–Visible, Mössbauer, and EPR spectroscopies. The studies showed it to possess two unpaired electrons on the FeO group that are coupled to a radical on the porphyrin ring. KIE studies on the reactivities of deuterated and nondeuterated substrates implicated a rate-determining hydrogen abstraction step for the reaction as proposed by Groves and coworkers in the late 1970s (*37*). As such, the catalytic cycle of P450 is significantly different from the nonheme enzymes like TauD. In particular, P450 enzymes require cofactors to donate electrons and protons to convert molecular oxygen into its active form, whereas nonheme iron systems do not require a cofactor but use a co-substrate such as αKG instead. These differences in catalytic cycle also have effects on the substrate hydroxylation reactions.

II. Computational Studies of the Catalytic Activity of Heme and Nonheme Enzymes

With the advances in density functional theory, these days calculations can be done with good accuracy to predict experimental results. In density functional theory, the wave function (Ψ) in the Schrödinger equation (Eq. 2) is described as a functional of the electron density $\rho(\mathbf{r})$ and is used to calculate the electronic energy E (*38,39*). The Hamiltonian (H) describes all perturbations working on the electrons, and in density functional theory, the most common method is the B3LYP method (*40,41*).

In density functional theory, the functional determines the description of the electron–electron interactions, which separate into exchange (x) and correlation (c) components. Thus, Becke developed a hybrid density functional method (Eq. 3), where the total energy calculated was benchmarked against a set of experimental ionization potentials, electron affinities, and proton affinities of high accuracy. These calculations provided Becke three fit parameters (A, B, and C) that appear to be general for all molecules (*42,43*). The hybrid density functional method B3LYP contains the local density approximations for exchange of Slater (E_x^{Slater}) and the one for correlation due to Vosko, Wilks, and Nusair (E_c^{VWN}), respectively (*44,45*). It also contains the Hartree–Fock exchange (E_x^{HF}), a correction factor to the exchange due to Becke ($\Delta E_x^{\text{Becke}}$), and a correction factor to the correlation from Lee, Yang, and Parr for nonlocal correlation effects (ΔE_c^{LYP}).

$$H\Psi = E\Psi \tag{2}$$

$$E_{xc}^{\text{B3LYP}} = AE_x^{\text{Slater}} + (1-A)E_x^{\text{HF}} + B\Delta E_x^{\text{Becke}} + E_c^{\text{VWN}} + C\Delta E_c^{\text{LYP}} \tag{3}$$

This hybrid density functional method has been extensively applied by our group to calculate the spectroscopic and catalytic properties of enzymatic intermediates, including the iron (IV)–oxo species of heme and nonheme oxidants (*46–48*). Let us summarize here first the direct calculations we did with respect to experimental data, including reproducing experimental rate constants, KIEs, and spectroscopic data.

Styrene epoxidation by a model of Cpd I of P450 was calculated using an iron(IV)–oxo porphyrin cation radical species with thiolate axial ligand, [Fe^{IV}═O($Por^{+\bullet}$)SH] (*49*). It was found that the reaction proceeds via two-state reactivity (TSR) on competing doublet and quartet spin state surfaces with free energies of activation of $\Delta G^{\ddagger}$=20.9 (21.6)kcal mol^{-1} on the quartet (doublet) spin state surfaces. In comparison, the experimental free energy of activation of styrene epoxidation by $P450_{cam}$ enzymes was determined to be 24–25 kcal mol^{-1} (*50*) so that our calculations reproduce experimental data within about 3 kcal mol^{-1}.

A direct comparison of computations with experimental data was done in a collaboration of our group with the Nam group in Seoul. These studies involved aromatic hydroxylation by a nonheme iron(IV)–oxo oxidant with pentadentate N4Py ligand system, where N4Py=*N*,*N*-bis(2-pyridylmethyl)-*N*-bis(2-pyridyl) methylamine (*51*). It was found that the rate-determining step is an electrophilic substitution to form a cationic intermediate

via a free energy of activation barrier of $\Delta G^{\ddagger}$=16.1 kcal mol^{-1} on a quintet spin state surface. The experimental free energy of activation for anthracene hydroxylation by the same oxidant was determined to be 19 kcal mol^{-1} at 298 K. These studies show that generally the B3LYP method predicts free energies of activation within about 3 kcal mol^{-1} from experiment, where the computations tend to underestimate the barrier heights.

Subsequently, our group studied a systematic set of aliphatic hydroxylation reactions by a model of Compound I of P450 (*52*) and the iron(IV)–oxo species of TauD (*53*). These studies showed that the barrier height of aliphatic hydroxylation correlates with the strength of the C—H bond that is broken via the C—H bond dissociation energy (BDE_{CH}). The trends gave good linearity and implicated that the 3 kcal mol^{-1} deviation between experimental and B3LYP calculated free energies of activation actually is a systematic error and that the reproducibility and linearity of the curves was within 1 kcal mol^{-1} (*52,53*).

The good agreement between experimental and calculated free energies of activation further prompted us to calculate KIEs (*54,55*). Initial calculated KIEs used the semiclassical Eyring equation (KIE_{Eyring}), Eq. (4), which takes the free energy of activation ($\Delta G^{\ddagger}$) difference of the hydrogen- and deuterium-substituted reactions. In Eq. (4), the temperature is given by T and R is the gas constant.

$$KIE_{Eyring} = \exp\left[(\Delta G^{\ddagger}_{D} - \Delta G^{\ddagger}_{H})/RT\right] \tag{4}$$

Subsequent models also included tunneling corrections to the KIE due to either Wigner (KIE_{Wigner}) or Bell (KIE_{Bell}), Eqs. (5)–(7). These models assume that the imaginary frequency (ν) in the transition state represents the potential well width and consequently represent the ability of tunneling. In Eqs. (5)–(7), the Boltzmann constant is given as k_B and Planck's constant as h.

$$KIE_{tunneling} = KIE_{Eyring}\, Q_{t,H}/Q_{t,D} \tag{5}$$

$$Q_{t,Wigner} = 1 + u_t^2/24 \quad \text{with} \quad u_t = h\nu/k_B T \tag{6}$$

$$Q_{t,Bell} = \frac{u_t}{2\sin(0.5u_t)} - \sum_{n=1}^{\infty}(-1)^n \frac{\exp((u_t - 2n\pi)\Delta E/u_t)}{(u_t - 2n\pi)/u_t} \tag{7}$$

The potential energy profile of *trans*-methylphenylcyclopropane and *trans*-d_1-methylphenylcyclopropane hydroxylation by Compound I of P450 was calculated using DFT methods, and product

isotope effects (PIEs) were estimated from the KIE values (*54,55*). The calculations predicted a PIE from the ratio of the hydrogen- and deuterium-substituted reactions of 1.03, 1.07, and 1.20 using the Eyring, Wigner, and Bell KIE models, respectively. These values compared very well with the experimental value of 1.14 (*56*).

Finally, we did extensive studies on spectroscopic parameters with respect to experiment. For instance, the iron(IV)–oxo vibration is known to have a strong dependence on the mass of the oxygen atom; hence a replacement of ^{16}O by ^{18}O gives a lowering of the Fe—O vibrational mode by about 35 kcal mol^{-1}. This, for instance, has been shown in TauD by Hausinger and coworkers (*25*), where the resonance Raman spectrum revealed several oxygen sensitive bands. Thus, the $^{16}O_2/^{18}O_2$ difference spectrum identified the iron(IV)–oxo vibration at 821 cm^{-1} in the $^{16}O_2$ spectrum, whereas it was redshifted by 34 cm^{-1} in the $^{18}O_2$ spectrum. Computational studies on TauD, prolyl-4-hydroxylase (P4H) and ribonucleotide reductase models gave similar results for analogous iron(IV)–oxo vibrations (*27,57,58*). Thus, in the case of TauD and P4H, molecular oxygen is activated on an iron(III) center, whereby the first oxygen atom reacts with αKG to form succinate and CO_2 and an iron(IV)–oxo species. One of the oxygen atoms from O_2 is included in a carboxylate group of succinate that is bound to iron, while the other one is the oxo group. Therefore, replacing $^{16}O_2$ with $^{18}O_2$ affects the Fe(IV)—oxo bond as well as the Fe(IV)—O—succinate bond. In order to identify these vibrations, we did a geometry optimization of a model of the iron (IV)–oxo species of P4H and replaced either the oxo or the carboxylate oxygen or both by ^{18}O (*58*). We find an Fe═O stretch vibration at $\nu_{Fe=O}$=811 cm^{-1}, while the stretch vibration along the Fe—O bond between the metal and the succinate group is located at $\nu_{Fe-OSucc}$=857 cm^{-1}. These frequencies shift by 33 and 18 cm^{-1}, respectively, upon replacement of $^{16}O_2$ by $^{18}O_2$. Our calculations support the experimental assignment and identify the individual vibrations. In addition, we located two bending vibrations in the carboxylic acid group of succinate at 557 cm^{-1} (out of plane) and 583 cm^{-1} (in plane). Although these frequencies give little shifts upon replacement of $^{16}O_2$ by $^{18}O_2$, we did notice sharp differences in the calculated Raman intensities, whereby the higher vibration is more Raman active in the $^{16}O_2$ spectrum, and the lower one more active in the $^{18}O_2$ spectrum. Because of this, they appear as a single peak in the resonance Raman spectrum that shifts by about 30 cm^{-1}, but in fact are two peaks with different Raman intensities in the $^{16}O_2$ and $^{18}O_2$ spectra.

Finally, others and us calculated Mössbauer parameters of TauD and P4H in comparison with experiment (*58,59*). Although the agreement for these types of calculations is not perfect, generally the correct trend is reproduced. Recent quantum mechanics/molecular mechanics studies on a doubly reduced form of structure **B** in the catalytic cycle of P450 were performed and focused on the possible low-lying electronic states (*60*). In particular, the relative energy difference and spectroscopic parameters (EPR) of an Fe^{I}-porphyrin versus Fe^{II}-porphyrin anion radical were compared.

In summary, DFT-calculated barrier heights and spectroscopic constants using model complexes give good reproducibility of experimental data. Generally, the deviation from experiment is systematic rather than random.

A. Compound I of P450

The cytochromes P450 use an iron(IV)–oxo heme cation radical active species as active oxidant, which is also known as Compound I (Cpd I). Cpd I has a special electronic configuration with three unpaired electrons: two located on orthogonal π^*_{FeO} orbitals (π^*_{xz} and π^*_{yz}), while a third is on the heme in an orbital that in D_{4h} symmetry has the label a_{2u} (*61,62*). Figure 4 shows the optimized geometry of Cpd I as taken from Refs. (*46,62*) and the high-lying occupied and low-lying virtual molecular orbitals that are critical for the hydroxylation reaction mechanism. The a_{2u} orbital is a heme-based orbital that mixes

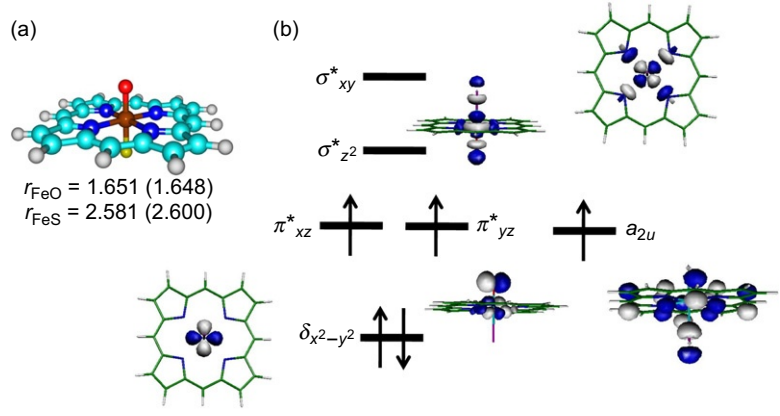

FIG. 4. (a) Optimized geometry of P450 Cpd I with bond lengths in angstroms. (b) High-lying occupied and low-lying virtual orbitals of Cpd I.

somewhat with a lone-pair π orbital on the axial ligand (*63*). Especially, a thiolate ligand mimicking a cysteinate residue gives significant contributions in the gas phase, although environmental effects, for example, through the protein have been shown to influence the mixing of the heme and lone-pair axial ligand orbitals (*63,64*). The high-lying occupied and virtual orbitals originate from the metal 3d orbitals, and in addition, there is a high-lying porphyrin-based orbital (a_{2u}). The metal 3d-type orbitals are occupied by four electrons: two in a low-lying nonbonding orbital ($\delta_{x^2-y^2}$) and the other two in antibonding orbitals for the Fe—O interaction. Two virtual orbitals are of σ* type and reflect the antibonding interactions of the metal with the distal and axial ligands (in σ^*_{z2}) and with the heme nitrogen atoms (in σ^*_{xy}). Thus, Cpd I has electron occupation $\delta_{x^2-y^2}{}^2\pi^*_{xz}{}^1\pi^*_{yz}{}^1a_{2u}{}^1$; however, since the interaction between the π* orbitals and the a_{2u} orbital is small, the system can appear in an overall quartet or doublet spin state with the same orbital occupation. In the doublet spin state, the two unpaired electrons in the π* orbitals are up-spin, whereas the unpaired electron in a_{2u} is down-spin. As a consequence, Cpd I has almost degenerate doublet and quartet spin states, which give rise to TSR patterns on competing doublet and quartet spin state surfaces (*31,65*). TSR leads to unequal transition states during substrate oxidation and may masquerade product distributions and KIEs.

B. Two-State Reactivity (TSR)

Cpd I reacts with an alkane (RH) by an initial hydrogen abstraction to form an iron–hydroxo complex, Equations (8) and (9). Hydrogen abstraction, however, includes a one-electron transfer from the substrate to Cpd I. Due to the fact that there are several close-lying orbitals in Cpd I this electron transfer can either fill the π^*_{xz} orbital or the a_{2u} orbital with a second electron. A transfer of an extra electron into the π* system gives an iron–hydroxo complex with the metal in oxidation state Fe^{III}, while the heme stays in the cation radical situation, that is, with electron configuration $\mathbf{I}_{III}=\delta_{x^2-y^2}{}^2\pi^*_{xz}{}^2\pi^*_{yz}{}^1a_{2u}{}^1\pi_R{}^1$. The latter orbital is the substrate radical restgroup. On the other hand, electron transfer from the substrate into the heme orbital keeps the metal in oxidation state Fe^{IV} and creates an intermediate with electronic configuration $\mathbf{I}_{IV}=\delta_{x^2-y^2}{}^2\pi^*_{xz}{}^1\pi^*_{yz}{}^1a_{2u}{}^2\pi_R{}^1$. Calculations on ethene epoxidation (*66*) and propene hydroxylation as well as epoxidation (*67,68*) showed that the two iron–hydroxo complexes, $[Fe^{IV}(OH)(Por)SH]$

and [Fe^{III}(OH)($Por^{+\bullet}$)SH], are close in energy and their ordering and relative energies are dependent on the nature of the environment.

$$[Fe^{IV} = O(Por^{+\bullet})SH] + RH \rightarrow [Fe^{IV}(OH)(Por)SH] + R^{\bullet} \quad (8)$$

$$\left[Fe^{IV} = O(Por^{+\bullet})SH\right] + RH \rightarrow \left[Fe^{III}(OH)(Por^{+\bullet})SH\right] + R^{\bullet} \quad (9)$$

In a subsequent step, the hydroxo group rebinds to the substrate radical restgroup to form the alcohol products, Eq. (10). This process transfers a second electron into the iron–-heme system and whether it starts from [Fe^{IV}(OH)(Por)SH] or [Fe^{III}(OH)($Por^{+\bullet}$)SH] it leads to the same products complexes [Fe^{III}(Por)SH—ROH] (**P**) with electronic configuration $^4\mathbf{P}=\delta_{x^2-y^2}{}^2\pi^*_{xz}{}^1\pi^*_{yz}{}^1\sigma^*_{z2}{}^1a_{2u}{}^2$ or $^2\mathbf{P}=\delta_{x^2-y^2}{}^2\pi^*_{xz}{}^2\pi^*_{yz}{}^1a_{2u}{}^2$.

$$\left[Fe^{IV}(OH)(Por)SH\right] + R^{\bullet} \rightarrow \left[Fe^{III}(Por)SH - - - ROH\right] \quad (10)$$

An example of a calculated reaction mechanism of an aliphatic hydroxylation process that passes the various Fe(III) and Fe(IV) iron–hydroxo complexes (**I**) as taken from Ref. (*68*) is shown in Fig. 5. Thus, the reaction proceeds via TSR on competing doublet and quartet spin state surfaces. The initial reaction is a hydrogen atom abstraction via barrier $\mathbf{TS}_H$ to form the intermediates. In the gas phase, the [Fe^{IV}(OH)(Por)SH] complexes are lower in energy than the [Fe^{III}(OH)($Por^{+\bullet}$)SH], but addition of the protein environment in quantum mechanics/molecular mechanics

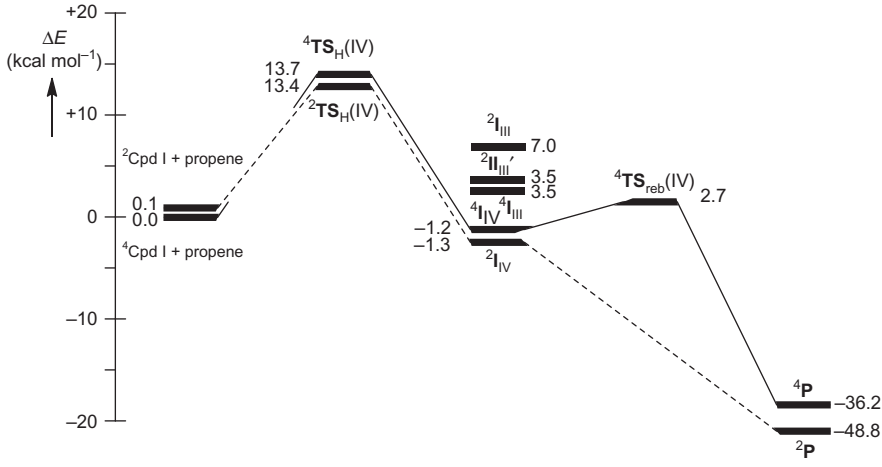

FIG. 5. Potential energy profile of aliphatic hydroxylation of propene by Cpd I via either Fe(III) or Fe(IV) intermediates. Data taken from Ref. (*68*).

calculations (*64*) reverses the ordering. In a subsequent step, the radical rebounds to the hydroxo group to form alcohol product complexes. This step is barrierless on the low-spin surface but encounters a rebound barrier of 3.9 kcal mol^{-1} from $^4\mathbf{I}_{IV}$. Note that in the low spin, there are two Fe(III) electronic configurations $^2\mathbf{I}_{III}$ and $^2\mathbf{I}_{III}{}'$ with occupation $^2\mathbf{I}_{III}=\pi^*_{yz}{}^{\uparrow}\ a_{2u}{}^{\downarrow}\ \pi_R{}^{\uparrow}$ and $^2\mathbf{I}_{III}{}'=\pi^*_{yz}{}^{\uparrow}\ a_{2u}{}^{\uparrow}\ \pi_R{}^{\downarrow}$. Thus, the TSR surface in Fig. 5 indicates that the high-spin intermediate ($^4\mathbf{I}_{IV}$) will have a finite lifetime due to an existing rebound barrier, whereas on the low-spin surface rebound is barrierless and the lifetime of $^2\mathbf{I}_{IV}$ will be negligible. These differences may affect product distributions as for instance rearrangement and stereochemical scrambling can occur during the lifetime of the intermediate, while this is unlikely on the low-spin surface (*69,70*).

C. VB Description of Potential Energy Surfaces

In this section, we explain the basic features of a VB curve-crossing diagram, which was designed to explain hydrogen abstraction barriers through electron transfer mechanisms (*71–74*). Figure 6 gives a basic description of a VB curve-crossing diagram. The system starts in the reactant geometry on the bottom left of the figure, where the system is described by the

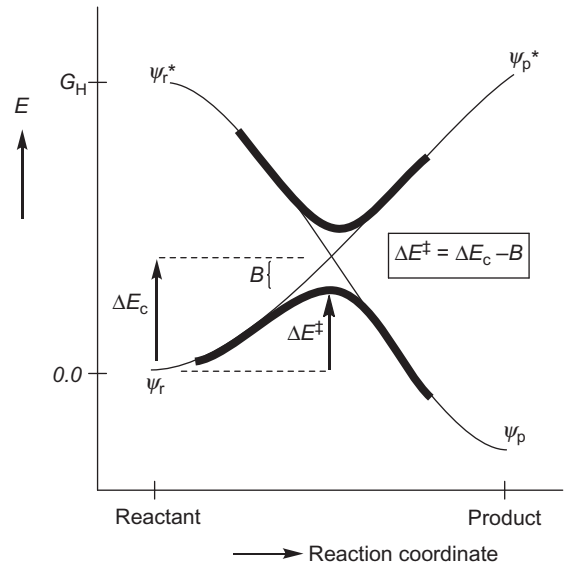

FIG. 6. General description of a VB curve-crossing diagram.

reactant wave function Ψ_r. On the right-hand side of the figure is the alcohol product complex, which has product wave function Ψ_p. The curve-crossing diagram is created by making a connection between the reactant and the product wave functions. These two wave functions are described by different electronic situations, that is, orbital occupation. Thus, the product electronic situation corresponds to an excited state in the reactant geometry with wave function Ψ_r*. Similarly, the reactant electronic situation is an excited state in the product geometry with wave function Ψ_p* and connects to Ψ_r. These reactant and product wave functions with their individual electron distributions cross each other and give rise to an avoided crossing, that is, a transition state for the reaction. In VB theory, the barrier height ($\Delta E^{\ddagger}$) is described as a function of the excitation energies of these processes. The excitation energy in the reactant geometry from the reactant wave function to Ψ_r* is defined through the promotion energy gap G_H. The height of the crossing point is ΔE_c but the actual transition state energy ($\Delta E^{\ddagger}$) is a bit lower in energy by a factor B that represents the resonance energy, Eq. (11). Moreover, substituting ΔE_c by a fraction of the excitation energy G_H gives the barrier height as a function of the resonance energy and the promotion gap (Eq. 11). The latter will be used to predict barrier heights of hydrogen abstraction reactions of which we will show several examples later in this review paper.

$$\Delta E^{\ddagger} = \Delta E_c - B = f\,G_H - B \tag{11}$$

In the next few sections, we will describe examples where we used VB curve crossing diagrams to predict trends in oxygen atom transfer reactions.

III. Trends in Substrate Oxidation Reactions

The cytochromes P450 catalyze a range of different reaction processes including aliphatic and aromatic hydroxylation, C═C double-bond epoxidation, heteroatom oxidation (sulfoxidation), N-dealkylation, and dehydrogenation. Many of these reaction mechanisms have been elucidated with computational studies that have given insight into the electron transfer processes and the reactions leading to by-products. The most intensely studied reaction mechanism is substrate hydroxylation, which has relevance to the biotechnological industry. Understanding the catalytic mechanism of substrate hydroxylation by the P450s, therefore, has always been a key target in this research area. We

will start with a detailed analysis of computational methods (DFT as well as VB) that have given fundamental insight into the reaction process in Section III.A. Figure 7 displays three more oxygen atom transfer processes catalyzed by the P450s, namely aromatic hydroxylation, sulfoxidation, and epoxidation. Electronically, the substrate epoxidation process, pathway (b) in Fig. 7, shows many similarities to aliphatic hydroxylation, and its mechanism and properties are discussed in Section III.B. Aromatic hydroxylation, pathway (c) in Fig. 7, and sulfoxidation, pathway (d) in Fig. 7, by contrast, proceed via electrophilic addition reactions, and therefore, we will discuss these mechanisms separately in Sections III.C and III.D, respectively.

A. Aliphatic Hydroxylation

To gain insight into the factors that determine the reactivity of oxidants, such as Compound I of P450 in substrate hydroxylation reactions, a systematic study on hydrogen atom abstraction reactions by [Fe^{IV}=O($Por^{+\bullet}$)SH] was performed (*52*). These studies used the following substrates: methane, ethane, propane (1° as well as 2° C—H bonds), propene (aliphatic), toluene (aliphatic), ethylbenzene (benzyl C—H bond), *trans*-methyl phenyl cyclopropane, *trans-i*-propyl phenyl cyclopropane, *N*,*N*-dimethyl aniline, and camphor. Initially, the potential energy profile of hydrogen atom abstraction was calculated and all showed similarity to the one shown above in Fig. 5. In all cases, the reactions are stepwise with a rate-determining step for the hydrogen atom

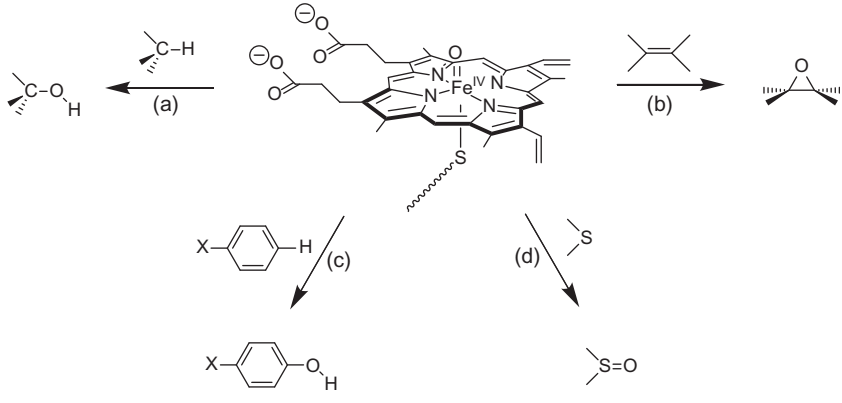

Fig. 7. Different reaction mechanisms catalyzed by Compound I of P450.

abstraction that is followed with a much smaller rebound barrier to form alcohol products. Experimental studies on hydrogen atom abstraction by a range of metal-oxo oxidants determined a linear correlation between the natural logarithm of the rate constant and the BDE_{CH} of the C—H bond broken in this process (*75–79*). The BDE_{CH} value representing the energy to break the C—H bond in substrate Sub–H is defined in Eq. (12).

$$\mathrm{Sub-H} \rightarrow \mathrm{Sub}^{\bullet} + \mathrm{H}^{\bullet} + \mathrm{BDE_{CH}} \qquad (12)$$

The correlation between hydrogen abstraction barrier ($\Delta E^{\ddagger}$) and BDE_{CH} for the 11 hydrogen atom abstraction reactions we calculated is given in Fig. 8. Indeed in agreement with experimental observations, a linear correlation between barrier height (or natural logarithm of the rate constant) and BDE_{CH} is observed. To understand the origin of this correlation between barrier height and BDE_{CH}, we have set up a VB curve-crossing diagram that explains the electron transfer processes for the hydroxylation reaction (see Fig. 9).

Figure 9 starts on the bottom left-hand side with the reactants configurations (Cpd I of P450+substrate, RH) and proceeds via a radical intermediate and finally leads to alcohol products. The π-system in the Fe—O bond in Cpd I is occupied with six electrons ($\pi_{xz}^{2}\pi_{yz}^{2}\pi^{*}_{xz}{}^{1}\pi^{*}_{yz}{}^{1}$): we display these electrons with a dot next to the atoms in Fig. 9. Thus, the group spin density of the half-filled π^{*}_{xz} and π^{*}_{yz} molecular orbitals in Cpd I gives approximately 50% spin density on the iron and 50% spin density on the oxygen atom. As a consequence, there are two electromers K_1 and K_2 with the same orbital occupation. In addition to

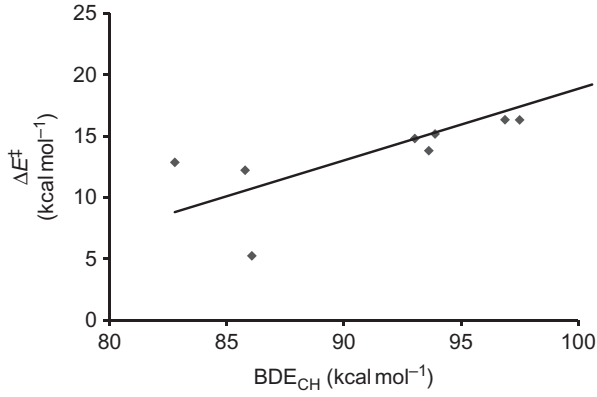

FIG. 8. Correlation between hydrogen abstraction barrier ($\Delta E^{\ddagger}$) and BDE_{CH} with data taken from Ref. (52).

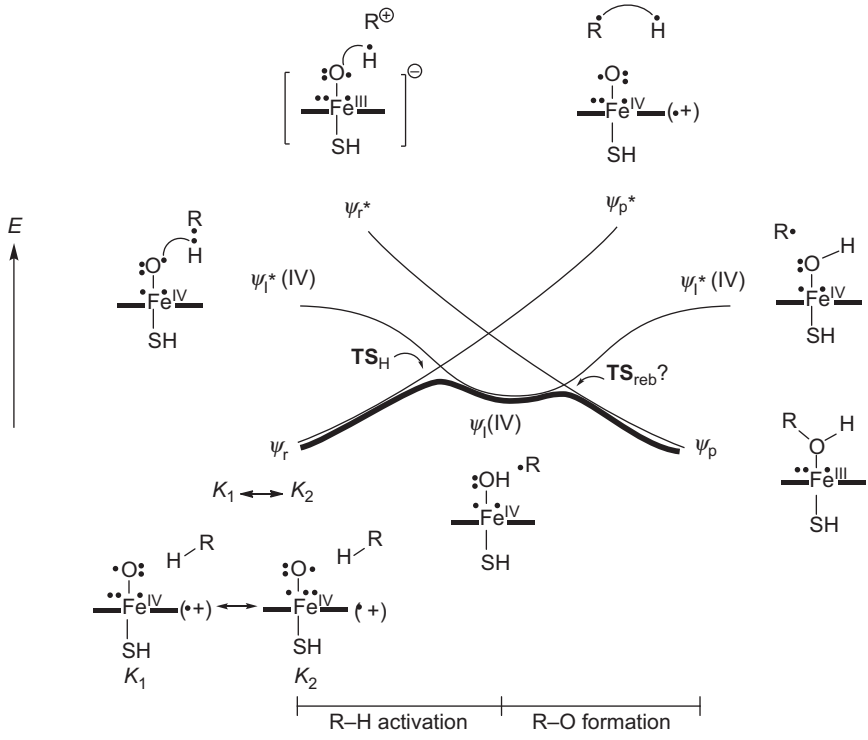

FIG. 9. VB curve-crossing mechanism for the hydroxylation reaction by the iron(IV)-oxo species of P450 via an [Fe^{IV}(OH)(Por)SH—R$^{\bullet}$] intermediate.

these two unpaired electrons in the π^*_{xz} and π^*_{yz} orbitals, there is another unpaired electron in a porphyrin-based orbital that in D_{4h} symmetry has the a_{2u} label. The reactant wave function with $\pi^*_{xz}{}^1\pi^*_{yz}{}^1a_{2u}{}^1$ configuration is Ψ_r. In VB theory, a reactant wave function is connected with an excited state in the product geometry with wave function Ψ_p*. The ground state products have the metal in oxidation state Fe(III) with doublet spin configuration $\delta^2\pi^*_{xz}{}^2\pi^*_{yz}{}^1a_{2u}{}^2$ or with quartet spin configuration $\delta^2\pi^*_{xz}{}^1\pi^*_{yz}{}^1\sigma^*_{z2}{}^1a_{2u}{}^2$. These product wave functions (Ψ_p) connect to an excited state in the reactant geometry (Ψ_r*). In principle, the two VB curves cross and give rise to an avoided crossing and a concerted barrier for hydrogen atom abstraction. However, the VB curve is intercepted by an intermediate wave function Ψ_I(IV) that represents a radical intermediate with [Fe^{IV}(OH)(Por)SH—R$^{\bullet}$] configuration and orbital occupation $\delta^2\pi^*_{xz}{}^1\pi^*_{yz}{}^1a_{2u}{}^2\phi_R{}^1$, where the latter orbital represents the radical on the substrate restgroup. The curve crossing between Ψ_I(IV) and Ψ_r gives rise to a hydrogen

atom abstraction barrier ($\mathbf{TS}_{H}$), while the one between Ψ_{I}(IV) and Ψ_{p} gives a rebound barrier ($\mathbf{TS}_{reb}$). We will focus here on the hydrogen atom abstraction barrier, however. Details on the rebound step can be found in Refs. (*52,73,74,80*).

The VB curve-crossing diagram displayed in Fig. 9 explains that the reaction is stepwise via a radical intermediate followed by a radical rebound barrier to give alcohol products. In VB theory, the barrier height can be described by Eq. (11) above and is proportional to the curve crossing energy and the resonance energy (B). The curve crossing energy is a function of the excitation energy (or promotion gap) from the ground state wave function to the product-type excited state wave function in the geometry of the reactants. As follows from the structures drawn in Fig. 9, this excitation energy refers to a singlet–triplet excitation in the C—H bond of the substrate. This energy difference is proportional to the strength of the C—H bond and hence will correlate with BDE_{CH}. We recently showed a correlation between barrier height and BDE_{CH} for aliphatic hydroxylation by $[Fe^{IV}{=}O(Por^{+\bullet})SH]$ as well as by the iron(IV)-oxo species of TauD (*52,53*).

The VB model (Eq. 11) was used to predict hydrogen abstraction barriers from empirical data (*52*). An average deviation from experiment of between 1.5 and 2.0 $kcal\,mol^{-1}$ was found for hydrogen atom abstraction from substrates by $[Fe^{IV}{=}O(Por^{+\bullet})SH]$. Similar reproducibility of DFT-calculated barrier heights was obtained using a nonheme iron(IV)-oxo oxidant mimicking the active species of TauD (*53*). Therefore, the VB model described by Eq. (11) can be used to predict hydrogen abstraction barrier heights of substrates.

Recent studies (*81*) on the axial ligand effect on substrate hydroxylation further generalized the H−abstraction trends and showed that the trends are also applicable when one substrate and a selection of oxidants is investigated. However, the free energy of activation in that case is proportional to BDE_{OH} rather than BDE_{CH}, which was explained with a VB diagram.

B. Epoxidation

P450 enzymes activate substrates with C=C double bonds, for instance from monounsaturated fatty acids, to form epoxides as an initial step in their metabolism. Quite a few biochemical studies focused on the products observed from double-bond activation using, for example, propene, cyclohexene, and styrene as substrates (*82–86*). Subsequent computational studies provided

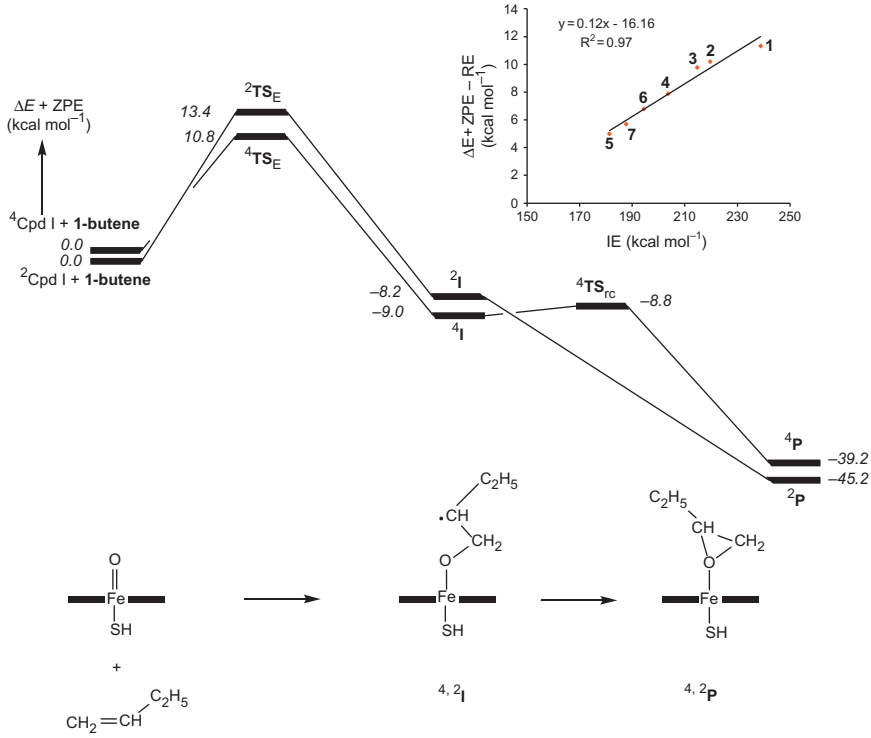

FIG. 10. Potential energy profile for the epoxidation reaction of 1-butene by ^{4,2}[Fe^{IV}=O(Por$^{+\bullet}$)SH] as calculated with DFT methods. Data taken from Ref. (*88*).

a mechanism of formation of epoxide products as well as by-products including suicidal complexes and aldehydes (*49,66–70*). Thus, it was found that the reaction is stepwise via a radical intermediate (**I**), while a concerted synchronous reaction proceeded via a second-order saddle point (*87*). A typically calculated reaction mechanism for 1-butene epoxidation by [Fe^{IV}=O(Por$^{+\bullet}$)SH] is shown in Fig. 10 with data taken from Ref. (*88*).

Alkene activation by Compound I of P450 takes place on close-lying doublet and quartet spin state surfaces with a rate-determining electrophilic addition of the oxo group to the terminal carbon atom of the double bond with transition state **TS**$_E$. The intermediates (^{4,2}**I**) are radicalar with orbital occupation $\delta^2\pi^*_{xz}{}^1\pi^*_{yz}{}^1a_{2u}{}^2\phi_R{}^1$, which resemble the configuration of the radical intermediates obtained after hydrogen atom abstraction. Similar to aliphatic hydroxylation, also substrate epoxidation

gives close-lying mechanisms via either iron(III)- or iron(IV)-based intermediates (*66–68*), but we will focus on the lowest lying mechanisms that pass an iron(IV) intermediate only here. A ring-closure transition state ($\mathbf{TS}_{rc}$) separates intermediates from epoxide products ($^{4,2}\mathbf{P}$). The ring-closure transition state is negligible on the low-spin surface and small on the high-spin surface due to electron transfer from the substrate in the low-lying π^*_{xz} orbital in the doublet spin state as compared to a virtual σ^*_{z2} orbital in the quartet spin state. This difference in barrier height has been assigned as the reason for the stereospecific epoxidation of substrates by P450 enzymes (*69*).

A systematic study of substrate epoxidation by [Fe^{IV}═O($Por^{+\bullet}$) SH] was done using a range of different olefins: ethene (**1**), propene (**2**), 1-butene (**3**), *trans*-2-butene (**4**), 1,3-cyclohexadiene (**5**), 1,4-cyclohexadiene (**6**), and styrene (**7**). All reactions proceed via TSR patterns with close-lying doublet and quartet spin states and a potential energy profile similar to that given for 1-butene in Fig. 10. In all cases, the first barrier (via $\mathbf{TS}_E$) is rate determining and the ring-closure barriers are small. It was reasoned (*88*) that the barrier height ($\mathbf{TS}_E$) is proportional to the breaking of the double bond in the olefin. Generally, the lowest ionization energy (IE) of an olefin refers to removal of an electron from a π-bond in the olefin, and hence, IE could be the controlling factor for the barrier height. The inset of Fig. 10 indeed confirms the hypothesis and displays the correlation between barrier height and olefin IE.

To explain the observed trends, a VB curve-crossing diagram was set up, which is summarized in Fig. 11. This diagram shows similarities to the one given above for aliphatic hydroxylation and is also anchored by the reactant and product wave functions, Ψ_r and Ψ_p. These curves are also bisected by an intermediate wave function for either an iron(III) or iron(IV) intermediate. Again the lowest lying surface in the gas phase is the one that passes the iron(IV) intermediate, so we will focus on this intermediate only. The curve crossing between the intermediate and reactant wave functions gives rise to an electrophilic addition barrier ($\mathbf{TS}_E$), which is proportional to the promotion gap in the reactant geometry for the singlet–triplet excitation in the C═C bond of the olefin. This singlet–triplet excitation is proportional to the IE of an electron from this bond and hence confirms the correlation between barrier height and IE. The VB diagram also explains why the reaction is stepwise via a radical intermediate.

Using DFT-calculated singlet-triplet π–π* excitation energies of substrates and the VB model in Eq. (11), barrier heights were predicted from empirical values. Generally, the DFT-calculated

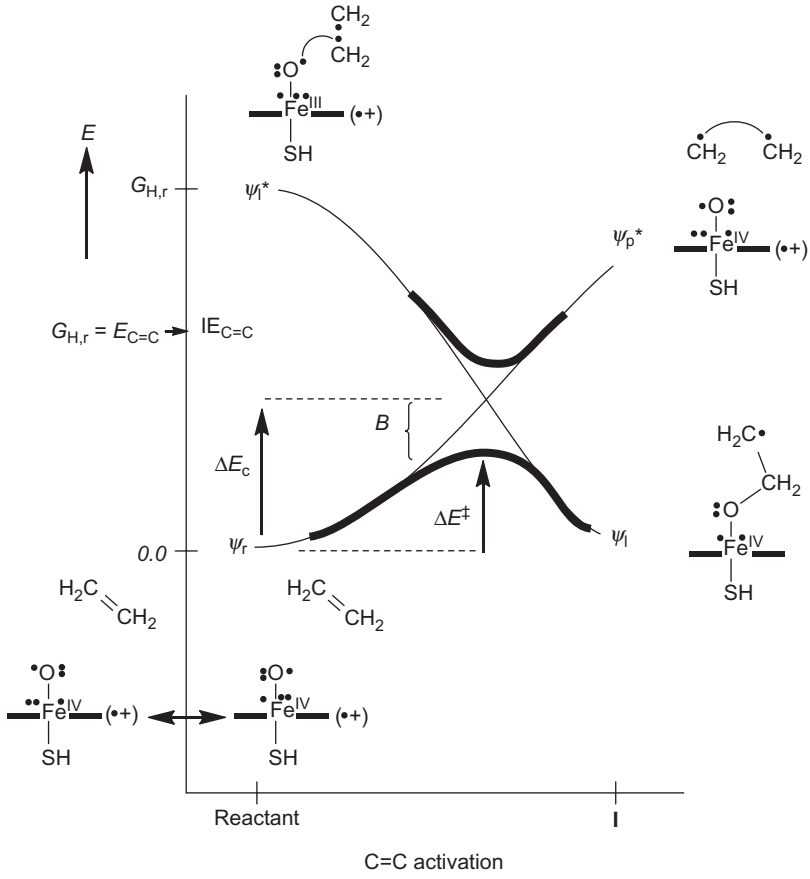

FIG. 11. VB curve-crossing diagram for substrate epoxidation by Compound I of P450.

barriers were reproduced within 1.4kcalmol^{-1}, and therefore, the model can be used to predict barrier heights.

C. SULFOXIDATION

Many P450 isozymes catalyze heteroatom oxidations, such as sulfoxidation, of substrates (*89–92*). Thus, the biodegradation of the pesticide aldicarb as well as neuroleptic drugs in the liver proceed through substrate sulfoxidation by P450 isozymes (*93,94*). Mechanistic studies on substrate sulfoxidation by P450 enzymes and biomimetic models have been performed (*95–99*) and

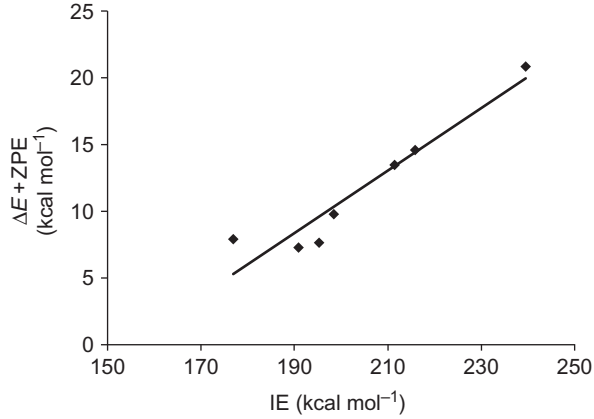

FIG. 12. Barrier heights (ΔE+ZPE) calculated at B3LYP level of theory as a function of ionization energy (IE) for a range of substrate sulfoxidation reactions by [Fe^{IV}=O($Por^{+\bullet}$)SH].

implicate a concerted reaction mechanism. Computational (DFT and QM/MM) studies supported the work and characterized the iron(IV)–oxo heme cation radical (Compound I, Cpd I) as the active oxidant (*100–104*). Watanabe and coworkers highlighted the relationship between the rate constant of substrate sulfoxidation by P450 enzymes with the ionization potential (IE) of the substrate (*105*). Recently, this correlation was explained using a VB curve-crossing diagram (*106,107*).

Figure 12 displays the correlation between barrier height for substrate sulfoxidation by [Fe^{IV}=O($Por^{+\bullet}$)SH] as a function of IE (*108*) using the following substrates: hydrogen sulfide, methylmercaptane, dimethylsulfide, ethylmercaptane, ethyl-methylsulfide, diethylsulfide, and ethyl-phenylsulfide. As can be seen that the correlation is good and confirms the trends observed by Watanabe and coworkers.

To understand the correlation between sulfoxidation barrier height and ionization potential of the substrate, also here a VB curve-crossing diagram was set up (*106*), which is shown in Fig. 13. In contrast to aliphatic hydroxylation and epoxidation discussed above, the sulfoxidation reaction is concerted without a reaction intermediate. Therefore, the reactants connect with products directly and the promotion gap as a result reflects the excitation energy from the reactant wave function to the product wave function in the reactant geometry. The excited wave function Ψ_p* essentially refers to the one-electron transfer from substrate to oxidant; hence it is proportional to the IE of the substrate and the electron affinity of the oxidant. Consequently, the correlation

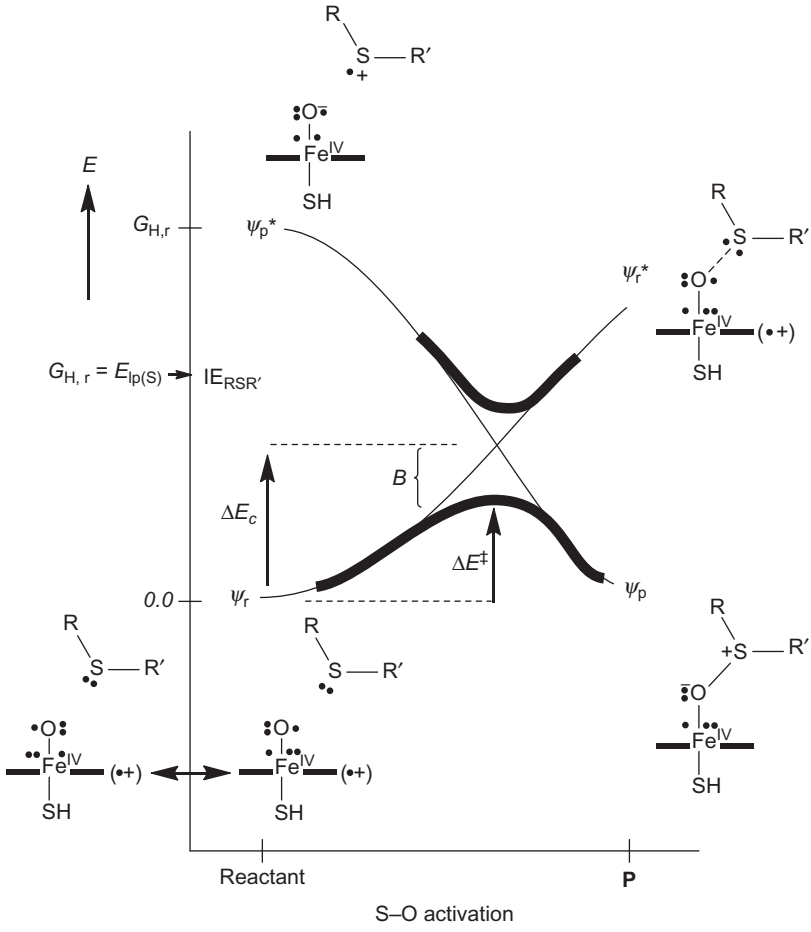

FIG. 13. Valence bond curve-crossing diagram for substrate sulfoxidation by $[Fe^{IV}{=}O(Por^{+\bullet})SH]$.

between ionization potential and barrier height is the result of the electron transfer processes during the reaction mechanism.

D. AROMATIC HYDROXYLATION

Recently, aromatic hydroxylation has also been described using VB curve-crossing diagrams (*108*). The cytochromes P450 hydroxylate arenes as a means of detoxification in the body. The activation of aromatic substrates by P450 enzymes generates several products, including phenols, arene oxides, and ketons. Experimental studies concluded that arene oxides are intermediates in the reaction leading to phenol products

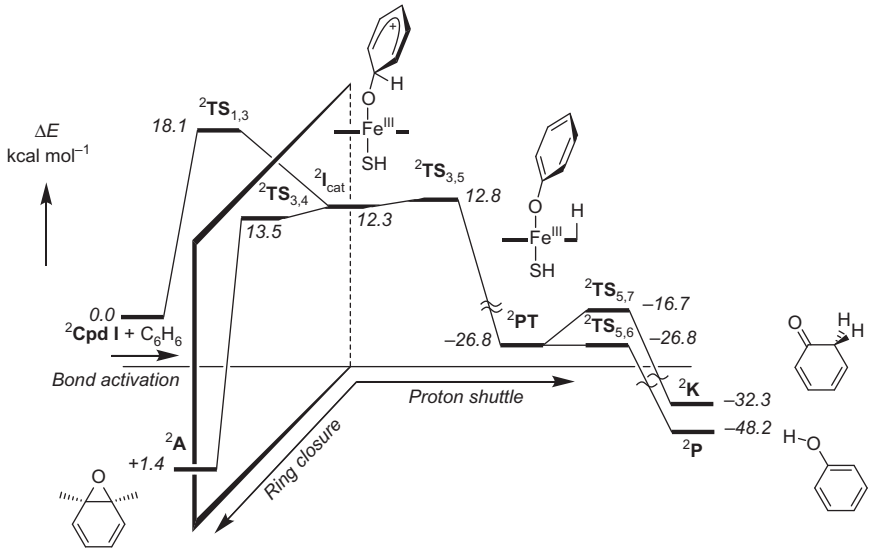

FIG. 14. B3LYP-calculated mechanism of the activation of benzene by [Fe^{IV}=O($Por^{+\bullet}$)SH] leading to phenol (**P**), keton (**K**), and arene oxide (**A**) products. Energies calculated in the gas phase relative to isolated reactants.

(*109–114*). Extensive density functional theory studies on the activation of aromatic substrates were performed and gave further insight into the mechanisms leading to phenols, arene oxides, and ketons (*102,115–121,122*).

The DFT-calculated mechanism of aromatic hydroxylation of benzene is schematically depicted in Fig. 14. Thus, aromatic hydroxylation starts with an electrophilic attack of the oxo group on one of the carbon atoms of the aromatic ring to form a cationic Meisenheimer complex ($^2\mathbf{I}_{cat}$) via a transition state ($^2\mathbf{TS}_{1,3}$) of about 18.1 kcal mol^{-1} in the gas phase. This intermediate is characterized with an orbital occupation of $\delta^2\pi^*_{xz}{}^2\pi^*_{yz}{}^1a_{2u}{}^2$ and consequently refers to a two-electron transfer from the substrate to oxidant. The cationic intermediate appears to be the central intermediate that leads to the formation of all possible reaction products, namely phenols, ketons, and arene oxides.

First, a ring-closure barrier ($^2\mathbf{TS}_{3,4}$) leads to arene oxide products directly. Second, a proton-shuttle mechanism transfers the *ipso*-proton from the substrate in $^2\mathbf{I}_{cat}$ to one of the nitrogen atoms of the porphyrin ring to give the proton-transfer intermediate ($^2\mathbf{PT}$) via a barrier $^2\mathbf{TS}_{3,5}$. In $^2\mathbf{PT}$, the aromaticity has come back into the ring, and the structure can be seen as a phenolate

bound to iron inside a protonated porphyrin group. From this point, the mechanism further bifurcates and gives reshuttle of the proton to either the oxygen atom to form phenol (^{2}**P**) or the *ortho*-carbon atom of phenolate to give 2,4-cyclohexenone (^{2}**K**) via transition state ^{2}**TS**$_{5,7}$. The calculations give a tiny barrier for formation of phenol products and a somewhat higher barrier (about 10.1 kcal mol^{-1}) leading to ketons.

In order to understand the calculated reaction mechanism, a VB curve-crossing diagram was set up (*108*), which is schematically depicted in Fig. 15. Similar to the curve-crossing diagrams discussed above, the reaction starts bottom left with the reactants configuration with wave function Ψ_r. For simplicity, we only give the mechanism leading to epoxide products, but the other pathways give similar curve-crossing diagrams. The product configuration (Ψ_p) connects to an excited state in the reactant geometry with a dominant charge-transfer (ionic)

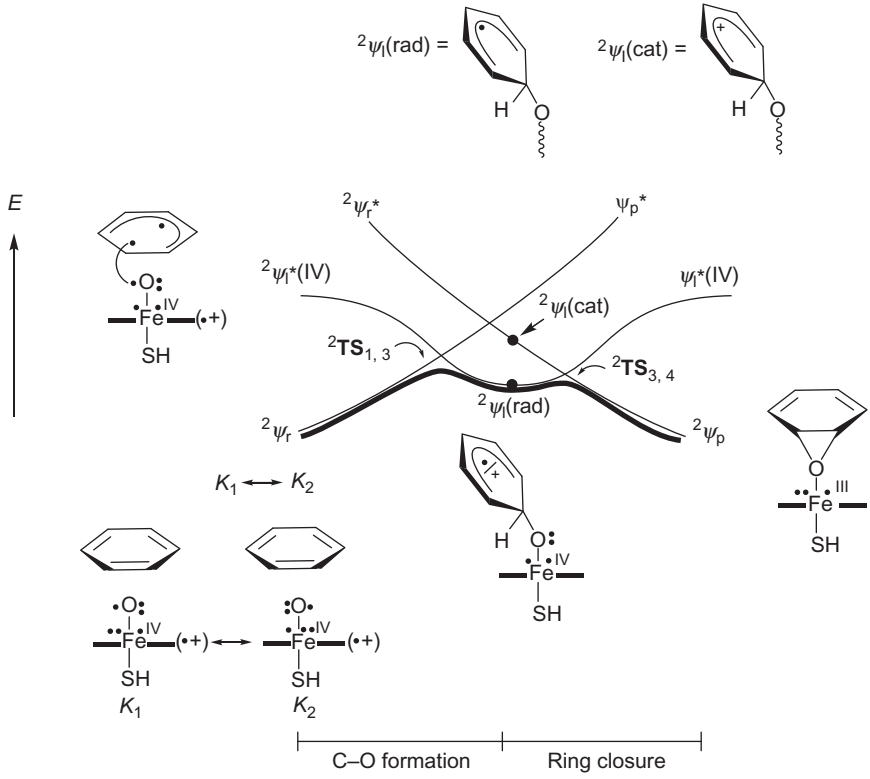

FIG. 15. VB curve-crossing diagram for aromatic hydroxylation by [Fe^{IV}=O(Por$^{+\bullet}$)SH].

configuration (Ψ_r*). Also here there is an intermediate curve via a radical intermediate and the curve crossing between the radical state and the reactants gives rise to a C—O activation barrier (^{2}**TS**$_{1,3}$), whereas the curve crossing between the radical state and the products gives a ring-closure transition state (^{2}**TS**$_{3,4}$). The excitation energy in the reactant configuration from Ψ_r to Ψ_I*(IV) reflects a one-electron transfer from π* to a_{2u} and splits the double-bond electrons into a triplet spin conformation. Thus, a singlet–triplet excitation in the aromatic ring is proportional to the IE of the substrate; hence, the barrier height correlates with IE as follows from the systematic studies. Since the charge-transfer curve in the intermediate structure is not far from the radical curve, mixing of both curves occurs in both the transition state (^{2}**TS**$_{1,3}$) and the intermediate complexes. Indeed, the DFT calculations gave transition states with noninteger charge and spin density on the benzene restgroup (*115*).

Recent studies of ours (*123*) on the axial ligand effect of aromatic hydroxylation by [Fe^{IV}=O($Por^{+\bullet}$)X] with X a variable axial ligand showed that the axial ligand effect manifests itself on the kinetics of a chemical reaction, whereby the free energy of activation was found to be proportional to BDE_{OH}.

IV. Outlook and Conclusions

This review gives a summary of recent attempts to rationalize oxygen atom transfer reactions by iron(IV)-oxo oxidants such as the active oxidant of P450 enzymes. Using VB curve-crossing models and systematic studies with density functional theory methods the factors that affect the rate-determining steps in the reaction mechanisms are rationalized. These studies have focused on aliphatic and aromatic hydroxylation, epoxidation and sulfoxidation. The studies give insight into the various mechanisms and the electron transfer processes that take place. Moreover, the calculations explain the regioselectivity of the various processes. Finally, the VB models can make predictions of barrier heights from empirical data.

References

1. Kadish, K. M.; Smith, K. M.; Guilard, R. (Eds.), "*Handbook of Porphyrin Science*"; World Scientific Publishing Co: New Jersey, **2010**.
2. Sono, M.; Roach, M. P.; Coulter, E. D.; Dawson, J. H. *Chem. Rev.* **1996,** *96*, 2841–2888.
3. Guengerich, F. P. *Chem. Res. Toxicol.* **2001,** *14*, 611–650.

4. Groves, J. T. *Proc. Natl. Acad. Sci. USA* **2003,** *100*, 3569–3574.
5. Ortiz de Montellano, P. R. (Ed.), "*Cytochrome P450: Structure, Mechanism and Biochemistry*"; (3rd edn.). Kluwer Academic/Plenum Publishers: New York, **2004**.
6. Higgins, L. J.; Yan, F.; Liu, P.; Liu, H.-W.; Drennan, C. L. *Nature* **2005,** *437*, 838–844.
7. Mishina, Y.; Duguid, E. M.; He, C. *Chem. Rev.* **2006,** *106*, 215–232.
8. O'Brien, P. J. *Chem. Rev.* **2006,** *106*, 720–752.
9. Yi, C.; Yang, C. G.; He, C. *Acc. Chem. Res.* **2009,** *42*, 519–529.
10. Solomon, E. I.; Brunold, T. C.; Davis, M. I.; Kemsley, J. N.; Lee, S.-K.; Lehnert, N.; Neese, F.; Skulan, A. J.; Yang, Y.-S.; Zhou, J. *Chem. Rev.* **2000,** *100*, 235–349.
11. Costas, M.; Mehn, M. P.; Jensen, M. P.; Que, L. Jr., *Chem. Rev.* **2004,** *104*, 939–986.
12. Abu-Omar, M. M.; Loaiza, A.; Hontzeas, N. *Chem. Rev.* **2005,** *105*, 2227–2252.
13. Nam, W. *Acc. Chem. Res.* **2007,** *40*, 522–531.
14. Bruijnincx, P. C. A.; van Koten, G.; Klein Gebbink, R. J. M. *Chem. Soc. Rev.* **2008,** *37*, 2716–2744.
15. Haines, D. C.; Tomchick, D. R.; Machius, M.; Peterson, J. A. *Biochemistry* **2001,** *40*, 13456–13465.
16. O'Brien, J. R.; Schuller, D. J.; Yang, V. S.; Dillard, B. D.; Lanzilotta, W. N. *Biochemistry* **2003,** *42*, 5547–5554.
17. Poulos, T. L.; Finzel, B. C.; Howard, A. J. *Biochemistry* **1986,** *25*, 5314–5322.
18. Veitch, N. C.; Smith, A. T. *Adv. Inorg. Chem.* **2000,** *51*, 107–162.
19. Que, L. Jr., *Nat. Struct. Biol.* **2000,** *7*, 182–184.
20. Bollinger, J. M.; Jr., Price, J. C.; Hoffart, L. M.; Barr, E. W.; Krebs, C. *Eur. J. Inorg. Chem.* **2005,** 4245–4254.
21. Bugg, T. D. H.; Ramaswamy, S. *Curr. Opin. Chem. Biol.* **2008,** *12*, 134–140.
22. Krebs, C.; Fujimori, D. G.; Walsh, C. T.; Bollinger, J. M. Jr., *Acc. Chem. Res.* **2007,** *40*, 484–492.
23. Borowski, T.; Bassan, A.; Siegbahn, P. E. M. *Chem. Eur. J.* **2004,** *10*, 1031–1041.
24. de Visser, S. P. *Chem. Commun.* **2007,** 171–173.
25. Proshlyakov, D. A.; Henshaw, T. F.; Monterosso, G. R.; Ryle, M. J.; Hausinger, R. P. *J. Am. Chem. Soc.* **2004,** *126*, 1022–1023.
26. Riggs–Gelasco, P. J.; Price, J. C.; Guyer, R. B.; Brehm, J. H.; Barr, E. W.; Bollinger, J. M.; Jr., Krebs, C. *J. Am. Chem. Soc.* **2004,** *126*, 8108–8109.
27. de Visser, S. P. *Coord. Chem. Rev.* **2009,** *253*, 754–768.
28. Grzyska, P. K.; Appelman, E. H.; Hausinger, R. P.; Proshlyakov, D. A. *Proc. Natl. Acad. Sci. USA* **2010,** *107*, 3982–3987.
29. Meunier, B.; de Visser, S. P.; Shaik, S. *Chem. Rev.* **2004,** *104*, 3947–3980.
30. Denisov, I. G.; Makris, T. M.; Sligar, S. G.; Schlichting, I. *Chem. Rev.* **2005,** *105*, 2253–2277.
31. Shaik, S.; Kumar, D.; de Visser, S. P.; Altun, A.; Thiel, W. *Chem. Rev.* **2005,** *105*, 2279–2328.
32. Sligar, S. G. *Biochemistry* **1976,** *15*, 5399–5406.
33. Schlichting, I.; Berendzen, J.; Chu, K.; Stock, A. M.; Maves, S. A.; Benson, D. E.; Sweet, R. M.; Ringe, D.; Petsko, G. A.; Sligar, S. G. *Science* **2000,** *287*, 1615–1622.
34. Davydov, R.; Makris, T. M.; Kofman, V.; Werst, D. E.; Sligar, S. G.; Hoffman, B. M. *J. Am. Chem. Soc.* **2001,** *123*, 1403–1415.

35. Mak, P. J.; Denisov, I. G.; Victoria, D.; Makris, T. M.; Deng, T.; Sligar, S. G.; Kincaid, J. R. *J. Am. Chem. Soc.* **2007,** *129*, 6382–6383.
36. Rittle, J.; Green, M. T. *Science* **2010,** *330*, 933–937.
37. Groves, J. T.; McClusky, G. A. *J. Am. Chem. Soc.* **1976,** *98*, 859–861.
38. Hohenberg, P.; Kohn, W. *Phys. Rev. B* **1964,** *136*, 864–871.
39. Kohn, W.; Sham, L. J. *Phys. Rev. A* **1965,** *140*, 1133–1138.
40. Becke, A. D. *J. Chem. Phys.* **1993,** *98*, 5648–5652.
41. Lee, C.; Yang, W.; Parr, R. G. *Phys. Rev. B* **1988,** *37*, 785–789.
42. Becke, A. D. *J. Chem. Phys.* **1992,** *96*, 2155–2160.
43. Becke, A. D. *J. Chem. Phys.* **1992,** *97*, 9173–9177.
44. Ziegler, T. *Chem. Rev.* **1991,** *91*, 651–667.
45. Vosko, S. H.; Wilk, L.; Nusair, M. *Can. J. Phys.* **1980,** *58*, 1200–1211.
46. de Visser, S. P.; Shaik, S.; Sharma, P. K.; Kumar, D.; Thiel, W. *J. Am. Chem. Soc.* **2003,** *125*, 15779–15788.
47. de Visser, S. P. *J. Am. Chem. Soc.* **2006,** *128*, 9813–9824.
48. de Visser, S. P. *J. Am. Chem. Soc.* **2006,** *128*, 15809–15818.
49. Kumar, D.; de Visser, S. P.; Shaik, S. *Chem. Eur. J.* **2005,** *11*, 2825–2835.
50. Vaz, A. D. N.; McGinnity, D. F.; Coon, M. J. *Proc. Natl. Acad. Sci. USA* **1998,** *95*, 3555–3560.
51. de Visser, S. P.; Oh, K.; Han, A.-R.; Nam, W. *Inorg. Chem.* **2007,** *46*, 4632–4641.
52. Shaik, S.; Kumar, D.; de Visser, S. P. *J. Am. Chem. Soc.* **2008,** *130*, 10128–10140.
53. Latifi, R.; Bagherzadeh, M.; de Visser, S. P. *Chem. Eur. J.* **2009,** *15*, 6651–6662.
54. Kumar, D.; de Visser, S. P.; Shaik, S. *J. Am. Chem. Soc.* **2003,** *125*, 13024–13025.
55. Kumar, D.; de Visser, S. P.; Sharma, P. K.; Cohen, S.; Shaik, S. *J. Am. Chem. Soc.* **2004,** *125*, 1907–1920.
56. Newcomb, M.; Aebisher, D.; Shen, R.; Esala, R.; Chandrasena, P.; Hollenberg, P. F.; Coon, M. J. *J. Am. Chem. Soc.* **2003,** *125*, 6064–6065.
57. de Visser, S. P. *Chem. Eur. J.* **2008,** *14*, 4533–4541.
58. Karamzadeh, B.; Kumar, D.; Sastry, G. N.; de Visser, S. P. *J. Phys. Chem. A* **2010,** *114*, 13234–13243.
59. Sinnecker, S.; Svensen, N.; Barr, E. W.; Ye, S.; Bollinger, J. M.; Jr., Neese, F.; Krebs, C. *J. Am. Chem. Soc.* **2007,** *129*, 6168–6179.
60. Porro, C. S.; Kumar, D.; de Visser, S. P. *Phys. Chem. Chem. Phys.* **2009,** *11*, 10219–10226.
61. Green, M. T. *J. Am. Chem. Soc.* **1999,** *121*, 7939–7940.
62. Ogliaro, F.; de Visser, S. P.; Cohen, S.; Kaneti, J.; Shaik, S. *ChemBioChem* **2001,** *11*, 848–851.
63. Ogliaro, F.; Cohen, S.; de Visser, S. P.; Shaik, S. *J. Am. Chem. Soc.* **2000,** *122*, 12892–12893.
64. Schöneboom, J. C.; Lin, H.; Reuter, N.; Thiel, W.; Cohen, S.; Ogliaro, F.; Shaik, S. *J. Am. Chem. Soc.* **2002,** *124*, 8142–8151.
65. Shaik, S.; de Visser, S. P.; Ogliaro, F.; Schwarz, H.; Schröder, D. *Curr. Opin. Chem. Biol.* **2002,** *6*, 556–567.
66. de Visser, S. P.; Ogliaro, F.; Harris, N.; Shaik, S. *J. Am. Chem. Soc.* **2001,** *123*, 3037–3047.
67. de Visser, S. P.; Ogliaro, F.; Sharma, P. K.; Shaik, S. *Angew. Chem. Int. Ed.* **2002,** *41*, 1947–1951.
68. de Visser, S. P.; Ogliaro, F.; Sharma, P. K.; Shaik, S. *J. Am. Chem. Soc.* **2002,** *124*, 11809–11826.

69. de Visser, S. P.; Ogliaro, F.; Shaik, S. *Angew. Chem. Int. Ed.* **2001,** *40*, 2871–2874.
70. de Visser, S. P.; Kumar, D.; Shaik, S. J. *Inorg. Biochem.* **2004,** *98*, 1183–1193.
71. Shaik, S. S. *J. Am. Chem. Soc.* **1981,** *103*, 3692–3701.
72. Shaik, S.; Shurki, A. *Angew. Chem. Int. Ed.* **1999,** *38*, 586–625.
73. Shaik, S.; Cohen, S.; Wang, Y.; Chen, H.; Kumar, D.; Thiel, W. *Chem. Rev.* **2010,** *110*, 949–1017.
74. Shaik, S.; Lai, W.; Chen, H.; Wang, Y. *Acc. Chem. Res.* **2010,** *43*, 1154–1165.
75. Bordwell, F. G.; Cheng, J.-P. *J. Am. Chem. Soc.* **1991,** *113*, 1736–1743.
76. Bordwell, F. G.; Cheng, J.-P.; Ji, G.-Z.; Satish, A. V.; Zhang, X. *J. Am. Chem. Soc.* **1991,** *113*, 9790–9795.
77. Mayer, J. M. *Acc. Chem. Res.* **1998,** *31*, 441–450.
78. Warren, J. J.; Tronic, T. A.; Mayer, J. M. *Chem. Rev.* **2010,** *110*, 6961–7001.
79. Mayer, J. M. *Acc. Chem. Res.* **2011,** *44*, 36–46.
80. Shaik, S.; Cohen, S.; de Visser, S. P.; Sharma, P. K.; Kumar, D.; Kozuch, S.; Ogliaro, F.; Danovich, D. *Eur. J. Inorg. Chem.* **2004,** 207–226.
81. de Visser, S. P. *J. Am. Chem. Soc.* **2010,** *132*, 1087–1097.
82. Groves, J. T.; Avaria-Neisser, G. E.; Fish, K. M.; Imachi, M.; Kuczkowski, R. L. *J. Am. Chem. Soc.* **1986,** *108*, 3837–3838.
83. Ortiz de Montellano, P. R.; Fruetel, J. A.; Collins, J. R.; Camper, D. L.; Loew, G. H. *J. Am. Chem. Soc.* **1991,** *113*, 3195–3196.
84. Alcalde, M.; Farinas, E. T.; Arnold, F. H. *J. Biomol. Screen.* **2004,** *9*, 141–146.
85. Dansette, P. M.; Bertho, G.; Mansuy, D. *Biochem. Biophys. Res. Commun.* **2005,** *338*, 450–455.
86. Yuan, X.; Wang, Q.; Horner, J. H.; Sheng, X.; Newcomb, M. *Biochemistry* **2009,** *48*, 9140–9146.
87. de Visser, S. P.; Ogliaro, F.; Shaik, S. *Chem. Commun.* **2001,** 2322–2323.
88. Kumar, D.; Karamzadeh, B.; Sastry, G. N.; de Visser, S. P. *J. Am. Chem. Soc.* **2010,** *132*, 7656–7667.
89. Werner, M.; Birner, G.; Dekant, W. *Chem. Res. Toxicol.* **1996,** *9*, 41–49.
90. Madan, A.; Parkinson, A.; Faiman, M. D. *Drug Metab. Dispos.* **1995,** *23*, 1153–1158.
91. Usmani, K. A.; Karoly, E. D.; Hodgson, E.; Rose, R. L. *Drug Metab. Dispos.* **2004,** *32*, 333–339.
92. Furnes, B.; Schlenk, D. *Drug Metab. Dispos.* **2005,** *33*, 214–218.
93. Perkins, E. J.; El-Alfy, A.; Schlenk, D. *Toxicol. Sci.* **1999,** *48*, 67–73.
94. Wójcikowski, J.; Maurel, P.; Daniel, W. A. *Drug Metab. Dispos.* **2006,** *34*, 471–476.
95. Goto, Y.; Matsui, T.; Ozaki, S.-i; Watanabe, Y.; Fukuzumi, S. *J. Am. Chem. Soc.* **1999,** *121*, 9497–9502.
96. Kato, S.; Yang, H.-J.; Ueno, T.; Ozaki, S.-i; Phillips, G. N.; Jr., Fukuzumi, S.; Watanabe, Y. *J. Am. Chem. Soc.* **2002,** *124*, 8506–8507.
97. Volz, T. J.; Rock, D. A.; Jones, J. P. *J. Am. Chem. Soc.* **2002,** *124*, 9724–9725.
98. Cho, K.-B.; Moreau, Y.; Kumar, D.; Rock, D. A.; Jones, J. P.; Shaik, S. *Chem. Eur. J.* **2007,** *13*, 4103–4115.
99. Benet-Buchholz, J.; Comba, P.; Llobet, A.; Roeser, S.; Vadivelu, P.; Wiesner, S. *Dalton Trans.* **2010,** *39*, 3315–3320.
100. Sharma, P. K.; de Visser, S. P.; Shaik, S. *J. Am. Chem. Soc.* **2003,** *125*, 8698–8699.

101. Kumar, D.; de Visser, S. P.; Sharma, P. K.; Hirao, H.; Shaik, S. *Biochemistry* **2005,** *44*, 8148–8158.
102. Rydberg, P.; Ryde, U.; Olsen, L. *J. Chem. Theory Comput.* **2008,** *4*, 1369–1377.
103. Li, C.; Zhang, L.; Zhang, C.; Hirao, H.; Wu, W.; Shaik, S. *Angew. Chem. Int. Ed.* **2007,** *46*, 8168–8170.
104. Porro, C. S.; Sutcliffe, M. J.; de Visser, S. P. *J. Phys. Chem. A* **2009,** *113*, 11635–11642.
105. Watanabe, Y.; Iyanagi, T.; Oae, S. *Tetrahedron Lett.* **1980,** *21*, 3685–3688.
106. Shaik, S.; Wang, Y.; Chen, H.; Song, J.; Meir, R. *Faraday Discuss.* **2010,** *145*, 49–70.
107. Kumar, D.; Sastry, G. N.; de Visser, S. P. *Chem. Eur. J.* **2011,** *17*, 6196–6205.
108. Shaik, S.; Milko, P.; Schyman, P.; Usharani, D.; Chen, H. *J. Chem. Theory Comput.* **2011,** *7*, 327–339.
109. Jerina, D. M.; Daly, J. W. *Science* **1974,** *185*, 573–582.
110. Jerina, D. M.; Daly, J. W.; Witkop, B.; Zaltzman-Nirenberg, P.; Udenfriend, S. *Arch. Biochem. Biophys.* **1968,** *128*, 176–183.
111. Jerina, D. M.; Daly, J. W.; Witkop, B.; Zaltzman-Nirenberg, P.; Udenfriend, S. *J. Am. Chem. Soc.* **1968,** *90*, 6525–6527.
112. Jerina, D. M.; Daly, J. W.; Witkop, B.; Zaltzman-Nirenberg, P.; Udenfriend, S. *Biochemistry* **1970,** *9*, 147–156.
113. Hanzlik, R.; Hogberg, K.; Judson, C. *Biochemistry* **1984,** *23*, 3048–3055.
114. Korzekwa, K. R.; Swinney, D. C.; Trager, W. F. *Biochemistry* **1989,** *28*, 9019–9027.
115. de Visser, S. P.; Shaik, S. *J. Am. Chem. Soc.* **2003,** *125*, 7413–7424.
116. de Visser, S. P. *Chem. Eur. J.* **2006,** *12*, 8168–8177.
117. Hazan, C.; Kumar, D.; de Visser, S. P.; Shaik, S. *Eur. J. Inorg. Chem.* **2007,** 2966–2974.
118. de Visser, S. P.; Tahsini, L.; Nam, W. *Chem. Eur. J.* **2009,** *15*, 5577–5587.
119. de Visser, S. P.; Latifi, R.; Tahsini, L.; Nam, W. *Chem. Asian J.* **2011,** *6*, 493–504.
120. Bathelt, C. M.; Ridder, L.; Mulholland, A. J.; Harvey, J. N. *J. Am. Chem. Soc.* **2003,** *125*, 15004–15005.
121. Bathelt, C. M.; Ridder, L.; Mulholland, A. J.; Harvey, J. N. *Org. Biomol. Chem.* **2004,** *2*, 2998–3005.
122. Rydberg, P.; Vasanthanathan, P.; Oostenbrink, C.; Olsen, L. *ChemMedChem* **2009,** *4*, 2070–2079.
123. Kumar, D.; Sastry, G. N.; de Visser, S. P. *J. Phys. Chem. B*. **2012**, in press, (DOI: 10.1021/jp2113522).

HEME-CONTAINING DIOXYGENASES

IGOR EFIMOV[a], JASWIR BASRAN[b], SARAH J. THACKRAY[c], SANDEEP HANDA[a], CHRISTOPHER G. MOWAT[c] and EMMA LLOYD RAVEN[a]

[a]Department of Chemistry, University of Leicester, Leicester, United Kingdom
[b]Department of Biochemistry, Henry Wellcome Building, University of Leicester, Leicester, United Kingdom
[c]EaStCHEM, School of Chemistry, University of Edinburgh, Edinburgh, United Kingdom

ABSTRACT

The heme dioxygenase enzymes involved in tryptophan oxidation catalyse the first and rate-limiting step in the kynurenine pathway—the O_2-dependent oxidation of l-tryptophan to *N*-formylkynurenine. In the past 10 years, there have been substantial new developments, including new structural information, bacterial expression systems for a number of dioxygenases, contributions from computational chemistry, and emerging

INORGANIC/BIOINORGANIC REACTION MECHANISMS
VOLUME 64 ISSN 0898-8838 / DOI: 10.1016/B978-0-12-396462-5.00002-7

mechanistic data from site-directed mutagenesis. This review summarizes these recent contributions.

Keywords: Heme; Iron; Dioxygenases.

I. Introduction

The heme dioxygenase enzymes involved in tryptophan oxidation catalyze the first and rate-limiting step in the kynurenine pathway—the O_2-dependent oxidation of L-tryptophan to *N*-formylkynurenine. This reaction is unique in heme chemistry and differentiates these enzymes from the better-known cytochrome P450 and peroxidase enzymes. These enzymes are referred to in the very early literature as "tryptophan pyrrolase" (*1–3*) (and even as "tryptophan peroxidase-oxidase" (*4*)) and only later did the nomenclature converge on either tryptophan 2,3-dioxygenase (TDO) or indoleamine 2,3-dioxygenase (IDO). In fact, both TDO and IDO catalyze the same reaction, with the different nomenclatures merely reflecting the generally wider substrate specificity of the IDOs, which react with variously substituted indole compounds, compared to the more substrate-specific TDOs.

The first report of activity towards tryptophan came more than 70 years ago (*1*), but the vast majority of the early work on purified enzymes was carried out in the 1970s and 1980s. This work has been previously reviewed by Sono and Dawson (*5*) as part of a larger review on heme-containing oxygenases. In the past 10 years, there have been substantial new developments, including new structural information, bacterial expression systems for a number of dioxygenases, contributions from computational chemistry, and emerging mechanistic data from site-directed mutagenesis. This review summarizes these recent contributions and attempts to present a concise, comparative summary that is relevant to those with a broader interest in heme protein structure and function.

II. Physiological Function

TDO and IDO activate molecular oxygen and catalyze its insertion into L-Trp to form *N*-formylkynurenine (Scheme 1) in the first and rate-limiting step in the kynurenine pathway. The kynurenine pathway is responsible for processing over 90% of the L-Trp utilized by humans so that both IDO and TDO play a central role in the

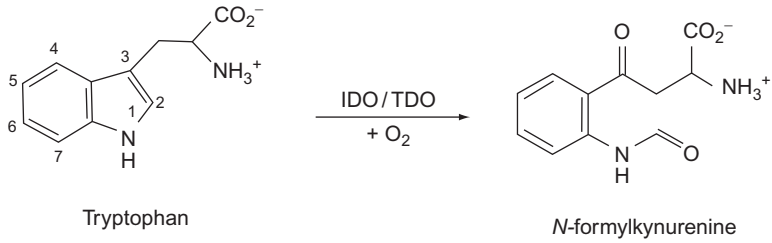

SCHEME 1. The reaction catalyzed by the heme dioxygenase enzymes.

physiological regulation of tryptophan, controlling the kynurenine pathway and influencing serotogenic regulation. The buildup of pathway metabolites such as quinolinic acid and L-kynurenine can lead to numerous physiological and pathophysiological conditions, such as multiple sclerosis, AIDS-related dementia, and ischemic brain injury (*6–8*). The kynurenine pathway metabolites 3-hydroxyanthranilic acid and 3-hydroxykynurenine have also been implicated in cataract formation when present at high concentrations (*9*), and some kynurenine pathway metabolites can contribute to immunosuppressive pathways and suppress proliferation (and even cause apoptosis) of T cells (although the mechanisms of action of such metabolites are unknown) (*10–12*). In addition, the local depletion of tryptophan by IDO/TDO is associated with antimicrobial responses or with immune regulation by IDO (*13*). Some pathogens are sensitive to tryptophan degradation, and this may be an effective mechanism for controlling their ability to proliferate.

Although both enzymes catalyze the same reaction, compartmentalization of IDO and TDO expression is thought to reflect their differing biological roles and it has been suggested (*14*) that the different substrate binding specificities of the ferric and ferrous forms of IDO and TDO might be linked to their physiological location. IDO is found in many eukaryotes where it is expressed ubiquitously throughout the body, except for in the liver. TDO expression, on the other hand, is normally restricted to the liver. IDO plays an active role in the human body's immune response, but there is little evidence to suggest that TDO plays a part in this process.

III. Heme Coordination Environment

In the absence of structural information, there was good reason to suppose that the heme active site in IDO and TDO contained a histidine residue. It had been noted that there was sequence homology with a group of IDO-like myoglobins, which were also presumed to contain a distal histidine (reviewed in Ref. (*15*)). The involvement

of an active site histidine in O_2 binding to the globins was well established (*16*) (the peroxidase enzymes also employ similar hydrogen bonding interactions (*17–20*)), which lent credibility to the proposal of a similar mechanism for stabilization of the O_2-bound complex. Additional evidence came from studies with enzyme inhibitors (*21*), from which it had been concluded that the reaction mechanism was critically dependent on the presence of an active site base, presumed to be histidine. Alongside this information, spectroscopic evidence at cryogenic temperatures (reviewed previously in some detail (*5*)) had suggested the presence of a low-spin heme species under certain conditions. Many of the spectroscopic features were similar to those found for bis-nitrogenous heme coordination and it was concluded that the distal pocket contained a histidine. These low-spin features were even observed later on for recombinant proteins too (*22,23*), but we now know that these data were somewhat misleading and are likely artifacts of the cryogenic conditions, since not all dioxygenases (human IDO is a good example) contain a distal histidine.

A consensus of spectroscopic data (EPR, MCD) for a number of dioxygenases has together revealed the presence of both water-bound, high-spin species and hydroxide-bound, low-spin species in solution (*14,22–25*), the populations of which are often pH dependent. The crystal structures of both human IDO (hIDO) and *Xanthomonas campestris* TDO in the ferric state a histidine residue ligating the heme iron in the proximal position (*26,27*). The precise balance of high-spin:low-spin heme likely varies between different enzymes and is probably affected by specific structural details contained within the active site. In the peroxidase enzymes, similar variations in heme coordination geometry are observed that do not appear to affect the reaction with peroxide to any great extent. By analogy, and since the reaction mechanism involves an initial reduction of the ferric heme to ferrous and complete loss of the water molecule, it is unlikely that the balance of high-spin:low-spin heme affects activity. Spectroscopic artifacts (often at cryogenic temperatures) relating to heme coordination are well known in other catalytic heme enzymes, and the earlier spectroscopic interpretations for TDO may well also have been complicated by the fact that the heme groups of the tetramer have now been shown to be inequivalent (*25*).

IV. Steady-State Activity

The dioxygenases are not spectacularly fast enzymes. The rate of catalysis varies slightly across the family of dioxygenases, with

k_{cat} values for L-Trp turnover of $\sim$1–2 s^{-1} for mammalian proteins and slightly faster rates of $\sim$15–20 s^{-1} for most bacterial TDO enzymes (*14,22,23,28–32*). Although both enzymes catalyze the same reaction, they are distinct not only in their ability to utilize different substrates but also in their stereospecificity. IDO catalyzes the insertion of dioxygen into both D- and L-tryptophan, while almost all TDO enzymes are completely inactive toward D-Trp. Historically, this distinction led to the categorization of the enzymes as either IDOs or TDOs, but two TDO enzymes (from *Bacillus brevis* and rat liver) have been shown to have limited D-Trp-dependent activity (*33*).

V. Expression Systems

In the past several years, expression systems for various enzymes have been published. The first was for human IDO (*34*). Table I gives a summary of bacterial expression systems for other mammalian and bacterial enzymes. This availability of new expression systems opened the door for mutagenesis and structural biology programs. In a few cases, structures have been published (*26,27,40*) as explained below.

VI. Crystal Structures

A. The Structure of Human IDO

The first crystal structure was for recombinant human IDO (*27*) which was crystallized with the inhibitor 4-phenylimidazole bound to the heme iron. Human IDO is a monomeric protein which is folded into two distinct domains: a large (C-terminal)

TABLE I

Summary of Expression Systems for IDO and TDO

Enzyme	Species	References
Indoleamine 2,3-dioxygenase	Human	*22,27,32,34,35*
	Mouse	*32*
	S. oneidensis	*26*
Tryptophan 2,3-dioxygenase	Human	*14,28,36*
	Rat	*37–39*
	X. campestris	*26*
	R. metallidurans	*40*
	Mosquito	*41,42*
	Scallop	*43*

domain and a small (N-terminal) capping domain, joined by a long loop (Fig. 1).[1] The larger domain is completely helical with a fold unique to this family of proteins, and interdomain contact is extensive. This larger domain is in essence topologically identical to the protomer of the tetrameric TDO, with all the structures readily superposable.

The heme-binding pocket of IDO is located mainly within the larger domain, close to the domain interface. The active site (Fig. 2) confirmed some of the earlier predictions but also contained some unexpected surprises (*27*). The structure revealed the presence of a proximal histidine, which was in agreement with predictions on the heme ligation from spectroscopy (*5*) and with more recent mutagenesis work in which His346 had been predicted (*45*) as the ligand. Asp274 on the proximal side had been suggested from mutagenesis (*45*) either to bind directly to the heme, which the structure shows

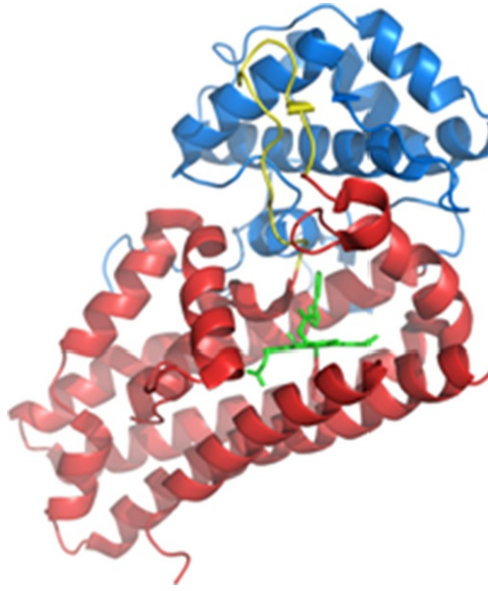

FIG. 1. The overall structure of human IDO (*27*), showing the large (red) and small (blue) domains, the loop region (yellow), the heme (in green), the proximal histidine residue (His346, red), and the bound inhibitor 4-phenylimidazole (green). This figure was prepared using Pymol (*44*).

[1]A small anomaly of the structure was that the enzyme crystallized as a cross-linked dimer linked by a disulfide bridge (Cys308 in each monomer), even though in solution there is no evidence for such a cross-link.

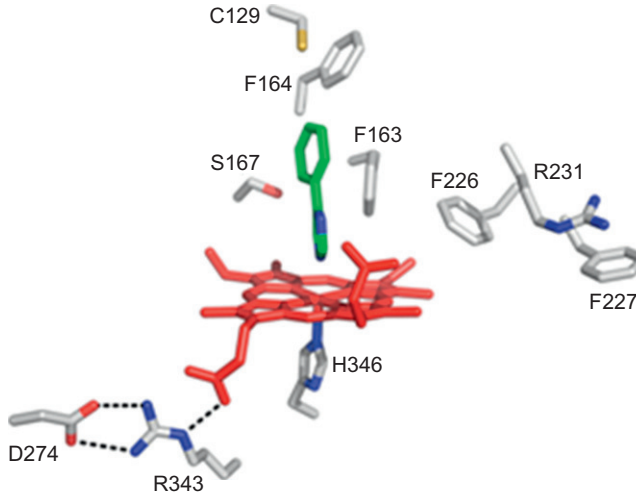

FIG. 2. The active site of human IDO (*27*) with the heme in red. There is a molecule of the inhibitor 4-phenylimidazole (green) bound to the heme iron in the structure, and two molecules of the crystallization buffer (CHES, not shown) in the active site. This figure was prepared using Pymol (*44*).

not to be the case, or to maintain a suitable conformation of the heme pocket. This latter hypothesis proved correct since there is an electrostatic interaction between this residue and Arg343 which is presumably important for maintaining the overall structure (Fig. 2). The IDO molecule as a whole contains a large number of hydrophobic Phe and Tyr aromatic residues (not shown), including in the distal heme pocket (Fig. 2), which presumably helps to accommodate binding of the hydrophobic side chain of the tryptophan substrate. Most surprisingly, and in direct conflict with the literature proposals on the mechanism (*5*) (see below), there is no histidine residue in the distal pocket. At least for IDO, therefore, the low-spin (presumed bis-nitrogenous (*5*)) species observed spectroscopically (*22,23,46*), Section III, cannot arise from coordination of a distal histidine to the heme. In fact, the entire IDO active site is almost completely devoid of polar residues: Ser167 is the only candidate (Fig. 2), but this residue was later shown by mutagenesis (*30*) not to be essential for O_2 or substrate binding, or for turnover.

A structure has also been published for the *Shewanella oneidensis* IDO (*26*), and this shows similar features in the active site.

B. The Structures of TDOs

The TDOs from *Ralstonia metallidurans* and *X. campestris* (xTDO) (*26,40*) have high (≈50%) sequence identity, and their overall structures are essentially identical. The overall structure of xTDO is shown in Fig. 3. Both TDOs are homotetrameric and are perhaps best described as a "dimer of dimers" because the N-terminal region (residues Arg21-Leu40 of the *X. campestris* enzyme; Fig. 3) of each monomer infiltrates the active site of the adjacent monomer and is crucial for substrate binding. The crystal structure of the bacterial *X. campestris* TDO to a large extent confirmed the generally hydrophobic nature of the active site and revealed high structural similarity between the TDO and IDO active sites (Fig. 4).

C. The Structure of the Substrate-Bound Complex and the Involvement of an Active Site Histidine

The structure of the substrate-bound complex of the *X. campestris* enzyme has also been published. There are ionic interactions with Arg117, also presumably present in hIDO

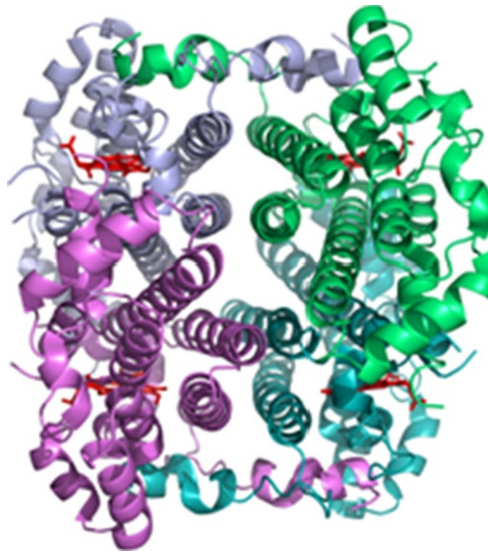

Fig. 3. The overall structure of xTDO (*26*), showing the tetrameric structure.

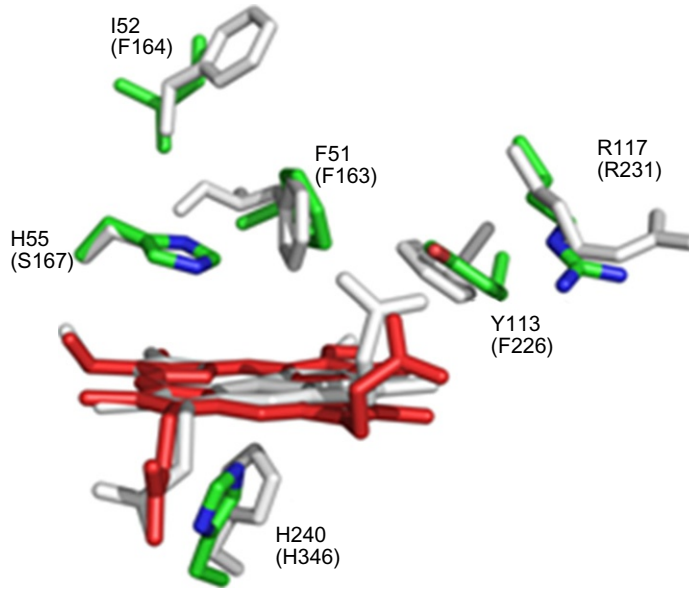

FIG. 4. An overlay of *X. campestris* TDO (green (*26*)) and hIDO (white (*27*)), showing the active site residues (in parentheses for hIDO).

(to Arg231) and *R. metallidurans* TDO (Arg134), and to the heme propionate (Fig. 5). These ionic interactions would explain why substrate binding is sensitive to substitutions at these charged positions (e.g., D-Trp, tryptamine, indole propionic acid, tryptophanol (*5,14,26,28,29,40,47,48*); Scheme 2) and in some cases (e.g., tryptamine, indole propionic acid, tryptophanol; Scheme 2) essentially eliminates activity altogether (*14*).

In contrast to hIDO, for the bacterial xTDO enzyme, there is a distal histidine residue (His55) which overlays with the equivalent (Ser167) residue in human IDO (Fig. 5), *and* which hydrogen bonds to the indole proton on N^1. Although, in principle, this seemed to imply that the base-catalyzed abstraction mechanism may indeed be possible, as discussed below (Scheme 4), site-directed mutagenesis data (*54*) do not support this because the *X. campestris* H55A variant is still catalytically active, albeit at a lower level (k_{cat} ca. 10% of the wild-type value). The interpretation is not completely unambiguous however, and others have drawn different conclusions (*29*). In human TDO, the residue corresponding to His55 in *X. campestris* is thought to be His76; mutation of His76 also reduces activity and by a similar amount

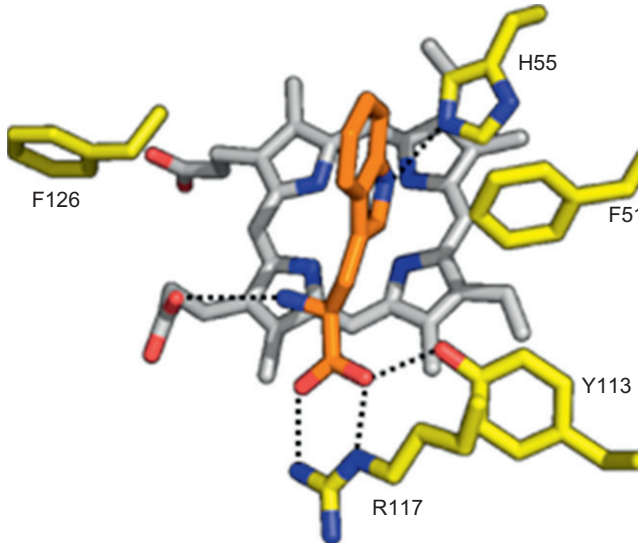

FIG. 5. The substrate binding site in *X. campestris* TDO (*26*), showing the substrate (orange) and the associated bonding interactions.

(k_{cat} ca. 10% of the wild-type value) to the H55 variants of *X. campestris*. This has been interpreted (*29*) as evidence for an essential role for His76 in TDO. In cases where His is present in the active site (for *X. campestris* and *R. metallidurans* TDO, for instance, and also assumed for hTDO (His76)), its full role is not yet established, although it might be involved in disfavoring substrate binding to the oxidized enzyme (*54*) or in holding the substrate in a very precise orientation suitable for cleavage of the C^2—C^3 bond. This would fit with spectroscopic work (*56*), which shows that substrate binding "locks" the bound O_2 into a single conformation (presumably suitably oriented for C^2—C^3 bond cleavage).

VII. Reaction Mechanism

A. Literature Proposals

The most cursory glance at the literature would quickly lead to one to conclude that the mechanism of catalysis was cast in stone. The reaction had been proposed as occurring through either Criegee (*49*) or dioxetane (*57*) pathways (Scheme 3) and has been

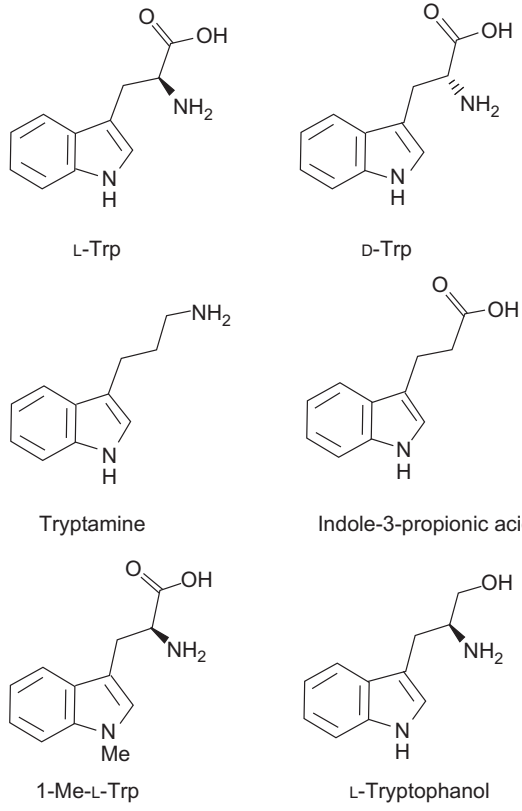

SCHEME 2. Structures of the various tryptophan analogues referred to in this work.

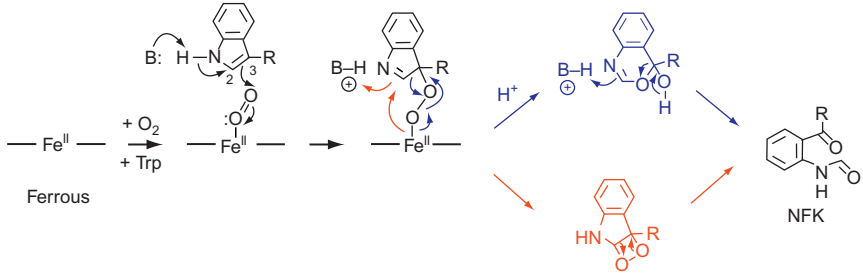

SCHEME 3. Previous proposals (*5,21,49*) for the reaction mechanism in the heme dioxygenases via either Criegee (blue) or dioxetane (red) pathways.

widely reproduced. It is a curiosity of the literature that these proposals became deeply entrenched despite the fact that there was barely any experimental evidence for either of them. One feature of the mechanism is that only a single initial reduction of the heme is required for turnover and that there is no further change in oxidation state of the heme iron during turnover, which is different from other O_2-dependent heme enzymes (e.g., P450s, NO synthases) in which a second reduction of the iron and protonation leads to formation of Compound I which then needs further re-reduction from a suitable reductase.

The first step of the mechanism had been proposed (*49*) as a base-catalyzed abstraction of the indole proton (Scheme 4a) and was based on the idea that only substrates containing a protonated indole nitrogen were active. Others (*21*) drew similar conclusions based on the observation that 1-methyltryptophan (Scheme 2) was an inhibitor of dioxygenase activity. But the complete absence of a distal histidine in hIDO quite obviously contradicted these proposals, and because of this it was suggested (*27*) that proton abstraction by the bound O_2 was more likely (a suggestion first put forward by Terentis *et al.* (*23*); Scheme 4b). In fact, we have noted (*31*) that the chemistry of indoles has a long and well-documented history, and they do not react by base-catalyzed proton abstraction (*58*). Indeed, there are chemical difficulties with both mechanisms drawn in Scheme 4a and b, since the electrons in the N—H (sigma) bond are perpendicular to the π-orbitals of the aromatic ring and so could not be used

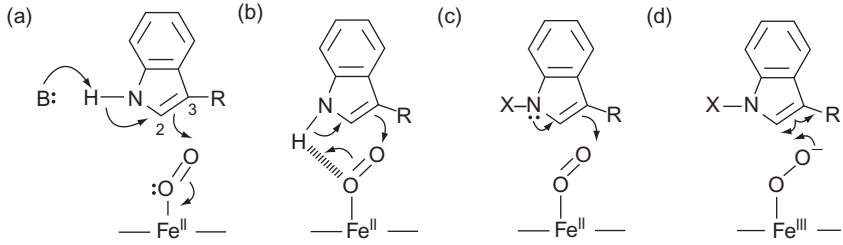

SCHEME 4. The variously proposed alternative reaction mechanisms for heme dioxygenases. (a) The base-catalyzed abstraction mechanism (*21,49*). (b) An alternative to the base-catalyzed mechanism, using proton abstraction by the bound O_2 (*23,27*). (c) Electrophilic addition (*31,50,51*). (d) Radical addition (*50–53*). The majority opinion from crystallography (*27*), mass spectrometry (*30*), mutagenesis (*54*), and computational work (*50*) concludes that (a) and (b) are unlikely. It is not yet known whether addition at C^3 or C^2 is most likely; both have been suggested (*31,50–53,55*).

to directly activate the aromatic ring for electrophilic attack onto oxygen. In addition, the theoretical pK_a of the indole proton is very high (pK_a≈17 (*59*)) and presumably out of range under catalytic conditions.

B. Revisions to Literature Proposals

Computational work (*50*) raised the first questions as to the likelihood of a base-catalyzed abstraction mechanism, and electrophilic addition was suggested as one of a number of alternative mechanisms. To date, the main experimental evidence comes from mass spectrometry (*31*) which has shown that 1-Me-Trp is not an inhibitor but actually a slow substrate for several dioxygenase enzymes. We have pointed out (*31*) that this rules out both mechanisms in Scheme 4a and b, as neither is possible with the methyl-substituted indole and would be consistent with mutagenesis data which show that when a distal histidine is present its removal does not shut down activity completely (*54*). Spectroscopic work using ^{1}H ENDOR (*56*) has since shown that the indole NH group is not hydrogen bonded to the bound O_2 in the ternary complex, further arguing against the mechanisms shown in Scheme 4b. Others (*52*) have drawn similar conclusions from computational work, and there now seems to be a consensus that base-catalyzed abstraction does not occur.

What happens instead? There are two alternative mechanisms, both of which would accommodate the reactivity of 1-Me-Trp (*31*). In the first case, the lone pair on nitrogen initiates electrophilic addition to the bound O_2 ligand (*31*) (Scheme 4c). This route was identified computationally (*50*) and suggested from mass spectrometry work (*31*). Electrophilic addition would be consistent with the known chemistry of indoles, but O_2 is typically not a very good electrophile and certainly in the case of the globins the ferrous-oxy bond is best formulated as an $Fe^{III}—O_2^-$ species (*60*). An alternative is radical addition (Scheme 4d) again identified as contender from computational work (*52,53*). This too would allow for reactivity of 1-Me-Trp (*31*) and is appealing in the sense that it would require a $Fe^{III}—O_2^-$ formulation for the ferrous-oxy heme, for which there is spectroscopic evidence (*53*).

As for NFK formation, the mechanism is not yet clear. The Criegee mechanism is well known in the nonheme iron literature (see, e.g., Ref. (*61*)), but there is no experimental evidence for either a Criegee (*49*) or a dioxetane (*57*) mechanism. As is clear from Scheme 3, neither mechanism requires a formal change in

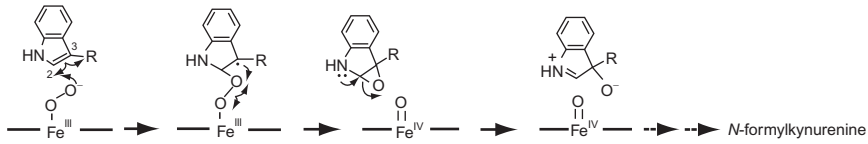

SCHEME 5. An alternative mechanism. Radical addition (instead of base-catalyzed abstraction) leading to species X is followed by formation of a ferryl heme species (Compound II) and a proposed epoxide species (*53*). Formation of an epoxide has also been suggested from computational work (*51*) (it was also considered in an earlier study, but initially considered energetically unfavorable in the gas phase (*50*)). Electrophilic addition (Scheme 4) could also involve epoxide formation through a similar (two-electron) mechanism. Possible ring opening of the epoxide is also indicated (third step).

oxidation state during turnover (which is unusual for heme-mediated catalysis). However, there is more than one report implicating the formation of a ferryl heme species during dioxygenase turnover. The first came from Yeh and coworkers (*53*) who have used resonance Raman methods to observe a stretching frequency characteristic of ferryl heme ($\nu_{Fe=O}$), assigned as a Compound II, during turnover in hIDO (but not in hTDO). These findings were corroborated independently later on (*62,63*). This has led to the suggestion (*53*) that simultaneous incorporation of both atoms of O_2 does not occur, but that instead sequential (stepwise) insertion of oxygen into the substrate is the preferred route, as depicted in Scheme 5. Recent computational work (*51*) supports epoxide formation as the first oxygenation step (although pathways involving high-valent iron ferryl heme had also been suggested from earlier work (*50*)) and its formation has been recently inferred from mass spectrometry analyses (*66*).

VIII. Wider Comparisons with Other Heme Enzymes

A. PRNB

The closely related PrnB enzyme catalyzes a similar reaction (Fig. 6a) and binds its substrate differently (*64*): in this case, the C^2—N^1 bond of 7-chloro-L-Trp is cleaved (without insertion of O_2) and Naismith and coworkers have shown that the L-typtophan binds in a different orientation to that of *X. campestris* TDO (Fig. 6b). This system may provide important clues as the details of the dioxygenase mechanism are unraveled.

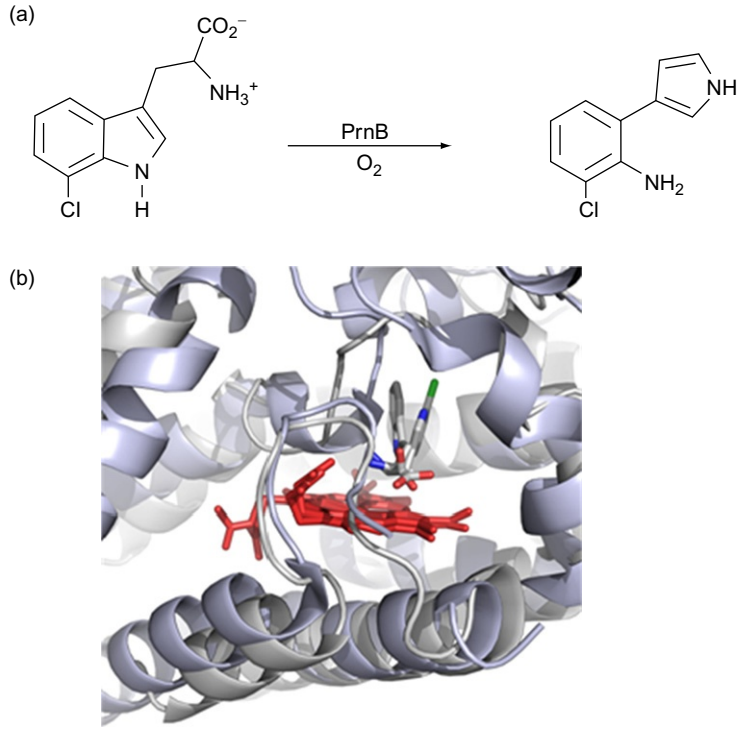

FIG. 6. (a) The reaction catalyzed by PrnB. (b) An overlay of the heme regions of *X. campestris* TDO (gray (*26*)) and PrnB (pale blue (*64*)), showing the different orientations of the substrate (L-Trp for TDO and 7-Cl-Trp for PrnB, both in gray with the Cl atom in green). The heme groups are overlaid in red.

B. OTHER CATALYTIC ENZYMES

The process of oxygen activation in most heme enzymes (e.g., P450s, peroxidases, etc.) is achieved through formation of highly oxidized iron intermediates. This demands continuous reduction of the heme group, through a suitable reductase/substrate (Scheme 6). There is evidence that the physiological partner reductase for IDO might be a cytochrome b_5 (*35,65*), but continuous re-reduction of an oxidized ferryl heme is not presumed because all of the available evidence so far indicates that the dioxygenases only require a single, initiating reduction of ferric heme. Further reduction and protonation of the ferrous-oxy heme would presumably not be a productive pathway for IDO or TDO, since it leads to

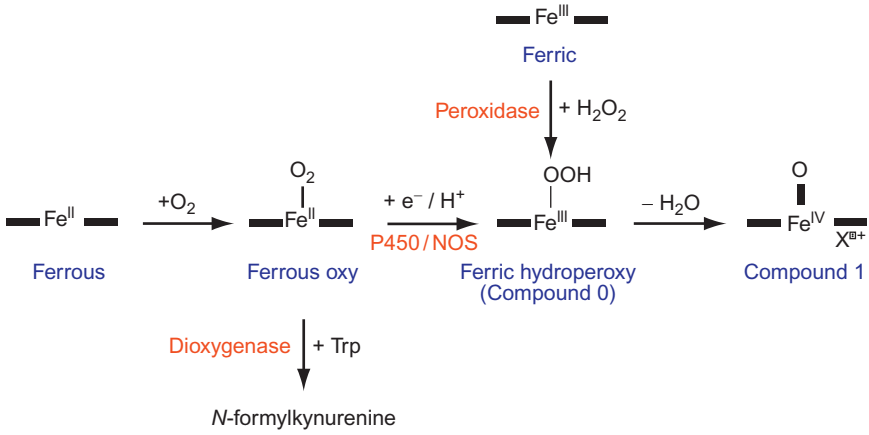

SCHEME 6. Comparison of the reaction mechanisms in various heme proteins. X represents the location of the radical in Compound I (most commonly a porphyrin π-cation radical).

Compound I formation. In fact, there is evidence from ENDOR work (*56*) that substrate binding shields the ferrous-oxy complex from protonation in dioxygenases, which may be one of the strategies that the dioxygenases employ to control the reactivity of the ferrous-oxy species and to avoid unproductive formation of Compound I (Scheme 6).

IX. Concluding Remarks

Interest in IDO and TDO originated many years ago, but there is much yet to learn. Information on the mechanism of NFK formation, structures for new enzymes, the similarities and differences with other heme proteins, and the controlling roles of individual residues all have to be firmly established. As the physiological roles become more firmly embedded, it is likely that these enzymes will continue to attract attention.

ABBREVIATIONS

hIDO	human indoleamine 2,3-dioxygenase
hTDO	human tryptophan 2,3-dioxygenase
IDO	indoleamine 2,3-dioxygenase

NFK	*N*-formylkynurenine
TDO	tryptophan 2,3-dioxygenase
xTDO	*X. campestris* tryptophan 2,3-dioxygenase

Acknowledgment

This work was supported by The Wellcome Trust (Project Grant 083636 to E. L. R. and C. G. M.).

References

1. Kotake, Y.; Masayama, I. *Z. Physiol. Chem.* **1936,** *243*, 237–244.
2. Yamamoto, S.; Hayaishi, O. *J. Biol. Chem.* **1967,** *242*, 5260–5266.
3. Tanaka, T.; Knox, W. E. *J. Biol. Chem.* **1959,** *234*, 1162–1170.
4. Knox, W. E.; Mehler, A. H. *J. Biol. Chem.* **1950,** *187*, 419–430.
5. Sono, M.; Roach, M. P.; Coulter, E. D.; Dawson, J. H. *Chem. Rev.* **1996,** *96*, 2841–2887.
6. Ohashi, H.; Saito, K.; Fujii, H.; Wada, H.; Furuta, N.; Takemura, M.; Maeda, S.; Seishima, M. *Arch. Biochem. Biophys.* **2004,** *428*, 154–159.
7. Saito, K.; Fujigaki, S.; Heyes, M. P.; Shibata, K.; Takemura, M.; Fujii, H.; Wada, H.; Noma, A.; Seishima, M. *Am. J. Physiol.* **2000,** *279*, F565–F572.
8. Tankiewicz, A.; Pawlak, D.; Buczko, W. *Postepy Hig. Med. Dosw.* **2001,** *55*, 715–731.
9. Aquilina, J. A.; Carver, J. A.; Truscott, R. J. W. *Exp. Eye Res.* **1997,** *64*, 727–735.
10. Grohmann, U.; Fallarino, F.; Puccetti, P. *Trends Immunol.* **2003,** *24*, 242–248.
11. Mellor, A. L.; Munn, D. H. *J. Immunol.* **2003,** *170*, 5809–5813.
12. Munn, D. H.; Mellor, A. L. *J. Clin. Invest.* **2007,** *117*, 1147–1154.
13. MacKenzie, C. R.; Heseler, K.; Mueller, A.; Daeubener, W. *Curr. Drug Metab.* **2007,** *8*, 237–244.
14. Basran, J.; Rafice, S. A.; Chauhan, N.; Efimov, I.; Cheesman, M. R.; Ghamsari, L.; Raven, E. L. *Biochemistry* **2008,** *47*, 4752–4760.
15. Suzuki, T.; Imai, K. *Cell. Mol. Life Sci.* **1998,** *54*, 979–1004.
16. Springer, B. A.; Sligar, S. G.; Olson, J. S.; Phillips, G. N.Jr., *Chem. Rev.* **1994,** *94*, 699–714.
17. Dunford, H. B. *Peroxidases and Catalases: Biochemistry, Biophysics, Biotechnology and Physiology* (2nd edn.). John Wiley: Chichester, **2010**.
18. Dunford, H. B. *Heme Peroxidases.* John Wiley: Chichester, **1999**.
19. Erman, J. E. *J. Biochem. Mol. Biol.* **1998,** *31*, 307–327.
20. Ortiz de Montellano, P. R. *Annu. Rev. Pharmacol. Toxicol.* **1992,** *32*, 89–107.
21. Cady, S. G.; Sono, M. *Arch. Biochem. Biophys.* **1991,** *291*, 326–333.
22. Papadopoulou, N. D.; Mewies, M.; McLean, K. J.; Seward, H. E.; Svistunenko, D. A.; Munro, A. W.; Raven, E. L. *Biochemistry* **2005,** *44*, 14318–14328.
23. Terentis, A. C.; Thomas, S. R.; Takikawa, O.; Littlejohn, T. K.; Truscott, R. J. W.; Armstrong, R. S.; Yeh, S.-R.; Stocker, R. *J. Biol. Chem.* **2002,** *277*, 15788–15794.

24. Makino, R.; Sakaguchi, K.; Iizuka, T.; Ishimura, Y. *Dev. Biochem.* **1980,** *16*, 179–187.
25. Gupta, R.; Fu, R.; Liu, A.; Hendrich, M. P. *J. Am. Chem. Soc.* **2010,** *132*, 1098–1109.
26. Forouhar, F.; Anderson, J. L.; Mowat, C. G.; Vorobiev, S. M.; Hussain, A.; Abashidze, M.; Bruckmann, C.; Thackray, S. J.; Seetharaman, J.; Tucker, T.; Xiao, R.; Ma, L. C.; Zhao, L.; Acton, T. B.; Montelione, G. T.; Chapman, S. K.; Tong, L. *Proc. Natl. Acad. Sci. USA* **2007,** *104*, 473–478.
27. Sugimoto, H.; Oda, S.-i.; Otsuki, T.; Hino, T.; Yoshida, T.; Shiro, Y. *Proc. Natl. Acad. Sci. USA* **2006,** *103*, 2611–2616.
28. Batabyal, D.; Yeh, S.-R. *J. Am. Chem. Soc.* **2007,** *129*, 15690–15701.
29. Batabyal, D.; Yeh, S.-R. *J. Am. Chem. Soc.* **2009,** *131*, 3260–3270.
30. Chauhan, N.; Basran, J.; Efimov, I.; Svistunenko, D. A.; Seward, H. E.; Moody, P. C. E.; Raven, E. L. *Biochemistry* **2008,** *47*, 4761–4769.
31. Chauhan, N.; Thackray, S. J.; Rafice, S. A.; Eaton, G.; Lee, M.; Efimov, I.; Basran, J.; Jenkins, P. R.; Mowat, C. G.; Chapman, S. K.; Raven, E. L. *J. Am. Chem. Soc.* **2009,** *131*, 4186–4187.
32. Austin, C. J. D.; Astelbauer, F.; Kosim-Satyaputra, P.; Ball, H. J.; Willows, R. D.; Jamie, J. F.; Hunt, N. H. *Amino Acids* **2009,** *36*, 99–106.
33. Watanabe, Y.; Fujiwara, M.; Yoshida, R.; Hayaishi, O. *Biochem. J.* **1980,** *189*, 393–405.
34. Littlejohn, T. K.; Takikawa, O.; Skylas, D.; Jamie, J. F.; Walker, M. J.; Truscott, R. J. W. *Protein Expr. Purif.* **2000,** *19*, 22–29.
35. Vottero, E.; Mitchell, D. A.; Page, M. J.; MacGillivray, R. T. A.; Sadowski, I. J.; Roberge, M.; Mauk, A. G. *FEBS Lett.* **2006,** *580*, 2265–2268.
36. Fukumura, E.; Sugimoto, H.; Misumi, Y.; Ogura, T.; Shiro, Y. *J. Biochem.* **2009,** *145*, 505–515.
37. Ren, S.; Liu, H.; Licad, E.; Correia, M. A. *Arch. Biochem. Biophys.* **1996,** *333*, 96–102.
38. Dick, R.; Murray, B. P.; Reid, M. J.; Correia, M. A. *Arch. Biochem. Biophys.* **2001,** *392*, 71–78.
39. Manandhar, S. P.; Shimada, H.; Nagano, S.; Egawa, T.; Ishimura, Y. *Int. Congr. Ser.* **2002,** *1233*, 161–169.
40. Zhang, Y.; Kang, S. A.; Mukherjee, T.; Bale, S.; Crane, B. R.; Begley, T. P.; Ealick, S. E. *Biochemistry* **2007,** *46*, 145–155.
41. Li, J. S.; Han, Q.; Fang, J.; Rizzi, M.; James, A. A.; Li, J. *Arch. Insect Biochem. Physiol.* **2007,** *64*, 74–87.
42. Paglino, A.; Lombardo, F.; Arca, B.; Rizzi, M.; Rossi, F. *Insect Biochem. Mol. Biol.* **2008,** *38*, 871–876.
43. Hu, X.; Bao, Z.; Hu, J.; Shao, M.; Zhang, L.; Bi, K.; Zhan, A.; Huang, X. *Aquacult. Res.* **2006,** *37*, 1187–1194.
44. DeLano, W. L. *The PyMOL Molecular Graphics System.* DeLano Scientific: San Carlos, CA, **2002**.
45. Littlejohn, T. K.; Takikawa, O.; Truscott, R. J. W.; Walker, M. J. *J. Biol. Chem.* **2003,** *278*, 29525–29531.
46. Sono, M.; Dawson, J. H. *Biochim. Biophys. Acta* **1984,** *789*, 170–187.
47. Capece, L.; Arrar, M.; Roitberg, A. E.; Yeh, S. R.; Marti, M. A.; Estrin, D. A. *Proteins* **2010,** *78*, 2961–2972.
48. Leeds, J. M.; Brown, P. J.; McGeehan, G. M.; Brown, F. K.; Wiseman, J. S. *J. Biol. Chem.* **1993,** *268*, 17781–17786.
49. Hamilton, G. A. *Adv. Enzymol. Relat. Areas Mol. Biol.* **1969,** *32*, 55–96.

50. Chung, L. W.; Li, X.; Sugimoto, H.; Shiro, Y.; Morokuma, K. *J. Am. Chem. Soc.* **2008,** *130*, 12299–12309.
51. Chung, L. W.; Li, X.; Sugimoto, H.; Shiro, Y.; Morokuma, K. *J. Am. Chem. Soc.* **2010,** *132*, 11993–12005.
52. Capece, L.; Lewis-Ballester, A.; Batabyal, D.; Di Russo, N.; Yeh, S. R.; Estrin, D. A.; Marti, M. A. *J. Biol. Inorg. Chem.* **2010,** *15*, 811–823.
53. Lewis-Ballester, A.; Batabyal, D.; Egawa, T.; Lu, C.; Lin, Y.; Marti, M. A.; Capece, L.; Estrin, D. A.; Yeh, S. R. *Proc. Natl. Acad. Sci. USA* **2009,** *106*, 17371–17376.
54. Thackray, S. J.; Bruckmann, C.; Anderson, J. L.; Campbell, L. P.; Xiao, R.; Zhao, L.; Mowat, C. G.; Forouhar, F.; Tong, L.; Chapman, S. K. *Biochemistry* **2008,** *47*, 10677–10684.
55. Guallar, V.; Wallrapp, F. H. *Biophys. Chem.* **2010,** *149*, 1–11.
56. Davydov, R. M.; Chauhan, N.; Thackray, S. J.; Anderson, J. L.; Papadopoulou, N. D.; Mowat, C. G.; Chapman, S. K.; Raven, E. L.; Hoffman, B. M. *J. Am. Chem. Soc.* **2010,** *132*, 5494–5500.
57. Hayaishi, O.; Rothberg, S.; Mehler, A. H.; Saito, Y. *J. Biol. Chem.* **1957,** *229*, 889–896.
58. Joule, J. A.; Mills, K. *Heterocyclic Chemistry* (4th edn.). Blackwell: Oxford, **2000**.
59. Yagil, G. *Tetrahedron* **1967,** *23*, 2855–2861.
60. Chen, H.; Ikeda-Saito, M.; Shaik, S. *J. Am. Chem. Soc.* **2008,** *130*, 14778–14790.
61. Kovaleva, E. G.; Neibergall, M. B.; Chakrabarty, S.; Lipscomb, J. D. *Acc. Chem. Res.* **2007,** *40*, 475–483.
62. Yanagisawa, S.; Yotsuya, K.; Hashiwaki, Y.; Horitani, M.; Sugimoto, H.; Shiro, Y.; Appelman, E. H.; Ogura, T. *Chem. Lett.* **2010,** *39*, 36–37.
63. Yanagisawa, S.; Horitani, M.; Sugimoto, H.; Shiro, Y.; Okada, N.; Ogura, T. *Faraday Discuss.* **2010,** *148*, 1–9.
64. Zhu, X.; van Pee, K. H.; Naismith, J. H. *J. Biol. Chem.* **2010,** *285*, 21126–21133.
65. Maghzal, G. J.; Thomas, S. R.; Hunt, N. H.; Stocker, R. *J. Biol. Chem.* **2008,** *283*, 12014–12025.
66. Basran, J.; Efimov, I.; Chauhan, N.; Thackray, S. J.; Krupa, J.; Eaton, G.; Griffith, G. A.; Mowat, C. G.; Handa, S.; Raven, E. L. J. *Am. Chem. Soc.* **2011,** *133*, 16251–16257.

REACTIVITY OF MANGANESE SUPEROXIDE DISMUTASE MIMICS TOWARD SUPEROXIDE AND NITRIC OXIDE: SELECTIVITY *VERSUS* CROSS-REACTIVITY

IVANA IVANOVIĆ-BURMAZOVIĆ and MILOŠ R. FILIPOVIĆ

Department of Chemistry and Pharmacy, University of Erlangen-Nürnberg, Egerlandstrasse 1, Erlangen, Germany

ABSTRACT

The (bio)chemistry and physiology of superoxide and nitric oxide and their interactions with metal centers are very complex issues, which require a multidisciplinary approach. We are still not fully aware of the reactions that occur in relatively simple *in vitro* conditions and we know even less about the real processes on a molecular level under the *in vivo* conditions. Systematic studies and reliable, comparable data on number of different

INORGANIC/BIOINORGANIC REACTION MECHANISMS
VOLUME 64 ISSN 0898-8838 / DOI: 10.1016/B978-0-12-396462-5.00003-9

manganese superoxide dismutase (MnSOD) mimetics, regarding their reactivity toward reactive oxygen and nitrogen species and corresponding reaction mechanisms, are required for the further progress in the field and possible biomedical application of the gained knowledge. We present here some important aspects of chemistry, in particular, redox activity, and biochemistry of superoxide and nitric oxide as well as their interaction with MnSOD mimetics that should be considered for the future design and pharmacological studies of manganese-based therapeutics and even diagnostic tools.

Keywords: Superoxide; Nitric oxide; Manganese superoxide dismutase; Manganese SOD mimetics (mimics); Peroxynitrite; Nitric oxide dismutation; Nitric oxide reduction.

I. General Facts About Superoxide

Dioxygen, a strangely reactive paramagnetic gas, is indispensable to our life on this planet. In our need to metabolize energy stores, we use it continuously. Oxygen-utilizing life forms have an efficient metabolism because of its high reduction potential ($E^0(O_2/H_2O)=+0.82$V vs. NHE), but this advantage comes with a price. Namely, a frequently encountered intermediate of dioxygen reduction is the superoxide radical anion ($O_2^{\bullet -}$), a deleterious metabolic by-product (*1*). For this reason, O_2^- activating species generally utilize two redox-active centers to circumvent this one-electron reduction (*2*). Nevertheless, small quantities of superoxide are produced. Earlier, $O_2^{\bullet -}$ was associated only with the effects of ionizing radiation, but now it is known to arise under ordinary circumstances during numerous biological reactions in living systems (*1*). It is generated by a large number of sources, including normal cellular respiration, in the metabolism of arachidonic acid, and as a result of neutrophil activation in response to infection or foreign antigens (*3a*).

Superoxide is usually referred to as a reactive species, which possesses multiple threats as a reducing agent in its anionic state and as an oxidant in its protonated form. It is potentially dangerous for all cellular macromolecules and it can engender other undesired reactive species. Importantly, although it is a radical and can initiate the free radical oxidation of sulfite and its scavenging inhibits, a number of biological free radical chain autoxidations (e.g., of epinephrine, pyrogallol), superoxide itself is not proven to be a highly reactive initiator of free radical

reactions in carefully controlled chemical experiments (*4a*). The true nature of its reactivity was a matter of a strong debate between Fridovich, on one side, and Sawyer and Valentine, on the other (*4b*). Two properties of superoxide are well documented: its nucleophilicity (e.g., toward alkyl halides and carbonyl systems such as esters, acyl halides, and CO_2) and its moderate reducing power in aprotic media, roughly equivalent to that of dithionite ion ($E^0(O_2^{\bullet -}/O_2)=-0.16$ V vs. SHE in aqueous solution or ca. -0.5 vs. NHE in aprotic solvents) (*4c,b*). A third confirmed reaction characteristic of superoxide is its capacity to effect proton removal from substrates and solvents (*4d*). Although its protonated HO_2 form, so-called hydroperoxyl radical is quite acidic ($pK_a=4.88$), which infers that superoxide is a weak base, the solutions of superoxide behave as if they are strongly basic. This is a result of the fact that superoxide protonation is coupled to strongly thermodynamically favored disproportionation, that is, dismutation, where besides electron transfer, protonation of the resulting peroxide anion occurs (Eq. (1)). Due to the extremely strong basicity of the "naked" peroxide dianion, superoxide ion solutions can promote proton transfer from substrates or solvents (HB in Eq. (2)) with pK_a values as low as 23, according to the overall reaction represented by Eq. (2).

$$2O_2^{\bullet -} + H_2O \rightarrow O_2 + HO_2^- + OH^- \tag{1}$$

$$2O_2^{\bullet -} + HB \rightarrow O_2 + HO_2^- + B^- \tag{2}$$

A property of superoxide to act as an oxidizing agent is much more ambiguous. Thermodynamically, an electron transfer to "bare" superoxide is almost impossible because the product of this reaction, peroxide dianion (O_2^{2-}), is highly unstable. Therefore, the reduction of superoxide is either a proton-coupled process (Eq. (3)) or metal-assisted reaction (Eq. (4)), where the latter requires coordination of $O_2^{\bullet -}$ and subsequent inner-sphere electron transfer. It is also possible to think in terms of hydrogen atom transfer reactions as a special sort of proton-coupled electron-transfer processes (Eq. (5)).

$$X\cdots O_2^-\cdots H-Y \rightarrow X^+ + HO_2^- + Y^- \tag{3}$$

$$M^{n+} + O_2^- \rightarrow M^{(n+1)+}(OO)^{2-} \xrightarrow{H^+} M^{(n+1)+} + H_2O_2 \tag{4}$$

$$H-Y\cdots O_2^- \rightarrow Y + HO_2^- \tag{5}$$

Thus, in aprotic media, superoxide is not a highly reactive oxidant for organic substrates (Eq. (6)) and it can rather oxidize those substrates that are susceptible to a hydrogen atom transfer mechanism (*4a*). Although oxidation of substrates by superoxide solutions can be observed, the true identity of an oxidant is not always clear. Namely, upon protonation of $O_2^{\bullet -}$, oxygen and hydrogen peroxide, or hydroperoxide anion, are formed (Eqs. (1)–(2)) that are considered to be the actual oxidizing agents (*4*).In aqueous solutions, that is, in the presence of sufficient proton concentrations, the redox potential for superoxide reduction is significantly more positive (Eq. (7)).

$$O_2^{\bullet -} + e^- (+\text{solvent}) \rightarrow HO_2^-; \quad (E_{pc})_{DMSO} = -1.75 \,\text{versus NHE} \tag{6}$$

$$O_2^{\bullet -} + e^- + 2H^+ \rightarrow H_2O_2; \quad E^{0'} = +0.89 \,\text{versus NHE(at pH 7)} \tag{7}$$

Considering the quite different redox behavior of superoxide in protic and aprotic media, it is important to study and understand its reactivity in both aqueous and nonaqueous solutions, which is also of biological relevance. Although we often tend to exclude the biological significance of chemical investigations in nonaqueous media, this definitely should not be the case when we deal with superoxide. Different cell compartments offer different reaction environment for superoxide. Whereas cytosol represents a more protic environment, mitochondria and, in general, biological membranes are lipophilic cell compartments, and as such much less protic. An important cascade of redox reactions within the electron transport chain take place on the inner mitochondrial membrane where, due to premature electron leakage to oxygen, superoxide is generated. Therefore, as it was stressed by Sawyer *et al*. (*5*), an even closer relation between the kinetic measurements in aprotic media than in bulk water can be drawn with the processes in mitochondria, which are the major source of superoxide in aerobic organisms, since aprotic media "may be representative of a hydrophobic biological matrix." Under less protic conditions, causing a longer half-life of $O_2^{\bullet -}$, efficient superoxide decomposition is even more desirable.

The effect of proton-coupled, that is, proton-assisted, reduction of superoxide is obvious and can be quantified (Eqs. (6) and (7)). However, how redox potentials for superoxide reduction and oxidation are changed upon its coordination to a metal center is not known and is usually completely neglected. It is of course not

easy to quantify the redox potential of coordinated superoxide, however, we need to be aware of the fact that these values are quite different from those that correspond to the outer-sphere oxidation and reduction (−0.16V vs. SHE and +0.89 vs. NHE at pH 7, respectively). This, so-called metal ion-coupled electron transfer (*6*) is an important mechanism for the activation of superoxide and other biologically relevant small molecules such as oxygen, hydrogen peroxide, and nitric oxide (NO) toward the electron-transfer process (*7*). It is crucial for superoxide dismutation (Eq. (1)) catalyzed by enzymatic and mimetic metal centers, as well as for understanding cross-reactions between these redox-active metal systems and other small molecules, viz. NO in the first place (*7*).

II. Life with Superoxide

Despite the fact that elementary reaction steps behind the chemical processes caused by the presence of superoxide in solutions are still not completely reviled, there is no doubt that *in vivo,* superoxide induces biologically harmful effects that are closely related to a wide range of disease states, some of them summarized in Fig. 1 (*3*). It belongs to the so-called reactive oxygen species (ROS), and its overproduction (or accumulation in lipophilic compartments) is related to oxidative stress, which is a situation where levels of ROS in tissues exceed the capacity of endogenous antioxidant defense systems to remove them. The toxicity of superoxide is significantly amplified by its cross link with other redox-active small molecules and metal centers available under physiological conditions, and consequently generation of its even more potent primary and secondary progenies such as hydrogen peroxide and peroxynitrite, as well as $OH^{\bullet}$ and $^{\bullet}NO_2$ radical species, respectively. For example, superoxide inactivates NO and suppresses its beneficial effects, and at the same time produces peroxynitrite ($ONOO^{-}$), which is one of the most potent biologically available oxidants, cytotoxic, and proinflammatory molecule. Peroxynitrite reacts with important biomolecules such as DNA, proteins, lipids, and sugars, leading to cell damage and eventually to cell death: apoptosis and/or necrosis (*8a,b,f*). Although actions of peroxynitrite in pathologies are numerous, a mechanism that is receiving greatest attention is its ability to nitrate tyrosine residues in proteins (*8b*). Nitration of manganese superoxide dismutase (SOD), for example, has been reported to be particularly specific for ischemia–reperfusion injury (*8c–e*). Further, nitration of critical targets such as tyrosine kinase receptors or

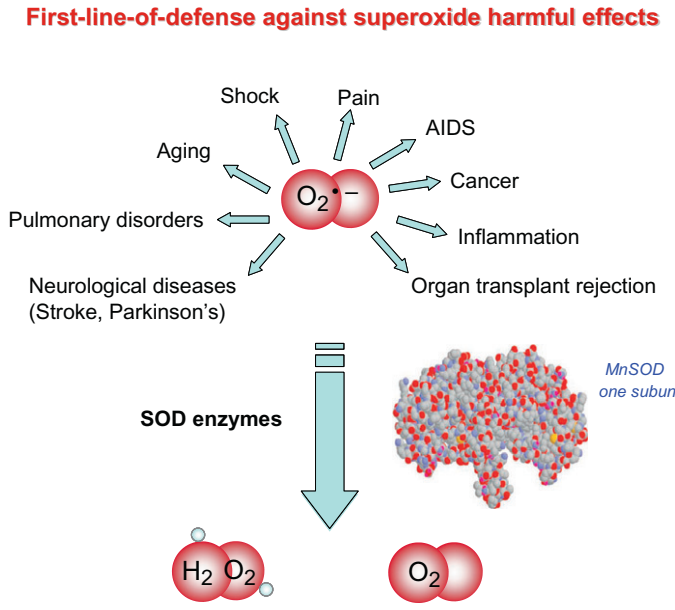

FIG. 1. Some disease states related to superoxide overproduction.

neurofilament proteins could injure motor neurons and is related to amyotrophic lateral sclerosis (*9*). Additionally, by reducing metal centers and generating hydrogen peroxide, superoxide can give rise to Fenton type reactions, where $OH^{\bullet}$ radicals, the strongest biological oxidants, are generated.

To diminish these threats, nature has created a family of metalloenzymes, the SODs. They catalyze the dismutation of superoxide to dioxygen and hydrogen peroxide (Eqs. (1) and (2)). They are differentiated by the redox-active metal: copper (Cu/Zn SOD), manganese (MnSOD), iron (FeSOD), or nickel (NiSOD) superoxide dismutases and fall into three evolutionary families (Fig. 2) (*10*). The iron and manganese SODs are structurally similar and are found in prokaryotes and in the matrix of mitochondria (near the electron transport chain), respectively. Nickel containing SODs are known in some prokaryotes, whereas Cu/Zn are present in the cytosols of virtually all eukaryotic cells and have an independent evolutionary history.

Under normal conditions, these enzymes are responsible for keeping the formation of superoxide under control. In disease states, the production of $O_2^{\bullet -}$ exceeds the ability of the endogenous SOD system to remove it, resulting in superoxide anion

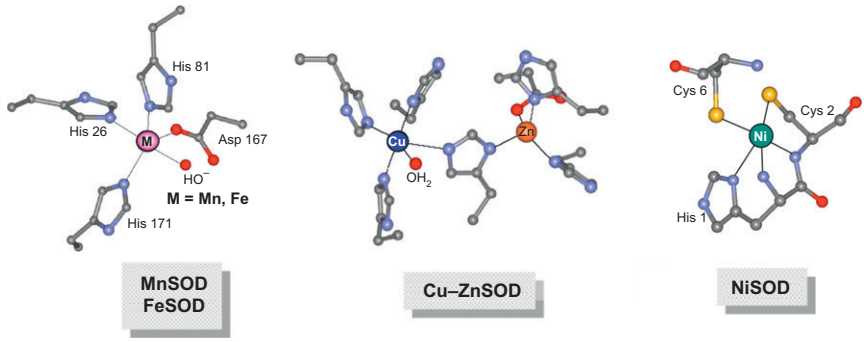

FIG. 2. Active centers of superoxide dismutases.

mediated damage. As mentioned above, many disease states can be related to $O_2^{\bullet -}$ and its progenies (Fig. 1) (*3*). For example, the crucial role of MnSOD has been demonstrated with knockout studies, where mice lacking MnSOD died within 10–21 days of life from cardiomyopathy, neurodegeneration, and metabolic acidosis (*11a,b*). From another side, the CuZnSOD knockout mice were fairly normal but more susceptible to neuronal injury (*11c*). The ability for MnSOD gene expression in response to oxidative stress decreases sharply with age. Thus, older people may be especially prone to degenerative diseases such as diabetes, Parkinson's disease, muscular dystrophy, and cancer (*3j*). As all these pathophysiological conditions are related to $O_2^{\bullet -}$, this commonality enables their treatment with an agent that removes superoxide anions.

For this purpose, the SOD enzymes (natural, recombinant, and modified) have been used in preclinical animal studies and clinical trials (*3a,b*) and have been shown to possess efficacy in the disease states associated with the overproduction of $O_2^{\bullet -}$. SODs have also proven useful as a probe for detection of this radical (*1*). An example is Orgotein® (bovine Cu/Zn SOD) which showed promising results as a human therapeutic (*12*). However, there are major drawbacks associated with the use of the enzymes as potential medicaments: immunological problems, lack of oral activity, short half-lives *in vivo*, costs of production, solution instability, reduced efficacy due to the large size, and inability to access the target tissues (e.g., native enzymes do not penetrate the blood brain barrier) (*3b*).

To overcome the problems associated with enzymes (Fig. 3), several investigations have been directed to design nonproteinaceous, synthetic, low molecular weight mimetics of the

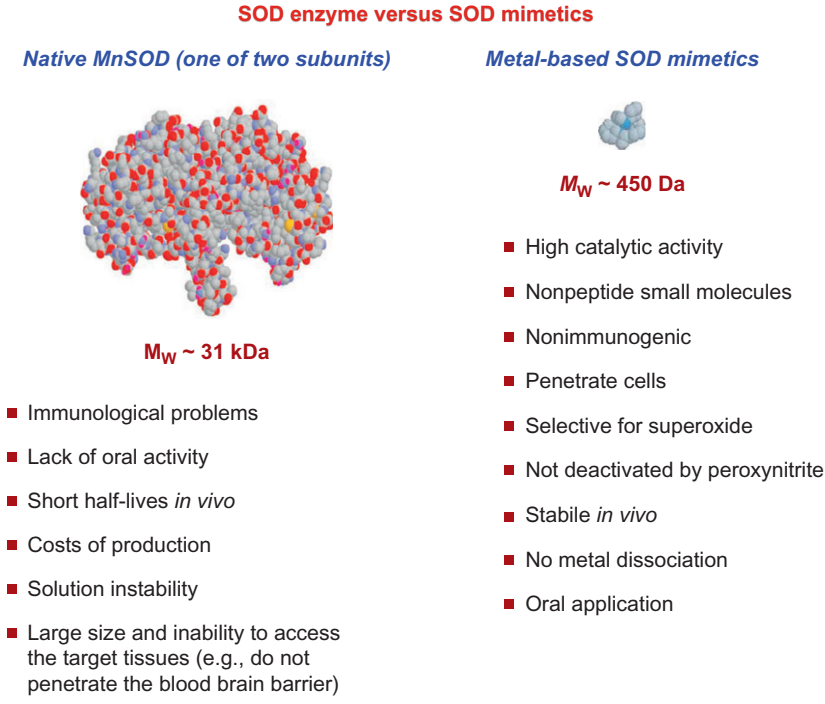

FIG. 3. SOD enzyme versus SOD mimetic.

SOD enzymes, which could serve as pharmaceutical intervention in various superoxide-related ailments.

III. Manganese Superoxide Dismutase Mimetics (MnSODm)

Among the SODm, manganese complexes have attracted a lot of attention, mostly due to the lower manganese toxicity in comparison to iron or copper (*3b*), that is, due to the fact that manganese is not prone to generate the hydroxyl radical in Fenton type reactions. There are three important classes of manganese SODm: Mn(III)Porphyrins, Mn(III)salen, and Mn(II)pentaazamacrocyclic complexes. The most active synthetic catalysts for superoxide disproportionation known to date are the Mn(II) seven-coordinate complexes with macrocyclic ligands derived from C-substituted pentaazacyclopentadecane [15]aneN5 (*13a*). Among Mn([15] aneN5)Cl_2 derivatives, the complexes with bis(cyclohexylpyridine) functionalities, such as M40403, have significant efficiency in animal models of inflammation and reperfusion injury (*13*), and the

2*S*,21*S*-dimethyl derivative of M40403 (M40401) possesses the highest catalytic rate for $O_2^{\bullet -}$ dismutation at pH=7.4 of any known synthetic mimetic, which exceeds that of native mitochondrial MnSOD (*13b*). Some of these complexes are the first SOD mimetics which entered clinical trials (*13*). It has been claimed that these compounds are highly selective, that is, they do not react with hydrogen peroxide or with other biological relevant oxidants such as NO or peroxynitrite radicals (*13*) (Scheme 1).

Parallel with an attempt to synthesize molecules possessing the function of human enzymes, it has been crucial to establish the method which allows precise measurement of the rate of $O_2^{\bullet -}$ dismutation. Studies by Riley *et al*. (*14*) on the evaluation of the activity of putative SOD mimics dictate the necessity of utilizing direct kinetic methods: stopped-flow kinetic analysis and pulse radiolysis (*vide infra*). Based on these measurements, it has been demonstrated that many so-called SOD mimetics do not actually possess catalytic active (*3b*). This was the consequence of applying indirect methodologies, as the cytochrome *c* assay, in the detection of SOD activity of these complexes, such as manganese complexes with desferal, 8-quinolol, cyclam, and aminopolycarboxylate complexes. Some authors are of the opinion that the indirect assays cannot distinguish true catalytic SOD activity (*14, 15a*). It seems that such complexes react stoichiometrically with $O_2^{\bullet -}$, or an apparent catalytic cycle is observed due to hydrogen peroxide contributing to the redox cycle (see Section IV.A).

Among the earliest reported "noncopper" SOD mimics are porphyrinato Fe(III) and Mn(III) complexes described by Pasternack and coworkers (*16a*), whereas the catalytic and biological function of Mn(III)porphyrins is covered by Duke University patents (*16b–d*). The metal porphyrin complexes as potential human pharmaceuticals suffer from a number of possible lethal side effects (toxicity due to the DNA/RNA nicking

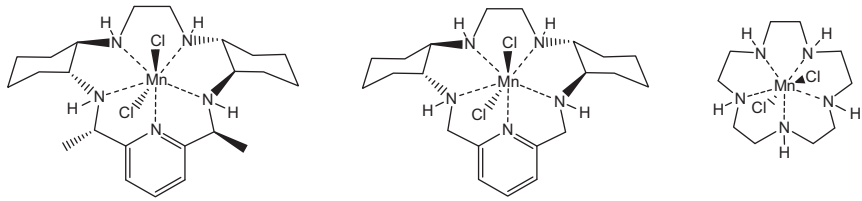

SCHEME 1. The most studied representatives of Mn(II) pentaazamacrocylic class of SOD mimics.

activity), low-yield porphyrin ligand syntheses, formation of oxo- or hydroxo-bridged dimers of lower activity, and generation of hydroxyl radicals in the Fenton reaction (*3b*). However, manganese porphyrins have exceptionally high stability, offer accessibility of several oxidation states of the manganese center and variety of structural modifications and therefore provoked extensive investigations (*17*). Remarkable work on manganese porphyrins as SOD mimetics including both *in vitro* and *in vivo* studies by Batinić-Haberle *et al.* has been recently summarized (*17b*). The presence of a peripheral charge and electron withdrawing groups on the porphyrin ligand influence the SOD activity of this class of complexes significantly. The electrostatic contribution plays an important role so that mono- versus pentacationic porphyrins differ in k_{cat} by 2 log units, whereas cationic versus anionic porphyrins differ in k_{cat} for more than two orders of magnitude (*17b*). The effect of the location of the peripheral positive charge, that is, alkyl groups on the pyridyl rings with respect to the porphyrin core *meso* positions, is also well understood. The closer the positive charge to the manganese center, the higher is the SOD activity (*17b*). Therefore, the *ortho* isomers are more potent SOD mimics than the *meta* analogues. Positive charge can also have drawbacks, because it increases the probability of toxic interactions with nucleic acids. Here, the bulkiness of the alkyl chains may restrict such interactions. Interestingly, the location of pyridinium nitrogens with respect to porphyrin *meso* position has an effect on the lipophilicity and planarity of the porphyrin complexes, which is important for their cytosolic accumulation. Exactly, these effects drive the higher accumulation of *meta* isomers inside *Escherichia coli* (they cross the cell wall more easily) and compensate for lower antioxidant potency when compared with *ortho* analogues (*17b*).

Besides electrostatics, redox potentials are crucial for the SOD activity or metal complexes in general. Thus dramatic effects were achieved by introducing halogenides, for example, in octabrominated $MnBr_8TM\text{-}4\text{-}PyP^{4+}$, where the reduction potential is shifted 420 mV more positively versus nonhalogenated analogues, resulting in a very high SOD activity ($\log k_{cat} \geq 8.67$) (*17b*). However, a more positive redox potential means stabilization of Mn(II), which is more labile and prone to dissociate (Scheme 2).

As mentioned above, due to electrostatics, manganese porphyrins with overall negative charge in general do not possess SOD activity. However, literature data regarding SOD activity for the negatively charged Mn(III)porphyrins are controversial (*3b,17b*). Their SOD activity has been concluded mainly based on

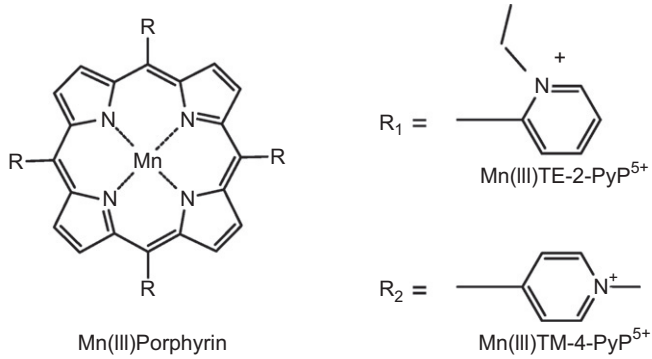

SCHEME 2. Typical representatives of Mn(III)(porphyrinato) SOD mimics.

a number of *in vivo* studies (where no explicit values were reported) or the cytochrome *c* assay (*17b*,*18*). However, recently it has been shown (*17b*) that false SOD activity of the negatively charged porphyrins Mn(III)TBAP^{3-} and Mn(III)TSPP^{3-} most probably results from some nonporphyrin Mn species present as impurities in commercial sources. There are also disagreements regarding *in vivo* action of Mn porphyrins that possess no charges on the periphery and formally bear one positive charge on the Mn site. Whereas Rosenthal *et al*. (*19a*) claimed that these so-called neutral Mn porphyrins have SOD and catalase activity, Batinić-Haberle *et al.* reveal a number of critical points questioning these compounds as functional SOD mimics (*17b*). This has recently even initiated a scientific debate (*19b,c*), where it was pointed out that from one side, SOD activity is not as important as other properties, such as catalase and other ROS or RNS scavenging properties, lipophilicity, lack of toxicity, or intracellular stability, in determining biological efficacy (*19b*), and from another side, that dissemination of compounds that are impure and/or of unknown chemistry may contribute to the abundance of misleading data (*19c*). It is really not a straightforward task to conceive what Mn porphyrins and other putative SOD mimics do *in vivo*, because, as we will also discuss latter, all these redox-active complexes are not selective toward one specific reactive oxygen or nitrogen species. But exactly because of this complexity and possibility of multiple actions of putative SOD mimetics and other redox-active metal complexes for biological/clinical studies, special research efforts should be exercise in order to assure high purity, defined speciation in solution, and reliable (re)activity data.

Beside the Mn([15]aneN5) derivatives and manganese porphyrins, the Mn(III)(salen) complexes have excellent potential

in manipulating a wide variety of disease states. Actually the Mn(II) pentaazamacrocyclic and Mn(III)(salen) complexes are those with the most reported results on the testing in animal models of human diseases. Two complexes of the Mn(III)(salen) class, EUK-8 and EUK-134, have been tested in a range of disease models related to oxidative stress and their structures, as therapeutics are patented by Eukarion, Inc. (*20a,b*). A substantial body of *in vitro* and *in vivo* results clearly demonstrate protective effects from Mn(III)salen complexes in diseases involving oxidative stress, especially in models for neurodegenerative diseases of aging (*21*). They are often referred to as multifunctional catalytic antioxidants that possess combined catalase and SOD activity (*21*), however, the latter has been questioned in the literature (*3b*). Their activity against reactive nitrogen species (RNS) is also observed (*21*).

However, there are no mechanistic details for these complexes, and although the Eukarion studies indicate their SOD catalytic activity, results from other groups clearly present a very low true SOD activity. Based on stopped-flow analysis of superoxide decay followed at a single wavelength, it has been reported (*3b*) that the Mn(III)salen complexes possess a low catalytic activity, that is, in general lower than $8\times10^5 M^{-1}s^{-1}$ at pH=8.0. Similar results have been obtained by a cytochrome *c* assay in phosphate buffer at pH=7.8 (*22*). In addition, some prior work by Taylor *et al.* (*23*) bore evidence of no observable reaction between Mn (III)(salen) complexes and superoxide. There is no doubt that EUK-8 and EUK-134 have protective effects in models of oxidative stress, but it is important to determine the key mechanism that is the source of the biological effect. An important observation is the fact that, although complexes with tetradentate Schiff base salen ligands do not react with $O_2^{\bullet-}$, complexes with the pentadentate salen analogues do react (*3b*). In general, these pentadentate ligands favor seven-coordinate geometry around the metal center, and exactly this structural feature of the metal complexes seems to be tailor made for successful SOD catalytic activity.

Recently, some manganese(II) complexes of tetraazamacrocyclic and acyclic polycarboxylate ligands have been reported as scavengers of superoxide and therapeutic agents against cell and tissue oxidative injury (*24*). However, the SOD-like activity has been studied by utilizing a sort of NBT (nitroblue tetrazolium) assay, which is not superoxide specific and is inevitably prone to artifacts (*19c*). Therefore, the superoxide scavenging properties of these complexes need to be properly reinvestigated in order to say something more precise about their mechanism of

action. Among these compounds, the most bioactive is the one with the higher lipophilic properties that can favor its transmembrane passage and distribution in the intracellular compartment (*24*). Interestingly, the corresponding metal free ligand alone showed a modest anti-inflammatory *in vivo* activity, which has been interpreted by its good chelating properties and ability to bind endogenous Mn(II), behaving as a prodrug (*24*).

IV. Some Methodological, Mechanistic, and Cross-reactivity Consideration

In summarizing this short overview on manganese SOD mimetics, we would like to stress that although some of them have proven to be effective in clinical trials in manipulating a variety of disease states related to reactive oxygen and nitrogen species, the key mechanisms behind their bioactivity are still elusive. In order to conceive the elementary reaction steps responsible for their beneficial physiological effects, it is first important to obtain reliable and comparable values for their SOD activities, for example, methodological approach in such studies needs to be carefully chosen. Further, the above-outlined arguments stress the need of a detailed understanding of the mechanisms by which putative SOD mimetics react with superoxide radicals, being essential for the rational design of efficient SOD catalysts. Finally, as a crucial element of such studies, detailed investigations of possible cross-reactions with other reactive oxygen and nitrogen species (such as hydrogen peroxide (H_2O_2), hydroxyl radicals ($OH^{\bullet}$), NO, nitroxyl (HNO/NO^-), peroxynitrite ($ONOO^-$), nitrogen dioxide (NO_2), etc.) as well as ligating agents (such as phosphates, carboxylates, etc.) should be performed, because it is still not clear which type of action(s) could be responsible for a certain bioactivity of applied putative SOD mimetics.

A. Methodological Approach: Indirect Versus Direct Methods for Detection of SOD Activity

Due to the fact that the reactions with superoxide are very fast and that superoxide solutions are unstable, kinetic and thermodynamic quantification of these processes requires a special approach. Already the self-decomposition of superoxide to hydrogen peroxide and oxygen in aqueous media ($k_{cat}=1\times10^5$ to 8×10^5

$M^{-1}s^{-1}$ in range of pH=8.1–7.1 (*14a*)) is, in itself, a fast process. Different methods are used for the determination of the rate constant for the catalytic SOD: direct methods (pulse radiolysis and stopped-flow measurements) (*14, 15a–e*) that follow decomposition of superoxide itself in the UV region; additionally indirect methods (different variations of cytochrome *c* or NBT/MTS/XTT assays) (*15f,g*) that follow the inhibition, by putative SODm, of the reaction between an indicator and *in situ* generated (usually by xanthine/xanthine oxidase system or ^{60}Co gamma irradiation) superoxide. In the case of indirect methods as well as pulse radiolysis, relatively low steady-state concentrations (ca. 0.5–50 μM) of superoxide are used, whereas in the stopped-flow experiment setup, much higher (millimolar) superoxide concentrations are applied (*15e*). It should be mentioned that widely utilized indirect methods need to be carefully assessed, because different components present in these assays may lead to side reactions (e.g., precipitation of formazan dye, interaction with the reduced form of xanthine oxidase, hydrogen peroxide-dependent oxidation of reduced cytochrome *c* by putative SODm, etc.) (*14b,15a, g,h*) and thus interfere in the determination of the SOD activity. There are cases in the literature, where the cytochrome *c* assay provided nearly identical data as pulse radiolysis (for MnTE-2-PyP^{5+}, $MnCl_2$, and Mn(III) biliverdin complex, (*15i*)). However, some authors have questioned their validity, emphasizing that indirect methods cannot differentiate between catalytic decomposition and stoichiometric scavenging of superoxide by compounds under study (*14,15a*).

The discovery and activity of SOD enzymes were first reported by Fridovich and McCord using a cytochrome *c* assay (*15j*). In this assay, the ferricytochrome *c* is reduced by superoxide to give the reduced form of cytochrome *c*, which results in a spectral change. Inhibition of this reduction of cytochrome *c* was taken as a measure of SOD activity. Since then, the cytochrome *c* assay and other indirect assays have been widely used by investigators to assess the SOD activity of enzymes and putative SOD mimetics. As mentioned above, difficulties with these indirect assays can arise from several sources, especially when low molecular weight redox-active substances are investigated. For example, an agent with putative SOD activity can oxidize the reduced cytochrome (possibly resulting in a false positive signal for SOD activity), reduce ferricytochrome *c* (potentially leading to a false negative signal), or react stoichiometrically, not catalytically, with superoxide (i.e., a scavenger of superoxide) (*14*). The question is only about the kinetic competition between cytochrome *c* and superoxide. However, the concentration of applied superoxide under its

steady-state production during the assay is quite low, significantly lower than the concentration of cytochrome *c* so that the reaction between the complex and cytochrome *c* can compete with the reaction between cytochrome *c* and superoxide (especially that the second-order rate constants for the reaction between cytochrome *c* and some complexes can be quite high ca. $10^6 s^{-1}M^{-1}$ (*15k*)). Due to the high positive charge on the surface of cytochrome *c*, the reaction between it and the metal complexes becomes less prominent or can be even fully suppressed by increase of the positive charge on the complex. Therefore, in the case of the porphyrin complexes with high positive charges, it is most probably safe to use this assay, at least in respect to the cross-reaction with cytochrome *c*.

The indirect assays do not discriminate among all these possible cross-reactions and, in addition, do not provide information regarding the mechanism of action of putative SOD mimetics. We have demonstrated that small molecular weight redox-active metal complexes in their different oxidation forms, in which they occur within the SOD catalytic cycle, inevitably react with indicator substance during the SOD assay (*5b*). Independent of the redox potential of studied putative SOD mimetics, the cross-reaction with an indicator substance, for example, cytochrome *c*, is very difficult to avoid (Fig. 4).

Therefore, direct kinetic methods are the only alternative. There are in general two methodological approaches: the pulse radiolysis and stopped-flow techniques. Pulse radiolysis has drawbacks because it produces a low steady-state concentration of $O_2^{\bullet -}$; thus, in such experiment, it is difficult to achieve real catalytic conditions (superoxide in a large excess). A common and cheap source of superoxide is KO_2, which can be dissolved in aprotic DMSO, where it is relatively stable. In that way, much higher concentrations of $O_2^{\bullet -}$ can be obtained than by pulse radiolysis. Riley *et al*. have utilized stopped-flow kinetic analysis as a direct technique for monitoring superoxide decay kinetics, via the spectrophotometric signature of superoxide at 245 nm, where a DMSO solution of KO_2 is rapidly mixed (<2 ms) with an aqueous buffered solution of the catalyst in approximately 1:20 volume ratio (*14*).

From this type of analysis, an uncatalyzed decay of superoxide (second-order kinetics) can be distinguished from a catalyzed decay of superoxide (first-order kinetics) in the presence of a large excess of superoxide over the complex being screened (Eq. (8)). A second-order catalytic rate constant (k_{cat}) can be obtained (Eq. (8)) for an agent with true catalytic SOD activity. This direct determination of a true k_{cat} can be used to directly

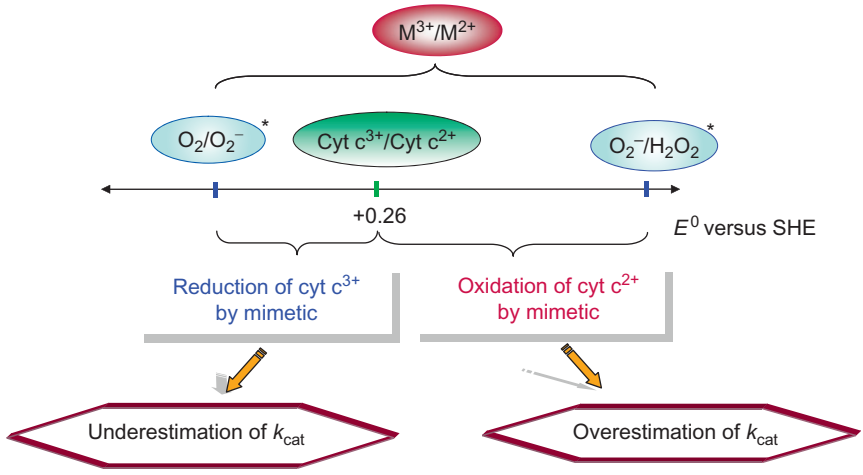

FIG. 4. Redox cross-reactions between metal-based SOD mimetic and cytochrome *c*.

compare and quantify the SOD activities of enzymes and/or mimetics under a given set of conditions (e.g., defined pH and temperature). No direct comparison can be made between the k_{cat} value and activity obtained from the cytochrome *c* assay or other indirect assays.

$$d\left[O_2^{\bullet -}\right]/dt = k_{self}\left[O_2^{\bullet -}\right]^2 + k_{cat}[\text{catalyst}]\left[O_2^{\bullet -}\right] \quad (8)$$

However, the above-mentioned method also has a limitation. Since the self-dismutation of superoxide, k_{self}, in 1:20 DMSO/H_2O mixture is already a very fast process, this technique can be used only for $k_{cat} > 10^{5.5} M^{-1} s^{-1}$. Even more problematic is to technically achieve rapid and efficient mixing of different volumes of two solutions with a big difference in viscosity. Further, DMSO itself has an absorption maximum in the same spectral range as superoxide, which requires significant dilution in order to be able to monitor the superoxide decay. Besides the work of Riley *et al.*, no one else could reproduce such experiments.

We have collaborated with the Bio-Logic company on optimizing their stopped-flow module μSFM-20 (Fig. 5a) for measurements with superoxide. This module is driven by high-speed stepping-motors with microprocessor control, enables

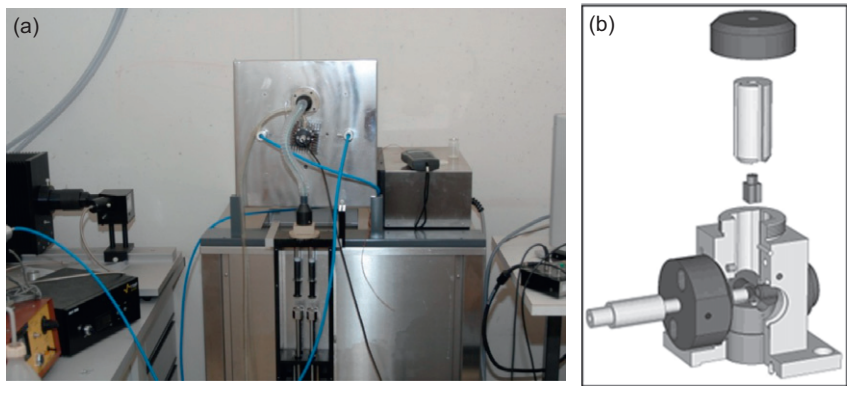

FIG. 5. The μSFM-20 module installed with the cryo-stopped-flow accessory (a) and the microcuvette accessory (b).

efficient and rapid mixing of solutions of high viscosity, and has a large solvent compatibility. It is the most powerful and flexible rapid mixing instrument existing today. Its high sample economy is even enhanced by a completely variable mixing ratio option. We have upgraded the μSFM-20 to a sub-millisecond mixing stopped-flow configuration (Fig. 5b) by combining it with a microcuvette accessory (with an optical path light of 0.8 mm) and a monochromator to minimize the dead time of the instrument. Studying the superoxide decomposition catalyzed by metal complexes by using only DMSO solutions (the DMSO spectrum is automatically subtracted from the sample spectra) and applying a microcuvette accessory (which reduced the dead time of the instrument to 0.4 ms), we can observe the pure catalyzed decay of superoxide at 270 nm as a first-order process. Uncatalyzed superoxide decomposition is suppressed in aprotic solvent; thus, the catalyzed process with any rate constant can be followed without the interference of the self-dismutation of $O_2^{\bullet -}$. In addition, mixing of two solutions of the same viscosity does not cause any unwanted effects. Further, as it was stressed by Sawyer *et al.* (*5a*), an even closer relation between the kinetic measurements in aprotic media than in bulk water can be drawn with the processes in mitochondria, which is the major source of superoxide in aerobic organisms, since aprotic media "may be representative of a hydrophobic biological matrix." Under less protic conditions, causing a longer half-life of $O_2^{\bullet -}$, efficient superoxide decomposition is even more desirable.

All the above-mentioned methods for the detection of SOD activity applied in the literature are based on single wavelength

measurements, which are used for the determination of the corresponding catalytic rate constants (k_{cat}). To achieve better control over the monitored process and to enable k_{cat} determination from the overall UV/vis spectral changes (global analysis of the entire time-resolved spectra), a double mixer stopped-flow system was combined with a fast diode array detector. For the first time, time-resolved spectroscopy has been utilized by us for the determination of SOD activities (Fig. 6) of different enzymatic and mimetic systems (25). Due to the short integration time (0.5 ms) for good quality spectra in the UV region, use of laser driven light source is recommended. Application of a high density mixer enables efficient mixing of aqueous buffer solutions containing SODm, with a DMSO solution of KO_2 (in a 10:1 ratio), so that this setup can be applied for the measurements in the presence of aqueous solutions too.

B. Enzymatic and Mimetic SOD Mechanism

The intriguing question is how the seven-coordinate geometry of metal complexes engenders its remarkable catalytic activity, exceeding that of the native mitochondrial MnSOD enzymes (Fig. 2), knowing that the coordination sphere of active metal centers in the native SOD enzymes is of different geometry.

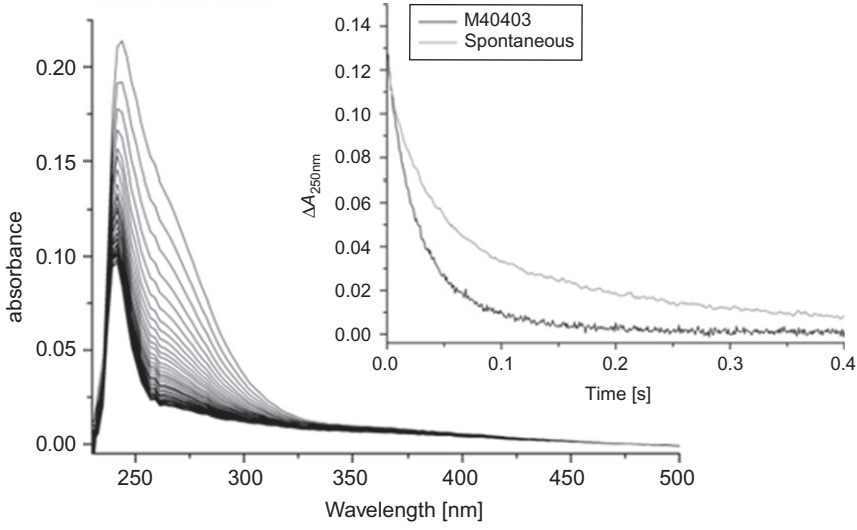

Fig. 6. Direct method for detection of SOD activity in aqueous solutions by time-resolved spectroscopy.

The arrangement of ligands in FeSODs is very similar to that in MnSODs, including human MnSOD, and both these classes of enzymes function in a fundamentally similar manner to that of Cu/Zn SODs. The geometry around Mn(III) and Fe(III) enzyme centers is trigonal bipyramidal with two histidines and one aspartate in the equatorial plane and with histidine and a solvent molecule (proposed to be OH^-) as axial ligands (Fig. 2) (*10a,26*). In all SOD enzymes, the metal cycles between oxidized and reduced states catalyzing the disproportionation of superoxide to dioxygen and hydrogen peroxide (Fig. 7), and in MnSODs and FeSODs, the metal alternates between five- and six-coordination. Ligated solvent (OH^-) acts as a proton acceptor in the reduction half-reaction; thus the water molecule becomes axially ligated to the Mn(II) and Fe(II) center, respectively. Both half-reactions, reduction and oxidation, are inner-sphere electron-transfer processes. The entering $O_2^{\bullet -}$ anion binds to the

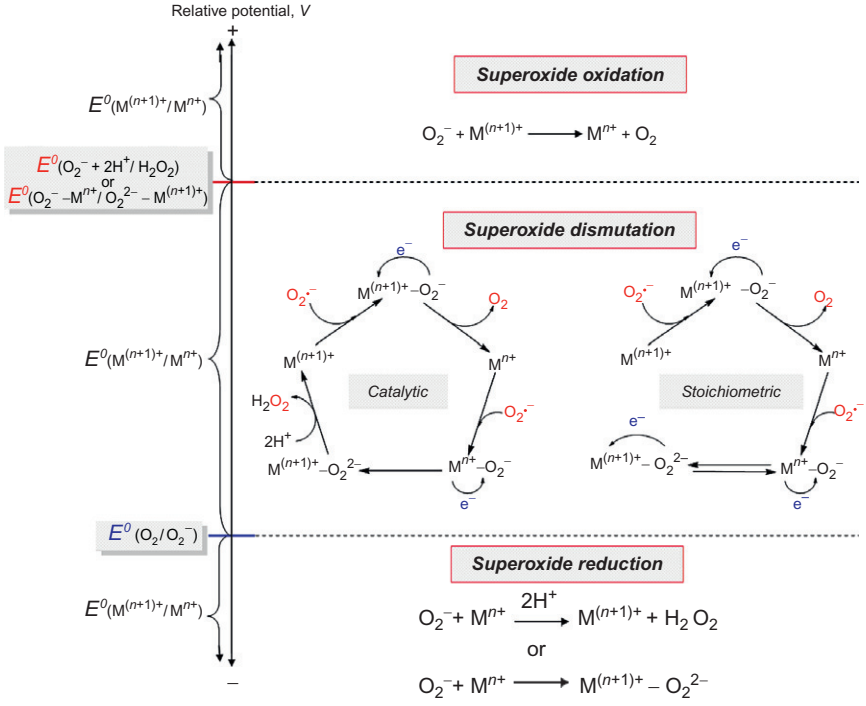

FIG. 7. Redox reaction between superoxide and metal centers: metal complexes can interact with $O_2^{\bullet -}$ either as catalysts for its dismutation (SOD mimetics) or in a stoichiometric manner.

metal in the *trans* position to the negative carboxylate aspartate group without displacement of the other metal ligands. Thus formation of the six-coordinate inner-sphere complexes is accompanied by very small perturbations of the metal and its ligands. In the iron SODs, protonation of Fe(III)-OH^- seems to be the rate-limiting step. The additional transfer of two protons takes place during the oxidative half-cycle, more precisely during the reduction of the coordinated superoxide anion. One proton comes from the ligated H_2O molecule to form Fe(II)-OOH^-, which dissociates a hydroperoxyl anion that is subsequently protonated to produce H_2O_2. Exactly this step, the dissociation of the peroxo complex promoted by proton transfer from the ligated H_2O to make peroxide a better leaving group, is the rate-determining step in the catalytic cycle of MnSOD enzymes. These crucial proton transfer pathways are not easy to infer from structural data, on which predominantly the proposed mechanisms are based (*10c*). As the assignment of species involved in proton transfer is notoriously difficult in the case of enzyme systems, relevant investigations on adequate model complexes could be of vast importance.

Without going into further details, it is important to point out that nature created the most efficient mechanism to enable fast catalytic turnover by selecting inner-sphere proton-coupled electron transfer as an efficient path that does not require charge separation in the transition state. It also requires minimal perturbations to form catalytic intermediates, without displacement of the other ligands in an associative manner. In contrast to the above-outlined mechanisms, the postulated mechanism for the catalytic action of the seven-coordinate Mn(II) SOD mimics (*13a*) is quite complicated, although resulting in amazingly fast catalytic processes. The postulated catalytic mechanism (Fig. 8) proceeds through two parallel but separated rate-determining steps, viz. pH-dependent outer-sphere and pH-independent inner-sphere oxidation of the Mn(II) complex. Both steps require profound conformational change of the pentadentate macrocyclic ligand, but these perturbations proceed also through two unique folding motifs yielding two different six-coordinate Mn(III) species. Mechanistic details are predominantly based on molecular mechanics calculations (*13a*), and there are not sufficient experimental data to support them. Therefore, a number of unresolved questions have arisen from the suggested reaction mechanism for the seven-coordinate Mn(II) type mimetics.

In the past years, it has been shown by us and others (*5b,15b,27*) that the mechanism of superoxide dismutation by small metal complexes proceeds predominantly by an inner-sphere mechanism,

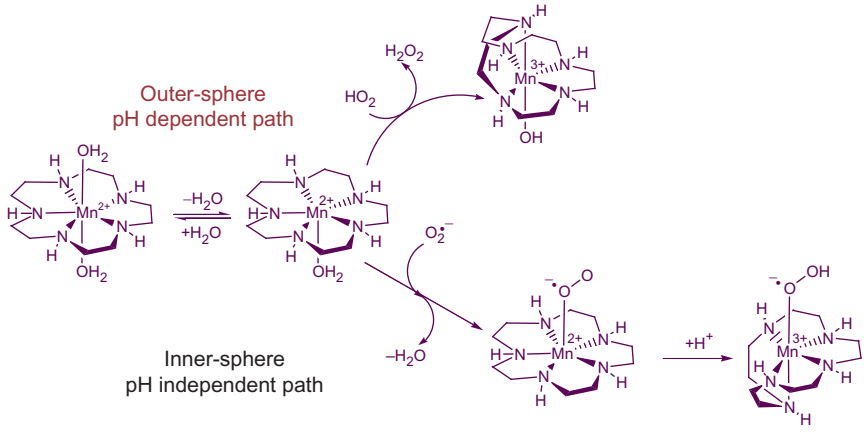

FIG. 8. Pustulated mechanism for superoxide dismutation by manganese pentaazamacrocyclic complexes (modified from Ref. *7b*).

which requires coordination of superoxide by substitution of a solvent molecule. The superoxide binding to the seven-coordinate metal centers follows an interchange associative rather than dissociative mechanism (*27*). This means that there is no need for the formation of a six-coordinate intermediate and a ligand conformational change along the catalytic pathway, as previously proposed (Fig. 8). In general, pentagonal–bipyramidal manganese and iron complexes bind nucleophiles according to an interchange associative mechanism and pass through an eight-coordinate transition state (Fig. 9). As a consequence, a pentadentate ligand can stay planar, that is, also conformational rigid ligand systems can be used for design of manganese and iron SOD mimetics.

C. Redox Properties and Interactions with Small Molecules

For the superoxide dismutation by a metal complex, it is necessary that the complex redox potential falls between the redox potentials for the reduction and oxidation of $O_2^{\bullet -}$ (Scheme 3). The potential range between -0.16V (or -0.33V with respect to a standard state of 1atm O_2 pressure; the reevaluated standard redox potential of the oxygen/superoxide couple is -0.137V) (*28*) and $+0.89$V versus NHE is commonly accepted in the literature as the range in which a metal center should exhibit its redox potential for having SOD activity (*29*). However,

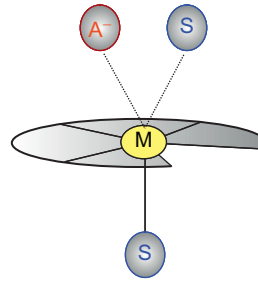

FIG. 9. Eight-coordinate transition state in an interchange associative mechanism of substitution reactions on a pentagonal–bipyramidal complex (S=solvent molecule, A^-=anionic monodentate ligand).

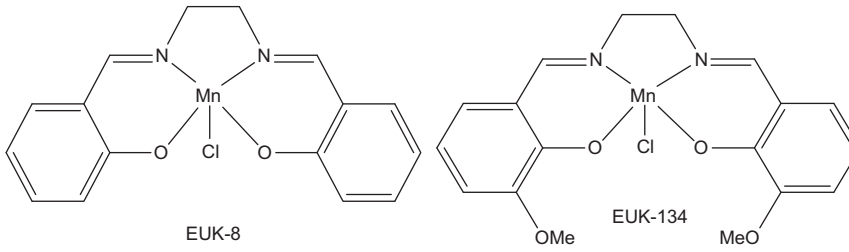

SCHEME 3. Two most studied representatives of Mn(III)(salen) type of SOD mimics.

the problem arises from the fact that these potentials correspond to the outer-sphere oxidation and reduction (at pH=7) of $O_2^{\bullet -}$ (*28*), respectively. In reality, metal complexes, with at least one labile monodentate ligand, usually react with superoxide according to an inner-sphere electron-transfer mechanism, due to the fact that $O_2^{\bullet -}$ is a very good nucleophile, which facilitates its coordination. Once $O_2^{\bullet -}$ is coordinated, its reduction potential shifts toward more positive values (Fig. 10) because peroxide, as the reduction product, is significantly stabilized by coordination to a positively charged metal center. To a certain extent, the oxidation potential of $O_2^{\bullet -}$ is also affected by its coordination, that is, it is also positively shifted, but this effect is not so prominent (Fig. 10). As a consequence, the redox potential of coordinated superoxide is difficult to predict and generalize, since it depends on the charge density and electronic properties of the metal center, which are in addition affected by the nature of the particular

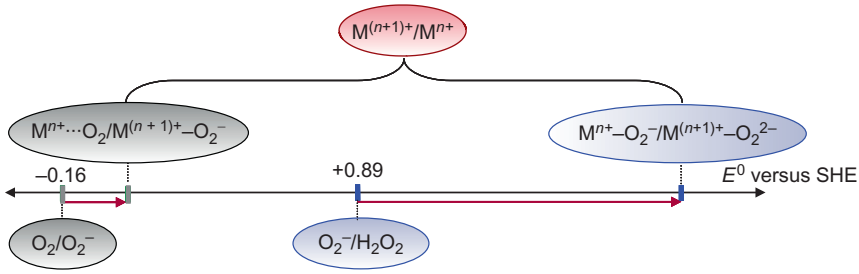

FIG. 10. Difference of reduction potentials for free and coordinated superoxide.

ligand system. Therefore, the correlations between the complex redox potentials and its SOD activity cannot be based on the known redox potentials for the outer-sphere oxidation and, in particular, reduction of $O_2^{\bullet -}$, as it is practiced in the literature (*30*), calling for systematic studies of this phenomenon in the future.

That inner-sphere electron transfer plays an important role within the SOD mechanism is shown by our preliminary experiments with the eight-coordinate Mn(II) complex (Fig. 11). Although the redox potential of this complex is similar to the redox potentials of some proven seven-coordinate Mn(II) SOD mimetics (approximately +0.78V vs. NHS) (*13a,g,31*), the studied eight-coordinate Mn(II) complex demonstrates no ability for catalytic superoxide dismutation. This can be explained in terms of the saturated coordination geometry around the metal center and shows that, for SOD activity, the complex redox potential is not the only important requirement. In the case of these complexes, with a relatively high redox potential, coordination of superoxide is crucial for its efficient reduction.

Besides the superoxide dismutation mechanism, the reactivity of metal centers, in particular manganese complexes, toward NO is very much dependent on the possibility for binding a substrate molecule. As it will be shown later, the possibility that MnSOD enzymes and some mimetics can react with NO has been wrongly excluded in the literature, simply based on the known redox potential for the (substrate) free enzymes, mimetics, and NO, respectively. Therefore, the general fact that, upon coordination, redox potentials of both the metal center and a coordinated species are changed should be considered in the case of any inner-sphere electron-transfer process as a possible reaction mechanism.

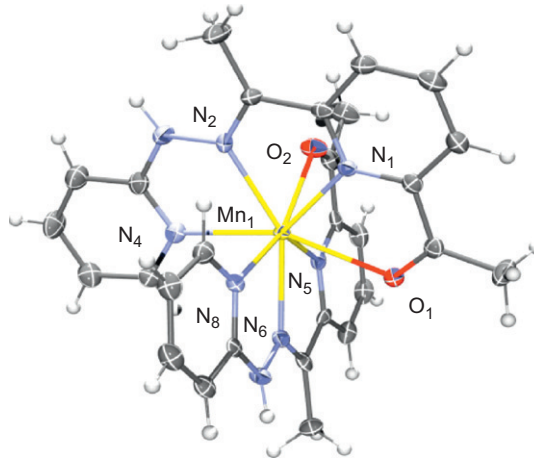

FIG. 11. Eight-coordinate Mn(II) complex.

V. Manganese SOD Enzymes and Reactive Nitrogen Species: Cross-reactivity, Not Selectivity

Although one of the major goals in designing SOD mimics is to "reproduce" strict selectivity of the natural enzyme, the past decade's research has seriously questioned the absolute selectivity of natural SOD enzymes toward superoxide. The first study to show that appeared in 1999 by Niketic *et al*. (*32*), where the authors demonstrated that Mn and Fe SOD enzymes (*E. coli*), but not CuZnSOD, react with NO under anaerobic conditions leading to the redox transformation of NO to nitroxyl (NO^-/HNO) and nitrosonium (NO^+) ions which produce enzyme modifications and inactivation, leading to the cleavage of the enzyme polypeptide chain.

Later, Quijano *et al*. (33) showed that both human recombinant and *E. coli* MnSOD react also with peroxynitrite with respective rate constants 1.0 ± 0.2 and $1.4\pm0.2 M^{-1}s^{-1}$. More importantly, this study demonstrated that removal of the metal center from the enzyme active site lowers the mentioned rate constant to $<10^4 M^{-1}s^{-1}$, whereas the reconstitution of the enzyme structure reestablishes the same reactivity toward peroxynitrite. The presence and the nature of the metal ion seem to be important for the observed reaction. While MnSOD showed reactivity toward peroxynitrite, the Zn-substituted enzyme did not. As a consequence of this reactivity, the characteristic tyrosine residue of the MnSOD enzyme is nitrated which causes the loss of the enzyme activity. Further, the produced $NO_2^\bullet$ is capable of reacting

with the surrounding molecules/tyrosine residues increasing the nitration yield. Quijano *et al*. (*33*) proposed that the manganese ion in MnSOD plays an important role not only in the decomposition kinetics of peroxynitrite but also in peroxynitrite-dependent nitration of self and remote tyrosine residues.

More recently, Filipovic *et al*. (*34*) readdressed the reaction of NO with MnSOD under both aerobic and anerobic conditions. In this study, Filipovic *et al*. (*34*) showed that MnSOD indeed reacts with NO under anaerobic conditions which leads to the complete loss of the enzyme activity. However, in the presence of glutathione, a possible scavenger of the proposed NO^+ and NO^- species, the activity of the enzyme remains preserved while the amount of removed NO increased, implying the catalytic process (Fig. 12). The authors proposed that this reaction should be referred to as NO dismutation:

$$Mn^{3+}(SOD) + NO \rightarrow Mn^{2+}(SOD)\cdots NO^+$$

$$Mn^{2+}(SOD) + NO \rightarrow Mn^{3+}(SOD)\cdots NO^-$$

In the same study (*34*), the reaction of MnSOD with NO under aerobic (and thus more physiological) conditions was also studied, and the second-order rate constant for the reaction of MnSOD (*E. coli*) with NO under aerobic conditions was determined to be $650 M^{-1}s^{-1}$. It should be mentioned that this rate constant is not the catalytic rate constant for NO removal by MnSOD, since the experimental conditions used in the study were not catalytic. Further, it is possible that this constant is largely underestimated because of the relatively slow response time of the NO electrode used in the study to follow the reaction. However, the authors demonstrate that dismutation indeed takes place and that even reduction of NO, considered to be thermodynamically impossible (*vide infra*), is possible. More importantly, they propose that this reaction could present a defense mechanism against overproduction of NO and its subsequent toxic effects due to the reaction with superoxide and peroxynitrite formation. These two reactions of MnSOD, one with NO and the other with ONOOH, stimulated further studies on SOD mimics with RNS and showed that none of them in fact posses strict selectivity toward superoxide.

VI. ROS Versus RNS

When talking about superoxide, its interaction with NO and NO signaling has to be taken into account. Since its discovery as an endothelium-derived relaxing factor (*35a*), NO has passed

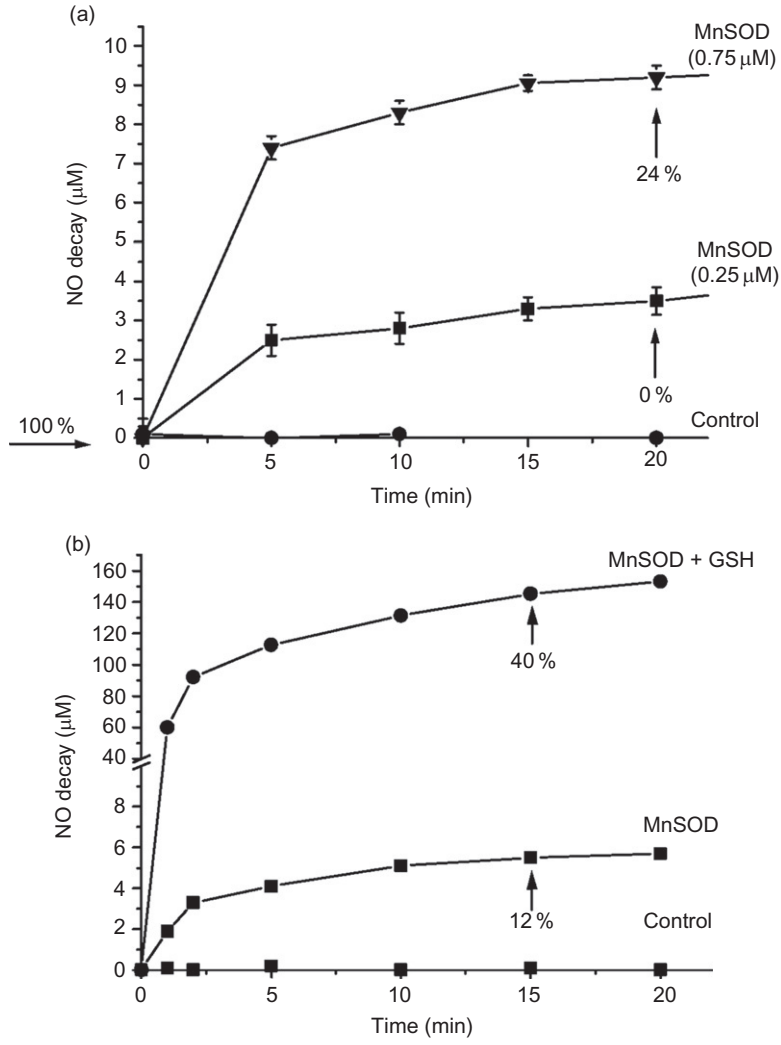

FIG. 12. MnSOD causes rapid NO decay in anaerobic solution. (a) Anaerobic NO solution (10 μM) in 50 mM phosphate buffer, pH 7.4, was incubated for 60 min at 23 C and subsequently for further 20 min following the injection of Ar-purged stock solution of MnSOD to the final indicated enzyme monomer concentrations. (b) Anaerobic NO solution (150 μM) in 50 mM phosphate buffer, pH 7.4, was incubated with MnSOD (0.45 μM subunit) with and without the supplementation with GSH (1 mM). Arrows indicate remaining enzyme activity as percentage of the control. Taken from Filipovic *et al*. (*34*).

from a signaling molecule involved in the regulation of blood pressure to the molecule that could alter the signaling of almost all metabolic pathways, as extensively reviewed elsewhere (*35b–j*). NO maintains these roles by reacting with metal centers of metalloenzymes (*35b,j*), by modulating SH groups of the protein (forming *S*-nitrosothiols or/and disulfides) (*36*), or/and by reacting with superoxide to form peroxynitrite (*37*). While the first two accounts for the physiological effects of NO, the latter mechanism is characteristic of pathological processes. SODs keep the level of superoxide below 10^{-10}M under normal, physiological conditions (*38*). However, when the enzyme activity is impaired or the enzyme level lowered, a possibility for peroxynitrite formation increases (Fig. 13) (*37a,b,13e*).

The reaction of NO and superoxide is diffusion controlled ($\sim 10^{10} M^{-1} s^{-1}$) (*37c*), and the chemistry, biochemistry, and pathophysiology of peroxynitrite have been extensively studied during the past two decades. Several excellent reviews are covering this subject (*37a,b,d,8f*). When produced, peroxynitrite modifies different biomolecules such as proteins (protein nitration, oxidation, aggregation), lipids (nitration and oxidation), DNA (oxidation) through nitration and oxidation reactions and as thus represents a very powerful toxic molecule (*37a,b,e,f,8c,f*). This is particularly the case during inflammation, which implies activation of immune cells and overproduction of both superoxide and NO (*37g,39*). Although addressed against pathogens as a defense mechanism, when prolonged, inflammation leads to severe tissue damage and represents the basis of numerous disease states (*13e,f*). The design of therapeutics against the inflammation-related diseases is thus traditionally divided into three levels: (i) aiming toward removal of superoxide (*13*), (ii) inhibition of iNOS (*40*), and recently, (iii) aiming toward scavenging peroxynitrite (*37a,d*). As presented in the following text, all the main three classes of SOD mimics maintain their strong pharmacological potential through reacting at more than one of the mentioned levels.

VII. Reaction of SOD Mimics with Peroxynitrite

Of the three most studied classes of MnSOD mimics, porphyrin-type mimics are most examined with respect to peroxynitrite (*41*). Reactivity of metal porphyrins with peroxynitrite was originally proposed by Stern *et al*. (*41a*), where authors showed that [Fe (III)TMPyP] possesses peroxynitrite isomerase activity. However, the activity of Mn porphyrins, particularly those that show SOD

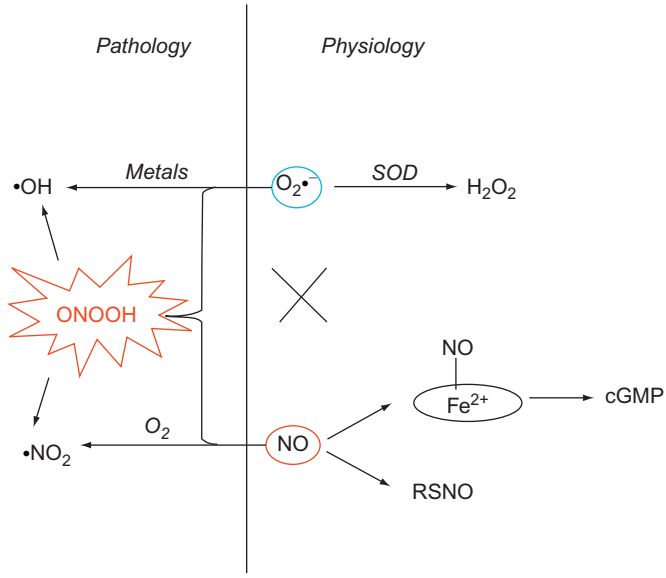

FIG. 13. Interplay of ROS and RNS in physiology and pathology. When produced at steady-state levels, superoxide is efficiently removed by SODs. Under these conditions, NO reacts mainly by activating soluble guanylate cyclase to produce cGMP and/or to induce posttranslational modification of protein by forming *S*-nitrosothiols. However, in different pathologies, when one or both of the molecules are overproduced or/and SOD levels reduced, NO and $O_2^{\bullet-}$ combine to give peroxynitrite, a powerful oxidant. Peroxynitrite can react directly with the biomolecules or can homolytically decompose to give OH and NO_2 radicals, both of which can additionally be formed in the reaction of superoxide with free metal ions and in reaction of NO with oxygen, respectively.

activity toward peroxynitrite, is mechanistically different. In the initial studies of Lee *et al.* (*41b*), it was shown that Mn(III)TMPyP reacts very fast with peroxynitrite, but only to produce the oxoMn (V) complex. Pseudo-catalysis is possible in the presence of reducing agents like ascorbate or glutathione, which would then reduce back the stable oxoMn(V) complex (Fig. 14).

In the paper following the discovery that MnSOD enzyme reacts with peroxynitrite, Ferrer-Sueta *et al.* (*41c*) examined a set of Mn porphyrins to show that they all react with peroxynitrite with the second-order rate constant being in the range of 10^5–$10^7 M^{-1}s^{-1}$. The authors noticed that the reactivity of the prophyrins toward $ONOO^-$ reflects an overall effect of the

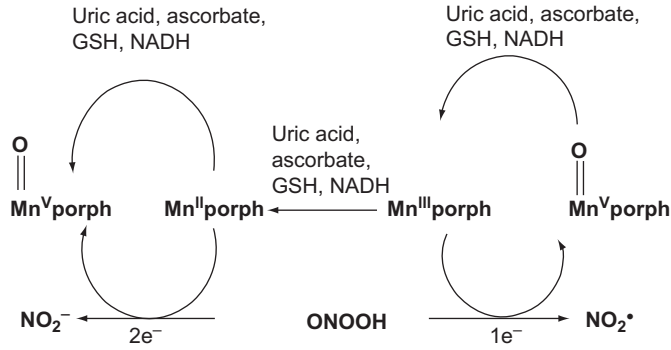

FIG. 14. Reaction mechanism for the Mn(III)(porphyrinato) SOD mimic-assisted peroxynitrite removal. For the detailed explanation, see the main text.

prophyrin ligand on the metal center, pointing out that the reaction proceeds by inner-sphere reaction mechanism with the rate-limiting step for the reaction being a coordination of peroxynitrite to the metal center. Conversely, the drawback of this reaction is the increased production of NO_2 and subsequent nitration of the surrounding molecules. In spite of this chemical notion, numerous physiological studies using porphyrin-based MnSOD mimics showed beneficial effects in peroxynitrite-caused pathologies (*37d,41d,e*). The answer could lie in the fact that, although applied as Mn(III)porphyrins, when distributed *in vivo*, these complexes get reduced easily by the reducing environment in the cells, which then changes the chemistry and the mechanism of their action. Mn(II) complexes react with peroxynitrite also to produce Mn(V)oxo porphyrin, but together with nitrite no NO_2 radicals (Fig. 14).

Reactivity of other SOD mimics toward peroxynitrite was scarcely studied. Sharpe *et al*. (*42*) reported that manganese salen complexes (EUK-8 and EUK-134) could react with peroxynitrite which leads to the formation of oxomanganese salen complex. This complex possesses different reactivity and readily reacts with NO.

Mn(II)pentaazamacrocyclic complexes are least studied in terms of any other reactive oxygen or nitrogen species except superoxide, as the authors always stressed that they posses strict selectivity. However, we showed (*43*) that some representatives of this class do react with NO (*vide infra*) and suggested that a reaction is possible with peroxynitrite (*44*) as well. Figure 15 clearly shows that when present in solution, Mn

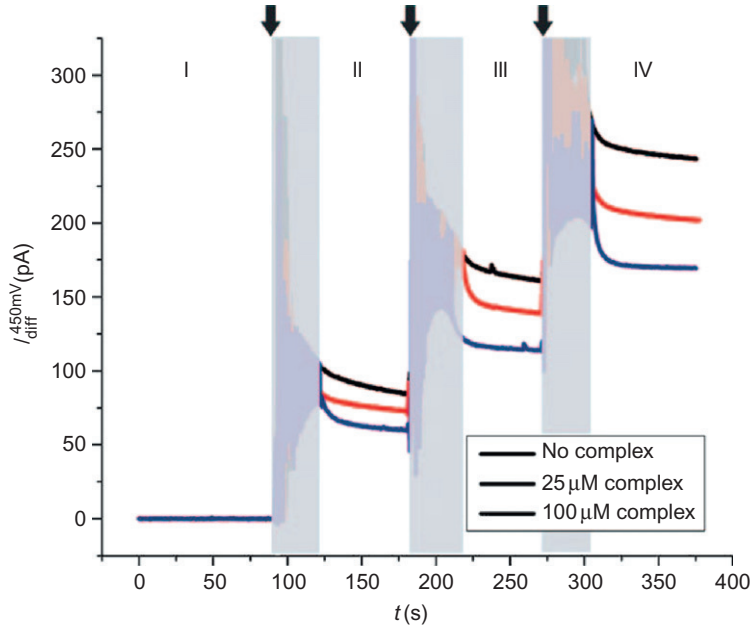

FIG. 15. Subtracted amperometric responses at +450 mV (I_{diff}^{450mV}) versus SSCE in PBS/NaOH (pH≈10.5) using the same platinized carbon microelectrode. The dotted curves were obtained in the absence of [Mn(II)(pyane)Cl_2], whereas the dashed and solid curves were obtained in the presence of 25 and 100 μM of the complex, respectively. Region I corresponds to the period prior to $ONOO^-$ addition, while regions II–IV correspond to the initial $ONOO^-$ concentrations of 12.8, 25.0, and 36.6 μM, respectively. The arrows and shaded areas correspond to injections of $ONOO^-$ and mixing of the solution. Taken from Filipovic *et al.* (*44*).

(II)(pyane) causes the removal of peroxynitrite as measured amperometrically. However, this observation warrants further investigation.

VIII. Reaction of MnSOD Mimics with NO

The main targets of successfully designed SOD mimics are said to be inflammation-based diseases where overproduction of superoxide takes place. SOD mimics would thus remove superoxide, producing H_2O_2, or could remove both (like in the case of salen complexes). In this way, the role of NO would remain

preserved and subsequent formation of peroxynitrite (which can additionally be removed efficiently by porphyrin-type of SOD mimics, as mentioned above) prevented. Because of this main dogma, interestingly, very few studies dared to test it and measure direct reaction of MnSOD mimics with NO. In the light of our previous findings that the MnSOD enzyme could react with NO through a possible dismutation mechanism (*34*), we studied in details the reaction of pentaazamacrocyclic SOD mimics with NO *in vitro* (*43*) and on a cellular model (*44*).

One of the main problems with studying nonporphyrin Mn complexes with SOD acitivity is that the UV–vis spectral properties are very limited and not well defined, so the need for combination of different other spectroscopic methods is needed. By combining the amperometric detection of NO consumption, with ATR-FTIR, EPR, and MS spectrometry, together with some analytical methods for detection of the products, we were able to detect all reaction steps behind the reaction of Mn(II) pentaazamacrocyclic SOD mimics and NO. The addition of SOD active [Mn(pyane)] and inactive [Mn(pydiene)] complexes (Scheme 4) into NO solution leads to immediate removal of NO. This process was followed by formation of three distinctive IR bands at 1840, 1653, and 1647 cm^{-1} assigned to $Mn(II)NO^+$ and six- and seven-coordinate $Mn(III)NO^-$, respectively, as Mn(III) is not very stable in seven-coordinate geometry and an equilibrium between seven- and six-coordinate species exists in the solution (*27*). Consequently, when followed by EPR, the cycling between EPR active Mn(II) and EPR inactive Mn(III) could be observed (Fig. 16).

Together with the detection of *S*-nitrosothiols (as a marker of NO^+ chemistry) (*45a*) and hydroxylamine (as a marker of NO^-/HNO chemistry) (*45b*), we proposed the following reaction mechanism:

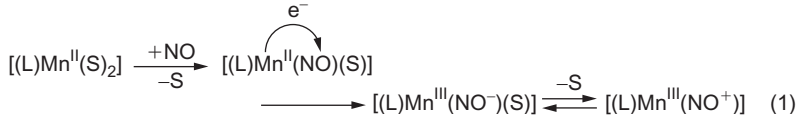

Different Mn complexes have been reported to react with NO, either to yield metal nitrosyls or to produce N_2O and metal

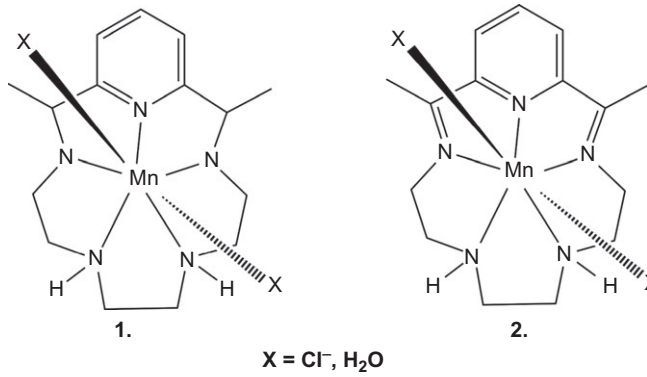

SCHEME 4. Chemical structure of two representatives of Mn (pentaazamacrocyclic) complexes studied for the reaction with NO. **1**, SOD active complex [Mn(II)(pyane)]; **2**, SOD inactive precursor of **1**, [Mn(II)(pydiene)].

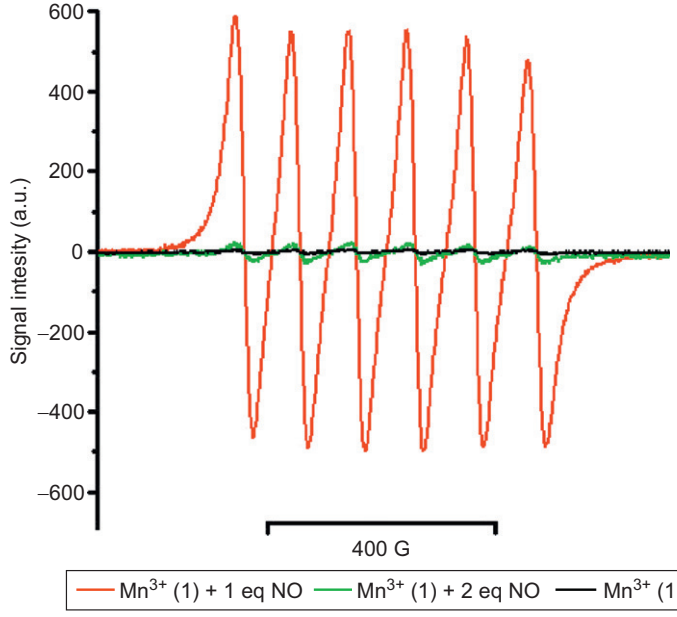

FIG. 16. Changes in the EPR spectra recorded during the reaction of NO with the Mn(III) form of **1** (200 μM) (T=25 °C, 50 mM phosphate buffer at pH 7.4). A synthetic NO donor (DEA-NONOate) was used as a source of NO (1eq=100 μM). Instrument settings: microwave frequency 9.51 GHz; power 10 mW; modulation amplitude 2 G; gain 2×10^4. Taken from Filipovic *et al*. (*43*).

nitrite complexes by NO disproportionation (*46*). To distinguish the mechanism proposed for Mn(II)pentaazamacrocyclic complexes and MnSOD enzyme from these processes, we proposed that the term NO dismutation should be used.

It should be emphasized that one of the reasons why most of the MnSOD mimics, in particular pentaazamacrocyclic complexes, have not been tested for the reaction with NO is because of the prevailing opinion that all of them do not have sufficiently high redox potential to reduce NO via outer-sphere electron transfer (redox potential of these MnSOD mimetics is >0.8 V, NHE) (*47a*). However, these complexes are generally prone to react with different monodentate ligands, and coordination of NO is quite feasible. Once NO coordinates, its redox potential shifts toward significantly more positive values, enabling an inner-sphere electron transfer resulting in the Mn(III)NO^- nitrosyl species.

Due to the same misinterpretation of the real meaning of the known redox potential for the MnSOD enzyme, it has been questioned whether MnSOD could reduce NO (*47b*). The question in most recent literature still exists: "Can we provide a definite answer to the endogenous HNO (nitroxyl) production paradox?" (*47b*). The authors conclude that NO reduction by MnSOD is highly endergonic and unlikely because the $NO,H^+/NO^-$(HNO) couple has the low redox potential of ca. -0.55 to -0.8V compared to $+0.3$V for MnSOD. However, as we have already mentioned and experimentally confirmed, the reduction of NO by Mn centers of even very high redox potentials (>0.8V, NHE) is possible if the reaction proceeds according to an inner-sphere mechanism, which is usually the case.

The reduction of NO to nitroxyl is of special biochemical and physiological significance and consequence. Although the chemistry and physiology of nitroxyl are not the subject of this review and could be found covered elsewhere (*47c–e)*, it should be mentioned that nitroxyl (NO^-/HNO) possesses physiological effects distinct to that of NO. It has been shown that unlike NO donors, HNO donors do not develop nitrate-tolerance and as thus possess strong pharmacological potential in the treatment of cardiovascular diseases (*47e*). HNO has been recently also shown to posses anticarcinogenic properties (*47c*). While the design of organic molecules that would serve as donors of HNO is an on-going process (*47f*), we believe that the rational design of metal complexes, which would posses NO reductase or NO dismutase activity, could be as efficient and beneficial.

The importance of our *in vitro* finding was further tested on a cellular model (*44*). As previously explained, the main target

for SOD mimic application are different inflammation-based diseases (*13*), all of which are characterized not only by increased superoxide formation but also by increased expression of inducible nitric oxide synthase (iNOS) that leads to overproduction of NO. Modern therapies rely on either inhibitors of iNOS or scavenging of superoxide. However, achieving the selective inhibition of iNOS is still a challenge and most of the molecules inhibit the activities of other NOS enzymes as well (*40*). We proposed that our observed NO dismutase activity coupled to SOD activity could be a new way to attack the inflammation from both sides.

We used a unique amperometric technique that allows measurement of hydrogen peroxide, NO, ONOOH, and NO_2^- on a single cell level, developed by the group of Amatore (*48*). In such experiments, a platinized carbon-disk microelectrode was positioned in close proximity to the cell membrane of a single macrophage. The release of the ROS/RNS is detected in real time by amperometry at a constant potential. This is, at the same time, the only known method for a direct detection and quantification of peroxynitrite (*48b,d*). Using immune-stimulated macrophages, as main actors in the production of ROS and RNS on the course of inflammation (*39*), we could actually measure the amount of the species released in untreated cells and [Mn(II)(pyane)]-treated cells. Treatment with pentaazamacrocyclic SOD mimics did not cause a change in cell morphology or survival. Surprisingly, however, the treatment with the SOD mimic completely abrogated the release of NO and peroxynitrite from the cells, but the protein and mRNA levels of iNOS remained unchanged implying that, as observed *in vitro*, [Mn(II)(pyane)] indeed efficiently scavenges NO, transforming it into less benign species. This method also allowed us to depict the chemical fate of each ROS and NOS species produced upon immune-stimulation of macrophages (Fig. 17).

To date, this is the first time that a chemical compound with a promising pharmacological effect has been reported to remove both superoxide and NO by transforming them into more benign species and without altering the normal enzymatic pathways for their production. This also questions the need for peroxynitrite scavengers when, in fact, this class of complexes efficiently prevents peroxynitrite generation and moderately reacts with it (see Fig. 17). Further studies on the possible disease models with emphasis on the ability to redox modulate NO metabolic pathways by this class of SOD mimics is the current goal of our studies.

The ability of Mn(III)(porphyrinato) SOD mimics to react with NO was first reported in the study by Pfeiffer *et al*. (*49*), where MnTMPyP was used. The authors observed no SOD activity of

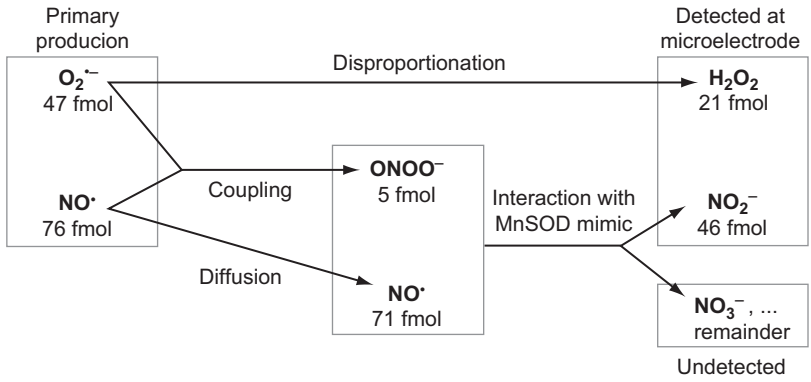

FIG. 17. Proposed scheme accounting for the detection of 21 fmol H_2O_2 and 46 fmol NO_2^- from the primary production of 76 fmol NO and 47 fmol $O_2^{\bullet-}$. Taken from Filipovic *et al.* (*44*).

this complex *in vivo*, arguing that this effect was overcome by inhibition of endothelial sGC at low concentration of the drug. More importantly, they observed that the present glutathione complex acts as a potent scavenger of NO. They proposed that it is the reduced Mn(II) form, formed when the complex was mixed with GSH, that binds NO so efficiently. Further, the complete removal of NO was observed even when substoichiometric concentrations of SOD mimic were used, implying a possible catalytic process. Spasojevic *et al.* (*50*) reported the reaction of another SOD mimic, manganese tetrakis(*N*-ethylpyridinium-2-yl)porphyrin (Mn(III)TE-2-PyP^{5+}), with NO. A rapid reaction of the reduced form of this complex with NO ($k \approx 1 \times 10^6 M^{-1} s^{-1}$) was observed with the formation of a manganese nitrosyl complex. The authors argue that the Mn(III) form of the complex does not react with NO, while Mn(II) binds NO. This raises the question of the actual physiological/pharmacological role of porphyrinato SOD mimics. As stated above, under physiological conditions, all Mn(III)porphyrins would be reduced so the observed reaction of NO binding (*50*) and/or its catalytic removal (*49*) could have important physiological effects and could account for some of the observed pharmacological effects. In Fig. 18, we present one of the possible reaction scenarios for the Mn(II)–NO complex formed in this reaction. Further, the observed peroxynitrite removal could be easily explained by the actual removal of both NO and superoxide and thus prevention of peroxynitrite formation rather than its removal. More importantly, Pfeiffer *et al.* (*49*) found that MnTMPyP also directly inhibits NOS, inhibiting thus further NO production and

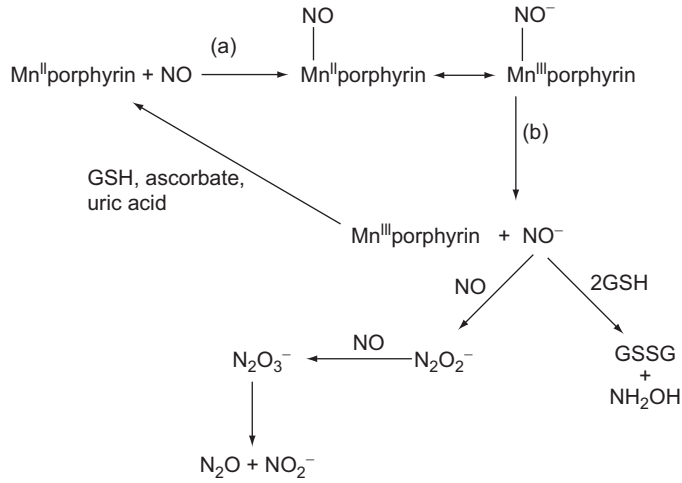

FIG. 18. Observed (a) and proposed (b) reaction pathways for the reaction of Mn(porphyrinato) SOD mimics with NO. As reported by Pfeiffer *et al*. (*49*), Mn(II)porphyrins bind NO efficiently (a) even causing its removal from the solution in substoichiometric concentrations implying a possible catalytic cycle. We propose (b) that the formed Mn(II)–NO complex exists also as Mn(III)–NO^-. NO^- could be released from the metal active site by further reaction with NO or glutathione (GSH) to form N_2O, nitrite, hydroxylamine, and GSSG. Mn(III) porphyrin that is released in this reaction could be reduced back to its Mn(II) form and react further in another cycle.

diminishing the peroxynitrite generation. Further studies on this are necessary, particularly in the direction of the chemical nature of the bound NO and its release from the porphyrin/reaction with another biomolecule.

Manganese salen complexes do not react with NO directly, but when exposed to different oxidants (H_2O_2, HOCl, ONOOH), they get oxidized to form a Mn(V)oxo salen complex which can then react with NO to form NO_2 or/and nitrite to form nitrate (Fig. 19) (*42*). The authors argue that Mn-Salens may prove to be therapeutic agents where NO overproduction is a factor in pathophysiology, for example, sepsis. Mn-Salens might prove useful in treating sepsis, and rational drug design or compound screening will locate Mn-Salens with poor catalase activity but rapid oxidation to oxoMn-Salens, which would result in a high level of oxoMn-Salen in the presence of oxidizing, inflammatory species. The oxoMn-Salens generated could then clear the body of a sepsis patient of excessive NO.

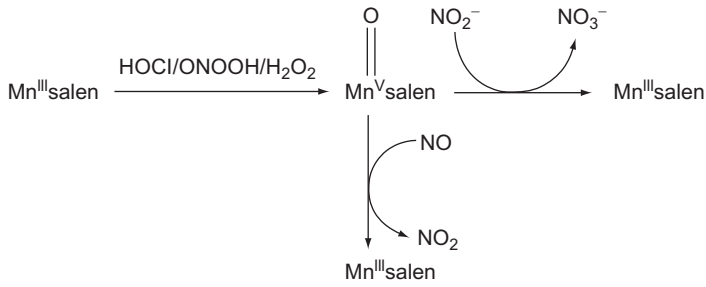

FIG. 19. Reaction of Mn(salen) SOD mimics with NO. For the detailed explanation, see the main text.

IX. Conclusion and Perspectives

The chemistry, biochemistry, and physiology of superoxide and NO and their interactions with metal centers are very complex issue, which requires a multidisciplinary approach. We are still not fully aware of the reactions that occur under relatively simple *in vitro* conditions, and we know even less about the real processes on a molecular level under *in vivo* conditions. Systematic studies and reliable, comparable data on number of different manganese SOD mimetics, regarding their reactivity toward reactive oxygen and nitrogen species and corresponding reaction mechanisms, are required for the further progress in the field and possible biomedical application of the gained knowledge. To date, there are very few studies which consider a number of different side reactions in which MnSOD mimetics may be involved, such as binding of physiologically relevant ligands (phosphates, oxalates, carbonate, carboxylates in general, chloride, different thiols, etc.) and their effects on the thermodynamic stability, kinetic lability, and reactivity toward NO and superoxide. These are very important questions, because Mn(II) complexes are in general quite labile, and under reductive intracellular conditions, the most probable oxidation state of all manganese centers is exactly 2+. It may even happen that *in vitro* SOD activity or NO reactivity of a designed Mn mimetic cannot be directly correlated with its physiological effects, because the complex can decompose and Mn can bind to other bioavailable nucleophiles resulting in different species with unknown reactivity. The role of the ligand in such cases would be just to deliver the manganese center to a particular cell compartment. Thus, future studies should be directed toward elucidation of the reactivity and speciation of Mn complexes *in vivo* by utilizing real time measurements, which are possible nowadays by applying

specially designed molecular fluorescence probes selective for NO, nitroxyl, superoxide, etc. Such methodology can be utilized for testing a possible decomplexation of Mn or distribution of Mn complex within the intracellular environment.

Due to the growing interest in the regulation of the cellular redox status and variety of signaling pathways aiming at modulating (patho)physiological processes for the benefit of health, the (bio) chemistry of manganese compounds and their reaction mechanisms certainly deserves innovative and visionary scientific approaches in the time ahead of us.

Abbreviations

SOD	superoxide dismutase
SODm	superoxide dismutase mimics
MnSOD	manganese superoxide dismutase
FeSOD	iron superoxide dismutase
Cu/ZnSOD	copper zinc superoxide dismutase
NiSOD	nickel superoxide dismutase
ROS	reactive oxygen species
RNS	reactive nitrogen species
GC	guanylate cyclase
cGMP	cyclic guanosine monophosphate
NOS	nitric oxide synthase
iNOS	inducible nitric oxide synthase
GSH	glutathione

Acknowledgment

We kindly acknowledge financial support from the Deutsche Forschungsgemeinschaft (SFB 583) and a grant from the University of Erlangen-Nuremberg (Emerging Field Initiative: Medicinal Redox Inorganic Chemistry).

References

1. (a) Fridovich, I. *Ann. N. Y. Acad. Sci.* **1999,** *893*, 13–28. (b) Fridovich, I. *J. Biol. Chem.* **1989,** *264*, 7761–7764.
2. Kaim, W.; Schwederski, B. *Bioinorganic Chemistry: Inorganic Elements in the Chemistry of Life.* Wiley: Chichester, England, **1994**.
3. (a) Salvemini, D.; Muscoli, C.; Riley, D. P.; Cuzzocrea, S. *Pulm. Pharmacol. Ther.* **2002,** *15*, 439–447. (b) Riley, D. P. *Chem. Rev.* **1999,** *99*, 2573–2587. (c) Dix, T. A.; Hess, K. M.; Medina, M. A.; Sullivan, R. W.; Tilly, S. L.; Webb, T. L. L. *Biochemistry* **1996,** *35*, 4578–4583. (d) Macarthur, H.; Westfall, T. C.; Riley, D. P.; Misko, T. P.; Salvemini, D. *Proc. Natl. Acad.*

Sci. USA **2000,** *97*, 9753–9758. (e) Aikens, J.; Dix, T. A. *Arch. Biochem. Biophys.* **1993,** *305*, 516. (f) Gryglewski, R. J.; Palmer, R. M.; Moncada, S. *Nature* **1986,** *320*, 454–456. (g) Liochev, S. I.; Fridovich, I. *IUBMB Life* **1999,** *48*, 157–161. (h) Mollace, V.; Nottet, H. S.; Clayette, P.; Torco, M. C.; Muscoli, C.; Salvemini, D.; Perno, C. F. *Trends Neurosci.* **2001,** *24*, 411–416. (i) Church, S. L.; Grant, J. W.; Ridenour, L. A.; Oberley, L. W.; Swanson, P. E. Meltzer. *Proc. Natl. Acad. Sci. USA* **1993,** *90*, 3113–3117. (j) Borgstahl, G. E. O.; Parge, H. E.; Hickey, M. J.; Johnson, M. J.; Boissinot, M.; Hallewell, R. A.; Lepock, J. R.; Cabelli, D. E.; Tainer, J. *Biochemistry* **1996,** *35*, 4287–4297.

4. (a) Sawyer, D. T.; Valentine, J. S. *Acc. Chem. Res.* **1981,** *14*, 393–400. (b) Sawyer, D. T.; Valentine, J. S. *Acc. Chem. Res.* **1982,** *15*, 200. (c) Sawyer, D. T.; Gibian, M. J.; Morrison, M. M.; Seo, E. T. *J. Am. Chem. Soc.* **1978,** *100*, 627–628. (d) Sawyer, D. T.; Gibian, M. J. *Tetrahedron* **1979,** *35*, 1471–1481.
5. (a) Chin, D. H.; Chiericato, G.; Jr., Nanni, E. J.; Jr., Sawyer, D. T. *J. Am. Chem. Soc.* **1982,** *104*, 1296–1299. (b) Liu, G.-F.; Filipovic, M.; Heinemann, F. W.; Ivanovic-Burmazovic, I. *Inorg. Chem.* **2007,** *46*, 8825–8835.
6. Morimoto, Y.; Kotani, H.; Park, J.; Lee, Y.-M.; Nam, W.; Fukuzumi, S. *J. Am. Chem. Soc.* **2011,** *133*, 403–405.
7. (a) Ivanovic-Burmazovic, I.; van Eldik, R. *J. Chem. Soc. Dalton Trans.* **2008,** 5259–5275. (b) Ivanovic-Burmazovic, I. *Adv. Inorg. Chem.* **2008,** *60*, 59–100.
8. (a) Ischiropoulos, H.; Beckman, J. S. *J. Clin. Invest.* **2003,** *111*, 163–169. (b) Ischiropoulos, H. *Biochem. Biophys. Res. Commun.* **2003,** *305*, 776–783. (c) MacMillan-Crow, L. A.; Cruthirds, D. L. *Free Radic. Res.* **2001,** *34*, 325–336. (d) MacMilln-Crow, L. A.; Thompson, J. A. *Arch. Biochem. Biophys.* **1999,** *366*, 82–88. (e) Filipovic, M. R.; Miljkovic, J.; Allgäuer, A.; Chaurio, R.; Shubina, T.; Herrmann, M.; Ivanovic-Burmazovic, I. *Biochem. J.* **2011,** in press. (f) Pacher, P.; Beckman, J. S.; Liaudet, L. *Physiol. Rev.* **2007,** *87*, 315–424.
9. Hart, P. J.; Valentine, J. S. In: "*Medicinal Inorganic Chemistry*"; Eds. Sessler, J. S., Doctrow, S. R., McMurray, T. J.; Lippard, S. J.; ACS and Oxford Press: New York, **2005**, pp. 348–365.
10. (a) Tierney, D. L.; Fee, J. A.; Ludwig, M. L.; Penner–Hahn, J. E. *Biochemistry* **1995,** *34*, 1661–1668. (b) Cass, A. E. G. In: "*Metalloproteins, Part I: Metal Proteins with Redox Roles*"; Ed. Harrison, P.; Verlag Chemie: Weinheim, **1985** pp. 121–156. (c) Barondeau, D. P.; Kassmann, C. J.; Bruns, C. K.; Tainer, J. A.; Getzoff, E. D. *Biochemistry* **2004,** *43*, 8038–8047.
11. (a) Lebovitz, R. M.; Zhang, H.; Vogel, H.; Cartwright, J.; Jr., Dionne, L.; Lu, N.; Huang, S.; Matzuk, M. M. *Proc. Natl. Acad. Sci. USA* **1996,** *93*, 9782–9787. (b) Li, Y.; Huang, T.-T.; Carlson, E. J.; Melov, S.; Ursell, P. C.; Olson, J. L.; Noble, L. J.; Yoshimura, M. P.; Berger, C.; Chan, P. H.; Wallace, D. C.; Epstein, C. J. *Nat. Genet.* **1995,** *11*, 376–381. (c) Reaume, A. G.; Elliott, J. L.; Hoffman, E. K.; Kowall, N. W.; Ferrante, R. J.; Siwek, D. F.; Wilcox, H. M.; Flood, D. G.; Beal, M. F.; Brown, R. H.; Jr., Scott, R. W.; Snider, W. D. *Nat. Genet.* **1996,** *13*, 43–47.
12. (a) Lefaix, J. L. *Int. J. Radiat. Oncol. Biol. Phys.* **1996,** *35*, 305–312. (b) Cuzzocrea, S.; Mazzon, E.; Dugo, L.; Caputi, A. P.; Riley, D. P.; Salvemini, D. *Eur. J. Pharmacol.* **2001,** *432*, 79–89.

13. (a) Riley, D. P.; Schall, O. F. *Adv. Inorg. Chem.* **2007,** *59*, 233–263. (b) Salvemini, D.; Wang, Z. Q.; Zweier, J. L.; Samouilov, A.; Macarthur, H.; Misko, T. P.; Currie, M. G.; Cuzzocrea, S.; Sikorski, J. A.; Riley, D. P. *Science* **1999,** *286*, 304–306. (c) Masini, E.; Cuzzocrea, S.; Mazzon, E.; Marzocca, C.; Mannaioni, P. F.; Salvemini, D. *Br. J. Pharmacol.* **2002,** *136*, 905–917. (d) Di Filippo, C.; Cuzzocrea, S.; Marfella, R., et al. *Eur. J. Pharmacol.* **2004,** *497*, 65–74. (e) Cuzzocrea, S.; Riley, D. P.; Caputi, A. P.; Salvemini, D. *Pharmacol. Rev.* **2001,** *53*, 135–159. (f) Muscoli, C.; Cuzzocrea, S.; Riley, D. P. J.; Zweier, L.; Thiemermann, C.; Wang, Z. Q.; Salvemini, D. *Br. J. Pharmacol.* **2003,** *140*, 445–460. (g) Salvemini, D.; Mazzon, E.; Dugo, L.; Riley, D. P.; Serraino, I.; Caputi, A. P.; Cxuzzocrea, S. *Br. J. Pharmacol.* **2001,** *132*, 19–29.

14. (a) Riley, D. P.; Rivers, W. J.; Weiss, R. H. *Anal. Biochem.* **1991,** *196*, 344–349. (b) Weiss, R. H.; Flickinger, A. G.; Rivers, W. J.; Hardy, M. M.; Aston, K. W.; Ryan, U. S.; Riley, D. P. *J. Biol. Chem.* **1993,** *268*, 23049–23054.

15. (a) Goldstein, S.; Michel, C.; Bors, W.; Saran, M.; Czapski, G. *Free. Radic. Biol. Med.* **1988,** *4*, 295–303. (b) Maroz, A.; Kelso, G. F.; Smith, R. A. J.; Ware, D. C.; Anderson, R. F. *J. Phys. Chem. A* **2008,** *112*, 4929–4935. (c) McClune, G. J.; Fee, J. A. *Biophys. J.* **1978,** *24*, 65–69. (d) Regelsberger, G.; Laaha, U.; Dietmann, D.; Rüker, F.; Canini, A.; Grilli-Caiola, M.; Furtmüller, P. G.; Jakopitsch, C.; Peschek, G. A.; Obinger, C. *J. Biol. Chem.* **2004,** *279*, 44384–44393. (e) Abreu, I. A.; Cabelli, D. E. *Biochim. Biophys. Acta* **1804,** *2010*, 263–274. (f) Barnese, K.; Gralla, E. B.; Cabelli, D. E.; Valentine, J. S. *J. Am. Chem. Soc.* **2008,** *130*, 4604–4606. (g) Beyer, W. F.; Jr., Fridovich, I. *Anal. Biochem.* **1987,** *161*, 559–566. (h) Diguiseppi, J.; Fridovich, I. *Arch. Biochem. Biophys.* **1980,** *203*, 145–150. (i) Spasojevic, I.; Batinic-Haberle, I.; Stevens, R. D.; Hambright, P.; Thorpe, A. N.; Grodkowski, J.; Neta, P.; Fridovich, I. *Inorg. Chem.* **2001,** *40*, 726–739. (j) McCord, J. M.; Fridovich, I. *J. Biol. Chem.* **1969,** *244*, 49–55. (k) Wherland, S.; Gray, H. B. *Proc. Natl. Acad. Sci. USA* **1976,** *73*, 2950–2954.

16. (a) Pasternack, R. F.; Banth, A.; Pasternack, J. M.; Johnson, C. S. *J. Inorg. Biochem.* **1981**, *15*, 261; (b) Duke University PCT Int. Appl. WO9609053, **1996**; (c) Duke University PCT Int. Appl. WO9640223, **1996**; (d) Duke University PCT Int. Appl. WO5227405, **1993**; (e) EUKARION, Inc. U.S. Patent US5696109, **1997**; (f) EUKARION, Inc. PCT Int. Appl. WO9640148, **1996**; (g) Coleman, N. W.; Taylor, L. T.; *Inorg, Chim. Acta.* **1982**, *61*, 13–17.

17. (a) Batinić-Haberle, I. *Methods Enzymol.* **2002,** *349*, 223–233. (b) Batinić-Haberle, I.; Rebouças, J. S.; Spasojević, I. *Antioxid. Redox. Signal.* **2010,** *13*, 877–918.

18. (a) Cuzzocrea, S.; Costantino, G.; Mazzon, E.; Zingarelli, B.; De Sarro, A.; Caputi, A. P. *Biochem. Pharmacol.* **1999,** *58*, 171–176. (b) Cuzzocrea, S.; Zingarelli, B.; Constantino, G.; Caputi, A. P. *Free Radic. Biol. Med.* **1999,** *26*, 25–33. (c) Ling, X.; Liu, D. *J. Neurosci. Res.* **2007,** *85*, 2175–2185. (d) Martin, R. C.; Liu, Q.; Wo, J. M.; Ray, M. B.; Li, Y. *Clin. Cancer Res.* **2007,** *13*, 5176–5182. (e) Muscoli, C.; Cuzzocrea, S.; Ndengele, M. M.; Mollace, V.; Porreca, F.; Fabrizi, F.; Esposito, E.; Masin, M.; Matuschak, G. M.; Salvemini, D. J. *J. Clin. Invest.* **2007,** *117*, 1–11. (f) Patel, M. *Aging Cell* **2003,** *2*, 219–224. (g) Khaldi, M. Z.; Elouil, H.; Guiot, Y.; Henquin, J. C.; Jonas, J. C. *Am. J. Physiol. Endocrinol. Metab.* **2006,** *29*, E137–E146. (h) McKinnon, R. L.; Lidington, D.; Tyml, K. *Microcirculation* **2007,** *14*, 697–707. (i)

Rebouças, J. S.; Spasojević, I.; Batinić-Haberle, I. *J. Inorg. Biol. Chem.* **2008,** *13*, 289–302.
19. (a) Rosenthal, R. A.; Huffman, K. D.; Fisette, L. W.; Damphousse, C. A.; Callaway, W. B.; Malfroy, B.; Doctrow, S. R. *J. Biol. Inorg. Chem.* **2009,** *14*, 979–991. (b) Rosenthal, R. A.; Doctrow, S. R.; Callaway, W. B. *Antioxid. Redox. Signal.* **2011,** *14*, 1173. (c) Batinic-Haberle, I.; Reboucas, J. S.; Spasojevic, I. *Antioxid. Redox. Signal.* **2011,** *14*, 1174–1176.
20. (a) EUKARION, Inc. U.S. Patent US5696109, **1997**; (b) EUKARION, Inc. PCT Int. Appl. WO9640148, **1996**.
21. Doctrow, S. R.; Baudry, M.; Huffmann, K.; Malfroy, B.; Melov, S. In: "*Medicinal Inorganic Chemistry*"; Eds. Sessler, J. S., Doctrow, S. R., McMurray, T. J.; Lippard, S. J.; ACS and Oxford Press: New York, **2005** pp. 319–347.
22. Pollard, J. M.; Rebouças, J. S.; Durazo, A.; Kos, I.; Fike, F.; Panni, M.; Gralla, E. B.; Valentine, J. S.; Batinić-Haberle, I.; Gatti, R. A. *Free Radic. Biol. Med.* **2009,** *47*, 250–260.
23. Coleman, N. W.; Taylor, L. T. *Inorg. Chim. Acta* **1982,** *61*, 13–17.
24. Failli, P.; Bani, D.; Bencini, A.; Cantore, M.; Mannelli, L. D. C.; Ghelardini, C.; Giorgi, C.; Innocenti, M.; Rugi, F.; Spepi, A.; Udisti, R.; Valtancoli, B. *J. Med. Chem.* **2009,** *52*, 7273–7283.
25. Friedel, F. C.; Lieb, D.; Ivanovic-Burmazovic, I. *J. Inorg. Biochem.* **2011,** in press.
26. Lah, M. S.; Dixon, M. M.; Pattridge, K. A.; Stallings, W. C.; Fee, J. A.; Ludwig, M. L. *Biochemistry* **1995,** *34*, 1646–1660.
27. Dees, A.; Zahl, A.; Puchta, R.; van Eikema Hommes, N. J. R.; Heinemann, F. W.; Ivanovic-Burmazovic, I. *Inorg. Chem.* **2007,** *46*, 2459–2470.
28. (a) Stanbury, D. M. *Adv. Inorg. Chem.* **1989,** *33*, 70–138. (b)Petlicki, J.; van de Ven, T. G. M. *J. Chem. Soc., Faraday Trans.* **1998,** *94*, 2763–2767.
29. Zhang, D.; Busch, D. H.; Lennon, P. L.; Weiss, R. H.; Neumann, W. L.; Riley, D. P. *Inorg. Chem.* **1998,** *37*, 956–963.
30. (a) Durot, S.; Policar, C.; Cisnetti, F.; Lambert, F.; Renault, J.-P.; Pelosi, G.; Blain, G.; Korri-Youssoufi, H.; Mahy, J.-P. *Eur. J. Inorg. Chem.* **2005,** *17*, 3513–3523. (b) Batinić-Haberle, I.; Spasojević, I.; Stevens, R. D.; Hambright, P.; Neta, P.; Okado-Matsumoto, A.; Fridovich, I. *Dalton Trans.* **2004,** 1696–1702.
31. (a) Riley, D. P.; Weiss, R. H. *J. Am. Chem. Soc.* **1994,** *116*, 387–388. (b) Riley, D. P.; Lennon, P. J.; Neumann, W. L.; Weiss, R. H. *J. Am. Chem. Soc.* **1997,** *119*, 6522–6528.
32. Niketic, V.; Stojanović, S.; Nikolić, A.; Spasić, M.; Michelson, A. M. *Free Radic. Biol. Med.* **1999,** *27*, 992–996.
33. Quijano, C.; Hernandez-Saavedra, D.; Castro, L.; McCord, J. M.; Freeman, B. A.; Radi, R. *J. Biol. Chem.* **2001,** *276*, 11631–11638.
34. Filipovic, M. R.; Stanić, D.; Raicević, S.; Spasić, M.; Niketić, V. *Free Radic. Res.* **2007,** *41*, 62–72.
35. (a) Palmer, R. M.; Ferrige, A. G.; Moncada, S. *Nature* **1987,** *327*, 524–526. (b) Moncada, S.; Palmer, R. M.; Higgs, E. A. *Pharmacol. Rev.* **1991,** *43*, 109–142. (c) Nediani, C.; Raimondi, L.; Borchi, E.; Cerbai, E. *Antioxid. Redox Signal.* **2011,** *14*, 289–331. (d) Paul, V.; Ekambaram, P. *Indian J. Med. Res.* **2011,** *133*, 471–478. (e) Zhang, Y.; Janssens, S. P.; Wingler, K.; Schmidt, H. H.; Moens, A. L. *Am. J. Physiol. Heart Circ. Physiol.* **2011,** *301*, H634–H646. (f) Otasevic, V.; Korac, A.; Buzadzic, B.; Stancic, A.; Jankovic, A.; Korac, B. *Front. Biosci.* **2011,** *3*, 1180–1195. (g) Singh, S.; Gupta, A. K. *Cancer Chemother.*

Pharmacol. **2011,** *67*, 1211–1224. (h) Baudouin, E. *Plant Biol.* **2011,** *13*, 233–242. (i) Hirst, D. G.; Robson, T. *Methods Mol. Biol.* **2011,** *704*, 1–13. (j) Cary, S. P.; Winger, J. A.; Derbyshire, E. R.; Marletta, M. A. *Trends Biochem. Sci.* **2006,** *31*, 231–239.

36. (a) Stamler, J. S.; Singel, D. J.; Loscalzo, J. *Science* **1992,** *258*, 1898–1902. (b) Foster, M. W.; Hees, D. T.; Stamler, J. S. *Trends Mol. Med.* **2009,** *15*, 391–404. (c) Hogg, N. *Annu. Rev. Pharmacol. Toxicol.* **2002,** *42*, 585–600.

37. (a) Szabo, C.; Ischiropoulos, H.; Radi, R. *Nat. Rev. Drug Discov.* **2007,** *6*, 662–680. (b) Ferrer-Sueta, G.; Radi, R. *ACS Chem. Biol.* **2009,** *4*, 161–177. (c) Kissner, R.; Nauser, T.; Bugnon, P.; Lye, P. G.; Koppenol, W. H. *Chem. Res. Toxicol.* **1997,** *10*, 1285–1292. (d) Trujillo, M.; Ferrer-Sueta, G.; Radi, R. *Antioxid. Redox Signal.* **2008,** *10*, 1607–1620. (e) Rubbo, H.; Trostchansky, A.; O'Donnell, V. B. *Arch. Biochem. Biophys.* **2009,** *484*, 167–172. (f) Liaudet, L.; Vassalli, G.; Pacher, P. *Front. Biosci.* **2009,** *14*, 4809–4814. (g) Ahmad, R.; Rasheed, Z.; Ahsan, H. *Immunopharmacol. Immunotoxicol.* **2009,** *31*, 388–396. (h) Szabó, C.; Módis, K. *Shock* **2010,** *Suppl. 1*, 4–14.

38. Halliwell, B.; Gutteridge, J. M. C. *Free Radicals in Biology and Medicine.* Oxford University Press: Oxford, **2007**.

39. (a) Bogdan, C.; Röllinghoff, M.; Diefenbach, A. *Curr. Opin. Immunol.* **2000,** *12*, 64–76. (b) Bogdan, C. *Nat. Immunol.* **2001,** *2*, 907–916.

40. (a) Fitzpatrick, B.; Mehibel, M.; Cowen, R. L.; Stratford, I. J. *Nitric Oxide* **2008,** *19*, 217–224. (b) Hesslinger, C.; Strub, A.; Boer, R.; Ulrich, W. R.; Lehner, M. D.; Braun, C. *Biochem. Soc. Trans.* **2009,** *37*, 886–891. (c) Leiper, J.; Nandi, M. *Nat. Rev. Drug Discov.* **2011,** *10*, 277–291. (d) Vallance, P.; Leiper, J. *Nat. Rev. Drug Discov.* **2002,** *1*, 939–950.

41. (a) Stern, M. K.; Jensen, M. P.; Kramer, K. *J. Am. Chem. Soc.* **1996,** *118*, 8735–8736. (b) Lee, J.; Hunt, J. A.; Groves, J. T. *J. Am. Chem. Soc.* **1998,** *120*, 7493–7501. (c) Ferrer-Sueta, G.; Vitturi, D.; Batinic-Haberle, I.; Fridovich, I.; Goldstein, S.; Czapski, G.; Radi, R. *J. Biol. Chem.* **2003,** *278*, 27432–27438. (d) Asayama, S.; Nakajima, T.; Kawakami, H. *Metallomics* **2011,** *3*, 744–748. (e) Nin, N.; El-Assar, M.; Sánchez, C.; Ferruelo, A.; Sánchez-Ferrer, A.; Martínez-Caro, L.; Rojas, Y.; Paula, M.; Hurtado, J.; Esteban, A.; Lorente, J. A. *Shock* **2011,** *36*, 156–161. (f) Soriano, F. G.; Lorigados, C. B.; Pacher, P.; Szabó, C. *Shock* **2011,** *35*, 560–566. (g) Rabkin, S. W.; Klassen, S. S. *Eur. J. Pharmacol.* **2008,** *586*, 1–8. (h) Crow, J. P. *Free Radic. Biol. Med.* **2000,** *28*, 1487–1494. (i) Patel, M.; Day, B. J. *Trends Pharmacol. Sci.* **1999,** *20*, 359–364.

42. Sharpe, M. A.; Ollosson, R.; Stewart, V. C.; Clark, J. B. *Biochem. J.* **2002,** *366*, 97–107.

43. Filipovic, M. R.; Duerr, K.; Mojović, M.; Simeunović, V.; Zimmermann, R.; Niketić, V.; Ivanovic-Burmazovic, I. *Angew. Chem. Int. Ed Engl.* **2008,** *47*, 8735–8739.

44. Filipovic, M. R.; Koh, A. C.; Arbault, S.; Niketić, V.; Debus, A.; Schleicher, U.; Bogdan, C.; Guille, M.; Lemaître, F.; Amatore, C.; Ivanovic-Burmazovic, I. *Angew. Chem. Int. Ed Engl.* **2010,** *49*, 4228–4232.

45. (a) Stamler, J. S.; Feelisch, M. In: "*Methods in Nitric Oxide Research*"; Eds. Feelisch, M.; Stamler, J. S.; John Wiley & Sons, Ltd.: Chichester, England, **1996** pp. 521–539. (b) Wink, D. A.; Feelisch, M. In: "*Methods in Nitric Oxide Research*"; Eds. Feelisch, M.; Stamler, J. S.; John Wiley & Sons, Ltd.: Chichester, England, **1996** pp. 403–412.

46. (a) Franz, K. J.; Lippard, S. J. *J. Am. Chem. Soc.* **1999,** *121*, 10504–10512. (b) Martirosyan, G. G.; Azizyan, A. S.; Kurtikyan, T. S.; Ford, P. C. *Chem. Commun.* **2004,** 1488–1489. (c) Ford, P. C.; Lorkovic, I. M. *Chem. Rev.*

2002, *102*, 993–1017. (d) Roncaroli, F.; Videla, M.; Slep, L. D.; Olabe, J. A. *Coord. Chem. Rev.* **2007,** *251*, 1903–1930.

47. (a) Bartberger, M. D.; Liu, W.; Ford, P.; Miranda, K. M.; Switzer, C.; Fukuto, J. M.; Farmer, P. J.; Wink, D. A.; Houk, K. N. *Proc. Natl. Acad. Sci. USA* **2002,** *99*, 10958–10963. (b) Doctorovich, F.; Bikiel, D.; Pellegrino, J.; Suárez, S. A.; Larsen, A.; Martí, M. A. *Coord. Chem. Rev.* **2011,** *255*, 2764–2784. (c) Flores-Santana, W.; Salmon, D. J.; Donzelli, S.; Switzer, C. H.; Basudhar, D.; Ridnour, L.; Cheng, R.; Glynn, S. A.; Paolocci, N.; Fukuto, J. M.; Miranda, K. M.; Wink, D. A. *Antioxid. Redox Signal.* **2011,** *14*, 1659–1674. (d) Choe, C. U.; Lewerenz, J.; Gerloff, C.; Magnus, T.; Donzelli, S. *Antioxid. Redox Signal.* **2011,** *14*, 1699–1711. (e) Bullen, M. L.; Miller, A. A.; Andrews, K. L.; Irvine, J. C.; Ritchie, R. H.; Sobey, C. G.; Kemp-Harper, B. K. *Antioxid. Redox Signal.* **2011,** *14*, 1675–1686. (f) DuMond, J. F.; King, S. B. *Antioxid. Redox Signal.* **2011,** *14*, 1637–1648.

48. (a) Amatore, C.; Arbault, S.; Bouton, C.; Drapier, J. C.; Ghandour, H.; Koh, A. C. *Chembiochem* **2008,** *9*, 1472–1480. (b) Amatore, C.; Arbault, S.; Guille, M.; Lemaitre, F. *Chem. Rev.* **2008,** *108*, 2585–2621. (c) Amatore, C.; Arbault, S.; Bouton, C.; Coffi, K.; Drapier, J. C.; Ghandour, H.; Tong, Y. H. *Chembiochem* **2006,** *7*, 653–661. (d) Amatore, C.; Arbault, S.; Bruce, D.; de Oliveira, P.; Erard, M.; Vuillaume, M. *Chem. Eur. J.* **2001,** 7, 4171–4179.

49. Pfeiffer, S.; Schrammel, A.; Koesling, D.; Schmidt, K.; Mayer, B. *Mol. Pharmacol.* **1998,** *53*, 795–800.

50. Spasojevic, I.; Batinic-Haberle, I.; Fridovich, I. *Nitric Oxide* **2000,** *4*, 526–5133.

AZANONE (HNO) INTERACTION WITH HEMEPROTEINS AND METALLOPORPHYRINS

FABIO DOCTOROVICH[a], DAMIAN E. BIKIEL[a], JUAN PELLEGRINO[a], SEBASTIÁN A. SUÁREZ[a] and MARCELO A. MARTÍ[a,b]

[a]Departamento de Química Inorgánica, Analítica y Química Física/INQUIMAE-CONICET, Buenos Aires, Argentina
[b]Departamento de Química Biológica, Facultad de Ciencias Exactas y Naturales, Universidad de Buenos Aires, Ciudad Universitaria, Pab. II (1428), Buenos Aires, Argentina

Abstract

Azanone (HNO), also called nitroxyl, is a highly reactive compound, with interesting yet poorly understood biological properties. Like its closely related sibling NO, its main biological targets are heme proteins, although significant differences in their

INORGANIC/BIOINORGANIC REACTION MECHANISMS
VOLUME 64 ISSN 0898-8838 / DOI: 10.1016/B978-0-12-396462-5.00004-0

reactivity and pharmacological effects are observed. Due to its high reactivity, azanone studies rely on the use of donors, molecules that therefore offer interesting therapeutic perspectives. In this review, we firstly describe the pharmacological potential of azanone, the chemistry of the available donors, and the main biological relevant HNO reactions with special focus on heme proteins and metalloporphyrins (Fe, Mn, and Co). Finally, we present evidence concerning the endogenous *in vivo* azanone production hypothesis, and how the recent porphyrin-based developed methods for its detection may contribute to solve this key physiological question.

Keywords: HNO; NO; Nitroxyl; Azanone; Nitroxyl anion; Nitrosyl; Porphyrin; Heme; Iron; Manganese; Ruthenium; Cobalt; Reductive nitrosylation; Kinetics; Oxidation; Protein; Myoglobin; NOS.

I. Introduction: Chemistry and Biology of Azanone

A. Structure

Azanone (HNO), also called nitroxyl (*1*), is a highly reactive compound. Although nowadays it is accepted that singlet ^{1}HNO is the most stable form, triplet ^{3}NOH is also a viable molecule, and both have been observed. The energy gap between these species is estimated to be relatively low, around 20 kcal mol^{-1} (*2–4*).

From the structural viewpoint, ^{1}HNO displays a bent structure with the N atom as the central one and an H—N═O angle of about 109°. The N—O bond distance is predicted to be 1.211 Å which is, as expected, larger than the N—O bond distance in nitric oxide due to the addition of electron density to the π* orbital. Due to this fact, the NO infrared stretching frequency for ^{1}HNO is ca. 200 cm^{-1} smaller than for nitric oxide.

B. HNO Physiology I: Pharmacological Perspectives

Intense interest in the biological effects of HNO has emerged mainly due to the wide variety of studies of its closely related sibling nitrogen oxide (NO). Nitrogen oxides, especially NO, play an important role in many physiological processes, specifically in cardiovascular functions. It regulates blood flow by transmitting the relaxation signal from the endothelium, where NO is produced by endothelial heme-protein NO synthase (eNOS) to the

NO responsive vascular smooth muscle cells. Which harbor the NO receptor, the heme-containing soluble guanylate cyclase (sGC) (*5,6*).

The almost 10 years of sustained research in the field of nitrogen oxide-releasing drug development has yielded important vasodilators such as nitroglycerin. Interestingly, and in spite of the closely related reactivity of NO and HNO, the biochemical pathways of HNO have recently been shown to be quite different from those of NO. This understanding was achieved about 10 years ago, when several studies showed clear demonstrations that the presence of NO donors *in vivo* results in different effects as those observed for HNO donors (*7*). A number of recent reviews have compared and contrasted both the pharmacology and toxicology of HNO and NO (see Wink and coworkers (*8–10*)).

The possibly most important physiological reported effect of HNO is to cause a vasorelaxation response. It is quite accepted that HNO donors, such as Angeli's salt (AS), act in a similar fashion to that of NO, possibly targeting sGC. However, a key difference between the observed effects of HNO donors and NO is that the former shows preferential venous dilation while the latter tends to affect arterial and venous sides equally (*11*). Interestingly, HNO donors also cause an increase in cardiac muscle contractility, via a combined positive effect on the force related with muscle contraction, with simultaneous relaxation of the cardiac muscles (inotropic and lusitropic effects, respectively), resulting in increased cardiac output. A number of studies have been reported where several models are proposed in order to explain the mechanism of the abovementioned HNO effects. For example, HNO has been found to target a critical cysteine residue in sarco/endoplasmic reticulum Ca^{2+}-ATPase (cysteine 674 in SERCA2a) (*12*). It has also been shown that HNO modifies critical thiols in phosphorylating phospholamban and increases SERCA2a activity by removing an inhibition of the Ca^{2+} pump (*13*). In summary, to the present date, a significant body of evidence has been collected pointing to possible positive effects of HNO in preventing heart failure, by acting on various potential targets via diverse mechanisms. This is a strong incentive for the development of new HNO donors for pharmacological applications.

Another therapeutic application of HNO (or its donors) may stem from the finding that it may be a powerful preconditioning agent that helps to alleviate the negative consequences of an ischemic event and reperfusion injury, characterized by blood flow deprivation followed by hypoxia and eventual heart tissue necrosis. The corresponding studies show that a dramatic decrease in the infarct size was achieved by pretreating heart tissues with AS, (the most common HNO donor). However, it

has been shown that HNO simultaneously increases the infarction size if administered during an ischemic event. In this case, the pharmacological effect of NO is drastically different from that of HNO, since NO was found to have protective properties in cardiac ischemia reperfusion injuries when given during the reperfusion phase (*14*). Finally, HNO prodrugs may also be effective as anticancer agents, as HNO has been shown to irreversibly hamper activity of glyceraldehyde 3-phosphate dehydrogenase (GAPDH)—a critical enzyme in glycolysis, which most solid tumors utilize as their energy source.

In summary, HNO-releasing agents have interesting perspectives as potential therapeutic compounds. However, more work is needed to understand the chemical mechanisms underlying the observed physiological effects.

C. HNO Physiology II: *In Vivo* Endogenous Production

A key question related with HNO and its biological role concerns the possibility of *in vivo* endogenous formation of HNO. The studies at this respect are contradictory and a definite answer is still missing. The most accepted pathway for *in vivo* HNO production has been speculated to result from the enzymatic activity of nitric oxide synthase (NOS) under particular cofactor conditions (*15–17*). In the proposed reaction, the substrate arginine is reduced by six electrons to yield HNO according to the following reaction (Eq. (1)):

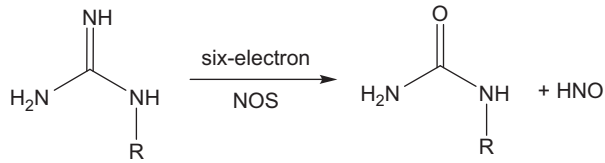

(1)

In the corresponding studies and based on N_2O and NH_2OH detection, the authors suggested that the product from NOS enzymatic turnover in the absence of the cofactor biopterin should be HNO and not NO (*16,18*). Additional evidence for endogenous HNO generation included detection of Fe(II)–NO coordination in NOS, rather than the usual ferric resting state (*16,19*). Very recently, Marletta and coworkers argued that in the last step of NO production by NOS, a biopterin-centered radical oxidizes the $\{FeNO\}^7$ to an $\{FeNO\}^6$ species, and then NO is released from the ferric iron. It remains, however, to be proven and seems unlikely that the $\{FeNO\}^7$ intermediate can actually

release $^3NO^-$ or ^1HNO (*20,21*). Although these and other results have been presented as evidence for HNO intermediacy in NOS metabolism, the HNO production mechanism has not been established conclusively and the results remain open to interpretation.

Another endogenous HNO source relies on the oxidation of hydroxylamine (HA), or other alcohol amine, such as hydroxyurea or *N*-hydroxy arginine. *In vivo*, such a process is postulated to depend on the activity of several heme proteins, which are able to stabilize oxo ferryl species (compound I and compound II), such as peroxidases. Recently, Donzelli *et al*. evaluated HNO production by this mechanism (*22*), with a newly developed selective assay in which the reaction products, $GS(O)NH^2$, in the presence of reduced glutathione (GSH) are quantified by HPLC. Their results showed that metmyoglobin, horse radish peroxidase, and myeloperoxidase were efficient HNO producers using hydroxylamine as substrate. However, there are several remaining unresolved questions concerning the proposed mechanism (which is outlined below, Eq. (2)).

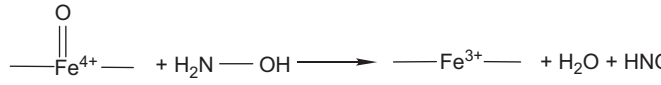

(2)

For example, one point of debate concerns whether the generated HNO molecule may escape from the ferric heme pocket, which seems unlikely given the HNO reactivity toward ferric hemes. Also important is the way in which the protein is driven to the formation of the oxo ferryl species *in vivo*, which *in vitro* was performed by the addition of H_2O_2 (*22,23*).

In the case of porphyrin models (*24*), it was proposed that for $[Fe^{III}(TPPS)]^{3+}$ the formation of HNO from hydroxylamine occurred by a two-electron *trans*-disproportionation of a bis-coordinated NH_2OH complex producing a low spin ferric intermediate $[Fe^{III}(Por)(NH_3)(HNO)]$. Based on the experimental kinetic evidence, and the obtained N_2/N_2O ratios from the reaction mixtures, a different mechanism was proposed for $Fe^{III}MP11$, in which the formation of $[Fe^{III}(Por)(NHis)(HNO)]$ was suggested to result from the reaction of free HA toward iron-bound HA.

Another endogenous suggested source of azanone stems from the reduction of NO to HNO by Mn or Fe superoxide dismutases (*25*) or by xanthine oxidase (XO) (*22*). Although both types of enzymes have been reported as capable of HNO production, the corresponding works relied on indirect methods for HNO detection which are sometimes difficult to interpret or unreliable.

Finally, there is at least one nonenzymatic proposed route for endogenous HNO production, which follows the decomposition of nitrosothiols (RSNOs) by other thiols (such as glutathione) according to the reaction shown below (Eq. (3)):

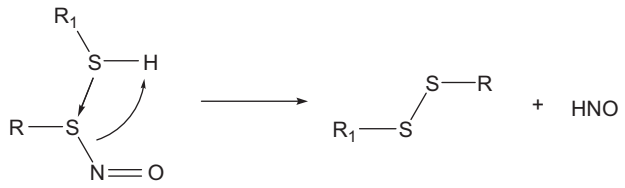

(3)

Although this mechanism has not been established for an *in vivo* process, *in vitro* studies show that the reactivity of excess thiol with RSNOs leads to disulfide and HNO formation (*26*). Moreover, HNO is also generated from the nitrosation of dithiol compounds such as dithiothreitol and lipoic acid (*22*).

It should be stressed that none of the mechanisms described above have been undoubtedly confirmed, primarily due to the difficulties with the unequivocal detection of HNO. Currently, the formation of N_2O, NH_2OH, or ferrous nitrosyl species is used as indirect evidence of HNO production, but clearly the development of reliable analytical methods for quantitative HNO detection is in high demand for the advancement of biomedical research in this area.

As a conclusion, HNO appears to have promising biochemical prospects. Three areas are emerging with regard to the potential biomedical applications of HNO-releasing molecules as therapeutic agents: cardiovascular therapy, reperfusion injury-preventive therapy, and anticancer treatment. However, endogenous *in vivo* HNO production still remains as an interesting hypothesis that needs to be proved or rejected.

D. HNO Donors

^{1}HNO and $^3NO^-$ are, as will be shown in next chapters, very reactive molecules. One of the key reactions is the reaction of ^{1}HNO with itself (i.e., dimerization) to yield hyponitrous acid ($H_2N_2O_2$) at nearly diffusional rate, which decomposes to water and N_2O. Therefore, nitroxyl solutions are not stable and HNO, if not produced continuously, readily disappears. Also, HNO cannot be isolated in the solid state, $^3NO^-$ is even more unstable, and its reactivity is less understood. To overcome these problems, working with ^{1}HNO (or $^3NO^-$) has always relied on the use of azanone

donor molecules, that is, compounds that under certain specific conditions spontaneously release ^{1}HNO or $^3NO^-$.

A number of reviews, dealing with the subject of ^{1}HNO or $^3NO^-$ generation, appeared over the past decade. Specifically, two reviews published in 2005 by Miranda and coworkers (*10,27*) include a deep description of the donor reactivity, as well as the more recent review by Doctorovich and coworkers (1). Here, we will briefly outline the key methods of HNO generation.

Historically, the first method for *in situ* generation of HNO was described by Angeli in 1896, from decomposition of $Na_2N_2O_3$. AS is still routinely used for this purpose. The accepted mechanism for spontaneous decomposition of AS to yield HNO and nitrite involves monoprotonation of AS anion between pH 4 and 8, as shown below (Eq. (4)):

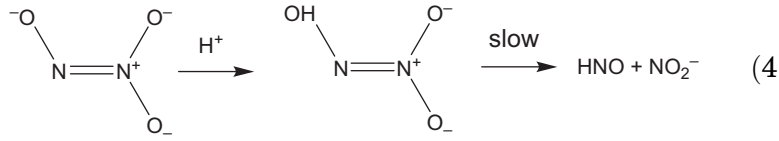

(4)

It should be noted that in strongly acidic media, (i.e., below pH 3), the relevant nitrogen-containing product of the decomposition of AS is NO (and not HNO). The mechanism for this process is not straightforward and is still under investigation. Equation (5) describes the sequence of proposed events leading to NO formation via an oxygen-deprotonated species:

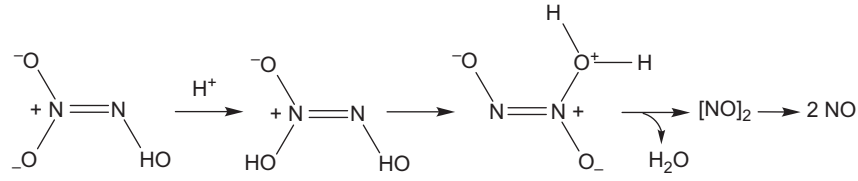

(5)

The close comparison of the experimentally determined and calculated rate constants values for the above equations supports the plausibility of this mechanism (*28*). Nitric oxide can also be generated from AS in a direct redox process with hexaammineruthenium(III) or hexacyanoferrate(III) in basic media according to Eq. (6),

$$(N_2O_3)^{2-} + M^{3+} \rightarrow NO + NO_2^- + M^{2+} \qquad (6)$$

In summary, AS is commonly regarded as a reliable HNO donor in near-neutral media, with a pH-dependent and first-order

thermal decomposition. From pH 4 to 8, the rate constant is practically invariable, being $6.8\times10^{-4}s^{-1}$ at 25°C, equivalent to a half-life of 17 min (*29–33*).

The second method of significance is generation of HNO from an organic compound, Piloty's acid (PA), via heterolysis in basic medium, according to the equation shown below:

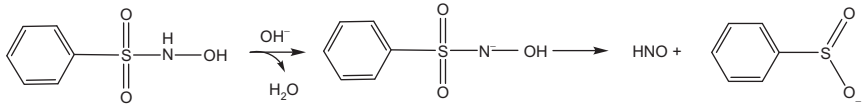

(7)

The reaction is spontaneous once the sulfohydroxamic moiety is deprotonated. Therefore, PA will spontaneous and continuously produce HNO above certain pH, which is related to the corresponding pK_a. Several PA derivatives have been synthesized recently (*34*), such as the *p*-nitro, 2,4,6-triisopropyl, *p*-methoxy, and other derivatives. These compounds also produce HNO and start to decompose at pH values as low as 1, therefore covering the whole pH range (Doctorovich and coworkers, manuscript in preparation). The rate constants for decomposition of PA at pH 13 and AS at pH 4–8 are comparable, with the values for both falling in the 10^{-3}–$10^{-4}s^{-1}$ range (at 25–35°C). Similar to AS in neutral and slightly acidic range, PA under basic conditions exhibits half-lives on the order of minutes (27 min at 25°C and 6 min at 35°C) (*35,36*). All PA derivatives show similar decomposition rates, although at different pH ranges.

Both PAs and AS are still widely used for generation of HNO for pharmacological studies. Of the two, AS has a comparative advantage of reliable generation of HNO under oxidative aerobic conditions and in neutral pH, as opposed to PAs giving off NO as main product in this case. However, the structure of AS anion is rigid and not amenable to derivatization. Hence, there is less flexibility in tailoring the function of HNO delivery for specific biomolecular targets. Moreover, the recent and facile preparation of several PA derivatives that can release HNO reliably at physiological (and almost any) pH shows that these compounds are probably the preferred donors to be used in future works in this area.

E. Reactions of HNO and NO with Biologically Relevant Small Molecules

In this chapter, we will briefly describe the fundamental chemistry of ^1HNO and $^3NO^-$, make note of new advances regarding

TABLE I

RATE CONSTANTS AND REDUCTION POTENTIALS FOR REACTIONS OF AZANONE, AZANONE ANION, AND NITRIC OXIDE WITH BIOLOGICALLY RELEVANT SMALL MOLECULES

Eq. #	Reaction	Rate constant[a]	Reference
19	$^1HNO+OH^-\rightarrow{}^3NO^-+H_2O$	$4.9\times10^4M^{-1}s^{-1}$	(*37*)
20	$^1HNO+{}^1HNO\rightarrow HONNOH$	$8\times10^6M^{-1}s^{-1}$	(*37*)
	$HONNOH\rightarrow N_2O+H_2O$	$5.0\times10^{-4}s^{-1}$	(*38*)
23	$^1HNO+O_2\rightarrow NO+HO_2$	$3–8\times10^3M^{-1}s^{-1}$	(*7,37,39*)
30	$^1HNO+NO\rightarrow N_2O_2^-+H^+$	$5.8\times10^6M^{-1}s^{-1}$	(*40*)
19	$^3NO^-+H_2O\rightarrow{}^1HNO+OH^-$	$1.2\times10^2s^{-1}$	(*37*)
21	$^3NO^-+{}^1HNO\rightarrow N_2O+OH^-$	$6.6\times10^9M^{-1}s^{-1}$	(*41*)
24	$^3NO^-+O_2\rightarrow ONOO^-$	$2.7\times10^9M^{-1}s^{-1}$	(*37*)
29	$^3NO^-+NO\rightarrow N_2O_2^-$	$3.0\times10^9M^{-1}s^{-1}$	(*40*)
25	$NO+O_2^-\rightarrow ONOO^-$	$4–7\times10^9M^{-1}s^{-1}$	(*42,43*)
26	$2NO+O_2\rightarrow2NO_2$	$2.54\times10^6M^{-2}s^{-1}$	(*44*)
		Potential versus NHE	Reference
$NO+H^++e^-\rightarrow{}^1HNO$		$E^\circ\approx-0.14V$	(*45*)
$NO+e^-\rightarrow{}^3NO^-$		$E^\circ<-0.8V$	(*46*)

[a]Rate constants are given at room temperature and pH=7.

this topic, and focus on the comparison with NO reactivity. Rate constants and some reduction potentials for the reactions mentioned below are summarized in Table I.

While NO is a free radical with a doublet ground state, and therefore involved in several radical reactions, ^1HNO has a singlet ground state (*47,48*). It is a weak acid with an accepted pK_a of 11.4 (*37,49*). Interestingly enough, its anion, $^3NO^-$, has a triplet ground state (*50,51*), the same as the isoelectronic O_2 molecule. Therefore, loss of a proton from HNO is not a simple acid/base equilibrium but a spin-forbidden slow deprotonation (Table I, Eq. (8)) (*37*):

$$^1HNO + OH^- \rightleftharpoons {}^3NO^- + H_2O \tag{8}$$

Reprotonation of $^3NO^-$ to ^1HNO is also slow (Table I) possibly due to the same reasons. Therefore, in physiological-like media (pH=7.4), ^1HNO is likely to be the dominant species, although if produced, $^3NO^-$ may live enough to be relevant.

E.1. Dimerization

HNO dimerizes with a second-order rate constant of ca. 10^7 to produce hyponitrous acid which finally decomposes to produce nitrous oxide (Table I, Eq. (9)) (*37,55,56*).

$$2\,HNO \rightarrow HONNOH \rightarrow N_2O + H_2O \qquad (9)$$

Between pH 7.5 and 10.5, where the species $HN_2O_2^-$ accounts for most of the hyponitrous acid in solution (pK_a=10.9), its decomposition rate exhibits a plateau with $k(25^\circ)=5.0\times10^{-4}s^{-1}$ (half-life 23 min) (*38*). Outside this pH range, the decomposition rate becomes even slower up to values of around $10^{-6}s^{-1}$. Below pH=5, and in the absence of radical scavengers, hyponitrous acid can decompose by a radical chain mechanism producing N_2 and NO_3^- (*57*), so it has to be taken into account that below pH=5 ethanol or other radical scavengers should be added to the reaction mixtures to avoid complications arising from the radical chain mechanism.

Regarding $^3NO^-$, although it has been suggested that it dimerizes with $k>8\times10^6M^{-1}s^{-1}$ (*27*), there is no experimental evidence to support this statement. According to Bonner and coworkers, "Coulomb barrier considerations lead one to expect inhibition of the dimerization reaction with increasing deprotonation of HNO" (*58*). However, it has been recently reported by Lymar and coworkers that the spin-forbidden reaction of $^3NO^-$ and ^1HNO takes place with a nearly diffusion-controlled rate constant of $6.6\times10^9M^{-1}s^{-1}$ (Eq. (10)) (*41*).

$$^3NO^- + {}^1HNO \rightarrow N_2O + OH^- \qquad (10)$$

It has to be kept in mind that this result is based on indirect kinetic observations. On the other hand, it is a surprising fact—even for the authors—that a spin-forbidden reaction would be so fast; according to Lymar and coworkers, this could be due to the very large driving force for this reaction (with an estimated ΔG of -80 kcal mol^{-1}). Although $^3NO^-$ is isoelectronic with O_2, due to its negative charge is expected to be more nucleophilic, so reaction 10 could be thought as a nucleophilic addition of nitroxyl anion to the N atom of ^1HNO to produce the intermediate $HONNO^-$ (after electronic rearrangement and a 1,2 H shift), which decomposes to produce N_2O (Eq. (11)). In principle, $^1HN{=}O$ could be expected to suffer this type of nucleophilic attack in a similar way to carbonyl ($R_2C{=}O$) compounds. However, this particular reaction is complicated by the different spin states of azanone. Further theoretical studies are needed to understand the reaction details. On the other hand, and unlike ^1HNO, NO has little tendency to dimerize to $(NO)_2$ with a small equilibrium constant $K=8.360\times10^{-2}$ (120 K) and therefore is rather stable in solution (*59*).

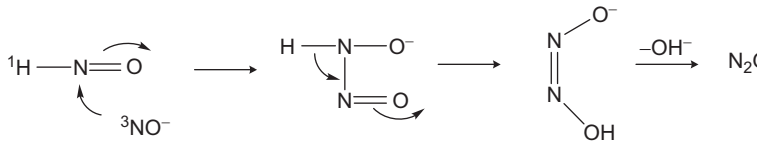

(11)

E.2. Reaction with oxygen

The reaction of ^{1}HNO with O_2 which has been studied in the gas phase (*60*) is rather slow, due to their different spin states, $k \approx 10^3 M^{-1} s^{-1}$ (see Table I). Strikingly, the reaction product is still unknown although it has been proposed that the reaction proceeds through Eq. (12), leading to NO and a radical hydroperoxy species (*37*).

$$^1HNO + O_2 \rightarrow NO^{\bullet} + HO_2^{\bullet} \tag{12}$$

On the other hand, $^3NO^-$ reacts with O_2 at nearly diffusion-controlled second-order rate to produce peroxynitrite (Eq. (13)) (*37*).

$$^3NO^- + O_2 \rightarrow ONOO^- \tag{13}$$

in a reaction isoelectronic with the also second-order diffusion-controlled reaction 14 (*27,42,43*).

$$NO + O_2^- \rightarrow ONOO^- \tag{14}$$

Nitric oxide, on the contrary, reacts with O_2 following third-order kinetics and at a slower rate. The mechanism of this reaction is shown in a simplified manner in Eqs. (15)–(17) (*44*).

$$2NO + O_2 \rightarrow\rightarrow\rightarrow 2NO_2 \tag{15}$$

$$NO_2 + NO \rightarrow N_2O_3 \tag{16}$$

$$N_2O_3 + H_2O \rightarrow 2NO_2^- + 2H^+ \tag{17}$$

E.3. Redox-related reactions

The accepted standard reduction potential for the NO/^{3}NO$^-$ couple is -0.8V (*49*). At physiological pH, ^{1}HNO is expected to be the main nitroxyl-related species, and it has an estimated $E^\circ(NO,H^+/^1HNO) \approx -0.14$V, becoming -0.55V at pH 7 (all values against NHE) (*37*). As a result, it is currently under discussion whether NO could be reduced to ^{3}NO$^-$ or ^{1}HNO in mammalian

systems since on one hand the reduction potentials mentioned above (−0.8 and −0.55V) are in the limit of biological-reducing agents, and other species which are present in higher concentrations, such as O_2, are more favorable to be reduced. On the contrary, $^3NO^-$ should function as a strong reducing agent yielding NO, while ^1HNO usually acts as an electrophile, as mentioned for reaction 10.

E.4. Reactions with NO

Last but not least, both $^3NO^-$ and ^1HNO react with NO, with quite distinct second-order rate constants which differ in three orders of magnitude favoring reaction with $^3NO^-$ (Table I, Eqs. (18) and (19)) (*40*):

$$^3NO^- + NO \rightarrow N_2O_2^- \tag{18}$$

$$^1HNO + NO \rightarrow N_2O_2^- + H^+ \tag{19}$$

The resulting $N_2O_2^-$ radical extremely rapidly acquires another NO molecule, producing the closed shell $N_3O_3^-$ anion, which decays to the final products N_2O plus NO_2^- with a rate constant of ca. $300\,s^{-1}$.

A summary of the reactions of NO and HNO/NO^- with small molecules is shown in Scheme 1.

II. Azanone Reactivity with Hemeproteins and Metalloporphyrins

A. Fe, Mn, and Co Porphyrin Nitrosyl Complexes

Besides the small molecules, described above, the main targets of NO and HNO in biological systems are thiols (*27,28*), and

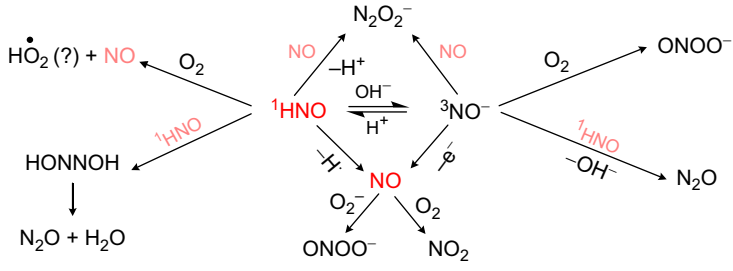

Scheme 1. Reactions of nitroxyl and nitric oxide.

metalloproteins, mainly heme proteins (*61,62*). In this context, much of the knowledge about the reaction of NO with hemes comes from the study of its reactivity with metalloporphyrins as isolated heme models, mainly of iron, but also manganese, cobalt, and ruthenium (*63*). There are two salient issues about metalloporphyrin nitrosyl complexes. The first concerns their formation and dissociation rates, the second is related to the NO geometry and its effect on other *trans* ligands. Usually NO binds to the metal via the nitrogen atom, and its character ranges (formally) from that of NO^+ to that of NO^- (*61,64*). A good and useful description of the metal–NO moieties was originally presented by Enemark and Feltham in the 1970s (*65–67*) and is depicted as $\{MNO\}^n$, where M is the corresponding metal center, and the key parameter is the number n, corresponding to the sum of the metal d electrons plus the nitrosyl π^* electrons.

Accordingly, for example, $\{FeNO\}^6$ complexes correspond to ferric nitrosyls, displaying NO^+ character, a linear Fe—N—O geometry and NO stretching mode $\upsilon_{NO} \approx 1937\,cm^{-1}$, while $\{FeNO\}^7$ complexes are ferrous nitrosyls with $NO^\bullet$ character, a bent Fe—N—O angle and $\upsilon_{NO} \approx 1670\,cm^{-1}$, as observed for several crystal structures of the corresponding Fe metalloporphyrin nitrosyl complexes (*68*). Besides the abovementioned complexes, iron porphyrins can yield also $\{FeNO\}^8$ species, which are supposed to have NO^- (nitroxyl) character, as will be described later (*69*). Concerning their stability, the $\{FeNO\}^7$ complexes are by far the most stable ones, with $K_d \approx 10^{-14}$ due to fast NO association to Fe(II) porphyrins (ca. $10^9 M^{-1}s^{-1}$) and very slow NO dissociation (*70*). On the other hand, $\{FeNO\}^6$ species show lower association rates (ca. $10^6 M^{-1}s^{-1}$) and significantly higher NO dissociation rates (between 1 and $500\,s^{-1}$) (*70*). A final very important point concerning the $\{FeNO\}^6$ complexes is their reactivity toward nucleophiles, usually OH^- and nitrite, which results in the reduction of the porphyrin metal center and the oxidation of NO to NO_2^- in a process called reductive nitrosylation. The net outcome of the reductive nitrosylation reaction is the formation of $\{FeNO\}^7$ species, when excess NO reacts with ferric porphyrins (*71,72*). For a recent review of the above described reactions, see the review by Ford and coworkers (*61*).

Manganese porphyrins also form nitrosyl complexes. Fast (ca. $10^6 M^{-1}s^{-1}$) reaction of Mn(II) with NO yields stable $\{MnNO\}^6$ complexes (*73*) that show a linear Mn—N—O geometry (*74*). Interestingly, no reductive nitrosylation is observed for the reaction of Mn(III) with NO (*73*). Cobalt porphyrins also form stable nitrosyl complexes. The $\{CoNO\}^8$ species obtained, for example, by reaction of NO with Co(II) porphyrins have been explored as isoelectronic

models for oxygenated heme (*75*). The $\{CoNO\}^8$ complexes are very stable, with high association and low NO dissociation rates (with values of ca. $10^9 M^{-1}s^{-1}$ and ca. $10^{-4}s^{-1}$, respectively) (*70,76*). On the other hand, the $\{CoNO\}^7$ complexes are less stable, with significantly lower association rates (*76*).

A final interesting point in relation to iron nitrosyl complexes directly related to HNO/NO^- chemistry concerns the nitric oxide reductase (NOR) reaction mechanism, as recently reviewed by Karlin (*77*). The NOR reaction is proposed to occur by binding of two NO molecules to two closely positioned ferrous hemes, which leads to N—N coupling and $N_2O_2^{2-}$ formation (i.e., NO^- dimerization), which finally leads to N_2O, H_2O, and two ferric hemes (*78,79*). Collman and coworkers succeeded in the synthesis of an inorganic functional model of NOR, containing an iron porphyrin center and a nonheme iron tri/tetracoordinated to imidazol and/or pyridine ligands, which is shown to react with two equivalents of NO to yield N_2O in the fully reduced state (*80,81*). Analysis of possible intermediates by EPR, Resonance Raman, and IR spectroscopy leads to suggest the existence of two different nitrosyl intermediates, assigned to mono and dinitrosyl species (*80*). The NOR reaction, as described, can therefore be interpreted as a coordination-mediated HNO/NO^- dimerization, depending on the order of ligand reduction, protonation, and N—N bond formation steps.

In summary, several metalloporphyrin nitrosyl complexes have been obtained and kinetically characterized. In the case of Fe, Mn, and Co as metal centers, the same nitrosyl complexes can be obtained by reaction of the corresponding M(III) porphyrins with HNO as will be described in the following sections.

B. Reactions of HNO with Fe, Mn, and Co Porphyrins

The first studied reactions of azanone with Fe porphyrins were not with isolated porphyrins, but directly with myoglobin, the benchmark of the heme proteins.

In this context, the reaction of azanone with isolated iron porphyrins seemed to be a relevant study to be carried out. The first experiments involved the reaction of common, previously described HNO donors such as trioxodinitrate (AS) and toluenesulfohydroxamic acid (a PA derivative, TSHA), with several model porphyrins, including the water soluble anionic *meso*-tetrakis(4-sulfonatophenyl)porphyrinate [Fe(III)TPPS]$^{3-}$, the cationic *meso*-tetrakis-*N*-ethyl pyridinium-2-yl porphyne [Fe(III)TEPyP]$^{5+}$, as well as the pentacoordinated heme-protein model

microperoxidase-11 (Fe(III)MP11) and the neutral *meso*-tetraphenyl porphyrinate (Fe(III)TPP) which is soluble in organic media (*52–54*).

As expected, all porphyrins yielded the corresponding $\{FeNO\}^7$ complexes, according to the general reaction 20.

$$^1HNO + Fe(III)Por \rightarrow Fe(II)PorNO + H^+ \qquad (20)$$

The reactions can be followed spectroscopically based on the corresponding reported spectral changes characteristic of the starting ferric and nitrosyl porphyrins, respectively. The observed changes in the position of the Soret and Q bands are, however, moderate.

Although ferrous heme proteins form stable Fe(II)(Prot)HNO adducts, as described above, isolated porphyrins such as FeTPPS or FeTPP do not, clearly suggesting that, without the protection provided by the protein matrix, the Fe(II)(Prot)HNO (or NO^-) adducts are unstable. We will describe below the obtention of the first stable $\{Fe(Por)NO\}^8$ porphyrin model, thanks to the presence of strongly electron-withdrawing substituents present in the porphyrin ring.

Besides the reactivity of azanone with iron porphyrins, other metalloporphyrins, namely with Co or Mn as the metal center, also react with HNO giving rise to interesting applications. When aqueous solutions of AS (at pH=7) or TSHA (at pH=10) are added to $[Mn(III)TEPyP]^{5+}$ under inert atmosphere, in equimolar or slight donor excess ratios, total conversion of $[Mn(III)TEPyP]^{5+}$ to $[Mn(II)TEPyP\text{-}NO]^{4+}$ is observed. Interestingly, and in opposition to what is observed for the Fe(III) porphyrins, there is a significant blue shift (more than 30 nm) of the Soret band, potentially providing a sensitive tool for HNO detection and quantification, as will be discussed in the next section. Similar spectral changes are observed for HNO donor reactions with $[Mn(III)TPPS]^{3-}$, although in these cases, excess donor is needed for the reaction to be completed, due to kinetic reasons that will be explained below.

Neither $[Mn(III)TEPyP]^{5+}$ nor $[Mn(III)TPPS]^{3-}$ react with NO (g) or NO donors (such as SNAP) under similar conditions, which means that the equilibrium constant for the formation of the Mn(III) nitrosyl product is not favorable and that these Mn(III) porphyrins do not suffer reductive nitrosylation to produce the Mn(II)(Por)NO complex as easily as the corresponding Fe(III) porphyrins do. Therefore, Mn(III) porphyrins show selective reactivity toward HNO, while Mn(II) porphyrins are selective for NO (Eqs. (21)–(24)) (*52,54*).

$$NO + Fe(III)Por \rightarrow Fe(II)(Por)NO \quad (21)$$

$$HNO + Fe(III)Por \rightarrow Fe(II)(Por)NO + H^{+} \quad (22)$$

$$NO + Mn(III)Por \rightarrow \text{Slow reaction/N.R.} \quad (23)$$

$$HNO + Mn(III)Por \rightarrow Mn(II)(Por)NO + H^{+} \quad (24)$$

Regarding Co porphyrins, the reaction with HNO of cobalt 5,10,15,20-tetrakis[3-(*p*-acetylthio-propoxy)phenyl]-porphyrin [Co(P)], which is soluble in organic media, was studied (*82*). This porphyrin has four sulfur anchors that allow it to be anchored to electrodes, as will be shown later. The reaction of NO(g) with Co^{II}(P) produces Co(III)(Por)NO^{-} in a few minutes, in agreement with previous data for other cobalt porphyrins (*83*). In a similar timescale, no spectral changes are observed for Co(II)Por in the presence of the nitroxyl donor TSHA. On the other hand, addition to Co(III)Por/TSHA of 1,8-diazabicyclo(5.4.0)undec-7-ene—that accelerates TSHA decomposition in organic solvent by deprotonation—slowly produces Co(III)(Por)NO^{-}, as confirmed by UV–vis and IR spectroscopy (ν_{NO}=1679 cm^{-1}). The UV–vis spectral changes are quite small, similarly to what happens with the corresponding reactions of iron porphyrins. In a similar timescale, no reaction takes place for Co(III)Por in the presence of NO(g) or any studied NO donor. The results, similarly to what is observed for Mn porphyrins, clearly show that Co^{II}Por reacts with NO and not with HNO, while Co^{III}Por reacts with HNO and not with NO (*82*).

In summary, while iron porphyrins cannot discriminate NO from HNO due to the reductive nitrosylation reaction, both Mn and Co porphyrins tend to differentiate NO from HNO: Co(II) and Mn(II) porphyrins react rapidly with NO but not with HNO, while Co(III) and Mn(III) porphyrins react rapidly with HNO but not with NO. On the other hand, Mn porphyrins tend to show an important shift in the UV–vis spectra (Soret band) when going from Mn(III) to Mn(II)NO porphyrins, while Co and Fe porphyrins do not (see Scheme 2).

C. Reactions of Azanone with Hemeproteins

The interest in HNO reactions with hemeproteins has several origins. Studies of the nitrogen cycle involved enzymes, with the intermediacy of assimilatory and dissimilatory nitrite

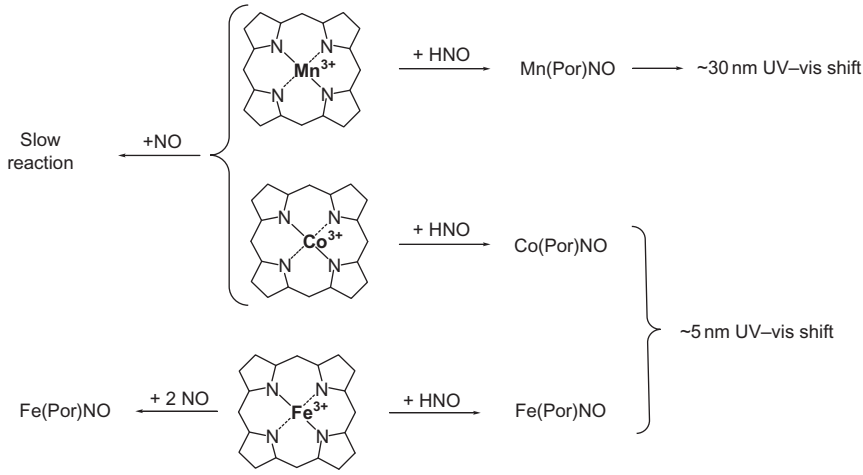

SCHEME 2. HNO versus NO reactivities of Mn, Co, and Fe porphyrins and UV–vis shifts of the Soret bands for the corresponding M(Por)NO products.

reductases. In this context, the complete six-electron reduction of nitrite to ammonia has been postulated to involve the presence of $\{Fe(H)NO\}^8$ (or azanone porphyrin) complexes in several of these heme-containing enzymes (*84*). An authentic Fe–HNO intermediate, for example, was supposed to be observed during turnover of the NO reductase cytochrome p450nor, after a two-electron reduction of a ferric nitrosyl complex by NADH. The postulated intermediate was characterized by UV–vis spectroscopy showing a Soret band with λ_{max} at 444 nm that reacts with NO to yield N_2O (*85,86*).

Back in 2000, Farmer and coworkers focused their attention to studies involving chemical reduction of the ferrous nitrosyl complexes of the paradigmatic heme-protein myoglobin and also studied the deoxymyoglobin (deoxyMb) reaction with HNO donors. Their results show that HNO can bind to deoxyMb forming a stable Fe(II)(Mb)HNO adduct which is the same complex obtained by reduction of the ferrous nitrosyl complex of Mb (*87,88*). Although the difference in the Soret and Q visible bands between the Fe(II)(Mb)NO and the corresponding Fe(II)(Mb)HNO complexes is relatively small, the last complexes are clearly identified by the characteristic peaks at ca. 15 ppm in the ^1H NMR spectra. Further evidence for the formation of Fe(II)(Mb)HNO is obtained by generating the corresponding $H^{15}NO$ adducts, which produce splitting of the HNO resonance in the ^1H NMR spectra, since ^{15}N is an NMR-active nucleus with $s=½$.

More recent studies also showed that the Fe(II)HNO complex can be obtained with globins such as hemoglobin, leghemoglobin, and the SH_2-binding globin from the clam *L. Pectinata*. The adducts are stable over a period of weeks and can be obtained by careful reduction of the ferrous nitrosyl adducts or by direct HNO trapping by the ferrous protein. Like the analogous O_2–Fe(II) adducts, the HNO adducts are diamagnetic and have therefore been proposed as oxy-heme models. In this regard, different kinetics were observed for the two subunits of human hemoglobin highlighting the use of HNO adducts as a unique tool sensitive to structural changes within the oxygen-binding cavity (*84,89*).

The other source of interest in HNO reactivity with hemeproteins arises due to possible physiological effects of either endogenously generated or externally delivered (as pharmacological agent) azanone. Besides the ferrous globin reactivity described above, main targets of HNO are ferric heme proteins as well as other metalloproteins. HNO, for example, reacts with ferric myoglobin and hemoglobin (in analogous manner as that described for ferric porphyrins) yielding the corresponding $\{FeNO\}^7$ complexes, in a reductive nitrosylation reaction (*89–92*). Ferric cytochromes and peroxidases also react in the same manner, showing an apparent lack of effect due to different proximal ligands, such as histidine, cysteine, or even tyrosine (*89*).

Finally, the most important and relevant target of HNO *in vivo* is the NO receptor sGC (*93,94*). The ferrous heme-protein sGC becomes activated upon NO binding, increasing the cyclic GMP (cGMP) levels that trigger relaxation of vascular smooth muscle cells increasing the blood flow in small vessels (*94,95*). The mechanism of signal transduction relies in the formation of an $\{FeNO\}^7$ adduct, which triggers proximal histidine release due to the NO trans effect and results in a conformational change that activates sGC (*93–96*). Recently, HNO was shown to be capable of activating sGC (*97*). This result is in contrast to previous studies that claimed that NO was the only nitrogen oxide capable of activating sGC (*98*). The striking feature of the recent results is that, although HNO-mediated sGC activation was shown to occur via interaction with the heme, unexpectedly it does not activate the ferric form of the enzyme. In addition, in the corresponding work, it was shown that higher HNO concentrations also lead to reaction with a cysteine leading to sGC inhibition (*97*). Although HNO-mediated sGC activation is an appealing hypothesis, several points remain to be elucidated in order to establish it as a definite fact. First, the reaction of HNO with both ferric and ferrous sGC must be studied in detail and its relation to sGC activity should be well defined. Second,

the outcome of the reaction with cysteine needs to be addressed as well as the resulting effect on the sGC functionality. Finally, the reaction conditions should be carefully controlled to avoid possible conversion of HNO to NO leading to inconsistent results.

D. HNO and NO Reaction Kinetics with Hemeproteins and Metalloporphyrins

D.1. Mechanistic analysis

A key determinant of the fate of nitroxyl in any given media, either *in vivo* or *in vitro*, will depend upon all the competing reaction rates. To study the ^{1}HNO-to-metalloporphyrin association kinetics, the UV–vis spectral changes corresponding to the formation of a nitrosyl porphyrin can be followed as a function of time for each reaction conditions, such as different donors (AS or TSHA), pH, and relative porphyrin to donor concentration ratios. Plots of the corresponding traces allow the determination of the initial observed rate υ_{obs} for the nitrosylation reaction. Even for reactions performed in strictly anaerobic media to avoid ^{1}HNO/^{3}NO$^-$ reactions with O_2, trace amounts of oxygen can be present since it is extremely difficult to remove O_2 from water below 10^{-7}M. The obtained exponential traces of nitrosyl product formation (when extreme ca. 100 donor to porphyrin ratios are used) are strongly indicative that, for all cases, the reaction is first order in porphyrin. Strikingly, two significantly different reaction times and stoichiometries are observed for peripheral negatively or positively charged iron and/or manganese porphyrins. For negatively charged porphyrins such as [Fe(III)TPPS]$^{3-}$ and [Mn(III)TPPS]$^{3-}$, the reaction with AS at pH 7 (where AS spontaneous decomposition has a half-life of about 900 s) (*90,92*) requires a large excess of AS to drive the reaction to completion, and for an equimolar ratio, the reaction half-life is ca. 120 min. On the other hand, the reaction of positively charged porphyrins such as [Fe(III)TEPyP]$^{5+}$ and [Mn(III)TEPyP]$^{5+}$ total conversion to the nitrosyl metalloporphyrin is obtained with an equimolar porphyrin to donor ratio in less than 10 s. A similar behavior is observed for the reactions with the HNO donor TSHA. These results clearly point to different reaction mechanisms operating depending on the porphyrin peripheral charge. The fact that the overall reaction rate for positively charged porphyrins by far exceeds the donor spontaneous decomposition strongly suggests that a direct porphyrin–donor interaction is taking place and that these porphyrins accelerate their decomposition. Therefore, Scheme 3

was proposed for the reactions of HNO donors with metalloporphyrins.

In Scheme 3, k_{on}(Donor) represents the bimolecular association rate constant of the metalloporphyrin with the HNO donor, k_{cat}(Donor) represents the porphyrin-accelerated donor decomposition rate constant, k_d represents the spontaneous donor decomposition rate constant to yield HNO, and k_{on}(HNO) is the bimolecular metalloporphyrin-to-HNO association rate. In order to obtain the rate constants, the following limiting cases have been analyzed: (case i) for negatively charged metalloporphyrins, the rate of HNO production due to spontaneous decomposition (k_{donor}) exceeds the reaction rate of HNO with the metalloporphyrin (k_{on}(HNO)), and the dimerization of HNO competes with the nitrosyl product formation. The shape of the υ_{obs} against AS plot is not linear, since when the HNO production is increased (due to an increase in donor concentration), the dimerization rate increases with the square of [HNO], as described by Eq. (25), and therefore, the relation between [HNO] and [Donor] is not linear. However, using the steady-state approximation for [HNO] (i.e., assuming that all HNO produced by the donor either reacts with the porphyrin or dimerizes according to k_{dim}=dimerization rate constant), the HNO concentration can be estimated according to Eq. (25). Using the estimated HNO concentration, a plot of υ_{obs} against [HNO] yields as expected a linear plot which allows determining the bimolecular HNO association rate constant k_{on}(HNO).

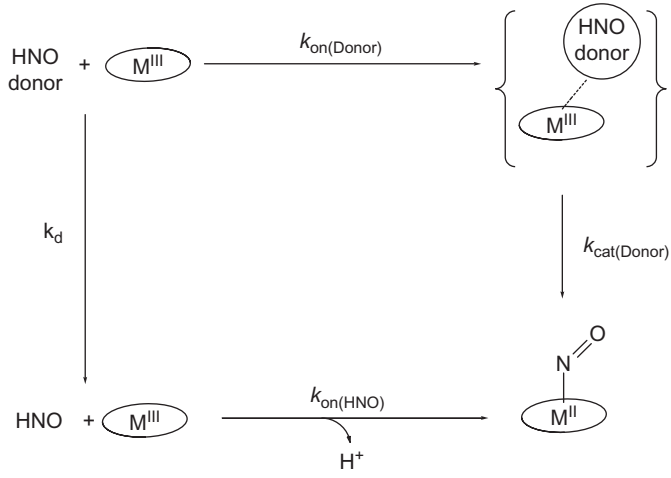

SCHEME 3. Proposed mechanism for the reactions of HNO donors with metalloporphyrins.

$$[\mathrm{HNO}] = \left[\left(k_{\mathrm{cat(Donor)}}[\mathrm{Donor}] - \upsilon_{obs}\right)/k_{\mathrm{dim}}\right]^{1/2} \qquad (25)$$

On the other hand, (case ii) if the reaction of the donor with the metalloporphyrin is faster than its spontaneous decomposition rate, the metalloporphyrin reacts directly with the donor, accelerating its decomposition rate and forming the corresponding nitrosyl complex by azanone transfer to the metal center. For these cases, almost no free HNO is produced, as evidenced by the quantitative formation of the nitrosyl product even for equimolar metalloporphyrin to donor ratios. In these cases, the υ_{obs} against [Donor] plot gives a straight line from which the bimolecular $k_{\mathrm{cat(Donor)}}$ rate constant can be obtained.

Further evidence for direct azanone transfer from AS to the metal center was obtained by the kinetic analysis of the reaction at pH 10, where AS is stable. Even under these conditions, the reaction with positively charged Mn porphyrins produces the nitrosyl product stoichiometrically in less than 5 s, while adding AS to the negatively charged $[\mathrm{Mn(III)TPPS}]^{3-}$ at pH 10 does not produce any reaction at all. Finally, DFT studies on the direct interaction of AS with both Mn and Fe porphyrins showed that AS ($N_2O_3^{2-}$, $(ON_a{=}N_bO_2)^{2-}$) is able to coordinate to either Mn(III) or Fe(III) by the N_a nitrogen, which results in a significant weakening of the N—N bond, therefore partially explaining the observed rate acceleration. It is expected that, being negatively charged, AS coordination to the metal center will be faster for positively charged metalloporphyrins.

Using the kinetic analysis described above, k_{on}(HNO) and/or k_{on}(Donor) were obtained for several Mn and Fe porphyrins and are shown in Table II.

Data shown in Table II are consistent with two alternative pathways for the reactivity of nitroxyl donors (AS, TSHA) in aqueous solutions: HNO transfers to the metal center through reaction of the porphyrin with azanone or with the HNO donor (see Scheme 3 above). Interestingly, and despite the fact that k_{on} for HNO binding are faster than k_{on} for the donors, donor concentrations are usually four orders of magnitude higher than those of HNO. Therefore, depending on the donor and porphyrin concentrations, one or the other pathway will predominate. At relatively high concentrations (10^{-4}M, assuming a 1:1=donor: porphyrin ratio), a faster rate is observed for the direct reaction with the donor, as observed for Mn(III) cationic porphyrins (*52*) and also for the ferric analogues (*53*).

Concerning the direct reaction between the donor and the metalloporphyrin, a redox mechanism could be operative for

TABLE II

KINETIC RATE CONSTANTS FOR THE REACTIONS OF MN(III) AND FE(III) PORPHYRINS WITH AS AND TSHA

Porphyrin (III)	$E_{1/2}$ $M^{3+/2+}$ versus NHE	$k_{on\ (donor)}$ ($M^{-1}s^{-1}$)		$k_{on\ (HNO)}$ ($M^{-1}s^{-1}$)		References
		AS (pH 7)	TSHA (pH 10)	AS (pH 7)	TSHA (pH 10)	
$[MnTEPyP]^{5+}$	+220 mV	1.2×10^4	1.0×10^4	–	–	(*52*)
$[MnBr_8TPPS]^{3-}$	+209 mV	3.7×10^3	7.9×10^3	–	–	MP[a]
$[FeTEPyP]^{5+}$	+380 mV	5.4×10^3	1.1×10^4	–	–	(*53,24*)
$[FeTPPS]^{3-}$	+23 mV	0.5	–	1.0×10^6	–	(*54*)
$[MnTPPS]^{3-}$	−160 mV	–	–	$\sim4.0\times10^4$	$\sim9.0\times10^4$	(*52*)
[FeMP11]	−360 mV	–	–	6.4×10^4	3.1×10^4	(*53,24*)

[a]MP=Doctorovich and coworkers, manuscript in preparation.

TSHA. PA has been shown to be oxidized by several iron complexes yielding the corresponding radical, which decomposes to produce NO and the reduced metal complex (*99*). This mechanism would imply that the reaction proceeds through an intermediate state with the reduced porphyrin (Fe(II)), TSHA radical, and free NO. Afterwards, NO would react very fast with the reduced iron porphyrin yielding the corresponding nitrosyl complex as the final product, as observed here. However, a mechanism involving an intermediate formed by TSHA and the metalloporphyrin followed by NO^- transfer to the porphyrins cannot be discarded and both mechanisms are compatible with the experimental observations. More interestingly, recently obtained data for a negatively charged bromated porphyrin $[MnBr_8TPPS]^{3-}$ indicates that the actual followed reaction mechanism (reaction of the porphyrin with nitroxyl or with the HNO donor) depends more on the reduction potential of the porphyrin metal center than on its peripheral charge. This is evidenced from the data in Table II showing that the negatively charged $[MnBr_8TPPS]^{3-}$, having a positive reduction potential due to the presence of the electron-attracting bromine substituents, reacts directly with the HNO donor, the same as the positively charged $[MnTEPyP]^{5+}$. However, the negatively charged $[MnTPPS]^{3-}$, with a reduction potential of −160 mV, reacts via the free HNO pathway.

The abovementioned scenario becomes even more complex in the presence of dioxygen, due to the reactivity of HNO and the M(Por)

TABLE III

KINETIC RATE CONSTANTS FOR THE RELEVANT REACTIONS OF $[Mn(TPPS)]^{3-}$ WITH AS

#	Reaction	Value	References
1	$HONNOH \rightarrow N_2O$	$5\times10^{-4}s^{-1}$	(*36*)
2	$HNO+HNO \rightarrow HONNOH$	$8\times10^{6}\ M^{-1}s^{-1}$	(*35*)
3	$AS \rightarrow HNO+NO_2^-$	$2.30\times10^{-3}s^{-1}$	(*29–33*)
4	$[Mn^{3+}(TPPS)]^{3-}+HNO \rightarrow [Mn^{2+}(TPPS)NO]^{3-}$	$1.0\times10^{5}M^{-1}s^{-1}$	(*52*)
5	$AS+[Mn^{3+}(TPPS)]^{3-} \rightarrow [Mn^{2+}(TPPS)NO]^{3-}+NO_2^-$	$20M^{-1}s^{-1}$	MP[a]
6	$O_2+[Mn^{2+}(TPPS)NO]^{3-} \rightarrow [Mn^{3+}(TPPS)]^{3-}+NO_3^-$	$5M^{-1}s^{-1}$	MP[a]
7	$O_2+HNO \rightarrow H^++NO_3^-$	$5\times10^{3}M^{-1}s^{-1}$	[b]

[a]MP=Doctorovich and coworkers, manuscript in preparation.

[b]This reaction has to be considered as:

(7a) $O_2+HNO \rightarrow HO_2+NO$, $k_{7a}=5\times10^{3}M^{-1}s^{-1}$ (average of lit. rate constants) (*7,39*)

(7b) $HO_2+NO \rightarrow ONOOH$, $k_{7b}=5\times10^{9}M^{-1}s^{-1}$ (*42*)

(7c) $ONOOH \rightarrow H^++NO_3^-$, $k_{7c}=1.2s^{-1}$ (*100*)

As the reactions 2 and 3 are very fast, and the intermediates have been obviated, we decided to use k_{7a} as the value for reaction 7.

NO porphyrins toward O_2. These reactions give place to oxygen and nitrogen reactive species (ORS and NRS) such as $ONOO^-$, NO, NO_2, HO_2, and others. The most important effects due to the presence of oxygen are the oxidation of the M(II)(Por)NO product back to the M(III)(Por) starting material (*52*) and the consumption of HNO, therefore lowering its effective concentration. In order to analyze this scenario, a set of more than 20 reactions involving the porphyrins as well as ORS and NRS have to be taken into consideration. These can be, however, analyzed using numerical simulations which take into consideration all the rate laws and kinetic constants involved. Previous results show that in order to describe correctly the kinetic reaction profiles at pH 7, only seven reactions are needed, which are shown in Table III and Scheme 4 for $[Mn(TPPS)]^{3-}$ with AS as the HNO donor (*1*).

The numerical results show that, if O_2 is present at a high concentration compared to AS, nitrite and nitrate are the main reaction products and nitrous oxide is practically not formed due to the competing reaction of HNO with O_2 to presumably produce initially HO_2 plus NO and ultimately NO_3^- (reactions 7a–c, Table III). Therefore, when the metalloporphyrin and AS coexist in solution under anaerobic conditions, the reaction of HNO with the M(III)Por competes not only with its dimerization but also with O_2. Moreover, since the M(II)PorNO product also reacts

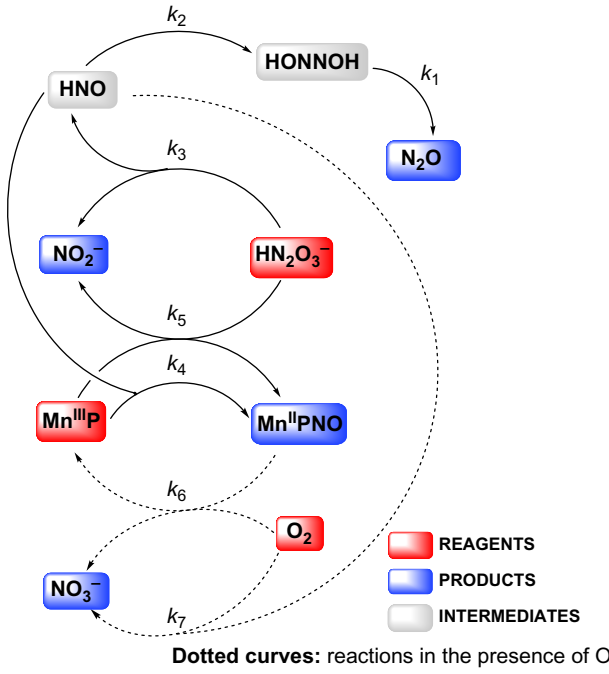

SCHEME 4. Reactions involved in the kinetic simulations which describe appropriately the reaction of metalloporphyrins with AS ($HN_2O_3^-$) in the absence and presence of dioxygen, at pH 7.

with O_2 to produce the starting material back (as described for Mn containing Mb) (*102*), little or no product is observed for relative low concentrations of AS and metalloporphyrin compared to O_2. On the contrary, when the concentrations of both AS and metalloporphyrin are at least one order of magnitude higher than [O_2], the M(II)PorNO product is formed and stays in solution. All the above observations could, in principle, be applied to other metalloporphyrins and/or HNO donors different from $[Mn(TPPS)]^{3-}$ and AS. The kinetic profiles should heavily depend on the most important rate constants involved, which are k_4 (k_{on}(HNO)), k_5 (k_{on}(donor)), and k_6 (k_{ox}(MPorNO)). The rate constant k_4 ranges from 10^4 to $10^6 M^{-1}s^{-1}$, k_5 from 1 to $10^4 M^{-1}s^{-1}$, and k_6 still has to be determined for a set of metalloporphyrins, although it can be estimated that, for the metalloporphyrins with positive reduction potentials, its value should be below $5 M^{-1}s^{-1}$ (Table III).

TABLE IV

BIMOLECULAR RATE CONSTANTS FOR HNO AND NO BINDING TO METALLOPORPHYRINS AND HEME PROTEINS

Target	Reactant	k_{on} ($M^{-1}s^{-1}$)	References
Fe(III)MP11	HNO	$3.1–6.4\times10^4$	(*53*)
Fe(III)MP11	NO	1.1×10^6	(*101*)
$[Fe(III)TPPS]^{3-}$	NO	4.5×10^5	(*70*)
metMb(Fe(III))	HNO	8×10^5	(*7*)
Cyt-c(Fe(III))	HNO	4×10^4	(*7*)
Catalase(Fe(III))	HNO	3×10^5	(*7*)
$[Fe^{II}TPPS]^{4-}$	NO	1.5×10^9	(*70*)
Mb(Mn(III))	HNO	3.4×10^5	(*102*)
Mb(Fe(II))	HNO	1.4×10^4	(*88*)
Mb(Fe(II))	NO	2.0×10^7	(*103*)
O_2	HNO	3×10^3	(*7*)

D.2. Comparative kinetic analysis

As with many biological small molecules, the comparative kinetics of azanone reactions with its possible biological targets will be the key factor in determining the physiological outcome. Table IV shows a comparison of the rate constants for the reactions of HNO and NO with several metalloporphyrins and heme proteins. It is clear from the data presented, that although lacking the protein scaffold, the soluble porphyrins and MP11 display reactivity toward HNO comparable to the observed reactivity of HNO with heme proteins (*7*). The bimolecular rate constants for HNO binding to ferric heme systems are in the order of 10^5–$10^6 M^{-1}s^{-1}$, similar to the values obtained for NO and probably represent an upper limit for the reaction with ferric hemes. However, these rates are more than 1000 times lower than the corresponding values for NO or CO binding to ferrous hemes (*70*) and heme proteins. This trend can be explained due to the fact that, for ferric hemes, the ligand binding rate is usually dependent on the lability of the leaving water ligand, in contrast with ferrous hemes, where the water ligand is weakly bound or the distal site is empty (*70*). This interpretation is further confirmed by the reported value for reaction of HNO with ferric cytochrome *c* (Cyt-*c*) which is ca. 20 times smaller compared to metMb. In Cyt-*c*, an endogenous ligand Methionine-80 blocks the distal site and HNO must displace it in order to coordinate to the iron. The slow displacement of the methionine ligand limits the HNO association rate (*7*).

E. Stabilization of {M(Por)HNO}^{8} Complexes by Fe Proteins and Heme and Nonheme Platforms

Nitroxyl (HNO/NO$^-$) heme-model complexes ({FeNO}^{8}, according to the Enemark–Feltham notation) have received special attention due to the intermediacy of nitroxyl-heme adducts in a variety of catalytic processes related to the biogeochemical cycle of nitrogen (*104*). For example, for the six-electron reduction of nitrite to ammonia that is catalyzed by cytochrome *c* nitrite reductase (ccNir), a heme{FeNO}^{8} complex is proposed as an intermediate (Scheme 5) (*105,106*). This intermediate has also been suggested for the reduction of NO to N_2O by P450nor (Scheme 6) (*107*). Then, the isolation of a suitable {FeNO}^{8} heme complex that allows structural and functional characterizations will help to understand the reaction mechanism of ccNir and other enzymes.

However, while there are several examples of HNO/NO$^-$ complexes with mainly second- or third-row transition metals in the literature (*108,109*), only few iron–nitroxyl complexes have been reported so far. In fact, stabilization of the heme Fe–HNO moiety has been achieved only for protein complexes Fe(globin) HNO (*87,110*) being the (Mb)HNO the most extensively characterized. Stabilization of the Fe(HNO) moiety in heme models, without the support of a protein environment, remains elusive, though a fairly stable {Ru(Por)HNO}^{8} complex, [Ru (TTP)(HNO)(1-MeIm)], was reported and the IR and ^{1}H NMR spectra were recorded, providing the diagnostic signatures to clearly identify the complex as an HNO adduct, without a crystal

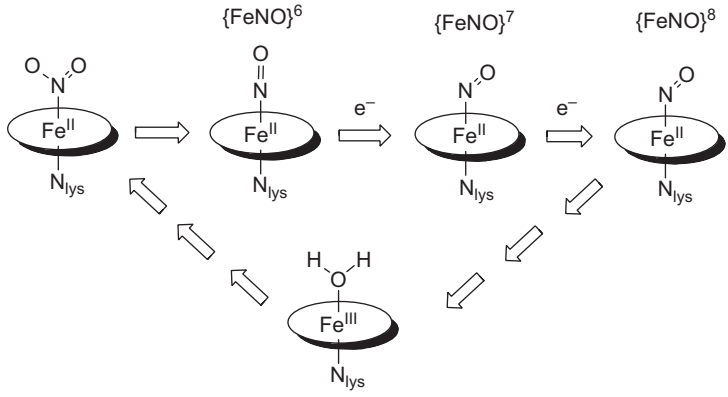

Scheme 5. Reduction of nitrite to ammonia by ccNiR. Proposed mechanism for the formation of the {FeNO}^{8} intermediate.

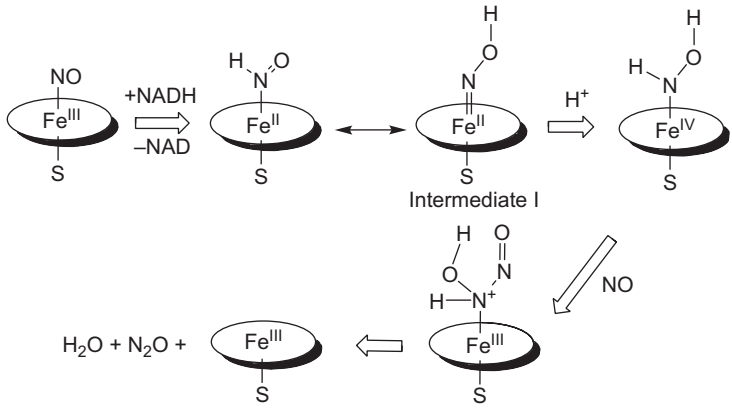

SCHEME 6. Proposed mechanism for the conversion of NO into N_2O by P450nor.

structure (*111*). Interestingly, the signal due to HNO in the ^1H NMR spectrum and the ν_{NO} matched well with the values obtained for (Mb)HNO (*87,88*), which suggest that the ruthenium porphyrinate platform could serve as a heme model. In contrast, the iron porphyrinates were proved to be able to stabilize the deprotonated $\{FeNO\}^8$ form, specially with macrocycles bearing highly electron-withdrawing substituents, but attempts to protonate the NO^- complexes to give the corresponding HNO adducts were unsuccessful, with reoxidation to the $\{FeNO\}^7$ (*69,112*). This difference in reactivity with (Mb)HNO is surely related to extra stabilization of the $\{Fe(H)NO\}^8$ moiety by distal amino acids; though taking into account the existence of the $\{Ru(Por)HNO\}^8$ mentioned above, the protein is not a compulsory platform to obtain a heme model of the $\{M(H)NO\}^8$ species. Apart from the ruthenium porphyrinate and the globin HNO adducts, there are two nonheme $\{FeNO\}^8$ complexes reported, the deprotonated complex Fe(NO)(cyclam-ac) (*113*) and the recently reported HNO adduct in aqueous solution, $[Fe(CN)_5HNO]^{3-}$, with a determined pK_a for coordinated HNO of 7.7 (*114*). One interesting point in relation to deprotonated $\{FeNO\}^8$ complexes is the difference in electronic structures between the heme and nonheme moieties. According to FTIR, UV–vis, ^{15}N NMR, and DFT results, the electronic structure of the $\{Fe(Por)NO\}^8$ complex $[Co(C_5H_5)_2]^+$ $[Fe(TFPPBr_8)NO]^-$ is best described as intermediate between $[Fe(II)(Por)NO]^-$ and $[Fe(I)(Por)NO]^-$ (*69*), as previously proposed for $[Fe(Porphine)NO]^-$ from DFT calculations (*115*), which is in sharp contrast with the

predominant Fe(II)NO^- character of known nonheme {Fe(Por)NO}^{8} complexes (*113*).

The high stability of the (Mb)HNO adduct (half-life in anaerobic aqueous solution greater than 6 months) made this complex the most appropriate model for characterization of the elusive {Fe(H)NO}^{8} moiety in a biologically relevant scenario. The structure and reactivity issues covered include different routes to the HNO adduct, full spectroscopic characterization: UV–vis, ^{1}H and ^{15}N NMR, Raman, X-ray absorption spectroscopy, reactivity with small molecules such as NO, NO_2^-, and O_2, and flash photolysis experiments. (Mb)HNO was first obtained in bulk and isolated in 2000 by chemical reduction of (Mb)NO with Cr(II)(EDTA) in aqueous solution, Eq. (26) (*87*). The higher yields were obtained at pH>9.5; the main byproduct at lower pH was deoxyMb. Some years later, the same group reported the efficient trapping of free HNO by deoxyMb, a second route to (Mb)HNO, Eq. (27) (*88*). Two HNO donors were used to generate free HNO, methylsulfonylhydroxylamine (MSHA), CH_3SO_2NHOH, at alkaline pHs or AS, $Na_2N_2O_3$, in neutral solutions.

Experiments with MSHA from stoichiometric to threefold excess of reagent were carried out and yields between 60% and 80% were obtained, with (Mb)NO as the main byproduct. At higher MSHA concentrations, the formation of (Mb)HNO took shorter times, but afterwards its concentration decreased rapidly. Without chromatographic purification the (Mb)HNO yield also decreased dramatically and this was attributed to further reaction with NO, HNO or with other MSHA decomposition products. A detailed kinetic analysis of the reaction of MSHA with deoxyMb gave an estimate of k=1.4x10^{4}M^{-1}s^{-1} for the trapping reaction, Eq. (27).

$$(\mathrm{Mb})\mathrm{NO} + \mathrm{Cr(II)(EDTA)} + \mathrm{H^+} \rightarrow (\mathrm{Mb})\mathrm{HNO} + [\mathrm{Cr(III)(EDTA)}]^+ \tag{26}$$

$$\mathrm{HNO} + \mathrm{deoxyMb} \rightarrow (\mathrm{Mb})\mathrm{HNO} \tag{27}$$

Reaction of AS with deoxyMb resulted more complicated due to the generation of metMb from the reaction of NO_2^- (byproduct of AS decomposition) with deoxyMb, Eq. (28).

$$\mathrm{deoxyMb} + \mathrm{NO_2^-} + \mathrm{H^+} \rightarrow \mathrm{metMb} + \mathrm{NO} + \mathrm{OH^-} \tag{28}$$

For example, stoichiometric reaction of AS with 4mM deoxyMb at pH 7 gave within 6min ca. 50% (Mb)HNO/(Mb)NO, 20% deoxyMb, and 30% metMb, while after half a day, the solution

contained more than 90% of (Mb)NO. Taking advantage of the first order on [H^+] of Eq. (28), the reaction of AS with deoxyMb in 1.5:1 ratio at pH 8 gave ca. 60% isolated (Mb)HNO after 30 min. Time-dependent UV–vis analysis showed a clear conversion to a (Mb)HNO/(Mb)NO mixture without formation of metMb.

More recently, a new route to (Mb)HNO was proposed, Eq. (29), that gave the desired product in >96% yield (*84*).

$$\mathrm{Mb} + \mathrm{NaNO_2} + \mathrm{NaBH_4} \rightarrow (\mathrm{Mb})\mathrm{HNO} \tag{29}$$

From this reactivity and from experiments with known HNO scavengers, it was concluded that the mixture $NaNO_2/NaBH_4$ generated free HNO, Eq. (30), that is then trapped by deoxyMb, as in Eq. (27).

$$\mathrm{HONO} + \mathrm{H^-} \rightarrow \mathrm{HNO} + \mathrm{OH^-} \tag{30}$$

Insight into the electronic structure of Mb(HNO) was attained by several spectroscopic methods. Protonation at the nitrogen was confirmed by ^{1}H NMR with a signal at 14.8 ppm, well downfield from the protein peaks, that splits into a doublet (J=72 Hz) in the labeled derivative, clearly a diagnostic signature of bound HNO (*87,114*). On the other hand, the chemical shift of (Mb)$H^{15}NO$ at +788 ppm versus $^{15}NH_4^+$ in the ^{15}N NMR is similar to several Co(III)NO^- complexes and is also considered a well-diagnostic feature for $\{MNO\}^8$ moieties (*116*), specially for unprotonated complexes which lack the characteristic ^{1}H NMR signal.

^{1}H NMR spectroscopy also afforded further insight into the structure of Mb(HNO) (*117*). The 2D NOESY maps showed 20 NOE connectivities with the HNO signal. A computer model of (Mb)HNO was generated by replacing the CO ligand by HNO in the crystal structure of (Mb)CO and fitting with the experimental ^{1}H NMR NOESY data. Surprisingly, only one orientation of the HNO ligand was found, almost perpendicular to proximal His93. This was suggested to be related to the π-acidity of both HNO and His ligands since the perpendicular orientation would minimize π back-bonding competition. A similar orientation was obtained upon simple energy minimization, which suggests a steric control of the orientation. The most significant difference between the residues of (Mb)HNO and (Mb)CO was the movement of the distal His64, by ca. 20° rotation to reach hydrogen bonding distance of the nitroxyl oxygen. Thus, the surprising stability of (Mb)HNO may be due in part to this hydrogen bonding interaction within the distal pocket, as in the isoelectronic (Mb)

O_2 adduct. On the other hand, given the absence of a proton acceptor close to the H atom of HNO, it was suggested that a water molecule could serve as the acceptor.

The structural characterization of the heme Fe(HNO) moiety in (Mb)HNO was achieved through X-ray absorption spectroscopy (*118*). As commonly observed in complexes $\{MNO\}^n$ with n=6, 7, and 8, the Fe—N(NO) bond lengths increase and the FeNO angles decrease in the order Mb(III)NO, Mb(II)NO, (Mb)HNO, that is, in the order n=6, 7, 8. The Fe—N(His) bond is also longer in the $\{FeNO\}^8$ adduct, as compared to that of the n=6 and 7 forms, while the Fe—N(Por) lengths are essentially the same for all three adducts. The stronger *trans* effect in $\{MNO\}^8$ complexes is well recognized. On the other hand, the N—O bond is longer in (Mb)HNO than in the n=6 and 7 forms, which is indicative of a high degree of ligand reduction, and is also consistent with the high shift in νN—O from 1617 cm^{-1} in (Mb)NO to 1385 cm^{-1} in (Mb)HNO. In contrast, the increase in νFe—N from 554 to 651 cm^{-1} is difficult to understand considering the observed lengthening of the Fe—N(NO) bond; this was attributed to the decrease in the reduced mass due to the lower FeNO angle in (Mb)HNO and/or a mixing with the bending Fe—N—O mode, which is not unlikely in highly bent geometries.

As we have reviewed above, (Mb)HNO served as a good model to afford structural insight into the elusive $\{Fe(Por)HNO\}^8$ species and to provide evidences for different routes to Fe(HNO) complexes. Some comments on the reactivity of this unusual adduct are also worth mentioning. Regarding the acid–base equilibrium, a change in the ^1H NMR signal due to HNO at 14.8 ppm was not observed from pH 6.5 to 10, suggesting a pK_a for (Mb)HNO higher than 10. Differently from $Fe(Por)NO^-$ (Por=TPP or $TFPPBr_8$) (*69,112*) or $[Ru(HNO)(\text{“pybuS}_4\text{”})]^+$ (*119*), Mb(HNO) is not oxidized upon protonation but is still a powerful one-electron reductant that is reoxidized to (Mb)NO by stoichiometric reaction with methyl viologen (*87*). Likewise, albeit (Mb)HNO has a half-life of ca. 6 months in anaerobic solutions, it is oxidized to metMb upon exposure to air over a period of minutes. Additionally, like the proposed nitroxyl intermediate of P450nor, (Mb)HNO reacts with NO to give (Mb)NO and N_2O over a period of minutes; the reaction with nitrite also yields (Mb)NO, at a pH-dependent rate. The same reactivity with NO was also observed for $RuHCl(HNO)CO(PiPr_3)_2$ (*120*). Finally, in contrast to other HNO adducts, (Mb)HNO is quite inert to displacement reactions and the HNO ligand is not displaced by CO (*108*). On the other hand, photolysis of solutions of (Mb)HNO yields metMb, which indicates that its geminate partner is the aminoxyl radical anion, HNO^-

(*121*). From the generation of metMb in the photolysis experiments, it was proposed that there is an important contribution of ferric character in the electronic structure of (Mb)HNO, that is, (Mb)Fe(III)HNO^-, analogous to the isoelectronic oxyMb, (Mb)Fe(III)O_2^-.

F. Electronic Structure Methods for Characterization of {Fe(Por)(H)NO}^{8} as Heme Protein Catalytic Intermediates

Several HNO-related species can be found in the literature, fundamentally as intermediates in catalytic cycles. Here, we will mention the application of electronic structure methodologies to three examples.

The first one is the ccNiR, which catalyzes the reduction of nitrite to ammonia. The active site of this protein comprises a protoporphyrin IX covalently linked to the backbone and a lysine as a proximal ligand (*122*). In this particular case, an HNO bound species was proposed as intermediate in the catalytic cycle. Using DFT calculations in a simplified model system including an iron porphyrin with proximal ammonia and different reaction intermediates as distal ligands, the different potential steps were studied (*105*). The proposed six-electron reduction mechanism (Scheme 5) involves as a first step the reduction from Fe(III)—H_2O to Fe(II)—H_2O followed by ligand displacement of water by nitrite in the active site. An heterolytic cleavage of one of the nitrite N—O bonds to produce an {FeNO}^{6} species is the second step. Calculations of the energy cost for different potential reactions suggest that the most plausible continuation of the mechanism has to be the reduction to {Fe(Por)NO}^{7} followed by a rapid one-electron reduction to {Fe(Por)NO}^{8}, which can then protonate to give the HNO bound species. The mechanism follows via a two-proton–two-electron step yielding an *N*-bound Fe(II)-hydroxylamine species. The next step involves incorporation of two protons and a reduction via one electron to produce an ammonia bound to an Fe(III) center, which is finally reduced to Fe(II). This species is ready to rebind a new nitrite, displacing the ammonia.

A second case comprises the key intermediates in the catalytic cycle of fungal NOR (P450nor). This enzyme converts NO to N_2O via a {FeNO}^{8} species (*123–125*). Using computational tools, Lehnert and coworkers have studied this mechanism (Scheme 6) (*115*), that involves coordination of NO to the Fe(III) form, a reducing step via NADH to yield an intermediate I (an Fe(II)(Por)NOH species) and finally a second reaction with NO to generate N_2O and the Fe(III) form. It has to be mentioned that

Intermediate I has been characterized via UV–vis and resonance Raman spectroscopy (*126,127*).

The calculations were carried out by modeling the systems with a six-coordinated porphyrin: an iron-porphine, nitrogenated species (NO, HNO, NOH, $N_2O_2^{2-}$, HN_2O_2, $H_2N_2O_2$), and 1-methylimidazole or methylthiolate as the proximal ligands. In order to get further insight into the biochemistry and to obtain vibrational information, the authors fully optimized the structures. An approximate pK_a for the protonation steps was also calculated taking into account the solvation effects by using an implicit solvent scheme (PCM model). Besides the results obtained regarding the mechanism, an interesting feature proposed by the authors is that, in contrast with the (Mb)HNO structure reported by Farmer, they suggested that the intermediate comprises a doubly protonated species. This Fe(IV)(Por)NHOH complex can react easily with the second NO molecule. The thiolate role is to stabilize this species and allows the double protonation.

These results are particularly important because the details of the heme-thiolate NOR (P450nor) catalytic mechanism are still controversial. One theory, supported by computational results (*128*), assumes two sequential one-electron transfers from NAD(P)H to an initial {Fe(Por)NO}^{6} complex. The {Fe(Por)NO}^{8} species thus formed would react with NO, eventually liberating the $ONNO^{2-}$ anion (most probably in its protonated form), which decomposes to N_2O and water. However, more recent experimental results (*107*) suggest the first step of the mechanism (Scheme 6) to be direct hydride transfer from NAD(P)H to {Fe(Por)NO}^{6}, presumably resulting in an iron-bound HNO unit. DFT geometry optimization of all the proposed reaction intermediates was reported, suggesting that the hydride transfer to {Fe(Por)NO}^{6} could produce {Fe(Por)NOH}^{8} or {Fe(Por)HNO}^{8}. Subsequent addition of NO to {Fe(Por)NOH}^{8}, but not to {Fe(Por)HNO}^{8} or {Fe(Por)N(H)OH}^{8}, is predicted to lead to immediate liberation of $HN_2O_2^-$ without any stable intermediates which finally decomposes to H_2O and N_2O. Contrary to what would be predicted according to the "thiolate push effect" dogma, the thiolate ligand at the heme active site is shown to obstruct NO reduction rather than facilitate it. It is in fact shown that replacement of the thiolate by a neutral nitrogen ligand (i.e., lysine, as found in the active site of ccNIR, mentioned above) clearly favors, from a thermodynamic point of view, NO reduction at the heme site (*129*).

Mentioned above, the third case is the interesting HNO–protein complex that has been obtained by Farmer *et al.* (*87,88*) and characterized theoretically by Linder and Rodgers

(*130*). Using DFT calculations on a model system to study the potential implicants of the different protonation schemes, the authors boarded the structural characterization of the HNO complex with myoglobin (MbHNO). The system was modeled as a [Fe(Por)HNO(ImH)]. Between the different questions that the authors intended to answer, they tried to understand where was the proton located. In order to resolve this issue, calculations of different coordination (O or N) and protonation (HNO or NOH) isomers were performed. The most stable isomer was found to be the N coordinated and protonated one. Another results showed that the geometrical parameters were almost insensitive to the rotation of the axial imidazole ligand ring, suggesting a decoupling of the Fe—N(H)O and Fe-ImH π-bonding, which agrees with the EXAFS structure showing the imidazole ring remaining almost in an eclipsed conformation respect to the pyrrolic ^{15}N atoms (*130*). The calculation of this rotated conformation is only 3.4kJ/mol higher than the ground state structure. Due to the fact that the rotational barrier around the Fe—N bond is low, the ligand conformation can be easily stabilized in the protein due to influences of the environment.

In a recent work, Zhang and coworkers focused on the importance of the computational tools to study compounds involving HNO and porphyrins, which are used thoroughly as models of heme proteins active sites (*131*). Using a quantitative structure observable relationship, the authors performed a large number of quantum calculations on heme models in order to evaluate potential methodologies to predict geometrical parameters: ^{1}H NMR displacements, ^{15}N NMR displacements, and ν_{NO} stretching frequencies of HNO and RNO bound moieties. Among the most interesting results, the authors explored the potential effect of water interaction with the HNO bound to an Fe(II) porphyrin, as a model for MbHNO. The calculations suggest that the IR frequency of the bound HNO in myoglobin can be explained by dual H_2O—HNO hydrogen bonding.

III. Azanone Detection with Metalloporphyrins and Heme Proteins

A. Colorimetric Detection of Azanone with Manganese Porphyrins

The high efficiency by which manganese porphyrins trap HNO, and the observed stability of {Mn(Por)NO}^{6} but not {Mn(Por)NO}^{5} complexes, suggested to test Mn(III) porphyrins as agents for HNO/NO discrimination. As mentioned in a previous chapter, differently from Fe(III) porphyrins, Mn(III) porphyrins do not

suffer reductive nitrosylation in the timescale of the reaction with HNO, and the conversion of Mn(III) porphyrins to Mn(II)(Por)NO results in a large shift of the UV–vis Soret band. Moreover, since water soluble metalloporphyrins (such as Mn(III)TPPS) or others which are soluble in organic solvents (such as Mn(III)TPP) can be used and show a similar shift, the method is useful for organic or aqueous solutions. An important disadvantage for this reaction is that the Mn(II)(Por)NO porphyrin obtained as a product reacts with O_2 to produce the starting Mn(III) back. Based on these data, Dobmeier *et al*. found a way to overcome this inconvenient (*132*) and designed a method for quantitative detection of nitroxyl with an estimated dynamic range of 24–290 nM. This optical sensor film, suitable for the quantitative determination of HNO, was obtained through encapsulation of Mn(III)TPPS within the anaerobic local environment of an aminoalkoxysilane xerogel membrane decorated with trimethoxysilyl-terminated poly(amidoamine-organosilicon) dendrimers, which were shown to be poorly O_2-permeable. This HNO-sensing films were tested with the HNO donors AS and sodium 1-(isopropylamino)diazene-1-ium-1,2-diolate (IPA/NO) and were found to provide a rapid means for determining HNO concentrations in aerobic solution. However, the rapid dimerization of HNO and relatively slow rate of HNO complexation in the xerogel film limit optimal sensor performance to environments with restricted HNO scavenging conditions and renders a narrow dynamic range.

Another way to circumvent the problem raised by the reactivity of the nitrosyl product toward O_2 is to protect the metalloporphyrin by a protein matrix which slows down the oxidation rate. In a recent report, Bari and coworkers described the reaction of Mn(III) protoporphyrinate IX reconstituted in apomyoglobin ($MbPIXMn^{III}$) and its chemical behavior toward HNO or NO donors, either under anaerobic or aerobic conditions (*102*). The Mn(III) reconstituted globin successfully reacted with the nitroxyl donor trioxodinitrate (AS), while it remained indifferent toward NO or NO donors, in good agreement with previously reported data on water soluble Mn(III) porphyrinates. As expected, and in contrast to what is observed for isolated Mn porphyrins, in the case of $MbPIXMn^{III}$, the formation of the characteristic nitrosyl complex $MbPIXMn^{II}(NO)$, due to reaction with free ^1HNO, is observed by UV–vis spectroscopy even in aerobic environment. The nitrosyl derivative is moderately stable in the presence of oxygen at room temperature, and it slowly retrieves the original reconstituted Mn(III) protein. Subsequent

additions of the HNO donor confirm the nature of the reaction product, as the nitrosyl derivative can be regenerated repeatedly.

Kinetic analysis show that the association rate constant for the reaction of the reconstituted globin with azanone is practically the same than that for the free porphyrinate, suggesting that the protein environment is not involved in the reaction mechanism. However, oxidation of the nitrosyl porphyrin inside the protein is ca. 1000 times slower than for the porphyrin in solution, a feature that is ascribed to the role played by the distal residues which protect the nitrosyl product inside the protein matrix (see Scheme 7).

Overall, these results clearly show that $MbPIXMn^{III}$ is a good candidate for a physiologically compatible HNO probe, while they also highlight the modulation of the reactivity of metallonitrosyl complexes toward O_2 by a protein environment.

A main disadvantage to be taken into account for both these colorimetric methods is that, due to the fact that the UV–vis measurements are done in a wavelength range where biological materials strongly absorb, these optical methods cannot be used for most *in vitro* or *in vivo* studies.

B. Electrochemical Detection of Azanone with a Cobalt Porphyrin

Metalloporphyrins are widely used in technical applications, including gas sensors (*133,134*), when coupled to a surface. Ordered monolayers of metalloporphyrins can be easily built, especially when surface molecule linking is based on the establishment of Au—S bonds, and a number or thiol bearing

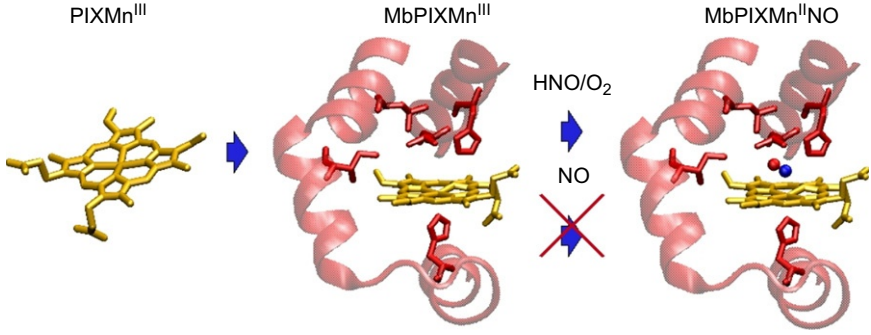

Scheme 7. Reaction of MbPIXMn(III) with HNO

porphyrins are available. Further, the use of *S*-acetyl protecting groups that undergo *in situ* cleavage on the surface allows the obtention of single porphyrin layers in a straightforward manner. Based on the previously described cobalt porphyrins reactivity toward NO and HNO (Section II.E), and the common use of surface-modified electrodes as electrochemical sensors, a porphyrin with four anchors, Co(II)-5,10,15,20-tetrakis[3-(*p*-acetylthiopropoxy) phenyl]porphyrin (Co(Por)), shown in Fig. 1, was immobilized on a gold surface by the formation of Au—S bonds (*82*). Both XPS and STM techniques show that most Co(Por) molecules are adsorbed in the lying down configuration by multiple linker binding to the gold surface, and that vacant gold sites are present that can be occupied in some cases by smaller lateral size adsorbates.

The reactions of HNO and NO with electrode bound Co(Por) were studied by electrochemical techniques. Previous studies by Kadish and coworkers showed that for nitrosyl complexes of Co (Por) in solution, four redox couples are found corresponding to the equilibria between $[Co(Por)NO]^{+2}$, $[Co(Por)NO]^{+1}$, $Co^{III}(Por)NO^{-}$, $[Co(Por)NO]^{-}$, and $[Co(Por)NO]^{2-}$ states (*135*).

Electrochemical measurements of Co(Por) bound to electrodes show the presence of three redox couples as well as the electrode bound nitrosyl porphyrin complex. The most significant feature of the electrochemical data is that for Co^{III}/Co^{II} couple (Eq. (31)); the obtained $E_{1/2}$ value is shifted ca. 400 mV to lower potentials compared to the $E_{1/2}$ in solution, strongly suggesting that Co(Por) adsorption on the gold electrode facilitates Co^{II} oxidation. On the other hand, for the nitrosyl porphyrin, the shift due to the gold surface effect is much smaller, and of only 60 mV

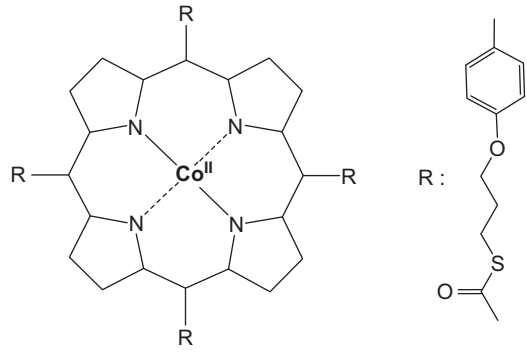

FIG. 1. Co(II)-5,10,15,20-tetrakis[3-(*p*-acetylthiopropoxy) phenyl] porphyrin.

(Eq. (32)). This is ascribed to charge donation from the gold surface which stabilizes the Co(III) state in $[Co(III)(Por)]^+$. This Co–Au interaction is weakened by NO coordination to the metal center.

$$[Co(III)(Por)]^+ + e^- \rightleftharpoons Co(II)(Por) \tag{31}$$

$$[Co(III)(Por)NO]^+ + e^- \rightleftharpoons Co(III)(Por)NO^- \tag{32}$$

Both NO reactivity and HNO reactivity of Co(Por) modified electrodes were tested in both the Co(II) and Co(III) oxidation states by electrochemical methods. While Co^{III}(Por) reacts efficiently with HNO, it does not so with NO. This is evidenced by the presence of the $[Co^{III}(Por)NO]^+/[Co^{II}(Por)NO]$ oxidation peak at 0.8V, after HNO addition to the Co(Por) electrode, and the lack of any electrochemical signal when NO donors are used instead. On the contrary, NO reacts rapidly with Co^{II}(Por) modified electrodes while HNO does not. In summary, Co(Por) attached to gold retains the same selective behavior toward HNO and NO, as observed in solution. Based on the redox-dependent selective reactivity observed for the Co(Por) bound electrodes toward NO and HNO, and the redox potential shift due to a surface effect, the reaction Scheme 8 was proposed to selectively detect HNO amperometrically. According to Scheme 8, the resting state electrode potential is set to 0.8V, a value where the porphyrin is stable in the Co^{III}(Por) state and no current flow is observed. Reaction with HNO yields, according to previous observations, the $Co^{III}(Por)NO^-$ complex, which under the described conditions is oxidized to Co^{III}(Por)NO. The resulting Co^{III}(Por)NO complex releases the NO ligand in a fast manner and yields Co^{III}(Por), which allows the catalytic cycle to start again. In this scheme, the current intensity should be

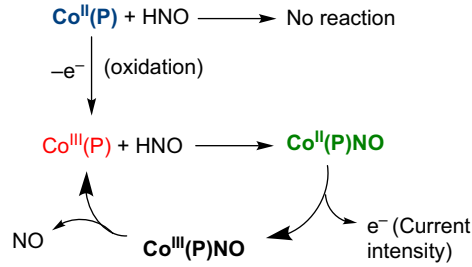

SCHEME 8. Reactions involved in the amperometrical detection of HNO by Co(Por).

proportional to the amount of HNO that binds the Co^{III}(Por). Consistent with the proposed scheme, measurement of the current versus time plot at 0.8V, where Co^{III}(Por) is stable, does not show any measurable current change. However, a few seconds after the addition of AS, the current intensity increases and is maintained during several minutes, due to the catalytic cycle, which is sustained by continuous HNO production from the donor, while no signal is produced by the addition of either NO(g) or NO donors. These results make a strong point for the use of Co^{III}(Por) electrodes as selective azanone sensors (*82*).

IV. Conclusions

The comparative analysis of azanone reactivity with small molecules and proteins in the context of physiological systems strongly suggests that its main targets are constituted by thiols such as cysteine (*22,28*), and metalloproteins, mostly ferric heme proteins. Reaction with abundant oxygen is too slow to be important, and nitroxyl does not react with superoxide anion (*69,89,136*). Reaction with heme proteins shows that although stable complexes have been reported for ferrous myoglobin and other globins, it is still not clear if this reaction is physiologically relevant (*84,88,110*). Moreover, kinetic studies related to the formation and decomposition of the corresponding complexes are needed in order to have a better estimation of their competing reactivity and stability. On the contrary, moderate to fast association rates, which results in a reductive nitrosylation that yields the quite stable ferrous nitrosyl complexes, characterize the reaction of HNO with ferric heme proteins and models. The studied examples include several cytochromes and peroxidases (*27,72,102,137,138*) as well as ferric porphyrines (*52,53*). In the case of proteins, the resulting complexes may be inactive for normal protein function providing an explanation for the observed HNO effects. Which specific protein is targeted will, however, depend on the local protein concentration and its specific reactivity, which in turns depends on the local environment of the heme, as for other ligands.

Concerning azanone detection, until recently, only indirect methods were available, the most popular being measurement of N_2O concentration (*27,82*). In the past few years, as described above, several metalloporphyrin methods have been developed to detect and quantify HNO in a reliable manner (*82,132,139,140*). UV–vis-based methods, such as manganese porphyrin-based xerogels or manganese reconstituted myoglobin, have severe limitations for biological samples because the signal to be observed

overlaps with the absorbance of heme proteins, which are the main targets under study. Also, they may interfere with the physiological state if used *in vivo*, since they have been shown to react with several other targets besides HNO (*73,141*). On the other hand, metalloporphyrin modified electrodes that produce an electrochemical response to HNO offer an excellent prospect for the development of a reliable, sensitive, selective, and physiologically compatible HNO sensor. Although clearly more work is needed in this area, present results indicate that HNO can be detected up to estimated concentrations of ca. 10 nM. This can be compared to the initial concentration of HNO produced by 10^{-3} M AS or PA in aerobic solutions at r.t. and pH 7.4: ca. 100 nM. Moreover, the already studied Co-porphyrin modified electrode discriminates HNO from NO (i.e., it is completely insensitive to NO) and responds to repeated additions of an HNO donor, without signal loss (*82*). What lies ahead is further development of this method in order to (i) test the response in the presence of possible interfering species, like NO_2^-, O_2, O_2^-, thiols, etc., (ii) calibrate the quantitative response to increasing HNO concentrations, (iii) improve the electrode by the use of nanostructured materials such as polyelectrolyte brushes (*142*) in order to increase the sensitivity to the pM level, and (iv) achieve electrode miniaturization for *in vivo, in situ*, and inside-cell measurements. In summary, a metalloporphyrin, reliable, sensitive, selective, and physiological compatible HNO-sensing device is expected to be available in the near future.

Acknowledgments

This work was financially supported by the University of Buenos Aires UBACYT X065 and UBACyT2010-12 to MAM, Agencia Nacional de Promoción Científica y Tecnológica (PICT 2006-2396 and PICT-07-1650) and CONICET PIP1207. M. A. M. and F. D. are members of CONICET.

References

1. Doctorovich, F., et al. *Coord. Chem. Rev.* **2011,** *255*(23-24), 2764–2784.
2. Bruna, P. *Chem. Phys. Lett.* **1979,** *67*, 109–114.
3. Guadagnini, R.; Schatz, G. C.; Walch, S. P. *J. Chem. Phys.* **1995,** *102*, 774.
4. Luna, A.; Merch, M.; Srn, B.; Roos, O. *Chem. Phys.* **1995,** *196*, 437–445.
5. Moncada, S.; Palmer, R. M.; Higgs, E. A. *Pharmacol. Rev.* **1991,** *43*, 109–142.
6. Ignarro, L. J. *Kidney Int.* **1996,** *49* (Suppl. 55), S2.
7. Miranda, K. M., et al. *Proc. Natl. Acad. Sci. USA* **2003,** *100*, 9196–9201.

8. Switzer, C. H., et al. *Biochim. Biophys. Acta* **2009,** *1787*, 835–840.
9. Paolocci, N., et al. *Pharmacol. Ther.* **2007,** *113*, 442–458.
10. Miranda, K. M.; Nagasawa, H. T.; Toscano, J. P. *Curr. Top. Med. Chem.* **2005,** *5*, 649–664.
11. Ma, X. L., et al. *Proc. Natl. Acad. Sci. USA* **1999,** *96*, 14617.
12. Tocchetti, C. G., et al. *Circ. Res.* **2007,** *100*, 96–104.
13. Lancel, S., et al. *Circ. Res.* **2009,** *104*, 720–723.
14. Ma, X. L.; Weyrich, A. S.; Lefer, D. J.; Lefer, A. M. *Circ. Res.* **1993,** *72*, 403–412.
15. Adak, S.; Wang, Q.; Stuehr, D. J. *J. Biol. Chem.* **2000,** *275*, 33554–33561.
16. Schmidt, H. H., et al. *Proc. Natl. Acad. Sci. USA* **1996,** *93*, 14492–14497.
17. Feelisch, M.; Te Poel, M.; Zamora, R.; Deussen, A.; Moncada, S. *Nature* **1994,** *368*, 62–65.
18. Ishimura, Y., et al. *Biochem. Biophys. Res. Commun.* **2005,** *338*, 543–549.
19. Hobbs, A. J.; Fukuto, J. M.; Ignarro, L. J. *Proc. Natl. Acad. Sci. USA* **1994,** *91*, 10992–10996.
20. Woodward, J. J.; Nejatyjahromy, Y.; Britt, R. D.; Marletta, M. A. *J. Am. Chem. Soc.* **2010,** *132*, 5105–5113.
21. Stoll, S., et al. *J. Am. Chem. Soc.* **2010,** *132*, 11812–11823.
22. Donzelli, S., et al. *Free Radic. Biol. Med.* **2006,** *40*, 1056–1066.
23. Donzelli, S., et al. *Free Radic. Biol. Med.* **2008,** *45*, 578–584.
24. Bari, S. E.; Amorebieta, V. T.; Gutiérrez, M. M.; Olabe, J.a.; Doctorovich, F. *J. Inorg. Biochem.* **2010,** *104*, 30–36.
25. Niketic, V.; Stojanovic, S.; Nikolic, A.; Michelson, A. M. *Free Radic. Biol. Med.* **1999,** *27*, 992–996.
26. Stoyanovsky, D. A., et al. *J. Am. Chem. Soc.* **2005,** *127*, 15815–15823.
27. Miranda, K. M. *Coord. Chem. Rev.* **2005,** *249*, 433–455.
28. Bartberger, M. D.; Fukuto, J. M.; Houk, K. N. *Proc. Natl. Acad. Sci. USA* **2001,** *98*, 2194–2198.
29. Veprek-Siska, J.; Pliska, V.; Smirous, F.; Visely, F. *Collect. Czech. Chem. Commun.* **1959,** *24*, 687–693.
30. Hughes, M. N.; Wimbledon, P. E. *Chem. Ind.* **1975,** 742–743.
31. Maragos, C. M., et al. *J. Med. Chem.* **1991,** *34*, 3242–3247.
32. Bonner, F. T.; Ravid, B. *Inorg. Chem.* **1975,** *14*, 558–563.
33. Hughes, M. N.; Wimbledon, P. E. *J. Chem. Soc. Dalton Trans.* **1976,** *8*, 703–707.
34. Porcheddu, A.; De Luca, L.; Giacomelli, G. *Synlett* **2009,** *2009*, 2149–2153.
35. Bonner, F. T.; Ko, Y. H. *Inorg. Chem.* **1992,** *31*, 2514–2519.
36. Seel, F.; Bliefert, C. *Z. Anorg. Allg. Chem.* **1972,** *394*, 187–196.
37. Shafirovich, V.; Lymar, S. V. *Proc. Natl. Acad. Sci. USA* **2002,** *99*, 7340–7345.
38. Buchholz, J. R.; Powell, R. E. *J. Am. Chem. Soc.* **1963,** *85*, 509–511.
39. Liochev, S. I.; Fridovich, I. *Free Radic. Biol. Med.* **2003,** *34*, 1399–1404.
40. Lymar, S. V.; Shafirovich, V.; Poskrebyshev, G. A. *Inorg. Chem.* **2005,** *44*, 5212–5221.
41. Lymar, S. V.; Shafirovich, V. *J. Phys. Chem. B* **2007,** *111*, 6861–6867.
42. Goldstein, S.; Czapski, G. *Free Radic. Biol. Med.* **1995,** *19*, 505–510.
43. Huie, R. E.; Padmaja, S. *Free Radic. Res. Commun.* **1993,** *18*, 195–199.
44. Goldstein, S.; Czapski, G. *J. Am. Chem. Soc.* **1996,** *118*, 3419–3425.
45. Smallwood, H. M. *J. Am. Chem. Soc.* **1929,** *51*, 1985–1999.
46. King, S.; Nagasawa, H. *Methods Enzymol.* **1999,** *301*, 211.
47. Orgel, L. E. *J. Chem. Soc.* **1953,** 1276–1278.

48. Walsh, A. D. *J. Chem. Soc.* **1953,** 2288–2296.
49. Bartberger, M. D., et al. *Proc. Natl. Acad. Sci. USA* **2002,** *99*, 10958–10963.
50. Szmytkowski, C.; Maciag, K. *J. Phys. B Atom. Mol. Phys.* **1991,** *24*, 4273.
51. Tennyson, J.; Noble, C. *J. Phys. B: At. Mol. Phys.* **1986,** *19*, 4025.
52. Martí, M. A.; Bari, S. E.; Estrin, D. A.; Doctorovich, F. *J. Am. Chem. Soc.* **2005,** *127*, 4680–4684.
53. Suárez, S. A., et al. *Polyhedron* **2007,** *26*, 4673–4679.
54. Bari, S. E.; Martí, M. A.; Amorebieta, V. T.; Estrin, D. A.; Doctorovich, F. *J. Am. Chem. Soc.* **2003,** *125*, 15272–15273.
55. Kohout, F. C.; Lampe, F. W. *J. Am. Chem. Soc.* **1965,** *87*, 5795.
56. Smith, P. A. S.; Hein, G. E. *J. Am. Chem. Soc.* **1960,** *82*, 5731–5740.
57. Buchholz, J. R.; Powell, R. E. *J. Am. Chem. Soc.* **1965,** *87*, 2350–2353.
58. Bonner, F. T.; Dzelzkalns, L. S.; Bonucci, J. A. *Inorg. Chem.* **1978,** *17*, 2487–2494.
59. Smith, A. L.; Johnston, H. L. *J. Am. Chem. Soc.* **1952,** *74*, 4696–4698.
60. Bryukov, M. G., et al. *Chem. Phys. Lett.* **1993,** *208*, 392–398.
61. Ford, P. C. *Inorg. Chem.* **2010,** *49*, 6226–6239.
62. Hoshino, M.; Laverman, L.; Ford, P. C. *Coord. Chem. Rev.* **1999,** *187*, 75–102.
63. Kadish, K. M. *The Porphyrin Handbook.* Academic Press: Boston, **2000**.
64. Richter-Addo, G. B.; Legzdins, P. *Metal Nitrosyls.* Oxford University: New York, **1992**.
65. Enemark, J. H.; Feltham, R. D. *J. Am. Chem. Soc.* **1974,** *96*, 5002–5004.
66. Westcott, B. L.; Enemark, J. H. *Inorganic Electronic Structure and Spectroscopy.* John Wiley & Sons: New York, **1999**.
67. Enemark, J. H.; Feltham, R. D. *Coord. Chem. Rev.* **1974,** *13*, 339–406.
68. Wyllie, G. R. A.; Scheidt, W. R. *Chem. Rev.* **2002,** *102*, 1067–1090.
69. Pellegrino, J.; Bari, S. E.; Bikiel, D. E.; Doctorovich, F. *J. Am. Chem. Soc.* **2010,** *132*, 989–995.
70. Laverman, L. E.; Ford, P. C. *J. Am. Chem. Soc.* **2001,** *123*, 11614–11622.
71. Wayland, B. B.; Olson, L. W. *J. Am. Chem. Soc.* **1974,** *96*, 6037–6041.
72. Hoshino, M.; Maeda, M.; Konishi, R.; Seki, H.; Ford, P. C. *J. Am. Chem. Soc.* **1996,** *118*, 5702–5707.
73. Spasojevic, I.; Batini-Haberle, I.; Fridovich, I. *Nitric Oxide* **2000,** *4*, 526–533.
74. Zahran, Z. N.; Lee, J.; Alguindigue, S. S.; Khan, M. A.; Richter-Addo, G. B. *Dalton Trans.* **2004,** 44–50.
75. Scheidt, W. R.; Hoard, J. L. *J. Am. Chem. Soc.* **1973,** *95*, 8281–8288.
76. Roncaroli, F.; Eldik, R. V. *J. Am. Chem. Soc.* **2006,** *128*, 8042–8053.
77. Schopfer, M. P.; Wang, J.; Karlin, K. D. *Inorg. Chem.* **2010,** *49*, 6267–6282.
78. Blomberg, M. R. A.; Siegbahn, P. E. M. *Biochim. Biophys. Acta* **2006,** *1757*, 969–980.
79. Praneeth, V. K. K.; Näther, C.; Peters, G.; Lehnert, N. *Inorg. Chem.* **2006,** *45*, 2795–2811.
80. Collman, J. P., et al. *J. Am. Chem. Soc.* **2008,** *130*, 16498–16499.
81. Collman, J. P., et al. *Proc. Natl. Acad. Sci. USA* **2008,** *105*, 15660–15665.
82. Suárez, S. A., et al. *Inorg. Chem.* **2010,** *49*, 6955–6966.
83. Whitten, D. G.; Baker, E. W.; Corwin, A. H. *J. Org. Chem.* **1963,** *28*, 2363–2368.
84. Kumar, M. R.; Fukuto, J. M.; Miranda, K. M.; Farmer, P. J. *Inorg. Chem.* **2010,** *49*, 6283–6292.

85. Shiro, Y., et al. *J. Biol. Chem.* **1995,** *270*, 1617.
86. Shiro, Y., et al. *Biochemistry* **1995,** *34*, 9052–9058.
87. Lin, R.; Farmer, P. J. *J. Am. Chem. Soc.* **2000,** *122*, 2393–2394.
88. Sulc, F.; Immoos, C. E.; Pervitsky, D.; Farmer, P. J. *J. Am. Chem. Soc.* **2004,** *126*, 1096–1101.
89. Miranda, K. M., et al. *J. Inorg. Biochem.* **2003,** *93*, 52–60.
90. Bazylinski, D. A.; Hollocher, T. C. *J. Am. Chem. Soc.* **1985,** *107*, 7982–7986.
91. Bazylinski, D. A.; Goretski, J.; Hollocher, T. C. *J. Am. Chem. Soc.* **1985,** *107*, 7986–7989.
92. Dutton, A. S.; Fukuto, J. M.; Houk, K. N. *J. Am. Chem. Soc.* **2004,** *126*, 3795–3800.
93. Denninger, J. W.; Marletta, M. A. *Biochim. Biophys. Acta* **1999,** *1411*, 334–350.
94. Poulos, T. L. *Curr. Opin. Struct. Biol.* **2006,** *16*, 736–743.
95. Hobbs, A. J.; Ignarro, L. J. *Methods Enzymol.* **1996,** *269*, 134–148.
96. Capece, L.; Estrin, D. A.; Marti, M. A. *Biochemistry* **2008,** *47*, 9416–9427.
97. Miller, T. W., et al. *J. Biol. Chem.* **2009,** *284*, 21788–21796.
98. Dierks, E. A.; Burstyn, J. N. *Biochem. Pharmacol.* **1996,** *51*, 1593–1600.
99. Wilkins, P. C.; Jacobs, H. K.; Johnson, M. D.; Gopalan, A. S. *Inorg. Chem.* **2004,** *43*, 7877.
100. Koppenol, W.; Moreno, J.; Pryor, W. A.; Ischiropoulos, H.; Beckman, J. *Chem. Res. Toxicol.* **1992,** *5*, 834–842.
101. Sharma, V. S.; Isaacson, R. A.; John, M. E.; Waterman, M. R.; Chevion, M. *Biochemistry* **1983,** *22*, 3897.
102. Boron, I.; Suárez, S. A.; Doctorovich, F.; Martí, M. A.; Bari, S. E. *J. Inorg. Biochem.* **2011,** *105*, 1044–1049.
103. Scott, E. E.; Gibson, Q. H.; Olson, J. S. *J. Biol. Chem.* **2001,** *276*, 5177–5188.
104. Averill, B. A. *Chem. Rev.* **1996,** *96*, 2951–2964.
105. Einsle, O.; Messerschmidt, A.; Huber, R.; Kroneck, P. M. H.; Neese, F. *J. Am. Chem. Soc.* **2002,** *124*, 11737–11745.
106. Simon, J. *FEMS Microbiol. Rev.* **2002,** *26*, 285–309.
107. Daiber, A., et al. *J. Inorg. Biochem.* **2002,** *88*, 343–352.
108. Farmer, P. J.; Sulc, F. *J. Inorg. Biochem.* **2005,** *99*, 166–184.
109. Farmer, P. J.; Kumar, M. R.; Almaraz, E. *Comments Inorg. Chem.* **2010,** *31*, 130–143.
110. Kumar, M. R., et al. *Biochemistry* **2009,** *48*, 5018–5025.
111. Lee, J.; Richter-Addo, G. B. *J. Inorg. Biochem.* **2004,** *98*, 1247–1250.
112. Choi, I. K.; Liu, Y.; Feng, D.; Paeng, K. J.; Ryan, M. D. *Inorg. Chem.* **1991,** *30*, 1832–1839.
113. Serres, R. G., et al. *J. Am. Chem. Soc.* **2004,** *126*, 5138–5153.
114. Montenegro, A. C., et al. *Angew. Chem. Int. Ed Engl.* **2009,** *48*, 4213–4216.
115. Lehnert, N.; Praneeth, V.; Paulat, F. *J. Comput. Chem.* **2006,** *27*, 1338–1351.
116. Mason, J.; Larkworthy, L. F.; Moore, E. A. *Chem. Rev.* **2002,** *102*, 913–934.
117. Sulc, F.; Fleischer, E.; Farmer, P. J.; Ma, D.; La Mar, G. N. *J. Biol. Inorg. Chem.* **2003,** *8*, 348–352.
118. Immoos, C. E., et al. *J. Am. Chem. Soc.* **2005,** *127*, 814–815.
119. Sellmann, D.; Gottschalk-Gaudig, T.; Häußinger, D.; Heinemann, F. W.; Hess, B. A. *Chem. Eur. J.* **2001,** *7*, 2099–2103.

120. Marchenko, A. V., et al. *Inorg. Chem.* **2002,** *41*, 4087–4089.
121. Pervitsky, D.; Immoos, C.; Veer, W. V. D.; Farmer, P. J. *J. Am. Chem. Soc.* **2007,** *129*, 9590–9591.
122. Einsle, O., et al. *Nature* **1999,** *400*, 476–480.
123. Richardson, D. J.; Watmough, N. J. *Curr. Opin. Chem. Biol.* **1999,** *3*, 207–219.
124. Ferguson, S. J. *Curr. Opin. Chem. Biol.* **1998,** *2*, 182–193.
125. Moura, I.; Moura, J. J. *Curr. Opin. Chem. Biol.* **2001,** *5*, 168–175.
126. Fujii, M. *J. Biol. Chem.* **1995,** *270*, 1617–1623.
127. Obayashi, E.; Takahashi, S.; Shiro, Y. *J. Am. Chem. Soc.* **1998,** *120*, 12964–12965.
128. Harris, D. L. *Int. J. Quantum Chem.* **2002,** *88*, 183–200.
129. Vincent, M.; Hillier, I.; Ge, J. *Chem. Phys. Lett.* **2005,** *407*, 333–336.
130. Linder, D. P.; Rodgers, K. R. *Inorg. Chem.* **2005,** *44*, 8259–8264.
131. Ling, Y.; Mills, C.; Weber, R.; Yang, L.; Zhang, Y. *J. Am. Chem. Soc.* **2010,** *132*, 1583–1591.
132. Dobmeier, K. P.; Riccio, D. A.; Schoenfisch, M. H. *Anal. Chem.* **2008,** *80*, 1247–1254.
133. Guillaud, G. *Coord. Chem. Rev.* **1998,** *178–180*, 1433–1484.
134. Davies, I. R.; Zhang, X. *Methods Enzymol.* **2008,** *436*, 63–95.
135. Richter-Addo, G. B., et al. *Inorg. Chem.* **1996,** *35*, 6530–6538.
136. Irvine, J. C., et al. *Trends Pharmacol. Sci.* **2008,** *29*, 601–608.
137. Bikiel, D. E., et al. *Phys. Chem. Chem. Phys.* **2006,** *8*, 5611–5628.
138. Doyle, M. P.; Mahapatro, S. N.; Broene, R. D.; Guy, J. K. *J. Am. Chem. Soc.* **1988,** *110*, 593–599.
139. Rosenthal, J.; Lippard, S. J. *J. Am. Chem. Soc.* **2010,** *132*, 5536–5537.
140. Tennyson, A. G.; Do, L.; Smith, R. C.; Lippard, S. J. *Nitric Oxide* **2007,** *26*, 4625–4630.
141. Batinic-Haberle, I., et al. *Inorg. Chem.* **1999,** *38*, 4011–4022.
142. Choi, E.-Y., et al. *Langmuir* **2007,** *23*, 10389–10394.

ADVANCES IN THE MECHANISTIC UNDERSTANDING OF SELECTED REACTIONS OF TRANSITION METAL POLYAMINECARBOXYLATE COMPLEXES

ARIANE BRAUSAM and RUDI VAN ELDIK

Department of Chemistry and Pharmacy, University of Erlangen-Nürnberg, Egerlandstr. 1, Erlangen, Germany

ABSTRACT

This review deals with the reaction mechanisms of polyaminecarboxylate complexes of different transition metals such as Fe, Mn, Ni, and Ru. Three types of chemical processes are treated, viz. water-exchange reactions, the binding of NO, and the activation of peroxides. In each case, the nature of the polyaminecarboxylate chelate and its influence on the underlying reaction mechanism are considered. In general, the complexes are either six- or seven-coordinate and all contain a coordinated water molecule. The lability of the latter is controlled by the nature of the polyaminecarboxylate chelate and the oxidation state of the metal ion. The binding of NO and the activation of peroxide are in turn controlled by the lability of the coordinated water molecule that is displaced during the interaction with these small molecules.

INORGANIC/BIOINORGANIC REACTION MECHANISMS
VOLUME 64 ISSN 0898-8838 / DOI: 10.1016/B978-0-12-396462-5.00005-2

Keywords: Reaction mechanisms; Activation of NO; Activation of peroxide; Polyaminecarboxylate complexes; Water-exchange reactions.

I. Introduction

Since Ferdinand Munz synthesized edta in the early 1930 for the first time (*1,2*), edta (ethylenediaminetetraacetate) and related chelating agents made a remarkable impact and are used in large quantities worldwide. The most prominent feature of polyaminecarboxylates is their outstandingly high formation constant for various metal cations. Therefore, they are often used in industrial processes, medical applications, and domestic products in order to solubilize and inactivate metal ions through complex formation. Applications of polyaminecarboxylic acids cover a wide range. They are used in detergents, textile and paper processing, photographic developing, water treatment, electroplating, and flue gas scrubbing. Due to the good solubility and high stability of the complexes formed with polyaminecarboxylic acids, they are also used in agricultural fertilizers. Polyaminecarboxylic acids are of particular interest in medicine and biology; they are used in heavy metal detoxification (*2*) and as contrast agents in magnetic resonance imaging. The common role of polyaminecarboxylic acids in this wide range of applications is the regulation of the metal ion concentration.

Their broad application spectrum gives rise to a consumption of more than 200,000 ton/a of polyaminecarboxylic acids worldwide (*3*). By far, the most used polyaminecarboxylates are edta and nta (*3*). Because of their good solubility and low biodegradability, especially of edta, polyaminecarboxylic acids can enter the water cycle via industrial and domestic wastewaters (*4*). For example, edta is so widely used that it has emerged as a persistent organic pollutant and can be found in ground water, lake water, and rivers in concentrations up to 100 nM (*5,6*). Once polyaminecarboxylates have reached the water cycle in higher concentrations, the danger of remobilization of bound cationic sediments and an increase in the concentration of dissolved metals in ground water through formation of highly stable polyaminecarboxylate complexes are at hand (*7,8*).

As already mentioned, polyaminecarboxylic acids form highly stable complexes with various metals. These complexes have in many cases at least one or two vacant coordination sites. In aqueous solution, these coordination sites are occupied by the readily dissociable ligand water. It is known that the displacement

of water molecules from the first coordination sphere of metal ions with kinetically inert multidentate ligands such as polyaminecarboxylates leads to the labilization of the remaining water molecules due to the labilizing effect of the chelating ligand (*9–11*). Thus, the chemical reactivity of polyaminecarboxylate complexes is controlled by the lability of the remaining water molecules. Many reactions involving the binding of small molecules like hydrogen peroxide (H_2O_2) (*12–14*), nitric oxide (NO) (*15,16*) and dioxygen (O_2) (*17*), or redox processes proceed via substitution of the bound water ligands. Therefore, it is crucial to understand the substitution mechanism and the factors that control the lability of the bound water molecules.

In principle, ligand substitution reactions can be divided into three main categories (*18*). For an associative mechanism (A), coordination of an entering ligand and the formation of an intermediate with an increased coordination number occur prior to the release of the leaving ligand. In contrast, for a dissociative mechanism (D), complete dissociation of a coordinated ligand coupled to the formation of an intermediate with a reduced coordination number occurs prior to the coordination of the entering ligand. Both these limiting mechanisms in principle involve two transition states, one for the formation of the intermediate and the other for the formation of the substitution product. The height of the energy barriers associated with these transition states controls the rate-determining step and the ability to detect or isolate the intermediate of increased or reduced coordination number, respectively. As a third possibility, the substitution reaction can occur in a single step that does not involve the formation of an intermediate, the so-called interchange mechanism (I). In this case, a continuous range of transition states can be observed depending on the degree of bond making of the entering ligand and bond breaking of the leaving ligand with the metal center, ranging from substantial associative (I_a mechanism) to substantially dissociative (I_d mechanism) in nature. In the case where the degree of bond formation and bond breakage is equal, a pure interchange (I mechanism) is operative. Thus the degree of bond formation and bond breakage during the interchange process controls the nature of the interchange mechanism in going from I_a to I and I_d mechanisms, respectively.

The different types of substitution mechanisms mentioned above are all characterized by a specific rate law, such that systematic kinetic measurements as a function of the entering ligand concentration can already reveal some mechanistic information. However, the rate law for some of these mechanisms can in some cases be rather similar such that further

measurements are required to differentiate between the different possibilities. One possibility that is usually employed is to determine the activation enthalpy, $\Delta H^{\neq}$, and the activation entropy, $\Delta S^{\neq}$, from a systematic kinetic study as a function of temperature and the application of the Eyring equation. It is especially the activation entropy that reveals information on the degree of order in the transition state, which in turn is controlled by the degree of bond formation or bond breakage on going to the transition state, that is, the intrinsic nature of the ligand substitution process. Another possibility that has received significant attention from various groups over the past few decades is to study the pressure dependence of the kinetics of the substitution reaction from which the volume of activation $\Delta V^{\neq}$ can be calculated that allows a more precise assignment of the underlying substitution mechanism (*19*). The volume of activation is defined as the difference between the partial molar volumes of the transition and reactant states and is a composite of intrinsic, $\Delta V^{\neq}_{\text{intr}}$, and solvational, $\Delta V^{\neq}_{\text{solv}}$, volume changes. In the case of water-exchange (or more general solvent exchange) reactions on metal centers, solvational changes are negligible and only intrinsic volume changes arising bond formation and bond breakage contributions have to be considered. With the activation volume in hand, the substitution mechanism of such processes can in most cases be assigned unambiguously. For an associatively activated exchange process, $\Delta V^{\neq}<0$ since it involves a volume collapse on going to the transition state, whereas $\Delta V^{\neq}>0$ for a dissociatively activated exchange process since it involves a volume expansion in going to the transition state.

On the basis of a semi-empirical model, Swaddle and Mak estimated the limiting activation volumes for water-exchange reactions on di- and trivalent transition metal aqua complexes to be $\Delta V^{\neq}\approx+13\text{cm}^3\text{mol}^{-1}$ for a D mechanism and $\Delta V^{\neq}\approx-13\text{cm}^3\text{mol}^{-1}$ for an A mechanism (*20,21*). Values of $\Delta V^{\neq}$ within these extreme values are usually interpreted in terms of I_d, I, or I_a mechanisms, respectively (*22*). With these values as a guideline, assignments which type of mechanism holds can be made with significant confidence.

^{17}O NMR is an excellent experimental method to investigate water-exchange reactions on metal centers through line-shape analysis, isotope labeling, and relaxation rate measurements (*23,24*). Transverse relaxation rates can be determined by employing the $H_2{}^{17}O$ line-broadening technique which improves the accuracy of the measurements. The available data on water-exchange rate constants of aquated metal complexes cover nearly 20 orders of magnitude (*25*). The rate constants depend

both on the metal center and spectator ligand properties. For fully aquated transition metal complexes, the reactivity is solely controlled by the d-orbital occupancy and charge of the complex. The higher the ligand field stabilization energy, the slower the water-exchange reaction. For complexes with the same d-electron configuration as in the case of Fe^{III} and Mn^{II}, a significantly slower exchange reaction for Fe^{III} is observed, which is caused by the higher charge density on the Fe^{III} center that coordinates the water molecules more strongly. Pressure- and temperature-dependent kinetic measurements allow the determination of rate constants, activation parameters, and mechanistic details on the exchange mechanism. From such data, information on the effect of steric constraint and chelation of the metal center on the exchange mechanism can be obtained. Due to the steric constraints introduced by polyaminecarboxylate ligands, a more dissociative mechanism is in principle expected.

Once fundamental and thorough knowledge about the water-exchange mechanism on polyaminecarboxylate complexes is gained via ^{17}O NMR studies, the next step is to investigate the activation of small molecules such as hydrogen peroxide (H_2O_2) and nitric oxide (NO) by such complexes. The crucial step in such activation processes in principle involves the coordination of the small molecule to the metal center, which in fact is a ligand substitution process involving the displacement of coordinated water. The activation of small molecules plays a fundamental role both in living systems and industrial processes. It is for instance known that the Fe^{2+}/H_2O_2 system is able to induce cleavage of single- and double-strand DNA in the presence of edta (*26,27*). Further, Fe^{II}(edta) can act as an effective NO scavenger in the BioDeNO$_x$ process (*28,29*). Ru^{III}(polyaminecarboxylate) complexes are promising NO scavengers (*30,31*). The low toxicity, high stability *in vivo*, and reactivity toward NO make these complexes ideal candidates for therapeutical applications. To further improve the efficiency of the above-described activation processes, it is crucial to understand the underlying mechanism of the binding of small molecules like H_2O_2 and NO. Kinetic measurements under various experimental conditions in aqueous solution give detailed information on rate and activation parameters, which in turn contributes to the elucidation of the underlying reaction mechanism.

The first part of this review deals with the influence of different polyaminecarboxylate ligands on the water-exchange reaction, the structure, and speciation in aqueous solution of Fe, Mn, Ni, and Ru polyaminecarboxylate complexes. The employed

metals differ in charge, d-electron configuration, and ionic radii, giving rise not only to different reaction rates but also to changes in the overall reaction mechanism of the water-exchange reaction. The employed chelates (see Scheme 1) play an important role in the studied reaction, and therefore, the role of the backbone, rigidity, and donor ability of the ligand on the structure and reactivity of the metal complexes will be presented in detail. Water-exchange reactions on Gd and other lanthanide polyaminecarboxylate complexes, which are often used as contrast agents in magnetic resonance imaging, were already discussed in the recent literature and will not be covered in this review (*11,32*).

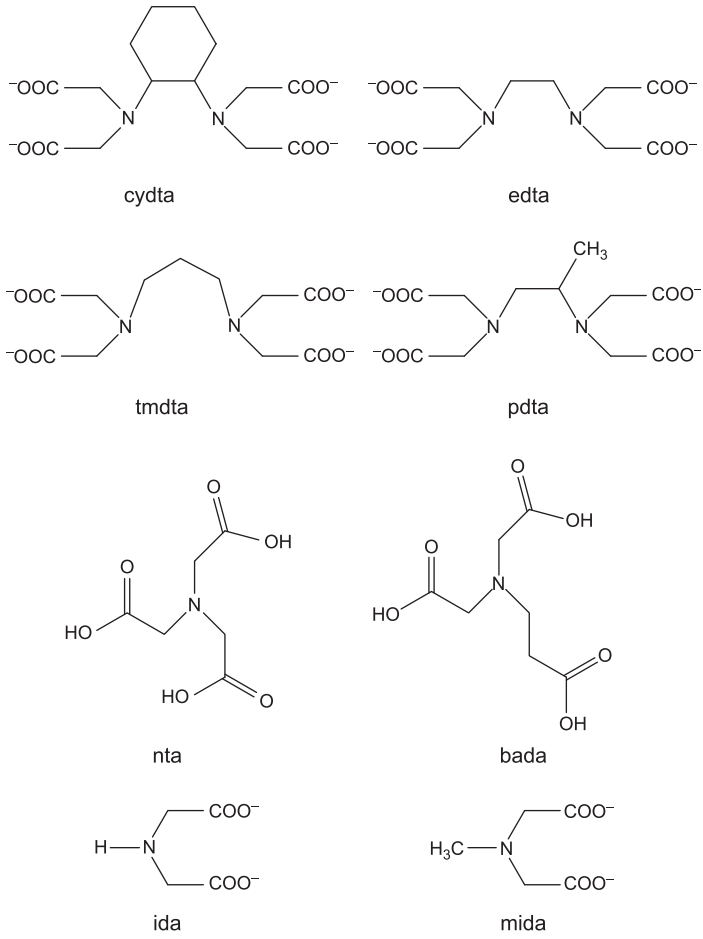

SCHEME 1. Schematic presentation of the polyaminecarboxylate chelates referred to in this chapter.

In the second part of this review, recent mechanistic findings on the activation of H_2O_2 and NO by the mentioned polyaminecarboxylate complexes in aqueous solution are presented. The different factors that influence the rate and the mechanism of the activation process by Fe and Ru polyaminecarboxylate complexes will be presented.

II. Water-Exchange Reactions on $[M(L)H_2O]$ Complexes ($M=Fe^{II/III}, Mn^{II}$)

X-ray analysis of edta and tmdta salts with different 3d transition metals shows that both six-coordination (L as hexadentate ligand) and seven-coordination are found in crystal structures. In six-coordinate 3d M^{III} and M^{II} complexes, no regular octahedron can be formed. Even small ions like Co^{III} have a too large ionic radius to be completely encircled by a ligand like edta. As a consequence, a "hole" is formed opposite to the central diamine ring in the architecture of the complex, which increases with increasing ionic radius of the central metal and increasing M—N bond lengths. With elongated M—N distances, a larger O_{G1}–M–O_{G2} angle is observed. This exocyclic angle is a direct measure of the "hole" size.

After dissolving M(L) type of salts in water, an equilibrium between the water free six-coordinate and the water containing seven-coordinate species is established (Eq. (1)).

$$[M(L)]^{n-} + H_2O \rightleftarrows [M(L)(H_2O)]^{n-}, \quad K_{6/7} \tag{1}$$

The correlations in Fig. 1 clearly show that nucleophilic attack of water at the metal center of 3d M–L complexes is facilitated with increasing ionic radius of the central metal and therefore also with a wider O_{G1}–M–O_{G2} angle.

In aqueous solution of M(L) complexes, a rapid $\Delta \leftrightarrow \Lambda$ enantiomerization takes place (*10,33*). This enantiomerization is accompanied by concerted rotations of the glycinate chelate rings (Scheme 2). This rotation is a concerted step in which the glycinate rings change their chirality by low-energy tunneling through a planar intermediate (*34,35*). This rotation can be visualized as a two-step process with a turn through space according to a Berry-like pseudorotation pathway (*36*), coupled to $\delta \leftrightarrow \lambda$ rearrangements of the four glycinate rings. During the rearrangement of the glycinate rings, the methylene carbon atom changes its hybridization state continuously from sp^3 to sp^2 and back (*37*). No metal–nitrogen bond rupture or a dechelation is observed during this process.

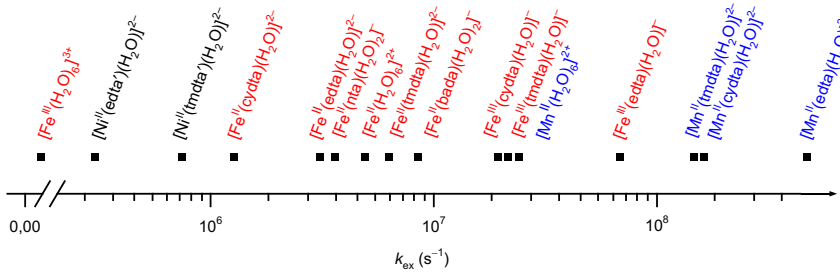

FIG. 1. Rate constants for water-exchange reactions on Mn^{II}-, Fe^{II}- and $Fe^{III}(L)H_2O$ complexes plotted on a logarithmic scale.

The ^1H and ^{13}C NMR spectra of paramagnetic high-spin $[Fe^{II}(edta)H_2O]^{2-}$ afford despite the enhanced relaxation due to the Fe^{II} center reasonable signals. Actually, six resonances in the ^1H spectrum of $[Fe^{II}(edta)H_2O]^{2-}$ would have been expected, but due to fast acetate interchange, signal averaging takes place and only three signals with relative intensities of approximately 1:1:1 are observed. The exchange of the glycinate rings between in-plane and out-of-plane positions leads to a single, time averaged signal for the protons of the ethylene backbone. This acetate arm exchange also leads to an equivalency of the glycinate methylene protons, but their protons in axial and equatorial positions remain magnetically inequivalent, causing two distinct resonances shifted to lower field.

Also solutions of $[Fe^{II}(tmdta)H_2O]^{2-}$ show fast $\Delta \leftrightarrow \Lambda$ enantiomerization. In the ^1H NMR spectrum, four contacted-shifted resonances are observed. Again, magnetically nonequivalent protons of the glycinate methylene group undergo a fast exchange. Table I sums up the chemical shifts and relative integrals for $[Fe^{II}(edta)H_2O]^{2-}$ and $[Fe^{II}(tmdta)H_2O]^{2-}$. This $\Delta \leftrightarrow \Lambda$ interconversion pathway is only accessible for polyaminecarboxylate ligands with a flexible backbone like edta and tmdta.

Introduction of constraints in the ligand backbone should hinder the fluxional behavior observed for edta type of complexes. Replacement of the flexible alkyl linker with the more rigid cydta ring in $[Fe^{II}(L)H_2O]^{2-}$ complexes leads to a nonaveraged resonance pattern in the ^1H NMR spectrum indicating that acetate scrambling is hindered (*10*). Also variable-temperature contact-shift measurements suggest that, throughout the available temperature range, no displacement for the detachment of the acetate group takes place. Since detachment of the M—N bonds

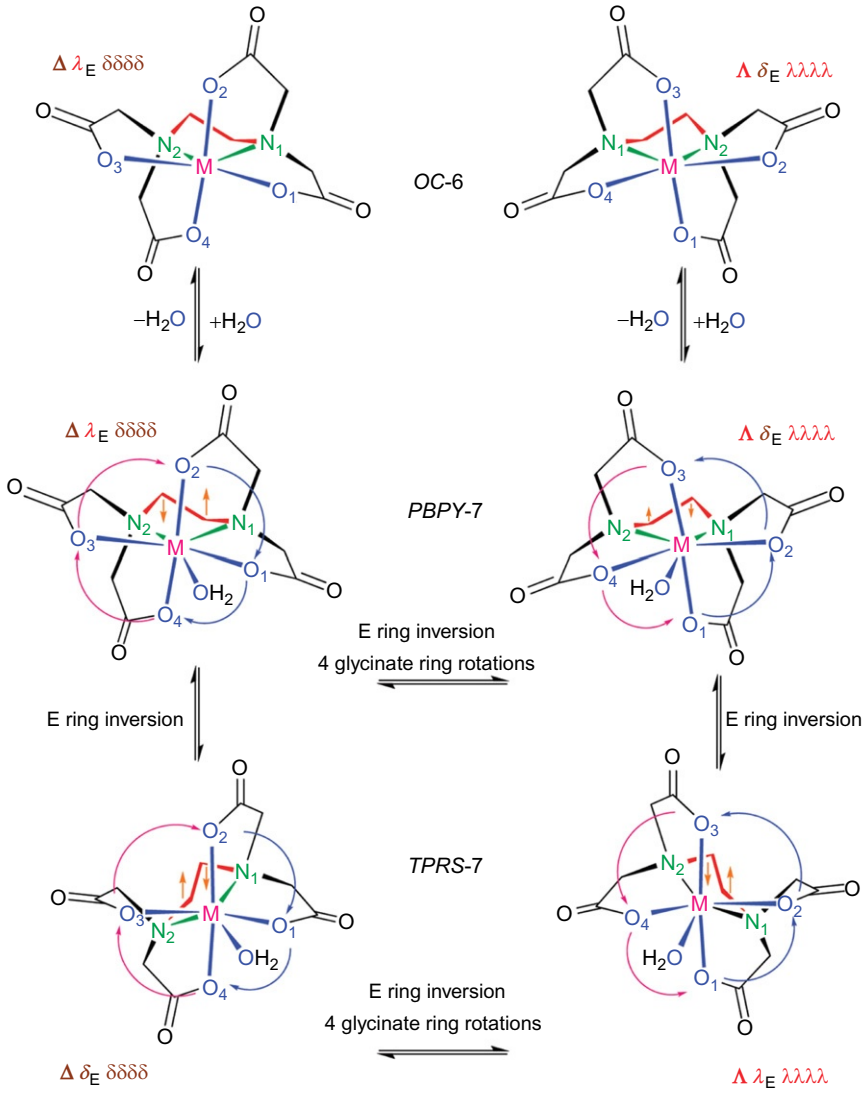

SCHEME 2. Schematic representations of the structure and dynamics of the diastereomers in the [M(edta)]/[M(edta)(H_2O)] system (*10*). Reprinted with permission from the American Chemical Society.

requires a high activation energy, the second pathway for $\Lambda \leftrightarrow \Lambda$ isomerization is also blocked. It can be assumed that nitrogen detachment is generally unfavorable for 3d transition metal

complexes; therefore, the static solution structure is caused only by the steric constraints in the cyclohexyl backbone of cydta. The structural investigation of Fe^{III} using NMR methods is not possible due to the large paramagnetic shifts and unresolved spectra.

Another striking difference in pK_a and dimerization constant K_d of polyaminecarboxylate complexes with rigid and flexible backbones can be explained with the altered tendency for $\Delta \leftrightarrow \Lambda$ interconversion. Dimerization takes place in solution of polyaminecarboxylate complexes at higher pH and higher complex concentration. A new and accurate approach to determine pK_a and K_d constants simultaneously makes use of the pH and complex concentration dependence of the intense absorption bands in the near UV region. These bands are assigned to charge transfer bands ($O_{oxo} \rightarrow Fe^{3+}$) of the Fe—O—Fe dimers. In the UV/vis spectra, aqua, hydroxo, and dimeric species can be distinguished.

Comparison of Fe^{3+}complexes of edta and cydta reveals that deprotonation of coordinated water in Fe-cydta takes place two pH units above that of Fe-edta and the dimerization constant K_d is two units lower for Fe-cydta. Table II gives a summary of the protolytic properties of various Fe^{3+} complexes. Fe^{III}pdta (pdta=1,2 propanediaminetetraacetate) with an intermediate backbone rigidity is included to gain a deeper understanding of the protolytic properties.

Equation (2) shows the overall reaction that finally leads to the deprotonated mono-hydroxo Fe^{III}cydta species. First the water

TABLE I

Comparison of ^1H NMR Data for Fe^{II}(polyaminecarboxylate) Complexes

Fe^{II}(edta)			Fe^{II}(tmdta)		
Shift (ppm)	Integral	Assignment	Shift (ppm)	Integral	Assignment
74.54	1.02	$2H_a^o$,$2H_e^i$	122.92	4.07	$2H_a^o$,$2H_e^i$
33.11	1.00	$2H_e^o$,$2H_a^i$	78.35	4.25	2α-CH_2
15.18	1.00	4en	64.45	4.00	$2H_e^o$,$2H_a^i$
			−77.70	2.00	β-CH_2

TABLE II

Protolytic Properties of Fe^{III}(polyaminecarboxylate) Complexes

	Fe^{III}(edta)	Fe^{III}(pdta)	Fe^{III}(cydta)
pK_{a1OH}	7.52±0.01	7.70±0.01	9.54±0.01
logK_d	2.64	2.28	1.07

molecule attacks the six-coordinate $[Fe^{III}(cydta)]^-$ to form $[Fe^{III}(cydta)H_2O]^-$, which is followed by deprotonation to yield $[Fe^{III}(cydta)OH]^{2-}$.

$$\left[Fe^{III}(cydta)\right]^- + H_2O \rightleftarrows \left[Fe^{III}(cydta)OH\right]^{2-} + H^+, \quad K^{III}{}_{a1OH} \quad (2)$$

Scheme 3 gives a more detailed insight into the different steps involved in the formation of hydroxo complexes of polyaminecarboxylate complexes. The active species in Scheme 3 is $[Fe^{III}(cydta)H_2O]^-$, since the equilibrium in Eq. (3) lies far on the right side for $Fe^{III}(L)$ complexes, because ring-opening of a glycinate ring is connected to an unfavorable entropy change.

$$\left[Fe^{III}(cydta)\right]^- + H_2O \rightleftarrows \left[Fe^{III}(cydta)H_2O\right]^- \quad (3)$$

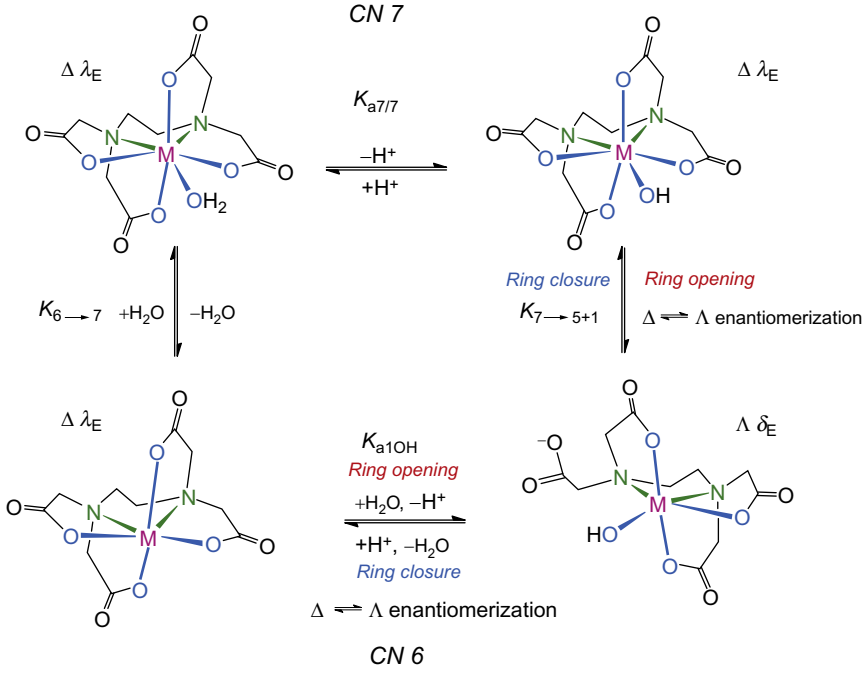

SCHEME 3. Schematic presentation of equilibrium and structural changes during the formation of ternary metal-edta-hydroxo complexes (*13*). Reprinted with permission from the American Chemical Society.

The $[Fe^{III}(cydta)OH]^{2-}$ complex exists in ring-closed and ring-opened forms that are interconnected. The equilibrium constant $K_{7\rightarrow5+1}$ is assigned to this reaction. Ring-opening takes place with complete enatiomerization for which all the rings undergo $\delta\leftrightarrow\lambda$ switches.From Scheme 3, it is clear that the experimentally determined pK^{III}_{a1OH} is an overall equilibrium constant (Eq. (4)), consisting of three constants for three consecutive steps.

$$K_{a1OH} = K_{6\rightarrow7}K_{a7/7}K_{7\rightarrow5+1} \tag{4}$$

For all three ligands, edta, pdta, and cydta, $K_{6\rightarrow7}$ values are large and the $K_{a7/7}$ values are of similar magnitude since the coordination of the three different ligands to the Fe^{III} center should not alter its electron withdrawing properties. As already mentioned above, the $\Delta\leftrightarrow\Lambda$ interconversion pathway is only accessible for polyaminecarboxylate ligands with a flexible backbone like edta. Therefore, $K_{7\rightarrow5+1}$ for Fe^{III}cydta is much smaller compared to Fe^{III}edta and Fe^{III}pdta, since $\delta\leftrightarrow\lambda$ switches are nearly blocked. Finally, this leads to an increase in pK_{a1OH}. In the case of Fe^{III}pdta, the additional methyl group in the backbone hinders the $\delta\leftrightarrow\lambda$ interconversion of the central diamine chelate ring by changing the CH_3 orientations from energetically favorable equatorial to unstable axial positions, only to a smaller extent, leading to only a slight increase in pK_{a1OH} compared to that for Fe^{III}pdta. The equilibrium concentration of the seven-coordinated hydroxo complex $[Fe^{III}(L)OH]^{2-}$ is highest for Fe^{III}cydta, and the concentration of the six-coordinate, ring-opened form is diminished. Since it is known that the active species in dimer formation is always the six-coordinate, ring-opened species $[Fe^{III}(L)(OH)_{5+1}]^{2-}$, the lower equilibrium concentration of $[Fe^{III}(L)(OH)_{5+1}]^{2-}$ is responsible for the drop in $\log K_d$ from 2.64 for Fe^{III}edta to 1.07 for Fe^{III}cydta.

As already mentioned, NMR is not a satisfactory method to investigate the conformational equilibria of Fe^{III} chelate complexes. A promising approach to distinguish between different isomers in aqueous solution of Fe^{III} polyaminecarboxylate complexes is the correlation of solid state Raman spectroscopy with Raman spectra calculated by DFT (*38*). Once a reasonable agreement between measured and calculated spectra is achieved, the calculated spectra can be used to simulate composite mixtures of conformations of Fe^{III} chelate complexes, which then can be correlated to experimentally determined Raman spectra of aqueous solutions of Fe^{III} polyaminecarboxylate complexes. For example, in the solid state structures of Fe^{III}tmdta, two different conformational isomers depending on the counter cation

are found, viz. the half-chair (hc) and twist-boat (tb) conformation. Depending on the counter cation, various ratios between hc and tb are found, but normally the tb conformation is the predominate one. On the basis of the calculated DFT Raman spectra, the most prominent bands could be assigned. Around ~440 cm^{-1}, a very intense band is observed in all tb spectra, whereas the Raman intensity is almost zero for the hc conformer and the most intense band appears at 480 cm^{-1}. A linear combination of the calculated spectra of the pure species give a 1:1 ratio of hc: tb for Fe^{III}tmdta.

An excellent method to investigate the rate and mechanism of water exchange on transition metal polyaminecarboxylate complexes are temperature- and pressure-dependent ^{17}O NMR measurements. The active species in the water exchange for Fe^{II}, Fe^{III}, and Mn^{II} is a seven-coordinate mono-aqua species. The exchange takes place between a coordinated and a bulk water molecule (Eq. (5)).

$$[M(L)H_2O]^{n-} + H_2^{O}17 \rightleftarrows [M(L)H_2{}^{17}O]^{n-} + H_2O \qquad (5)$$

For a given ligand, the rate of the water-exchange process mainly depends on the d-electron configuration, and k_{ex} increases along the series $Ni^{II}(L) < Fe^{II}(L) < Fe^{III}(L) < Mn^{II}(L)$ (see Table III and Fig. 1). This reflects exactly what is observed for the fully aquated metal ions $[M(H_2O)_6]^{2+}$. Although Fe^{III} and Mn^{II} have the same d-electron configuration, still the water-exchange rates for the Fe^{III} complexes are significantly smaller. Here, another effect is responsible for this clear difference. In all the examined complexes, the Fe^{III} species have a lower charge density compared to the Mn^{II} species and a decrease in k_{ex} is observed.

For Ni^{II} complexes, the slowest exchange rates are observed. The d^8-electron configuration and accordingly a strong preference for octahedral configuration in the active species lead to totally different exchange mechanism (see Section III).

Chelation leads to a significant drop in rate for the edta and cydta complexes of Fe^{II} compared to the fully aquated species. A similar trend is observed for the corresponding Gd^{III} and Eu^{II} species. One reason for this is a disfavored attack of the entering water molecule, by increasing steric constraints around the metal center introduced by the chelating ligand. Further, a lower degree of flexibility for the ligand framework can be assumed in polyaminecarboxylate complexes compared to the hexa-aqua species. Therefore, rearrangements of the metal coordination environment to reach the transition state are easier for [Fe

TABLE III

WATER-EXCHANGE DATA FOR Mn^{II}-, Fe^{II}- AND Fe^{III}(POLYAMINECARBOXYLATE)H_2O COMPLEXES

	k_{ex} (s^{-1})	$\Delta H^{\neq}$ (kJ mol^{-1})	$\Delta S^{\neq}$ (JK^{-1} mol^{-1})	$\Delta V^{\neq}$ ($cm^3 mol^{-1}$)
$[Mn^{II}(H_2O)_6]^{2+}$ (*39*)	2.1×10^7	33±1	+6±5	−5.4
$[Mn^{II}(edta)(H_2O)]^{2-}$ (*9*)	$(3.2\pm0.1)\times10^8$	36.6±0.8	+43±3	+3.4±0.2
$[Mn^{II}(tmdta)(H_2O)]^{2-}$ (*9*)	$(1.3\pm0.1)\times10^8$	37.2±0.8	+35±3	+8.7±0.6
$[Mn^{II}(cydta)(H_2O)]^{2-}$ (*10*)	$(1.4\pm0.2)\times10^8$	42.5±0.8	+54±3	+9.4±0.9
$[Fe^{II}(H_2O)_6]^{2+}$ (*39*)	$(4.3\pm0.1)\times10^6$	48.2±0.6	+44±2	+4.1
$[Fe^{II}(edta)(H_2O)]^{2-}$ (*33*)	$(2.7\pm0.1)\times10^6$	43.2±0.5	+23±2	+8.6±0.4
$[Fe^{II}(cydta)(H_2O)]^{2-}$ (*10*)	$(1.1\pm0.3)\times10^6$	17±2	−71±2	
$[Fe^{II}(nta)(H_2O)_2]^{-}$ (*40*)	$(3.1\pm0.4)\times10^6$	43±3	+25±9	+13.2±0.6
$[Fe^{II}(tmdta)(H_2O)]^{2-}$ (*9*)	$(5.5\pm0.5)\times10^6$	43±3	+30±13	+ 15.7±1.5
$[Fe^{II}(bada)(H_2O)_2]^{-}$ (*40*)	$(7.4\pm0.4)\times10^6$	40±3	+22±9	+13.3±0.8
$[Fe^{III}(H_2O)_6]^{3+}$ (*41*)	1.6×10^2	64	12.1	−5.4
$[Fe^{III}(edta)(H_2O)]^{-}$ (*13*)	$(6.0\pm0.3)\times10^7$	24.3±0.7	−14±2	+3.6±0.1
$[Fe^{III}(cydta)(H_2O)]^{-}$ (*13*)	$(1.7\pm0.2)\times10^7$	40±1	+28±5	+2.3±0.1
$[Fe^{III}(tmdta)(H_2O)]^{-}$ (*9*)	$(1.9\pm0.8)\times10^7$	42±3	+36±10	+7.2±2.7
$[Ni^{II}(H_2O)_6]^{2+}$ (*39*)	3.15×10^4			+7.2
$[Ni^{II}(edta')(H_2O)]^{2-}$ (*9*)	$(2.6\pm0.2)\times10^5$	34±1	−27±2	+1.8±0.1
$[Ni^{II}(tmdta')(H_2O)]^{2-}$ (*9*)	$(6.4\pm1.4)\times10^5$	22±4	−59±5	+5.0±0.6

$(H_2O)_6]^{2+}$ than in $[Fe(L)H_2O]^{2-}$ leading to a increased water-exchange rate in the former case. Upon comparing the activation volumes for the different Fe^{II} polyaminecarboxylate complexes, a clear change in mechanism is evident upon going from L=edta and cydta to L=nta, tmdta, and bada. This changeover in mechanism hampers comparison of exchange rate constants for Fe^{II} complexes of the various ligands. The pronounced dissociative mechanism may account for the observed accelerated rate for tmdta and bada compared to $[Fe(H_2O)_6]^{2+}$.

Although steric hindrance is evident for the polyaminecarboxylate complexes of Fe^{III} and Mn^{II}, a significant increase in k_{ex} is observed for all the considered complexes in comparison to the fully aquated species. Here, a second effect outweighs steric constraints induced by the chelating ligand. Coordination of the polyaminecarboxylate ligand to the Fe^{III} center leads to donation of electron density to the metal center through the σ and π donating properties of the ligand N (σ-donation) and O (σ- and π-donation) donor atoms. This leads to a decreased surface-charge density accompanied by a considerably weaker Fe^{III}—OH_2 bond than found in $[Fe(H_2O)_6]^{2+}$. For Fe^{II} complexes, the role of electron donation does not play such a dominating role. This is also

reflected in the activation volumes for Fe^{II} and Fe^{III} complexes of edta and tmdta. In the Fe^{II} case, a more dissociative mechanism with more positive volumes of activation is found, requiring considerably more bond weakening of the bound water molecule as compared to the corresponding Fe^{III} complexes.

Upon going from an edta complex to the cydta analogue, a decrease in k_{ex} for the water-exchange reaction is observed for all employed metals. With a water exchange nearly 3.6 times slower for cydta compared to edta, this decrease is especially evident for the Fe^{III} species, whereas for Mn^{II} and Fe^{II} species, only a decrease in reactivity by a factor of 2.5 is observed. The main reason for this decrease in reactivity is the lack of flexibility of the ligand backbone for cydta species. Rearrangements necessary to reach the transition state are hindered in the rigidified metal coordination environment in the case of M-cydta complexes. In the case of Fe^{III} as central metal, it is known that exchange of a water molecule only involves cleavage of the $Fe^{III}—OH_2$ bond. Due to the structural peculiarities of cydta, a change in coordination number from 7 to 6 always requires the concomitant flip of the four glycinate rings in the cdta ligand (see Scheme 4).

Introduction of a polyaminecarboxylate ligand leads to a more dissociative mechanism compared to the fully aquated hexa-aqua complexes. For Fe^{3+} and Mn^{2+}, a complete changeover from an I_a mechanism for the aquated species to an I_d mechanism is observed. Due to the encapsulation of the metal center, bond breakage of the bound water plays a more important role than binding of the entering water ligand (see Fig. 2).

Elongation and introduction of constraint in the ligand backbone as in the case of tmdta and cydta lead to a more pronounced dissociative mechanism compared to the edta species. In the case of tmdta, a more effective shielding is responsible for the observed larger values for the volume of activation. For cydta, an increase in rigidity of the ligands results in constraints in reaching the transition state during water exchange, making a more dissociative mechanism necessary.

III. Water-Exchange Reactions on $[Ni(L)H_2O]$ Complexes

In contrast to the seven-coordinate species discussed so far for $Fe^{II/III}$ and Mn^{II} complexes, $[M^{II/III}(L)(H_2O)]^{2-/-}$, the water containing species for Ni^{II} is a six-coordinate with one bound water molecule and a pentadentate polyaminecarboxylate ligand with a non-coordinating carboxyl group, $[Ni^{II}(L')H_2O]^{2-}$ (Eq. (6)).

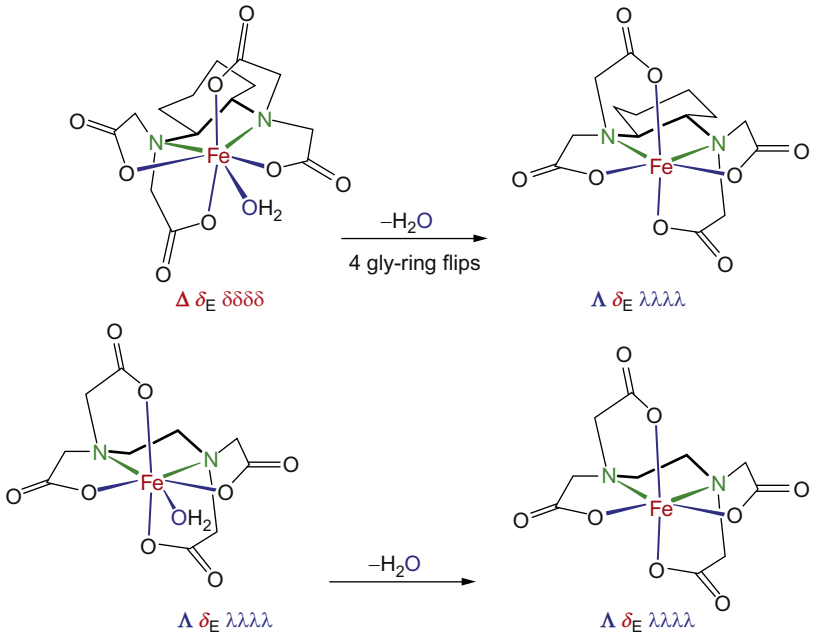

SCHEME 4. Differences between the water-exchange reactions of $[Fe^{III}(cydta)(H_2O)]^-$ (top, the ligand acting here is (*S*,*S*)-cydta) and $[Fe^{III}(edta)(H_2O)]^-$ (bottom) (*13*). Reprinted with permission from the American Chemical Society.

There were ongoing debates in the literature whether only a ring-closed hexadentate (*42–45*) species exists or a minor fraction of a ring-opened aqua-pentadentate species is in equilibrium with the ring-closed species (*46–50*) in aqueous solutions of Ni polyaminecarboxylate complexes.

$$\left[Ni^{II}(L)\right]^{2-} + H_2O \rightleftarrows \left[Ni^{II}(L')H_2O\right]^{2-} \qquad (6)$$

For L=edta, a water containing fraction of ~32% was found at ambient temperature (*9*). For tmdta, the obtained value of $P_m = 1.23 \times 10^{-4}$ reveals a smaller fraction of ~3% of $[Ni^{II}(tmdta')(H_2O)]^{2-}$ in solution (*9*). The preference for sixfold coordination can be related to the electronic configuration $(t_{2g}{}^6 e_g{}^2)$ of Ni^{II}. In an octahedral field, a strong LFSE effect can be expected. A certain affinity of Ni^{II}-edta for ring-opening also reflects in less angular strain upon going from the heptadentate edta form to the aqua-pentadentate form. Comparison of the

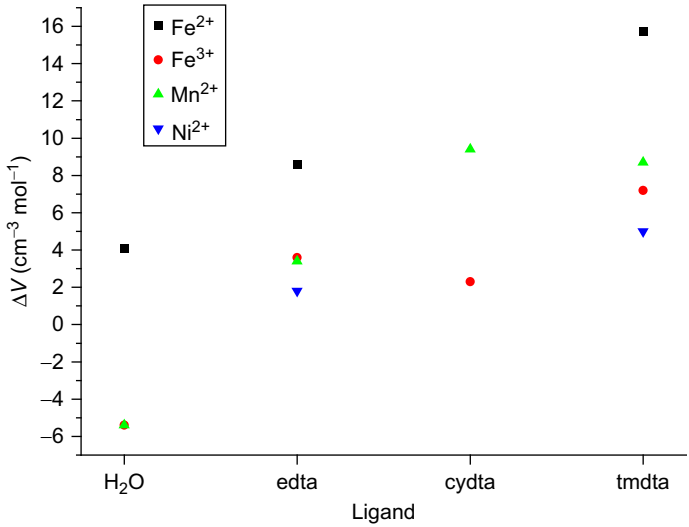

FIG. 2. Dependence of the activation volume of the water-exchange reaction on the bound ligand.

average twist angle Φ, the ratio s/h, and the angle θ, estimated for the di-anion in $Ca[Ni(edta)]\times 4H_2O$ (*51*), and the protonated mono-anion in $Li[Ni(Hedta)(H_2O)]\times H_2O$ (*52*), also shows a clear trend to ideal octahedral geometry and therefore preference for sixfold coordination.

$$\left[Ni^{II}(edta)\right]^{2-} + H_3O^+ \rightleftarrows \left[Ni^{II}(Hedta)H_2O\right]^- \qquad (7)$$

An appropriate access to the equilibrium in Eq. (6) is found in the proton-assisted ring-opening reaction given in Eq. (7). Already in the mid 1960s, an increase in the molar absorbance for the $^3A_{2g}\rightarrow {}^eT_{1g}(P)$ transition at 380 nm was found (*43,44*). A corresponding increase in absorbance at 380 nm was found during spectrophotometric titrations between pH 5.6 and 1.5 (*9*) related to the proton-assisted ring-opening given in Eq. (7). This type of absorbance increase is connected to the opening of a glycinate chelate arm, induced by the introduction of a ternary ligand at the Ni^{II} center. During temperature variable UV–vis experiments, an increased formation of the ring-opened pentadentate aqua species is observed (*9*), which is in agreement with the thermodynamic parameters $\Delta H = -14.2\,kJmol^{-1}$ and $\Delta S = -58.5\,JK^{-1}mol^{-1}$ reported by Evilia (*50*) for the exothermic reaction. The limiting values for the molar extinction coefficient

were estimated to be $\epsilon_{RO}=15.39 M^{-1}cm^{-1}$ for the ring-opened and $\epsilon_{RC}=9.13 M^{-1}cm^{-1}$ for the ring-closed species (*9*) at pH 5.6. The equilibrium constant was determined to be $K=0.52$ by spectrophotometric titration and $K=0.54$ by ^{13}C NMR (*50*). Variable pressure measurements at pH 5.6 showed the expected increased formation of the ring-opened aqua species upon going to higher pressures. Coordination of a water molecule, and dechelation of an acetate arm which is accompanied by significant charge creation, shift equilibrium (1) to the right on increasing pressure. Both these processes are expected to cause a volume collapse. From the isomeric equilibrium constant as function of pressure, the reaction volume was calculated to be $\Delta V=-7.9\pm0.2 cm^3mol^{-1}$ for the ring-opening in Eq. (1). For $[Co^{III}(edta)]^-$, a similar equilibrium with a $\Delta V=-9.5\pm0.4 cm^3mol^{-1}$ was reported (*53*). To summarize, the aqua-pentadentate ring-opened from is favored at elevated temperatures and pressures.

In ^{17}O NMR measurements, the activation parameters were determined to be $\Delta S^{\neq}=-27\pm2 JK^{-1}mol^{-1}$, $\Delta H^{\neq}=34\pm1 kJmol^{-1}$, and $\Delta V^{\neq}=+1.8\pm0.1 cm^3mol^{-1}$. The rate of the departure of the coordinated water molecule for the ring-opened species was found to decrease with increasing pressure. Several mechanistic explanations are possible. Either the coordinated water molecule exchanges with the bulk water or the bound water is substituted by the free carboxylate arm during the ring-closure reaction. The first possibility can be ruled out because of the strong preference of Ni^{II} for octahedral coordination. As in the case of $[Ni^{II}(H_2O)_6]^{2+}$ ($\Delta V^{\neq}=+7.2 cm^3mol^{-1}$), a strongly dissociative process could be expected for water exchange on $[Ni^{II}(edta')H_2O]^{2-}$. On the basis of the small measured volume of activation, an exchange of coordinated with bulk water can be excluded as underlying mechanism. The second proposed mechanism, viz. de-coordination of water and subsequent ring-closure of the carboxylate arm, consists of three components that can all contribute to the observed volume of activation: a positive contribution due to de-coordination of a water molecule, a negative contribution due to coordination of the COO^- group, and a positive contribution due to a decrease in electrostriction as a result of charge neutralization. The combination of the three different contributions accounts for the small positive value of $\Delta V^{\neq}$.

In summary, the observed kinetics reflect the ring-closure reaction of the aqua-pentadentate $[Ni^{II}(edta')H_2O]^{2-}$. It does not reflect a simple coordinated versus bulk water exchange as in the case of the seven-coordinate iron and manganese polyaminecarboxylate complexes. The activation volume $\Delta V_{RC}^{\neq}$ (volume of activation for the ring-opening process starting from

the ring-closed species) was estimated from $\Delta V^0 = \Delta V_{RC}^{\neq} - \Delta V_{RO}^{\neq}$ to be $-6.1 cm^3 mol^{-1}$. Again three processes contribute to the overall value of $\Delta V_{RC}^{\neq}$, viz. binding of water (negative contribution), de-coordination of the COO^- group (positive contribution), and increase in electrostriction due to charge creation (negative contribution).

Due to the small fraction of the water containing aqua-pentadentate complex (Eq. (3)) for Ni^{II}-tmdta, detailed variable temperature and pressure measurements of the equilibrium in Eq. (8) were impossible. The observed spectral changes are too small to be exploited.

$$\left[Ni^{II}(L)\right]^{2-} + H_2O \rightleftarrows \left[Ni^{II}(L')H_2O\right]^{2-} \tag{8}$$

Since a comparable pressure dependence for the $[Ni^{II}(L)]^{2-}/[Ni^{II}(L')H_2O]^{2-}$ equilibrium for edta and tmdta can be assumed, the activation volume $\Delta V_{RO}^{\neq}$ for the ring-closure reaction can be estimated to be $+5.0 \pm 0.6 cm^3 mol^{-1}$ considering the pressure dependence of P_m and the experimentally accessible reaction volume of the edta system ($\Delta V^0 = -7.9 cm^3 mol^{-1}$). As in the case of the corresponding iron and manganese complexes, a more pronounced dissociative character is observed for the water substitution upon going from Ni^{II}-edta to Ni^{II}-tmdta

In contrast to Ni^{II}-edta and Ni^{II}-tmdta, no significant effects on line widths or chemical shifts were apparent for Ni^{II}-cydta, indicating either the absence of any chemical exchange or the existence of only a very small fraction of the water containing species. Again a strong preference for octahedral coordination can be assumed, as in the case of Ni^{II}-edta and Ni^{II}-tmdta. Therefore, formation of a seven-coordinate water containing species can be ruled out. Due to the steric constraints caused by the cyclohexyl ring in the backbone of the chelate, formation of a ring-opened aqua-pentadentate species is energetically disfavored (*10,50*) All four carboxylate arms are virtually 100% coordinated in Ni^{II}-cydta at each time and no water exchange is possible.

IV. Binding of Nitric Oxide to $[Fe^{II}(edta)(H_2O)]^{2-}$

As already mentioned, $[Fe^{II}(edta)(H_2O)]^{2-}$ is used in flue gas scrubbing. A promising application for removal of NO_x from flue gas is the BioDeNO$_x$ process (*29,54–57*). During this process, gaseous nitric oxide, NO, is chemically absorbed by $[Fe^{II}(edta)(H_2O)]^{2-}$. During this reaction, a very stable and highly soluble $[Fe^{III}(edta)(NO^-)]^{2-}$ complex is formed via a dissociative reaction

pathway (*58,59*). In a subsequent step, the bound NO is biologically reduced to N_2. The most common electron donor for reduction of bound NO is ethanol (*28*), but also $[Fe^{II}(edta)(H_2O)]^{2-}$ itself can be used as reduction agent (*60*). Besides NO, there are several other components like CO_2, O_2, SO_2, or NO_2 present in flue gas. A special challenge is the presence of O_2, since the extremely oxidation sensitive $[Fe^{II}(edta)(H_2O)]^{2-}$ can easily be converted to $[Fe^{III}(edta)(H_2O)]^{-}$, which is not an active NO absorber at all. In fact, $[Fe^{III}(edta)(H_2O)]^{-}$ could be reduced by dissimilatory iron-reducing bacteria (e.g., *Escherichia coli*), but an additional reducing agent is needed. Since the presence of the NO containing complex $[Fe^{III}(edta)(NO^{-})]^{2-}$ and $[Fe^{II}(edta)(H_2O)]^{2-}$ leads do a significant decrease in cell growth (*61*), recovery of the active $[Fe^{II}(edta)(H_2O)]^{2-}$ species is not very sufficient. It turned out that not the reduction of bound NO, but the reduction of $[Fe^{III}(edta)(H_2O)]^{-}$ is the rate-limiting step in the Bio-DeNO$_x$ process; therefore, prevention of $[Fe^{II}(edta)(H_2O)]^{2-}$ oxidation by dioxygen should be a main goal.

The first step during the oxidation of $[Fe^{II}(edta)(H_2O)]^{2-}$ is displacement of the labile water ligand by dioxygen (*62*). Displacement of the labile coordinated water molecule by the more inert ligand fluoride proved to be a promising way to inhibit the oxidation reaction (*15*). Due to the low nucleophilicity of the fluoride ligand, a relatively low mixed-ligand formation constant for $[Fe^{II}(edta)(H_2O)]^{2-}$ with F^{-} was found to be ($K_{MLF}{}^{F}=1.3\pm0.2M^{-1}$). As a consequence, high F^{-} concentrations are required to reach a significant concentration of $[Fe^{II}(edta)(F)]^{3-}$ in solution. A high $[F^{-}]$ up to 1M did not lead do a decreased formation of the nitrosyl complex $[Fe^{III}(edta)(NO^{-})]^{2-}$ but reduced the oxidation rate of $[Fe^{II}(edta)(H_2O)]^{2-}$ with O_2 by 57%. Further, theoretical studies showed that binding of the resulting NO^{-} to the Fe^{III} center is stronger than binding of $O_2{}^{-}$ due to different bonding interactions (*63*).

Both nitrosylation with NO and oxidation with dioxygen proceed via substitution of the labile water molecule in $[Fe^{II}(edta)(H_2O)]^{2-}$. Due to the large formation constant of $(2.1\pm0.5)\times 10^{6}M^{-1}$ for the $[Fe^{III}(edta)(NO^{-})]^{2-}$ species, the equilibrium with NO shown in Scheme 5 lies entirely on the product site. The connected equilibrium with F^{-} is therefore shifted to the aqua side. In contrast to the binding of O_2 to the $[Fe^{II}(edta)(H_2O)]^{2-}$ species, which is less favored compared to NO, the equilibrium with F^{-} lies more on the fluoride side (see Scheme 5).

Therefore, addition of fluoride still allows complete conversion to the nitrosyl complex and simultaneously inhibits the unwanted oxidation to the Fe^{III} species.

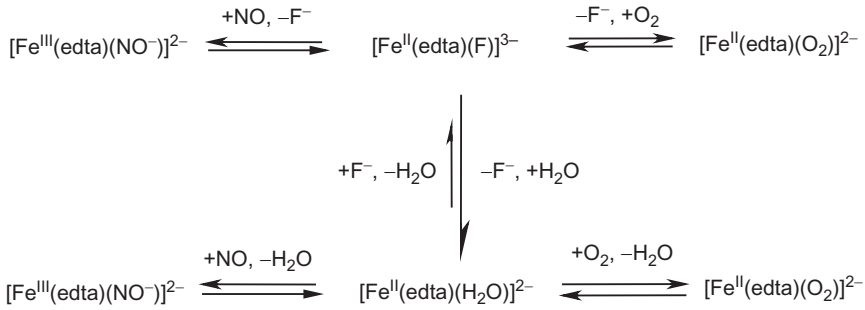

SCHEME 5. Scheme of equilibria connected with the formation of the ternary fluoride, nitrosyl, and dioxygen complexes of $[Fe^{II}(edta)(H_2O)]$ (*15*).

Mechanistic information on the reaction of $[Fe^{II}(edta)(H_2O)]^{2-}$ with NO in the absence of fluoride is also available for Fe^{II} complexes with other polyaminecarboxylate ligands besides edta, viz. Hedtra, nta, and mida (see Eq. (9)) (*58*).

$$Fe^{II}(L)H_2O + NO \underset{k_{off}}{\overset{k_{on}}{\rightleftharpoons}} Fe^{II}(L)NO + H_2O, \quad K = k_{on}/k_{off} \qquad (9)$$

With $k_{on}=2.4\times10^8 M^{-1}s^{-1}$ for L=edta, this complex exhibits the fastest rate constant for the binding of NO to the aqua complex at pH 5 along this series of selected chelates, making this complex an ideal candidate for exhaust gas denitrification. The different complexes of Fe^{II} with edta, Hedtra, and mida react with NO according to a dissociatively activated interchange mechanism (I_d), as indicated by the positive volumes of activation obtained for the reaction with NO. For Fe^{II}(edta), Fe^{II}(mida) and $Fe^{II}(mida)_2$ (*58*), an I_d mechanism was also found for the water-exchange reaction, supporting the assumption that water-exchange controls the mechanism of the substitution process with NO. The Fe^{II}(nta) complex is an exception in that a dissociative mechanism was found for the water-exchange reaction (see Table III), and a clearly associatively activated mechanism with a small negative volume of activation was found for the binding of NO (see Table IV). This is presumably an effect of the six-coordinate character of the Fe^{II}(nta) complex in solution in comparison to the seven-coordinate complexes for the other chelates.

The release of NO is throughout the series of complexes much slower than the binding reaction, which leads to high formation constants for the binding of NO to the Fe^{II} complexes. Again for

TABLE IV

SUMMARY OF KINETIC AND THERMODYNAMIC PARAMETERS AT 25°C FOR THE REVERSIBLE BINDING OF NO TO A SERIES OF Fe^{II}(CHELATE) COMPLEXES (*58*)

Complex	k_{on} ($M^{-1}s^{-1}$)	k_{off} (s^{-1})	$\Delta H^{\neq}$ ($kJmol^{-1}$)	$\Delta S^{\neq}$ ($JK^{-1}mol^{-1}$)	$\Delta V^{\neq}$ (cm^3mol^{-1})	K (k_{on}/k_{off}) (M^{-1})	Method
Fe^{II}(edta)	$(2.4\pm0.1)\times10^8$		24±1	−4±3	+4.1±0.2		fp
		91.0±0.4	61±2	−5±7	+7.6±0.6 (10.4° C)		sf
						$(2.1\pm0.5)\times10^6$	
Fe^{II}(hedtra)	$(6.1\pm0.1)\times10^7$		26±1	−12±3	+2.8±0.1		fp
		4.2±0.1	73±1	+11±4	+4.4±0.8		sf
						$(1.1\pm0.4)\times10^7$	
Fe^{II}(nta)	$(2.1\pm0.1)\times10^7$		24±1	−22±3	−1.5±0.1		fp
		9.3±0.6	66±1	−5±4	−3.5±0.7		sf
						$(1.8\pm0.3)\times10^6$	
Fe^{II}(mida)	$(1.9\pm0.1)\times10^6$		40±1	8±3	+7.6±0.4		fp
		57.3±0.4	47±2	−55±5	+6.8±0.4 (10.3° C)		sf
						$(2.1\pm0.6)\times10^4$	
$Fe^{II}(mida)_2$	$(1.8\pm0.1)\times10^6$		34±1	−13±3	+8.1±0.2		fp
		62.2±0.6	64±1	+5±5	+5.1±0.5 (10.0° C)		sf
						$(3.0\pm0.4)\times10^4$	

the different edta, Hedtra, and mida complexes, positive values for the volume of activation indicate a dissociative interchange mechanism for the release of NO. In contrast, for Fe^{II}(nta) an I_a mechanism is operative for the release of NO (*58*).

Table IV summarizes the available kinetic data for the reversible binding of NO to a series of Fe^{II} polyaminecarboxylate complexes at 25°C and pH 5. Rate constants for the forward reaction were obtained by flash photolysis (fp) and stopped-flow (sf) experiments with $[Ru(edta)H_2O]^-$ as NO scavenger (see Section V) for the backward reaction.

V. Binding of Nitric Oxide to $[Ru^{III}(edta)(H_2O)]^-$

A detailed account of the reactions of polyaminecarboxylate complexes of ruthenium(III) is given elsewhere in this volume (*64*). It has been reported in the literature (*65*) that $[Ru^{III}(edta)(H_2O)]^-$ is an excellent scavenger for NO, very similar to that of $[Fe^{II}(edta)(H_2O)]^{2-}$ as discussed in the previous section, although the nature of this complex is quite different. The $[Ru^{III}(edta)(H_2O)]^-$ complex has been shown to be pentadentate in aqueous solution with the sixth coordination site being occupied by either a water molecule. In aqueous solution, the complex exists in three forms, viz. $[Ru^{III}(Hedta)(H_2O)]$, $[Ru^{III}(edta)(H_2O)]^-$, and $[Ru^{III}(edta)(OH)]^{2-}$, depending on the pH according to:

$$\left[Ru^{III}(Hedta)(H_2O)\right] \rightleftarrows \left[Ru^{III}(edta)(H_2O)\right]^- + H^+, \quad pK_1 = 2.4$$

$$\left[Ru^{III}(edta)(H_2O)\right]^- \rightleftarrows \left[Ru^{III}(edta)(OH)\right]^{2-} + H^+, \quad pK_2 = 7.6$$

The pK_1 value corresponds to the deprotonation of the uncoordinated carboxylic acid group of the $Hedta^{3-}$ ligand, and the more basic pK_2 corresponds to that of coordinated water (*65*). Of these three complexes, $[Ru^{III}(edta)(H_2O)]^-$ is the most labile one and binds NO most efficiently with a binding constant of $9\times10^7 M^{-1}$ at 25°C. Davies *et al.* (*66*) were the first to study the kinetics of NO binding to $[Ru^{III}(edta)H_2O]^-$ using sf techniques and showed that $[Ru^{III}(edta)(H_2O)]^-$ scavenges NO rapidly with a rate constant of $2.6\times10^7 M^{-1}s^{-1}$ at 7°C to form $[Ru^{III}(edta)NO]^-$. A detailed reinvestigation of the system (*65*) showed that the uptake of NO appeared to be irreversible as judged from experiments in which a stream of Ar was used to remove NO

from solution, which is in agreement with the high binding constant and consistent with the overall reaction:

$$\left[Ru^{III}(edta)(H_2O)\right]^- + NO \rightarrow \left[Ru^{III}(edta)(NO)\right]^- \leftrightarrow \left[Ru^{II}(edta)(NO^+)\right]^-$$

In order to clarify the nature of the reaction product, detailed IR and ^{15}N-labeled NMR experiments were performed, from which it was concluded that the nitrosyl product can formally be described as a Ru^{II}–NO^+ complex. Note that in the case of NO binding to $[Fe^{II}(edta)(H_2O)]^{2-}$, the nitrosyl product was found to be a Fe^{III}–NO^- species (*58,59*). Detailed kinetic studies using sf and fp experiments (*65*) confirmed the very rapid binding constant reported before (*66*). In addition, NO trapping experiment using $[Fe^{II}(edta)(H_2O)]^{2-}$ showed that it was impossible to remove the coordinated NO from $[Ru^{II}(edta)(NO^+)]^-$, even in the presence of a very large excess of $[Fe^{II}(edta)(H_2O)]^{2-}$, which demonstrated the very efficient binding of NO to $[Ru^{III}(edta)(H_2O)]^-$.

A pH dependent study revealed that NO binding to $[Ru^{III}(Hedta)(H_2O)]$ and $[Ru^{III}(edta)(OH)]^{2-}$ at very low and high pH, respectively, to eliminate the reaction with $[Ru^{III}(edta)(H_2O)]^-$ (see Scheme 6), revealed that k_1 and k_3 are orders of magnitude slower than k_2, which is in agreement with the lability of these complexes (*65*). As a general remark on such reactions, it is important to note that the lability of $[Ru^{III}(edta)(H_2O)]^-$ is drastically influenced by the use of buffer components (such as acetate in the pH range 4–6) that can coordinate to this labile complex and thereby suppress the reaction with ligands such as NO.

Very recently, $Ru^{III}(edta)$ was used as a trap for NO in the ionic liquid 1-ethyl-3-methylimidazolium dicyanamide, [emim][dca], in order to study the kinetics of the release of NO from $[Fe^{III}(dca)_5(NO^-)]^{3-}$ (*67,68*). The anionic component of the selected ionic liquid, viz. dca^-, was found to coordinate rapidly to the

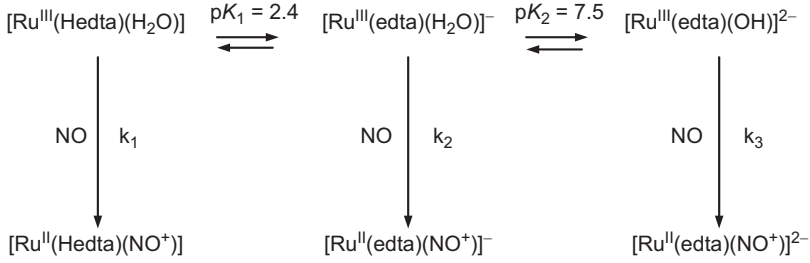

SCHEME 6. pH dependence of the reaction between $Ru^{III}(edta)$ and NO.

Ru^{III}(edta) complex and hindered its successful application (*67*). Further investigations in aqueous solution revealed thermodynamic and kinetic data for the formation of the $[Ru^{III}(edta)(dca)]^{2-}$ complex and its reaction with NO to form the corresponding nitrosyl complex. For the reaction of $[Ru^{III}(edta)(H_2O)]^-$ with dca^- at pH 6, the linear plot of k_{obs} versus $[dca^-]$ gave $k_{on}=90.5\pm0.4 M^{-1}s^{-1}$ and $k_{off}=0.056\pm0.003 s^{-1}$ at 25°C from which the overall equilibrium constant was found to be $K_{eq}=k_{on}/k_{off}=1614\pm93 M^{-1}$, which is in close agreement with the thermodynamically determined value of $957\pm15 M^{-1}$ (*68*). Kinetic parameters for the binding of dca^-, viz. $\Delta H^{\neq}=39.5\pm0.2 kJmol^{-1}$, $\Delta S^{\neq}=-75.2\pm0.5 JK^{-1}mol^{-1}$, and $\Delta V^{\neq}=-10.2\pm0.5 cm^3mol^{-1}$, clearly support the associative character of the substitution process (*67*). The subsequent reaction of $[Ru^{III}(edta)(dca)]^{2-}$ with NO in aqueous solution was studied at high pH, ca. 9, to simulate the conditions in the ionic liquid which is expected to be basic (*68*). Surprisingly, the values of k_{obs} showed a nonlinear dependence of k_{obs} on [NO] and suggested the binding of two molecules of NO to $[Ru(edta)(dca)]^{2-}$ according to the reaction shown in Eq. (10). The data could be fitted with a rate law of the form presented in Eq. (11), which suggests the subsequent binding of two NO molecules.

$$[Ru(edta)(dca)]^{2-} + 2NO \rightarrow \left[Ru(edta)(NO)_2\right]^- + dca^- \qquad (10)$$

$$k_{obs} = k_1[NO] + k_2[NO]^2 \qquad (11)$$

The calculated rate constants were found to be $k_1=(3.9\pm0.4)\times 10^3\ M^{-1}\ s^{-1}$ for the binding of the first and $k_2=(8.9\pm0.5)\times 10^6 M^{-2}s^{-1}$ for the second NO molecule at 25°C. These results clearly show that the reaction between NO and $[Ru(edta)(dca)]^{2-}$ under conditions similar to that in [emim][dca] is much slower than the reaction between NO and the most reactive aqua complex $[Ru(edta)(H_2O)]^-$ ($k=1\times10^8 M^{-1}s^{-1}$)generally used as scavenger for NO. For this reason, the Ru^{III}(edta) complex is not suitable as a trap for NO in the ionic liquid [emim][dca] as reaction medium (*67,68*).

VI. Binding of Hydrogen Peroxide to Fe^{III}(L) Complexes

During the reaction of hydrogen peroxide with the Fe^{II}(edta) system, hydroxyl radicals according to a Fenton type of mechanism are produced. This system is capable of inducing oxidative cleavage of double stranded native and synthetic DNA (*69*). In contrast, Fe^{III} polyaminecarboxylate systems do not produce

oxygen-based radicals, but different Fe^{III}-peroxo species are generated (*12,13,70,71*), which can be characterized by a variety of techniques like Mößbauer spectroscopy (*71,72*), low temperature UV–vis spectroscopy, variable-temperature and variable-field circular dichroism (*73*), and paramagnetic resonance spectroscopy (*73,74*). These peroxo species only have a limited stability in solution, depending on the chain length of their backbone (see Scheme 7) (*74*). For the ligands with the shorter backbone (PAC 5), addition of hydrogen peroxide leads to formation of purple side-on bound peroxo complexes, which all have an absorption maximum around 520 nm. Their color fades within 10 s at pH values around 10. For the PAC 6 chelates, the purple peroxo species were even shorter lived, and significant formation of Fe^{II}-PAC 6 and superoxide, O_2^-, was observed in the EPR spectra compared to that found for the Fe^{III}-PAC 5 complexes (*74*).

Cyclic voltammograms showed quasi-reversible Fe^{III}/Fe^{II} redox behavior at pH 4 in buffered solution. Redox potentials of the Fe^{III}-PAC 5 complexes are lower than those of the Fe^{III}-PAC 6

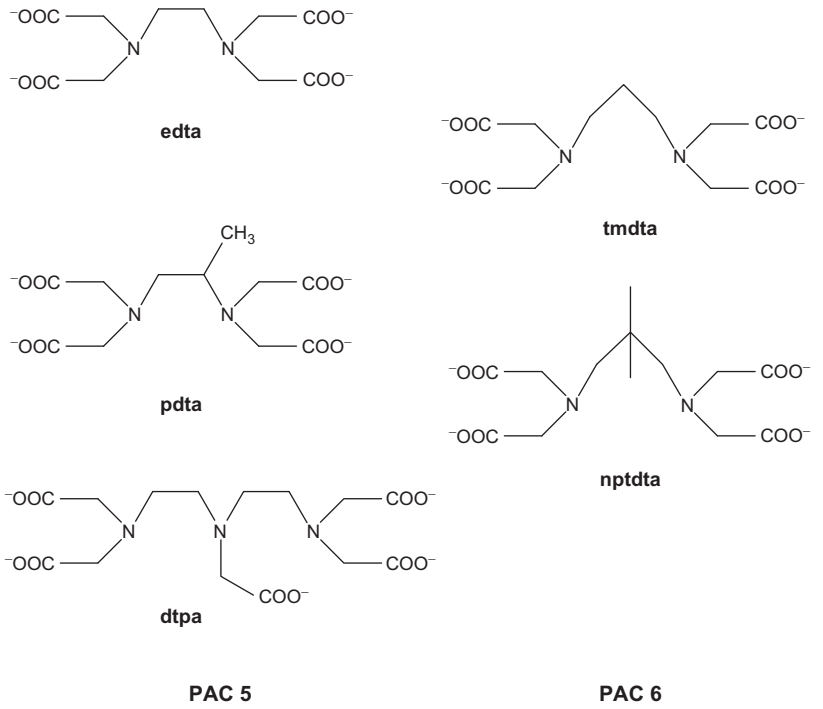

SCHEME 7. Polyaminecarboxylate ligands with different chain lengths of their backbone.

TABLE V

ELECTROCHEMICAL DATA OF Fe(L) COMPLEXES

Ligand	$E_{1/2}$ (V)[a]
edta	−0.284
pdta	−0.275
dtpa	−0.195
tmdta	0.090
nptdta	0.015

[a]Scan rate, 100 mV s^{-1}, measured versus Ag/AgCl.

complexes (see Table V), suggesting that depending on the reducibility to the corresponding Fe^{II} form of the respective complex, a longer lived side-on bound Fe^{III}-peroxo species is generated.

Detailed kinetic information is presently available for the coordination of hydrogen peroxide to $[Fe^{III}(edta)H_2O]^-$ and $[Fe^{III}(cydta)H_2O]^-$ (*12,13*). Both complexes have low Fe^{III}/Fe^{II} redox potentials, leading to relatively long-lived purple side-on bound peroxo complexes with an absorption maximum at 521 nm (edta) and 545 nm (cydta), well characterized by Mößbauer spectroscopy (*13,71,72*) Formation of the peroxo complex is only observable at pH values above the pK_a value of the respective $[Fe^{III}(L)H_2O]$ complex. For both complexes, a two-step mechanism was found. The first step involves coordination of hydrogen peroxide to give an end-on bound Fe^{III}-hydroperoxo complex, followed by ring-closure to the Fe^{III} high-spin side-on bound peroxo complex independent of the H_2O_2 concentration in the second reaction step. For both complexes $[Fe(edta)(H_2O)]^-$ (*16*) and $[Fe(cydta)(H_2O)]^-$ (*13*), it was found that both forward and back reactions of the coordination of hydrogen peroxide are affected by general acid catalysis. In the case of $[Fe(edta)(H_2O)]^-$, the forward reaction can proceed via a spontaneous, nonacid-catalyzed reaction pathway, which could involve proton transfer from hydrogen peroxide to the $[Fe(L)OH]^-$ complex. In contrast to $[Fe(edta)(H_2O)]^-$, no evidence for an additional proton catalyzed reaction pathway was found. In the case of $[Fe(edta)(H_2O)]^-$, only sterically unhindered buffers have a catalytic effect on the second reaction step, whereas for $[Fe(cydta)(H_2O)]^-$, sterically hindered buffers like CAPS also affect the second reaction step. A small contribution of the concentration of hydrogen peroxide was found in both cases at higher pH, indicating that deprotonated H_2O_2 can act as a proton scavenger. Scheme 8 gives an overview of the reaction pathways of $[Fe(cydta)(H_2O)]^-$

with H_2O_2. The mechanism can be transferred to the reaction of $[Fe(edta)(H_2O)]^-$ with hydrogen peroxide.

For the first reaction step, positive volumes of activation were found for coordination of H_2O_2 to the iron center, indicating an I_d mechanism. This is in line with the finding that the reactivity of the coordinated water controls the substitution behavior of Fe–polyaminecarboxylate complexes. For the back reaction, which only could be observed in the case of $[Fe(edta)(H_2O)]^-$, very large and positive $\Delta S^{\neq}$ and $\Delta V^{\neq}$ values were observed, suggesting an even stronger dissociative character. For the second reaction step, negative $\Delta S^{\neq}$ and $\Delta V^{\neq}$ values were found for the intramolecular rearrangement for both complexes, which is in agreement with an I_a type of mechanism for the peroxide chelation reaction. For the second reaction step with $[Fe(cydta)(H_2O)]^-$, no back reaction could be observed. In contrast, in the case of $[Fe(edta)(H_2O)]^-$ where the second step was followed at lower pH, the back reaction (de-coordination of the peroxo moiety) follows an I_a type of mechanism. Table VI summarizes the rate constants and activation parameters for the two-step reactions of $[Fe(cydta)(H_2O)]^-$ and $[Fe(edta)(H_2O)]^-$ with hydrogen peroxide.

VII. Binding of Hydrogen Peroxide to $[Ru^{III}(edta)(H_2O)]^-$

A series of papers have appeared on the binding of hydrogen peroxide to $[Ru^{III}(edta)(H_2O)]^-$, and a detailed account of this work is given elsewhere in this volume (*64*). In principle, the observed reactions can be summarized as follows:

$$\left[Ru^{III}(edta)(H_2O)\right]^- + H_2O_2 \overset{K_1}{\rightleftarrows} \left[Ru^{III}(edta)(OOH)\right]^{2-} + H_3O^+ \tag{12}$$

$$[Ru^{III}(edta)(OOH)]^{2-} \xrightarrow{H^+} \begin{cases} \xrightarrow{k_2} [Ru^{V}(edta)(O)]^- + H_2O & (13a) \\ \xrightarrow{k_3} [Ru^{IV}(edta)(OH)]^- + OH^\bullet & (13b) \end{cases}$$

At pH 5, H_2O_2 rapidly binds to $[Ru^{III}(edta)(H_2O)]^-$ to form $[Ru^{III}(edta)(OOH)]^{2-}$ which subsequently undergoes heterolytic or homolytic cleavage of the O—O peroxo bond to form

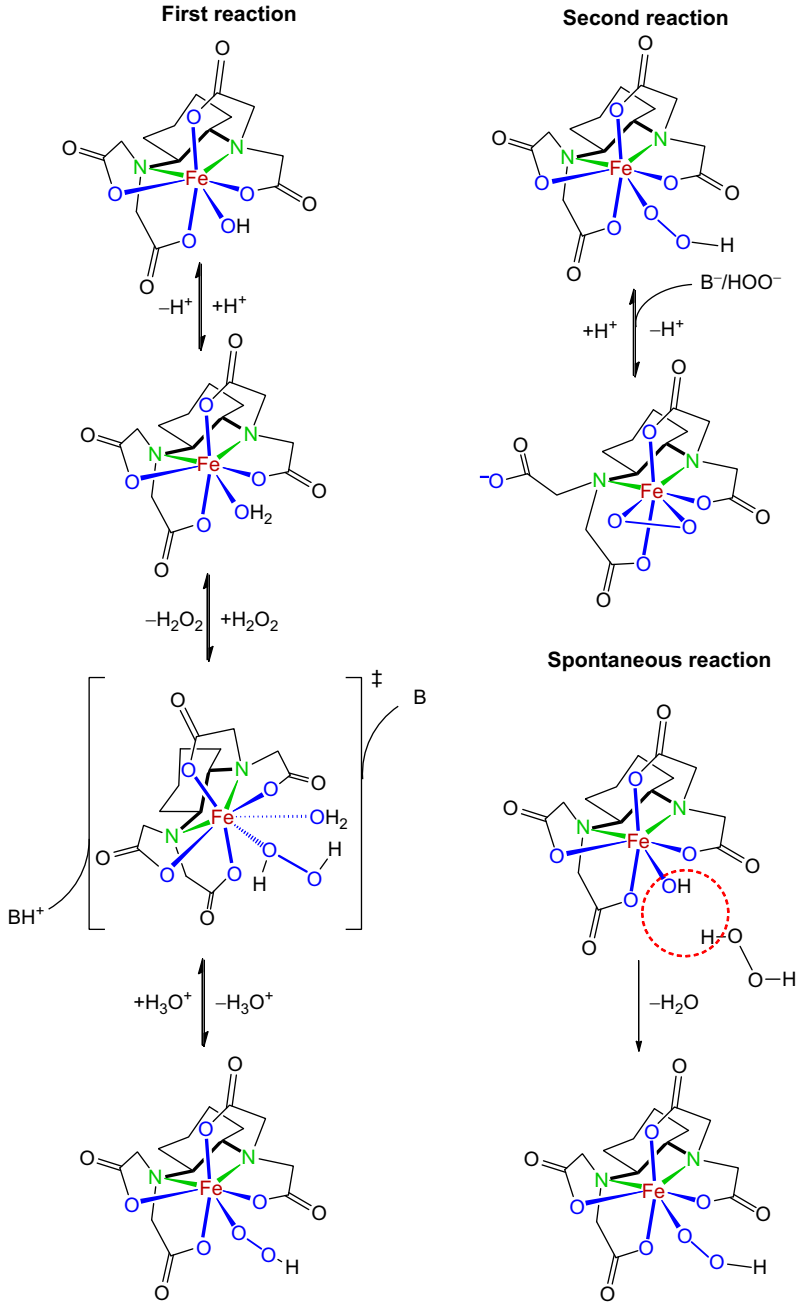

SCHEME 8. Suggested mechanism for the overall reaction of $[Fe^{III}(cydta)]^-$ with H_2O_2 in buffered solution (*13*). Reprinted with permission from the American Chemical Society.

TABLE VI

SUMMARY OF RATE AND ACTIVATION PARAMETERS FOR THE TWO-STEP REACTIONS (*12,13*)

	pH 9.0	pH 9.0	pH 10.5	pH 8.5
		$[Fe(edta)(H_2O)]^-$		
Rate constant at 25°C	k_1 4000 ± 141 $M^{-1}s^{-1}$	k_{-1} $145\pm4\,s^{-1}$	k_{2obs} $0.259\pm0.002\,s^{-1}$	k_{-2obs} $5.4\pm0.1\,s^{-1}$
$\Delta H^{\neq}$, $kJ\,mol^{-1}$	37 ± 4	101 ± 2	79 ± 2	86 ± 2
$\Delta S^{\neq}$, $JK^{-1}mol^{-1}$	-53 ± 14	$+135\pm6$	-10 ± 5	$+56\pm6$
$\Delta V^{\neq}$, cm^3mol^{-1}	$+6.8\pm0.8$	$+18.4\pm0.6$	-2.3 ± 0.1	$+5.1\pm0.2$
	pH 11.0	pH 11.0	pH 11.0	pH 11.0
		$[Fe(cydta)(H_2O)]^-$		
Rate constant at 25°C	k_1 6129 ± 467 $M^{-1}s^{-1}$	k_{-1} $26\pm13\,s^{-1}$	k_2 $2.78\pm0.05\,s^{-1}$	k_2*[a] $33\pm2\,M^{-1}s^{-1}$
$\Delta H^{\neq}$, $kJ\,mol^{-1}$	41 ± 3	109 ± 5	55 ± 3	52 ± 2
$\Delta S^{\neq}$, $JK^{-1}mol^{-1}$	-37 ± 10	$+142\pm18$	-33 ± 11	-61 ± 5
$\Delta V^{\neq}$, cm^3mol^{-1}	$+6\pm1$	–	-12 ± 2	-9 ± 2

[a]Rate constant for the buffer anion $[B^-]$ assisted deprotonation of the hydroperoxo complex (only observable with cydta as ligand).

$[Ru^V(edta)(O)]^-$ or $[Ru^{IV}(edta)(OH)]^-$, respectively. In principle, all three species, viz. $[Ru^{III}(edta)(OOH)]^{2-}$, $[Ru^V(edta)(O)]$, and $[Ru^{IV}(edta)(OH)]^-$, can act as oxygenation agents similar to the biological equivalents Compounds 0, I, and II, respectively. In fact, preliminary spectral evidence for the intermediate formation of $[Ru^{III}(edta)(OOH)]^{2-}$ was reported (*14*). In a more recent study (*75*), reaction conditions were found where it was possible to observe the formation of $[Ru^{III}(edta)(OOH)]^{2-}$ as an intermediate at 425 nm, followed by the subsequent formation of $[Ru^V(edta)(O)]$ and $[Ru^{IV}(edta)(OH)]^-$ as shown in Fig. 3.

Most surprising was the observation that the $Ru^{III}(edta)/H_2O_2$ system showed its highest catalytic activity for the degradation of Orange II (ORII) under the conditions where $[Ru^{III}(edta)(OOH)]^{2-}$ was formed right at the start of the reaction when $[Ru^{III}(edta)(H_2O)]^-$ was mixed with H_2O_2. This can be clearly seen from the degradation traces for ORII observed after different delay times before addition of ORII to the mixture of $Ru^{III}(edta)$ and H_2O_2 as shown in Fig. 4.

The kinetic data reported in Fig. 4b shows a decrease in the observed degradation rate constant by a factor of 10 during the delay of 50 s before addition of ORII to the reaction mixture. This

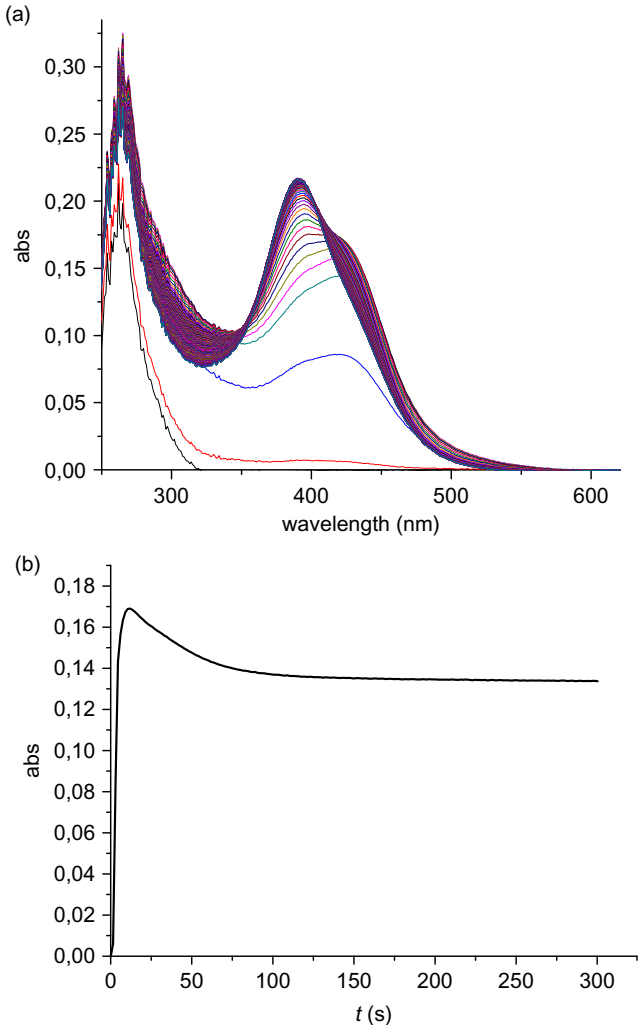

FIG. 3. (a) Spectral changes observed for the reaction of $[Ru^{III}(edta)(H_2O)]^-$ with a high excess of H_2O_2. (b) Absorbance versus time trace at 425nm. Experimental conditions: $[Ru^{III}]=4\times10^{-5}$M, $[H_2O_2]=1\times10^{-2}$M, pH=4.0 (1mM acetate buffer), temperature 22°C (*75*). Reprinted with permission from the Royal Society of Chemistry.

clearly suggests that $[Ru^{III}(edta)(OOH)]^{2-}$ immediately formed on the addition of H_2O_2 to $[Ru^{III}(edta)(H_2O)]^-$ must be responsible for the very rapid degradation of ORII prior to the formation of $[Ru^{IV}(edta)(OH)]^{2-}$ and $[Ru^{V}(edta)(O)]^-$ under such conditions.

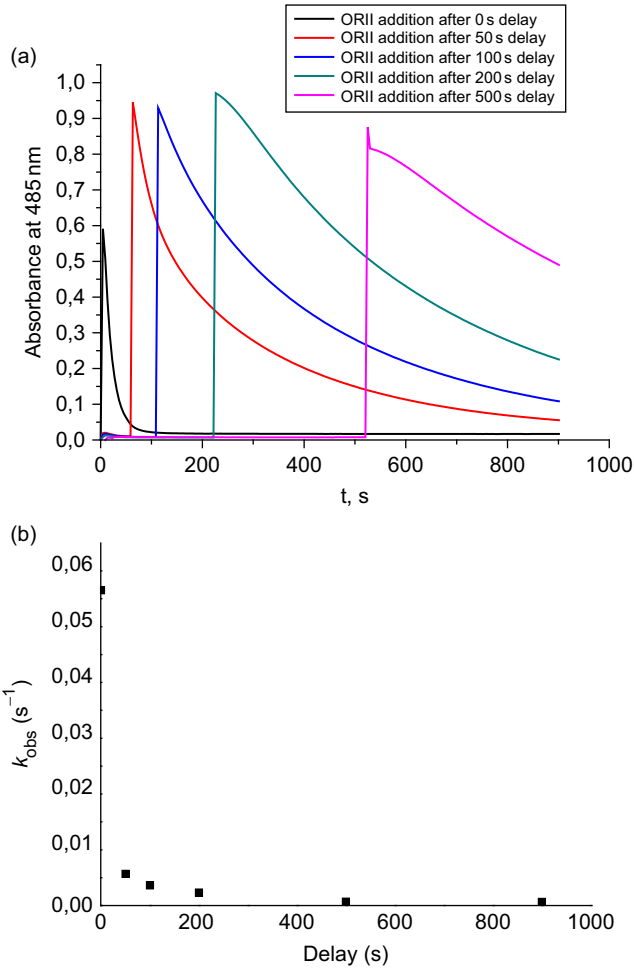

FIG. 4. (a) Absorbance versus time traces observed at 485 nm following the addition of 5×10^{-5}M Orange II to a solution consisting of 2×10^{-5}M$[Ru^{III}(edta)(H_2O)]^-$ and 1×10^{-2}MH_2O_2 after different delay times at pH 4 (1 mM acetate buffer) and 25°C. (b) Plot of the calculated first-order degradation rate constant versus the delay time for the addition of ORII (*75*). Reprinted with permission from the Royal Society of Chemistry.

The results can be accounted for in terms of the reaction scheme expressed in Scheme 9.

Detailed kinetic studies were performed in the pH range 1–5 to evaluate the effect of pH on the overall catalytic degradation of

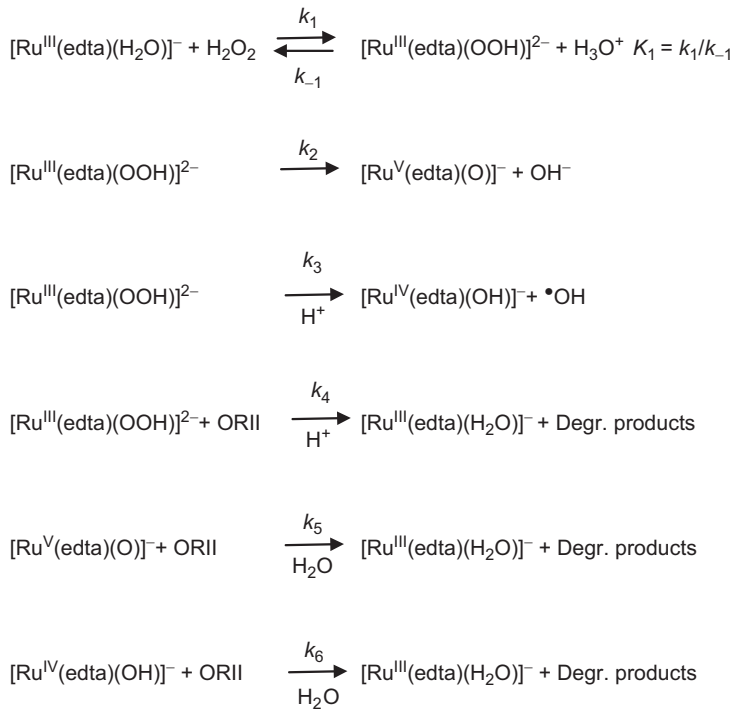

SCHEME 9. Proposed reaction scheme for the $[Ru^{III}(edta)(H_2O)]^-$ catalyzed degradation of ORII by H_2O_2.

ORII. The pH dependence of the observed first-order rate constant showed that a maximum degradation rate was observed at pH 3.5–4.0. This partly results from the fact that the most labile form of the $Ru^{III}(edta)$ complex, viz. $[Ru^{III}(edta)(H_2O)]^-$, is present in the pH range 4.0–6.0 as a result of the pK_a values given in Section V of this chapter. Further, the role of the dangling acetate arm can also contribute toward the stabilization of the $[Ru^{III}(edta)(OOH)]^{2-}$ complex as shown schematically in the overall catalytic cycle summarized in Scheme 10. The studies also showed that the degradation reaction catalyzed by $[Ru^{V}(edta)(O)]^-$ and $[Ru^{IV}(edta)(OH)]^-$ are orders of magnitude slower than found for $[Ru^{III}(edta)(OOH)]^{2-}$ (*75*).

The suggested formation of $[Ru^{III}(edta)(OOH)]^{2-}$ as the intermediate with the highest catalytic activity at pH 4 could be considered as unreasonable in light of the finding that the corresponding $[Fe^{III}(edta)(OOH)]^{2-}$ complex can only be formed as a stable intermediate at pH>7.5 (*12*). It should, however, be

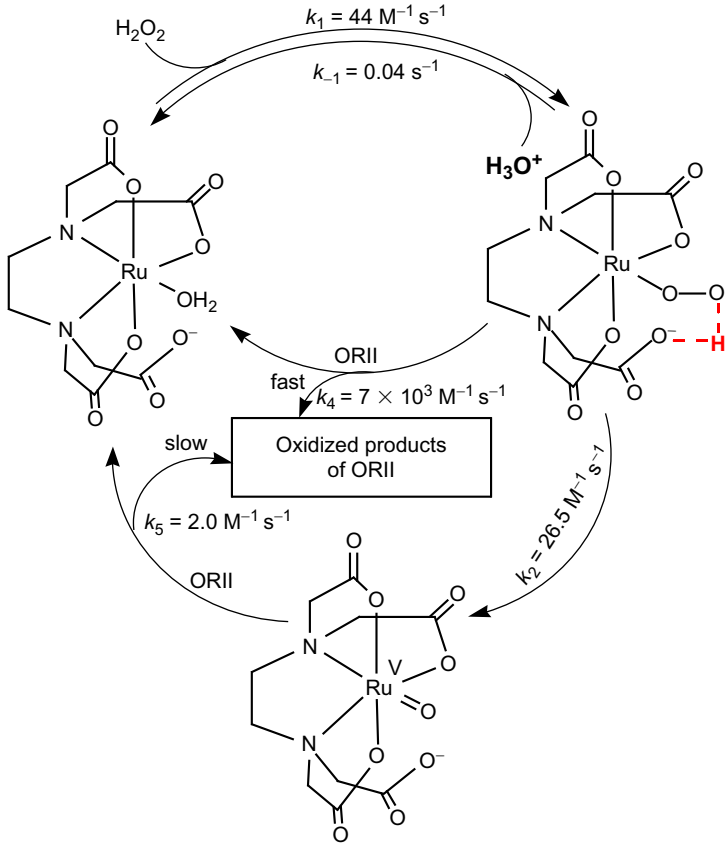

SCHEME 10. Proposed catalytic cycle and apparent role of the dangling acetate arm of $edta^{4-}$ (*75*). Reprinted with permission from the Royal Society of Chemistry.

kept in mind that the starting complex in the latter case, viz. $[Fe(edta)H_2O]^-$, is a seven-coordinate species, whereas $[Ru(edta)H_2O]^-$ is a six-coordinate species with a chelate dangling acetate arm. Further, in contrast to $[Ru^{III}(edta)(OOH)]^{2-}$, the $[Fe^{III}(edta)(OOH)]^{2-}$ complex does not undergo any subsequent homolytic or heterolytic cleavage of the peroxo bond. We, therefore, propose that the dangling acetate arm can lead to the stabilization of the hydroperoxo complex $[Ru^{III}(edta)(OOH)]^{2-}$ in a much lower pH range, than in the case of $[Fe^{III}(edta)(OOH)]^{2-}$, by assisting

the intramolecular deprotonation of the coordinated hydrogen peroxide to form the stable hydroperoxo intermediate (*75*). At lower pH, protonation of the dangling acetate arm will not allow this intramolecular stabilization of the hydroperoxo intermediate and leads to a decrease in the concentration and catalytic activity of the complex. The dangling acetate ligand is also held responsible for the subsequent homolytic and heterolytic cleavage of the peroxo bond in $[Ru^{III}(edta)(OOH)]^{2-}$.

The study illustrated the remarkably high activity of $[Ru^{III}(edta)(OOH)]^{2-}$, the Ru equivalent of Compound 0, as compared to $[Ru^{V}(edta)(O)]^{-}$ and $[Ru^{IV}(edta)(OH)]^{-}$, the Ru equivalents of Compounds I and II, respectively, toward the degradation of ORII. In the proposed formation of $[Ru^{III}(edta)(OOH)]^{2-}$ as the intermediate with the highest catalytic activity at pH 4, the role of the dangling acetate arm assisting the intramolecular deprotonation of the coordinated hydrogen peroxide that leads to the stabilization of the hydroperoxo complex $[Ru^{III}(edta)(OOH)]^{2-}$ is schematically demonstrated in Scheme 10. Thus, the complexes that are equivalents for Compounds I and II are practically nonreactive on the time scale observed for the degradation catalyzed by $[Ru^{III}(edta)(OOH)]^{2-}$ (*75*).

In a recent related study (*76*), $[Ru^{III}(edta)(H_2O)]^{-}$ was used to mediate the oxidation of cysteine by H_2O_2. Cysteine (RSH) is known to rapidly bind to $[Ru^{III}(edta)(H_2O)]^{-}$ to form $[Ru^{III}(edta)(SR)]^{2-}$ which subsequently undergoes direct oxidation with H_2O_2 at a much faster rate than with $[Ru^{V}(edta)(O)]^{-}$ and $[Ru^{IV}(edta)(OH)]$ produced in the direct reaction of $[Ru^{III}(edta)(H_2O)]^{-}$ with H_2O_2. The kinetic traces exhibit a clear induction period which can be accounted for in terms of the reformation $[Ru^{III}(edta)(SR)]^{2-}$ that rapidly occurs in the presence of an excess of RSH following the oxidation of coordinated RSH with H_2O_2. To illustrate this, some typically observed and simulated kinetic traces are given in Figs. 5 and 6 as a function of H_2O_2 and cysteine concentration, respectively.

The absorbance-time traces in Figs. 5 and 6 were simulated on the basis of the mechanism outlined in Scheme 11. A summary of the experimental and simulated rate constants are given in Table VII.

The experimental and simulated absorbance-time traces, as well as the experimental and simulated rate constants, are indeed in good agreement with the only exception of the value of k_6 in Table VII. The value of this rate constant is so small that it hardly contributes on the time scale of the observed oxidation

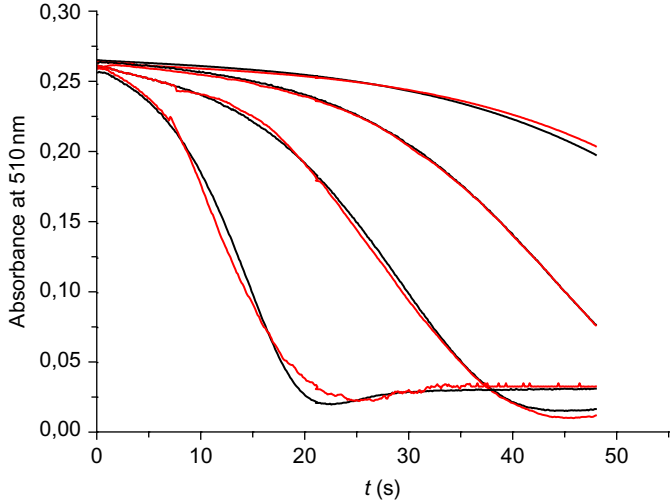

FIG. 5. Experimental (black) and simulated (red) absorbance-time traces at 510nm for the reaction of $[Ru^{III}(edta)(SR)]^{2-}$ (preformed by reacting $[Ru^{III}(edta)(H_2O)]^{-}$ with cysteine in the ratio 1:1) with different concentrations of H_2O_2. Experimental conditions: [**1**]$=1\times10^{-4}$M, [cysteine]$=1\times10^{-4}$M, $[H_2O_2]=(1, 2, 3, \text{and } 6)\times10^{-3}$M (increasing from right to left), pH 5.1 (1mM acetate buffer), temperature 20°C.

reactions. For this particular system, it was not possible to check the eventual role of $[Ru^{III}(edta)(OOH)]^{2-}$ that should be formed as an intermediate during the formation of $[Ru^{V}(edta)O]^{-}$.

VIII. Conclusions

NMR techniques represent an excellent tool to gain insight into the solution structure of polyaminecarboxylate complexes. Comparison of kinetic and mechanistic data allows to deduce the general principles and influencing factors responsible for the rate and mechanism of water-exchange processes on M(L) complexes. With these guidelines in hand, qualitative predictions for related complexes can be made. It turned out that steric constraints in the ligand backbone influence both the structure and reactivity of polyaminecarboxylate complexes. Based on the fundamental knowledge of the water-exchange reaction, other substitution processes, for example, binding of nitric oxide or

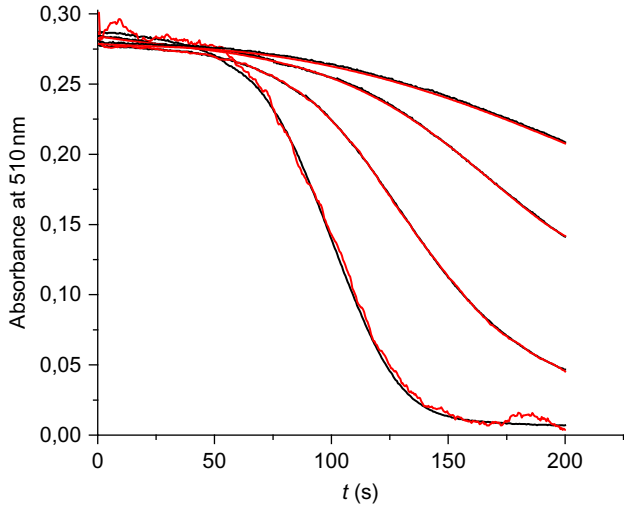

FIG. 6. Experimental (black) and simulated (red) absorbance-time traces at 510 nm for the reaction of $[Ru^{III}(edta)(SR)]^{2-}$ (preformed by reacting $[Ru^{III}(edta)(H_2O)]^{-}$ with different concentrations of cysteine) with a fixed excess of H_2O_2. Experimental conditions: [**1**]$=1\times10^{-4}$M, [cysteine]$=(2, 3, 4, \text{and } 5)\times10^{-4}$M (increasing from left to right), $[H_2O_2]=1\times10^{-3}$M, pH 5.1 (1 mM acetate buffer), temperature 20°C.

$$[Ru^{III}(edta)(H_2O)]^{-} + RSH \underset{k_{-1}}{\overset{k_1}{\rightleftharpoons}} [Ru^{III}(edta)(SR)]^{2-} + H_3O^{+} \quad K_1 = k_1/k_{-1}$$

$$[Ru^{III}(edta)(SR)]^{2-} + H_2O_2 \xrightarrow{k_2} [Ru^{III}(edta)(SROH)]^{-} + OH^{-}$$

$$[Ru^{III}(edta)(SROH)]^{-} + H_2O_2 \xrightarrow{k_3} [Ru^{III}(edta)(H_2O)]^{-} + RSO_2H$$

$$[Ru^{III}(edta)(SROH)]^{-} + RSH \xrightarrow{k_4} [Ru^{III}(edta)(H_2O)]^{-} + RSSR$$

$$[Ru^{III}(edta)(H_2O)]^{-} + H_2O_2 \xrightarrow{k_5} [Ru^{V}(edta)O]^{-} + 2H_2O$$

$$[Ru^{V}(edta)O]^{-} + RSH \xrightarrow{k_6} [Ru^{III}(edta)(SROH)]^{-}$$

SCHEME 11. Proposed catalytic cycle for the $[Ru^{III}(edta)(H_2O)]^{-}$-mediated oxidation of cysteine by H_2O_2.

TABLE VII

SUMMARY OF EXPERIMENTAL AND SIMULATED RATE CONSTANTS DETERMINED FOR ALL KINETIC EXPERIMENTS AT 20°C IN WHICH BOTH THE H_2O_2 AND CYSTEINE CONCENTRATIONS WERE VARIED [A]

Rate constant	Experimental value	Simulated value
k_1	$170\pm6\,M^{-1}s^{-1}$	$177\pm13\,M^{-1}s^{-1}$
k_{-1}	$(5.7\pm0.3)\times10^{-4}s^{-1}$	$(5\pm1)\times10^{-4}s^{-1}$
k_2	$22\pm1\,M^{-1}s^{-1}$	$21.6\pm1.1\,M^{-1}s^{-1}$
k_3	–	$153\pm7\,M^{-1}s^{-1}$
k_4	–	$928\pm64\,M^{-1}s^{-1}$
k_5	$15.4\pm0.6\,M^{-1}s^{-1}$	$15.8\pm0.6\,M^{-1}s^{-1}$
k_6	$0.089\pm0.007\,M^{-1}s^{-1}$	$0.83\pm0.07\,M^{-1}s^{-1}$

[a]Experimental conditions: $[Ru(edta)]=1\times10^{-4}M$, $[RSH]=(1–4)\times10^{-4}M$, $[H_2O_2]=(1–10)\times10^{-3}M$, pH=5.1 (1mM acetate buffer).

hydrogen peroxide to M(L) type of complexes can be understood. For example, the presence of fluoride can significantly lower the oxygen sensitivity of $[Fe^{II}(edta)(H_2O)]^{2-}$ in the BioDeNO$_x$ process without changing its NO binding ability. Kinetic measurements of the reaction of $[M^{III}(edta)H_2O]^-$ (M=Fe,Ru) with hydrogen peroxide using sf techniques helped to clarify the mechanism for the formation of peroxo intermediates. In contrast to catalytically inactive and unstable $[Fe^{III}(edta)OOH]^{2-}$, the corresponding Ru complex $[Ru^{III}(edta)OOH]^{2-}$ showed the highest catalytic activity compared to the possible Ru^{IV} species. The surprising stability of the $[Ru^{III}(edta)OOH]^{2-}$ complex at lower pH was ascribed to the dangling acetate arm present in the $[Ru^{III}(edta)H_2O]^{2-}$ species. In summary, understanding the fundamental processes in water-exchange reactions on polyaminecarboxylate complexes can help to explain, control, and improve related ligand substitution processes.

ACKNOWLEDGMENTS

The authors gratefully acknowledge continued financial support from the Deutsche Forschungsgemeinschaft initially through SFB 583 (Redox-active metal complexes) and thereafter, as well as the important contributions from numerous collaborators over many years (their names are cited in the references).

References

1. Munz, F. Polyamino carboxylic acids, **1935**.
2. Andersen, O. *Chem. Rev.* **1999,** *99*, 2683–2710.
3. Jager, H.-U.; Schul, W. *Muench. Beitr. Abwasser Fisch. Flussbiol.* **2001,** *54*, 207–226.
4. Schmidt, C. K.; Fleig, M.; Sacher, F.; Brauch, H.-J. *Environ. Pollut.* **2004,** *131*, 107–124.
5. Bergers, P. J. M.; deGroot, A. C. *Water Res.* **1994,** *28*, 639–642.
6. Kari, F. G.; Giger, W. *Water Res.* **1996,** *30*, 122–134.
7. Jardine, P. M.; Jacobs, G. K.; Wilson, G. V. *Soil Sci. Soc. Am. J.* **1993,** *57*, 945–953.
8. Kraus, K. *Muench. Beitr. Abwasser Fisch. Flussbiol.* **2001,** *54*, 187–194.
9. Maigut, J.; Meier, R.; Zahl, A.; van Eldik, R. *J. Am. Chem. Soc.* **2008,** *130*, 14556–14569.
10. Maigut, J.; Meier, R.; Zahl, A.; van Eldik, R. *Inorg. Chem.* **2008,** *47*, 5702–5719.
11. Helm, L.; Merbach, A. E. *Chem. Rev.* **2005,** *105*, 1923–1959.
12. Brausam, A.; van Eldik, R. *Inorg. Chem.* **2004,** *43*, 5351–5359.
13. Brausam, A.; Maigut, J.; Meier, R.; Szilagyi, P. A.; Buschmann, H.-J.; Massa, W.; Homonnay, Z.; van Eldik, R. *Inorg. Chem.* **2009,** *48*, 7864–7884.
14. Chatterjee, D.; Mitra, A.; van Eldik, R. *Dalton Trans.* **2007,** 943–948.
15. Maigut, J.; Meier, R.; van Eldik, R. *Inorg. Chem.* **2008,** *47*, 6314–6321.
16. Czap, A.; van Eldik, R. *Dalton Trans.* **2003,** 665–671.
17. Seibig, S.; van Eldik, R. *Eur. J. Inorg. Chem.* **1999,** 447–454.
18. Langford, C. N.; Gray, H. B. *Ligand Substitution Processes.* W.A. Benjamin: New York, **1966**.
19. van Eldik, R.; Klärner, F.-G. *High-Pressure Chemistry.* Wiley-VCH: Weinheim, **2002**.
20. Swaddle, T. W.; Mak, M. K. S. *Can. J. Chem.* **1983,** *61*, 473–480.
21. Swaddle, T. W. *Adv. Inorg. Bioinorg. Mech.* **1983,** *2*, 95–138.
22. De, V. D.; Weber, J.; Merbach, A. E. *Inorg. Chem.* **2004,** *43*, 858–864.
23. Helm, L.; Nicolle, G. M.; Merbach, A. E. *Adv. Inorg. Chem.* **2005,** *57*, 327–379.
24. Sandström, J. *Dynamic NMR Spectroscopy.* Academic Press: London, **1982**.
25. Helm, L.; Merbach, A. E. *Coord. Chem. Rev.* **1999,** *187*, 151–181.
26. Hertzberg, R. P.; Dervan, P. B. *Biochemistry* **1984,** *23*, 3934–3945.
27. Schultz, P. G.; Dervan, P. B. *J. Am. Chem. Soc.* **1983,** *105*, 7748–7750.
28. van der Maas, P.; Manconi, I.; Klapwijk, B.; Lens, P. *Biotechnol. Bioeng.* **2008,** *100*, 1099–1107.
29. Zhang, S.-H.; Mi, X.-H.; Cai, L.-L.; Jiang, J.-L.; Li, W. *Appl. Microbiol. Biotechnol.* **2008,** *79*, 537–544.
30. Bambagioni, V.; Bani, D.; Bencini, A.; Biver, T.; Cantore, M.; Chelli, R.; Cinci, L.; Failli, P.; Ghezzi, L.; Giorgi, C.; Nappini, S.; Secco, F.; Tine, M. R.; Valtancoli, B.; Venturini, M. *J. Med. Chem.* **2008,** *51*, 3250–3260.
31. Cameron, B. R.; Darkes, M. C.; Yee, H.; Olsen, M.; Fricker, S. P.; Skerlj, R. T.; Bridger, G. J.; Davies, N. A.; Wilson, M. T.; Rose, D. J.; Zubieta, J. *Inorg. Chem.* **2003,** *42*, 1868–1876.
32. *The Chemistry of Contrast Agents in Medical Magnetic Resonance Imaging.* John Wiley & Sons: Chichester, **2001**.

33. Maigut, J.; Meier, R.; Zahl, A.; van Eldik, R. *Inorg. Chem. (Washington, DC, US)* **2007,** *46*, 5361–5371.
34. Gollogly, J. R.; Hawkins, C. J.; Wong, C. L. *Inorg. Nucl. Chem. Lett.* **1970,** *6*, 215–219.
35. Hawkins, C. J.; Palmer, J. A. *Coord. Chem. Rev.* **1982,** *44*, 1–60.
36. Berry, R. S. *J. Chem. Phys.* **1960,** *32*, 933–938.
37. Pavelcik, F. *J. Coord. Chem.* **1984,** *13*, 299–307.
38. Meier, R.; Maigut, J.; Kallies, B.; Lehnert, N.; Paulat, F.; Heinemann, F. W.; Zahn, G.; Feth, M. P.; Krautscheid, H.; van Eldik, R. *Chem. Commun.* **2007,** 3960–3962.
39. Ducommun, Y.; Newman, K. E.; Merbach, A. E. *Inorg. Chem.* **1980,** *19*, 3696–3703.
40. Maigut, J.; Meier, R.; Zahl, A.; van Eldik, R. *Magn. Reson. Chem.* **2008,** *46* (Suppl. 1), S94–S99.
41. Swaddle, T. W.; Merbach, A. E. *Inorg. Chem.* **1981,** *20*, 4212–4216.
42. Felmy, A. R.; Qafoku, O. *J. Solution Chem.* **2004,** *33*, 1161–1180.
43. Bhat, T. R.; Radhamma, D.; Shankar, J. *J. Inorg. Nucl. Chem.* **1965,** *27*, 2641–2651.
44. Bhat, T. R.; Krishnamurthy, M. *J. Inorg. Nucl. Chem.* **1963,** *25*, 1147–1154.
45. Matwiyoff, N. A.; Strouse, C. E.; Morgan, L. O. *J. Am. Chem. Soc.* **1970,** *92*, 5222–5224.
46. Hunt, J. P.; Grant, M.; Dodgen, H. W. *J. Chem. Soc. D* **1970,** 1446–1447.
47. Grant, M. W.; Dodgen, H. W.; Hunt, J. P. *J. Am. Chem. Soc.* **1971,** *93*, 6828–6831.
48. Higginson, W. C. E.; Samuel, B. *J. Chem. Soc. A* **1970,** 1579–1586.
49. Erickson, L. E.; Young, D. C.; Ho, F. F. L.; Watkins, S. R.; Terrill, J. B.; Reilley, C. N. *Inorg. Chem.* **1971,** *10*, 441–453.
50. Evilia, R. F. *Inorg. Chem.* **1985,** *24*, 2076–2080.
51. Nesterova, Y. M.; Porai-Koshits, M. A. *Koord. Khim.* **1984,** *10*, 129–138.
52. Polynova, T. N.; Filippova, T. V.; Porai-Koshits, M. A. *Koord. Khim.* **1986,** *12*, 273–279.
53. Yoshitani, K. *Bull. Chem. Soc. Jpn.* **1994,** *67*, 2115–2120.
54. van der Maas, P.; van den Brink, P.; Klapwijk, B.; Lens, P. *Chemosphere* **2009,** *75*, 243–249.
55. Kumaraswamy, R.; Muyzer, G.; Kuenen, J. G.; Loosdrecht, M. C. M. *Water Sci. Technol.* **2004,** *50*, 9–15.
56. Kumaraswamy, R.; Kuenen, J. G.; Kleerebezem, R.; Loosdrecht, M. C. M.; Muyzer, G. *Appl. Microbiol. Biotechnol.* **2006,** *73*, 922–931.
57. Kumaraswamy, R.; van Dongen, U.; Kuenen, J. G.; Abma, W.; van Loosdrecht, M. C. M.; Muyzer, G. *Appl. Environ. Microbiol.* **2005,** *71*, 6345–6352.
58. Schneppensieper, T.; Wanat, A.; Stochel, G.; van Eldik, R. *Inorg. Chem.* **2002,** *41*, 2565–2573.
59. Schneppensieper, T.; Wanat, A.; Stochel, G.; Goldstein, S.; Meyerstein, D.; van Eldik, R. *Eur. J. Inorg. Chem.* **2001,** 2317–2325.
60. Van Der Maas, P.; Van De Sandt, T.; Klapwijk, B.; Lens, P. *Biotechnol. Prog.* **2003,** *19*, 1323–1328.
61. Li, W.; Wu, C.-Z.; Zhang, S.-H.; Shao, K.; Shi, Y. *Environ. Sci. Technol.* **2007,** *41*, 639–644.
62. Zang, V.; van Eldik, R. *Inorg. Chem.* **1990,** *29*, 4462–4468.
63. Schenk, G.; Pau, M. Y. M.; Solomon, E. I. *J. Am. Chem. Soc.* **2004,** *126*, 505–515.

64. Chatterjee, D.; van Eldik, R., accompanying Chapter in this volume.
65. Wanat, A.; Schneppensieper, T.; Karocki, A.; Stochel, G.; van Eldik, R. *J. Chem. Soc. Dalton Trans.* **2002,** 941–950.
66. Davies, N. A.; Wilson, M. T.; Slade, E.; Fricker, S. P.; Murrer, B. A.; Powell, N. A.; Henderson, G. R. *Chem. Commun. (Cambridge)* **1997,** 47–48.
67. Begel, S.; van Eldik, R. *Dalton Trans.* **2011,** *40*, 4892–4897.
68. Begel, S.; Heinemann, F. W.; Stopa, G.; Stochel, G.; van Eldik, R. *Inorg. Chem.* **2011,** *50*, 3946–3958.
69. Wang, W.; Lee, G. J.; Jang, K. J.; Cho, T. S.; Kim, S. K. *Nucleic Acids Res.* **2008,** *36*, e85/1–e85/7.
70. Sharma, V. K.; Millero, F. J.; Homonnay, Z. *Inorg. Chim. Acta* **2004,** *357*, 3583–3587.
71. Sharma, V. K.; Szilagyi, P. A.; Homonnay, Z.; Kuzmann, E.; Vertes, A. *Eur. J. Inorg. Chem.* **2005,** 4393–4400.
72. Horner, O.; Jeandey, C.; Oddou, J.-L.; Bonville, P.; Latour, J.-M. *Eur. J. Inorg. Chem.* **2002,** 1186–1189.
73. Neese, F.; Solomon, E. I. *J. Am. Chem. Soc.* **1998,** *120*, 12829–12848.
74. Fujii, S.; Tsueda, C.; Yamabe, K.; Nakajima, K.; Sakai, H. *Inorg. Chim. Acta* **2008,** *361*, 1207–1211.
75. Chatterjee, D. E.; Ember, E.; Pal, U.; Gosh, S.; van Eldik, R. *Dalton Trans.* **2011,** *40*, 10473–10480.
76. Chatterjee, D. E.; Ember, E.; Pal, U.; Gosh, S.; van Eldik, R. *Dalton Trans.* **2011,** (in press), 10997–11004.

POLYAMINECARBOXYLATERUTHENIUM(III) COMPLEXES ON THE MOSAIC OF BIOINORGANIC REACTIONS. KINETIC AND MECHANISTIC IMPACT

DEBABRATA CHATTERJEE[a] and RUDI VAN ELDIK[b]

[a]Chemistry and Biomimetics Group, CSIR-Central Mechanical Engineering Research Institute, Durgapur, India
[b]Department of Chemistry and Pharmacy, University of Erlangen-Nürnberg, Egerlandstr. 1, Erlangen, Germany

Abstract

Ru-pac complexes (pac=polyaminecarboxylate) are prospective in many ways for biological applications. They have unique features that make them suitable for biological applications. For instance, Ru-pac complexes can bind to biomolecules through a rapid and facile aqua-ligand substitution reaction and have a range of accessible and stable oxidation states. Ru-pac complexes also have some notable catalytic properties that mimic the enzymatic hydrocarbon oxidation by cytochrome P450 under homogeneous conditions, which is of immense significance toward developing Ru-pac-based agents for oxidative cleavage of DNA and artificial nuclease in DNA footprinting experiments.

INORGANIC/BIOINORGANIC REACTION MECHANISMS
VOLUME 64 ISSN 0898-8838 / DOI: 10.1016/B978-0-12-396462-5.00006-4

The advancement of Ru-pac-mediated bioinorganic reactions in terms of unraveling the mechanistic information has not been systematically reviewed till date. Hence, the subject of this review comprises mostly kinetic and mechanistic studies of bioinorganic reactions involving Ru-pac complexes. This review highlights the mechanistic aspects of recent investigations on the reactions of Ru-pac complexes that emphasize the prospect of the biological application of such complexes and ascertain the likely mechanisms of action of the Ru-pac complexes in some bioinorganic processes.

Keywords: Ru-pac complex; Kinetics; Reaction mechanism; Catalysis; —O—O— bond activation; DNA binding; DNA cleavage; Thio-amino acid oxidation; PTP inhibition; Dye degradation; NO scavenging; Redox reactions; Biomolecules.

I. Introduction

During the past three decades, [Ru(pac)(H_2O] complexes (pac= polyaminecarboxylate) have received much attention because of their kinetic lability toward aqua substitution along with a range of accessible and stable oxidation states, making them attractive candidates for different applications, particularly in biological studies. Most of the work published in earlier periods was limited to the aqueous chemistry of these compounds, mainly concerning the substitution behavior of Ru-edta complexes (*1–3*), including some electrochemical studies (*4–6*). In the recent past, the catalytic activity of ruthenium polyaminecarboxylate complexes in various organic transformations has been demonstrated. Moreover, a number of mixed ligand complexes of ruthenium-containing pac ligands have been synthesized, and among these complexes, some are of biological importance. The aim of this chapter is to bring into focus the intriguing areas of this system which have not been reviewed hitherto. This review is mainly concerned with the kinetics and mechanistic aspects of Ru-pac complexes that concern reactions of biological significance.

II. Background Chemistry

The donor character of the pac ligand is quite similar to many biological enzymes, which make use of carboxylate and amine donors from amino acids to bind to the metal center. The pac

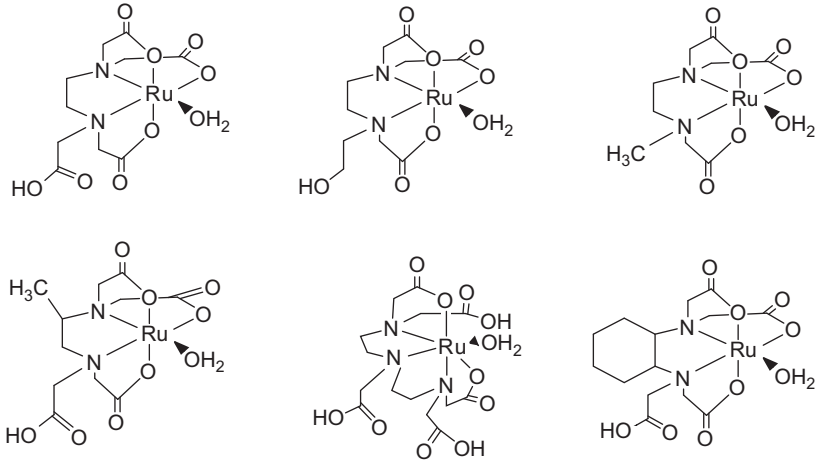

FIG. 1. Schematic representation of various ruthenium complexes bearing the pac ligand, $[Ru^{III}(pac)(H_2O)]$.

ligands form very stable 1:1 metal complexes with ruthenium. It was shown earlier (*5,6*), and later established by crystallographic studies (*7,8*), that pac ligands function as pentadentate ligands (presented in Fig. 1) toward ruthenium. While Ru(III) is the predominant oxidation state under physiological conditions, Ru(II), Ru(IV), and Ru(V) oxidation states are readily accessible in the presence of biological reductants (e.g., ascorbate or thiols) or oxidants (e.g., O_2 or H_2O_2), respectively.

III. Substitution of Ru(III)-pac Complexes

The chemistry of edta-type complexes of Ru(III) is dominated by their lability toward the aqua-substitution reaction (Scheme 1), which affords a facile and straightforward synthesis to mixed ligand complexes. Matsubara and Creutz also observed the unusual lability of the $[Ru(edta)(H_2O]^-$ ($edta^{4-}$=ethylenediaminetetraacetate) complex toward substitution with various aromatic N-heterocycles (*3*). The reaction was characterized by the rapid formation of a 1:1 (metal to ligand) substituted product complex, [Ru(edta)L].

Stopped-flow kinetics of the aqua-substitution reaction revealed that under pseudo-first-order conditions of an excess of the incoming nucleophile (δ), the values of the observed rate constant (k_{obs}) increase linearly with the concentration of the entering ligand (δ). The plots exhibited no meaningful intercepts,

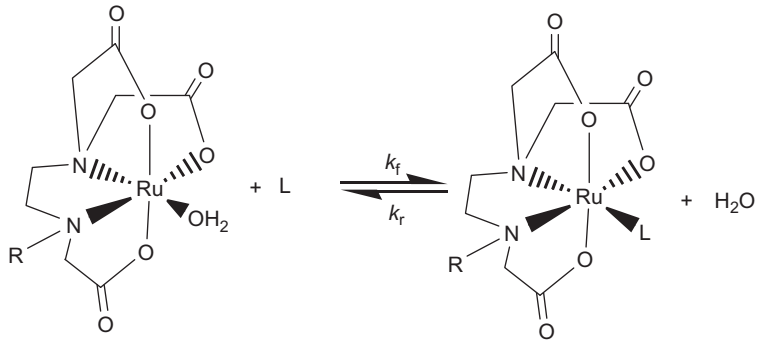

R = CH_2COO^- for edta; R = CH_2CH_2OH for hedtra and R = CH_3 for medtra

SCHEME 1. Mechanism of substitution of Ru(III)-pac complexes with nucleophile (L).

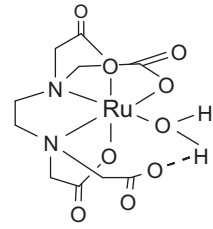

SCHEME 2. Hydrogen bonding between oxygen atom of dangling carboxylate group and coordinated H_2O.

indicating the absence of a reverse aquation reaction under the conditions employed. The maximum reactivity of the substitution reaction was observed in the pH range 4–6. The unusual lability of the $[Ru(edta)(H_2O]^-$ complex (which exists predominantly in the pH range 4–6) may be explained in terms of internal hydrogen bonding (*3*) between an oxygen atom of the uncoordinated carboxylate group (COO^-) and the coordinated water molecule, which either creates an open area for access to the entering ligand or labilizes the coordinating water molecule by affecting the Ru—OH_2 bond strength (Scheme 2).

A different mechanism involving transient coordination of a pendant group which assists the elimination of the coordinated water molecule (Scheme 3) in the $[Ru(edta)(H_2O]^-$ complex appeared in the literature (*9,10*).

Subsequently, Bajaj and van Eldik in a series of publications (*11–13*) reporting on the effect of pressure on the substitution

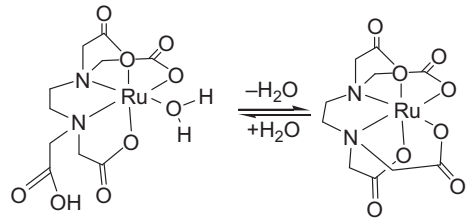

SCHEME 3. Transient coordination of pendant carboxylate group.

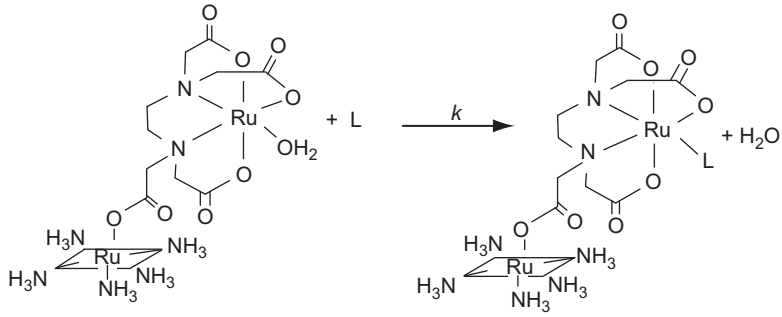

SCHEME 4. Mechanism of substitution reaction of $[(Ru^{III}(NH_3)_5(edta)Ru^{III}(H_2O)]^{2+}$ with nucleophile (L).

reaction established that it is neither hydrogen bonding nor transient coordination of the dangling carboxylate group, but the carbonyl oxygen atom by virtue of its *syn* lone pair of electrons, which labilizes the coordinated water molecule. Compelling evidence in favor of this was reported (*14*) when substitution of $[(Ru^{III}(NH_3)_5(edta)Ru^{III}(H_2O)]^{2+}$ was carried out with thiourea (Scheme 4). Although the incorporation of a pendant carboxylate group into the $[Ru^{III}(NH_3)_5]^{3+}$ moiety prevented the transient coordination as proposed by Ogino *et al*. (*10*), the rate of substitution was found to be higher than for $[Ru(hedtra)(H_2O)]$ (*12*) and $[Ru(medtra)(H_2O)]$ (*13*), where the pac chelates do not contain any pendant carboxylate group.

Kinetic data for the substitution of the $[Ru(pac)(H_2O)]^-$ complex with various nucleophiles (*15*) revealed that within the series of aqua/hydroxo complexes, the substitution rate constants decrease substantially along the series edta $\gg$ hedtra $>$ medtra. This is accompanied by a general increase in $\Delta H^{\neq}$ and almost constant $\Delta S^{\neq}$ (*15*). From this trend, the highest lability is induced for the pendant group when $R=CH_2COO^-$, with significantly decreased lability for $R=CH_2CH_2OH$ and even further for $R=CH_3$. This

substantiates the important role of the dangling pendant carboxylate group, as discussed earlier in the labilization of the coordinated water molecule in the $[Ru^{III}(edta)(H_2O)]^-$ complex. Substitution reactions that involve the displacement of the water molecule from $[Ru(pac)(H_2O)]$ follow associative interchange $[I_a]$ pathways, but the $[Ru^{III}(edta)(H_2O)]^-$ complex has an internal I_a pathway via its own pendant $—COO^-$ group which lowers the activation barrier by ca. 10 kJ/mol.

Substitution reactions of the corresponding Ru(II)-pac complexes have not received much further attention. The reason could be the disadvantage in working with the Ru(II) species as the Ru(II)-pac complexes are very sensitive to aerial oxidation and the presence of Ru(III) in the system causes erroneous results. Further, it was reported (*3*) that the substitution behavior of edta complexes of Ru(II) does not differ much from other Ru(II) complexes. Notwithstanding the above facts, the substitution kinetics of $[Ru^{II}(edta)(H_2O)]^{2-}$ with CH_3CN, SCN^-, and isonicotinamide was studied earlier (*3*) and found that the driving force which arises due to the unprotonated free carboxylate group in the corresponding Ru(III) complex is not operative in the Ru(II)-edta system. Labilization in the Ru(II)-edta system was ascribed to the coordination of the chelating edta ligand and lowering of the effective positive charge on the metal center which reduces the barrier to a dissociative substitution process.

IV. Reactions of Ru^{III}-pac Complexes with DNA Constituents

The $[Ru^{III}(pac)(H_2O)]$ complexes, due to their lability toward aqua substitution, are of oncological significance as they could bind DNA constituents in a facile and straightforward manner. The antitumor activity of Ru(IV)-cdta (cdta = cyclohexylethylenediaminetetraacetate) has been reported earlier (*16,17*). Literature relating to the inhibition of DNA recognition (*18*) by *cis*-$[Ru^{III}(pdta)Cl_2]$ (pdta = propylene-1,2-diaminotetraacetate) and cancer cell proliferation by $[Ru^{III}(pac)(H_2O)]$ have been reviewed in the recent past (*19*). The results of cell proliferation studies with Ru-pac complexes (*20*) using MCF-7 (breast cancer), NCI-H460 (lung cancer), and SF-268 (central nervous system) cell lines revealed that $[Ru^{III}(edta)(H_2O)]^-$ and $[Ru^{III}(pdta)(H_2O)]^-$ are much more efficient inhibitors of these cell lines than complexes, where pac = $hedtra^{3-}$ and $medtra^{3-}$. $[Ru^{III}(hedtra)(H_2O)]$ and $[Ru^{III}(medtra)(H_2O)]$ have insignificant activity that is presumably associated with a much lower rate of binding of the purine-base nucleotides than in the case of the

corresponding $edta^{4-}$ and $pdta^{4-}$ complexes. Results of kinetic and mechanistic studies on the interaction of [Ru-(pac)(H_2O)] complexes with various purine and pyrimidine bases and their corresponding nucleosides and 5′-nucleotides (Fig. 2) leading to the formation of [Ru-(pac)(Nu)] have been reported (*20–23*), ascertaining the most likely mechanisms of such complexes in the biological medium.

Reactions of [Ru^{III}(pac)(H_2O)] complexes with different nucleophiles, viz. AMP (adenosine-5′-monophosphate), ADP (adenosine-5′-diphosphate), ATP (adenosine-5′-triphosphate), GMP (guanosine-5′-monophosphate), IMP (inosine-5′-monophosphate), UMP (uridine-5′-monophosphate), CMP (cytidine-5′-monophorphate), and TMP (thymidine-5′-monophosphate), were scrutinized spectrophotometrically and kinetically (*20–23*). During spectrophotometric measurements, it was noticed that the spectral changes were not appreciable for kinetic studies on the reaction of Ru-pac complexes with pyrimidine-base nucleotides. Therefore, kinetic investigations could not be performed for pyrimidine-base nucleotides, but with purine-base nucleotides. The kinetics of the interaction of [Ru^{III}(pac)(H_2O)] with AMP appeared to be two exponential as seen in Fig. 3 typically for the reaction of [Ru^{III}(hedtra)(H_2O)] with AMP.

Analysis of the kinetic trace yielded two rate constants. The values of the observed rate constant corresponding to the first step increased linearly with increasing AMP concentration (Fig. 4), whereas the values of the observed rate constant for the second step were found to be independent of [AMP] (*21,23*).

Based on these kinetic results and on considering that the N-7 atom is the most probable coordination site of purines (*22*), the overall reaction shown in Scheme 5 involves rapid coordination through N-7 of adenine moiety of AMP in a [AMP]-dependent step, followed by a [AMP]-independent ring-closure step in which the exocyclic NH_2 group (at C-6 of the adenine base) of AMP binds to the ruthenium center by dislodging the adjacent carboxylate group of the coordinated pac ligand (Scheme 5).

The reaction of Ru-pac complexes with purine-base nucleotides other than AMP, showed a linear dependence of the observed rate constant on the concentration of Nu, however, did not reveal any [Nu]-independent ring-closure step as observed in the case of AMP. The kinetic behavior could be rationalized in terms of the reactions outlined in Scheme 6 for which the rate expression is given in Eq. (1).

$$k_{obs} = k_1[Nu] + k_{-1} \tag{1}$$

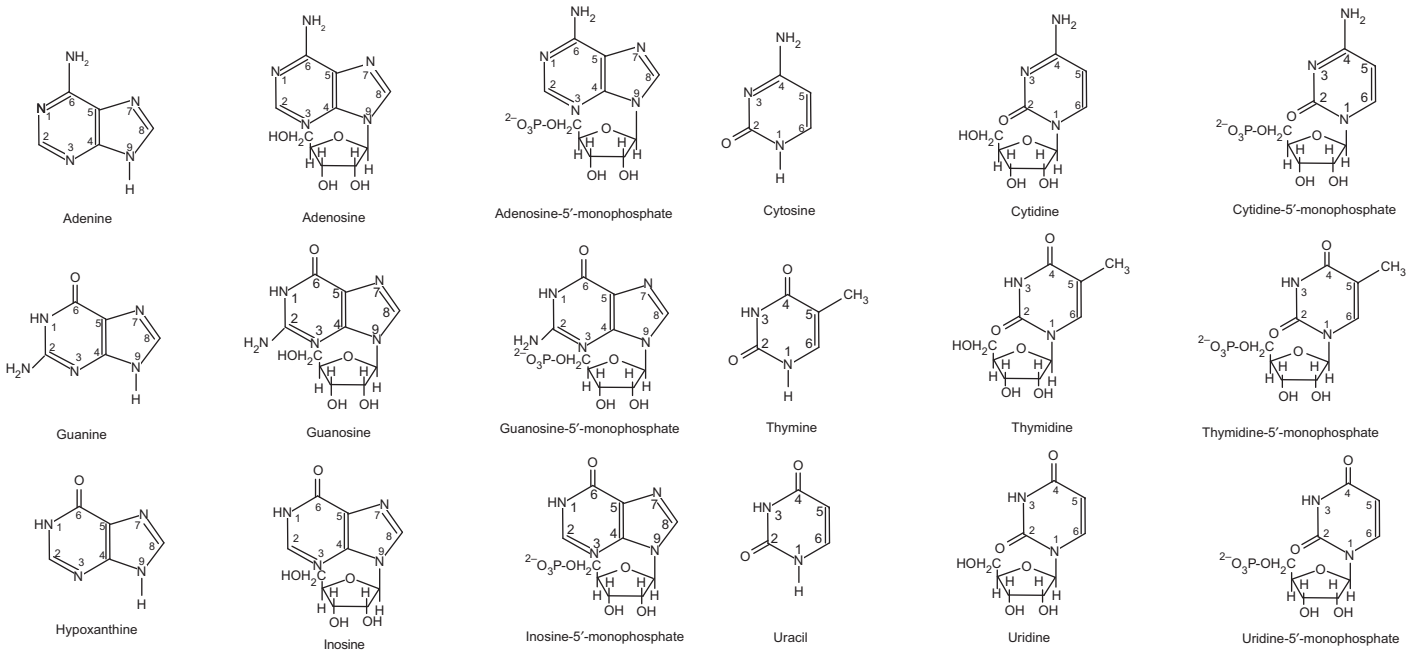

FIG. 2. Schematic presentation of purine and pyrimidine bases and their corresponding nucleosides and nucleotides.

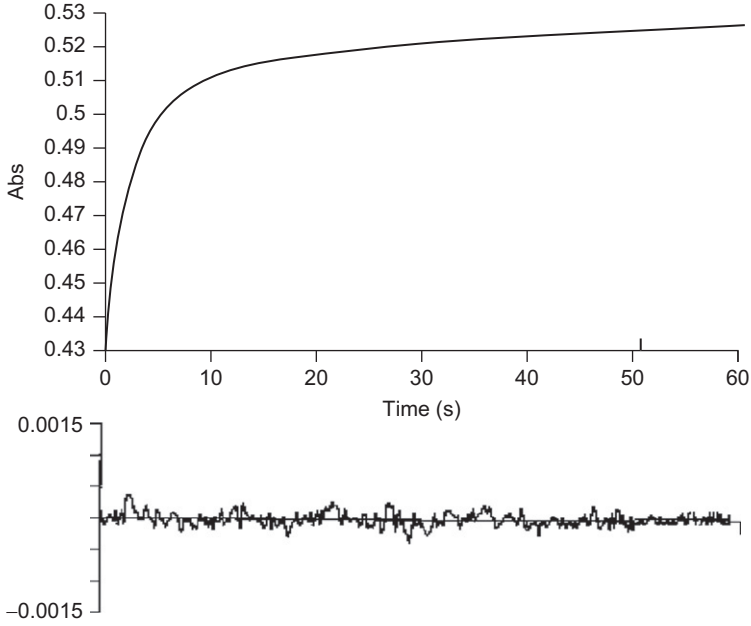

FIG. 3. Typical kinetic trace for the reaction between [Ru^{III}(pac)(H_2O)] and AMP at pH 4.5 and 25°C. The trace was fitted to double exponentials by following the growth in absorbance at 320 nm. The lower trace represents the difference between the experimental and the calculated curves.

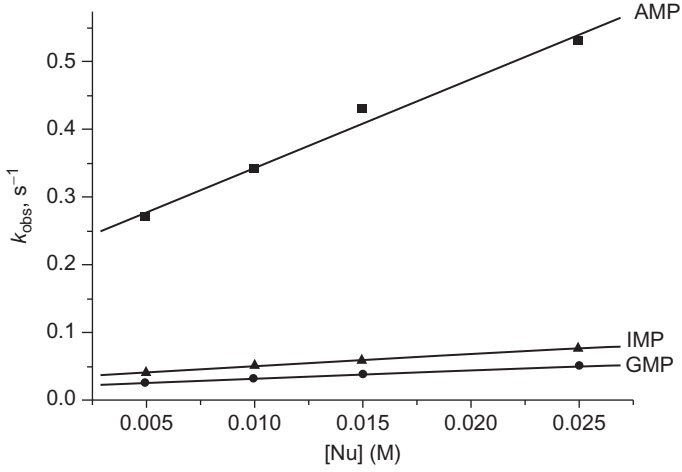

FIG. 4. Plot of k_{obs} versus [Nu] for the reaction of [Ru^{III}(pac)(H_2O)] with different 5-nucleotides [Nu] at 25°C. [Ru^{III}] = 5.0×10^{-4} M, pH 4.5, and $I = 0.1$ M ($NaClO_4$).

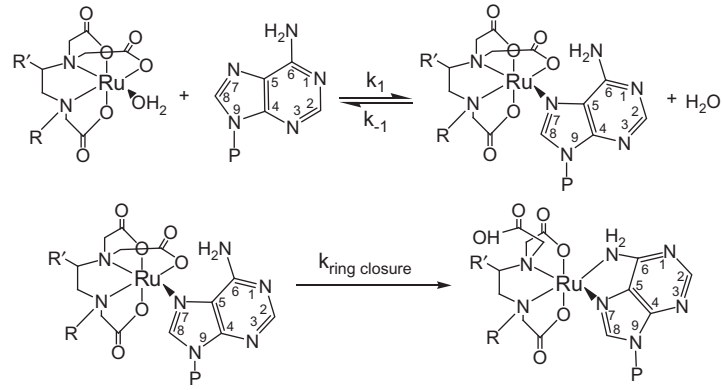

SCHEME 5. Mechanism of the reaction of $[Ru^{III}(edta)(H_2O)]^-$ with AMP.

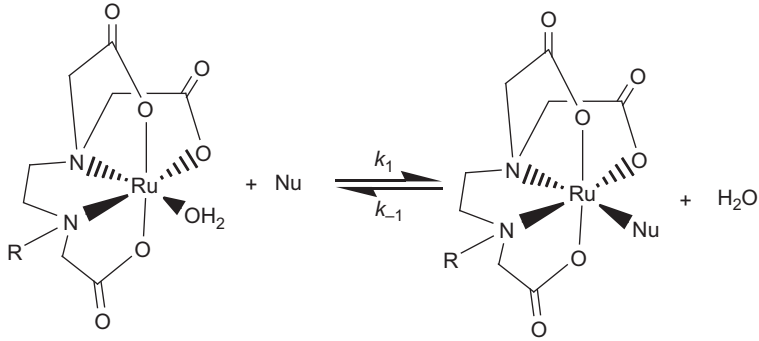

R = CH_2COO^- for edta; R = CH_2CH_2OH for hedtra and R = CH_3 for medtra

SCHEME 6. Mechanism of the reaction of Ru(III)-pac complexes with purine-base nucleotides [NU] other than AMP.

In practice, plots of k_{obs} versus [Nu] were linear (*20,21,23*) as shown typically for the reaction of $[Ru^{III}(hedtra)(H_2O]$ with GMP and IMP in Fig. 4 underlying the validity of the proposed scheme. The values of k_1 and k_{-1} determined from the slopes and intercepts of such plots, respectively, are summarized in Table I.

Comparison of the rate constants (k_1) listed in Table I suggests that the lability of the $[Ru^{III}(pac)(H_2O)]$ complexes toward aqua substitution is as follows: $[Ru^{III}(edta)(H_2O)]^- \gg [Ru^{III}(hedtra)(H_2O)] > [Ru^{III}(medtra)(H_2O)]$. All the complexes react with purine bases faster than nucleosides, whereas the rate of reaction is comparatively the slowest for nucleotide bases. However,

TABLE I

RATE CONSTANTS FOR THE REACTION OF [Ru^{III}(pac)(H_2O)] WITH DNA FRAGMENTS (L) AT 25°C

Complex	[Ru^{III}(pac)(H_2O)]					
	[Ru^{III}(edta)(H_2O)]$^-$		[Ru^{III}(hedtra)(H_2O)]		[Ru^{III}(medtra)(H_2O)]	
L	k_1 ($M^{-1}s^{-1}$)	k_{-1} (s^{-1})	k_1 ($M^{-1}s^{-1}$)	k_{-1} (s^{-1})	k_1 ($M^{-1}s^{-1}$)	k_{-1} (s^{-1})
Adenine	8902	14.5	44.2	1.4	4.7	0.1
Adenosine	8840	12.5	37.1	1.1	3.3	0.08
AMP	2904	22.5	13.1	0.51	1.1	0.07
ADP	2100	21.2	12.2	0.44	0.92	0.04
ATP	1069	20.8	9.8	0.21	0.8	0.02
Guanine	68.4	2.8	4.8	0.12	0.73	0.07
Guanosine	59.2	1.6	3.2	0.08	0.58	0.04
GMP	29.1	0.6	1.2	0.03	0.34	0.05
Xanthene	72.3	3.1	5.5	0.14	0.82	0.04
Inosine	61.2	2.8	3.4	0.12	0.7	0.02
IMP	38.3	2.4	1.8	0.09	0.57	0.02

[Ru^{III}] = 5×10^{-4} M, pH 4.5, and I = 0.1 M ($NaClO_4$).

all Ru-pac complexes chosen for this study exhibit a similar reactivity order toward binding nucleotides, viz. AMP ≫ IMP > GMP. The values of $\Delta H^{\neq}$ and $\Delta S^{\neq}$ determined from temperature dependence studies lie in the range $39 > \Delta H^{\neq} > 27\,kJ\,mol^{-1}$ and $-80 > \Delta S^{\neq} > -110\,JK^{-1}mol^{-1}$ and are in good agreement with those reported for the substitution of [Ru^{III}(pac)(H_2O)] complexes with other ligands (*15*), which signifies the operation of an associative interchange mechanism in the present case. Results of the kinetics and mechanism of the binding of [Ru^{III}(pac)(H_2O)]$^-$ to DNA bases, nucleosides and nucleotides, led us to conclude that [Ru^{III}(pac)(H_2O)] complexes bind to adenine base units of single strand calf-thymus DNA in a kinetically preferred pathway (*20–23*).

V. Reactions of Ru^{III}-pac Complexes with Sulfur-Containing Biomolecules

The [Ru^{III}(pac)(H_2O)] complexes can also bind sulfur-containing biomolecules (RSH) rapidly due its lability toward aqua substitution (*24–26*).

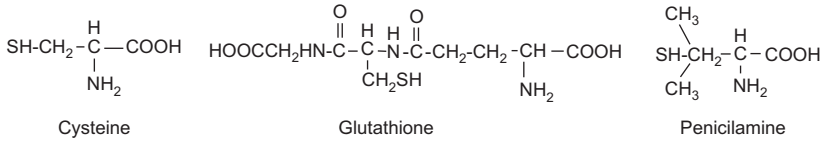

FIG. 5. Schematic presentation of the thiols selected in this work.

It is noteworthy that addition of RSH (Fig. 5) to an aqueous solution of $[Ru^{III}(pac)(H_2O)]$ complexes results in an immediate color change from pale yellow to red due to the formation of $[Ru^{III}(pac)(RS^-)]$. The intense band that appears in the visible region (510–516 nm) in the spectra of the $[Ru^{III}(pac)(RS^-)]$ complexes is typical for the formation of a sulfur–ruthenium bond. The binding to sulfur-containing biomolecules available in the cells is considered as one of the reasons for the postulated mechanism of "drug resistance' and "toxicity" of *cis*-platin like drugs. The binding to thio-macromolecules in the cell decreases the intracellular accumulation of such metallo-drugs, and consequently, it cannot reach the DNA inside the cell to cause cell death. Therefore, it appears that the kinetic understanding of the interaction of such metal complexes with DNA fragments vis-à-vis sulfur-containing biomolecules would be of importance in the rationalization of the antitumor activity as well as toxicity of such metallo-drugs. Hence, the reactivity of $[Ru^{III}(pac)(H_2O)]$ complexes with some biologically important thio-amino acids has been studied kinetically using the stopped-flow technique (*24–26*). Results of kinetic studies revealed that thio-ligands (RSH) directly replace the coordinated water molecule in $[Ru^{III}(pac)(H_2O)]$. The rate of reaction was found to be first order with respect to the concentration of the Ru-pac complexes. Under pseudo-first conditions, the values of the observed rate constant (k_{obs}) increased linearly with increasing concentration of the thio-ligands. The above kinetic behavior was rationalized in terms of the rate expression in Eq. (2).

$$k_{obs} = k_f[RSH] \tag{2}$$

The values of specific rate constants estimated from Eq. (2) are summarized in Table II. A comparison of the rate constants reveals the following reactivity of complexes: $[Ru^{III}(edta)(H_2O)]^- \gg [Ru^{III}(hedtra)(H_2O)] > [Ru^{III}(medtra)(H_2O)]$.

The activation parameters, $\Delta H^{\neq}$ ($52 > \Delta H^{\neq} > 38$ kJ mol^{-1}) and $\Delta S^{\neq}$ ($-58 > \Delta S^{\neq} > -77$ J K^{-1} mol^{-1}), obtained (*24–26*) for the substitution of $[Ru^{III}(pac)(H_2O)]$ by thio-amino acid ligands clearly

TABLE II

RATE CONSTANTS FOR THE REACTION OF $[Ru^{III}(pac)(H_2O)]$ WITH THIO-AMINO ACIDS (L) AT 25°C

RSH	k_f ($M^{-1}s^{-1}$)		
	$[Ru^{III}(edta)(H_2O)]^-$	$[Ru^{III}(hedtra)(H_2O)]$	$[Ru^{III}(medtra)(H_2O)]$
Cysteine	170	2.59	0.67
Glutathione	260	1.97	0.88
Pencilliamine	160	1.78	0.45
N-Acetylcysteine	270	2.53	0.77

$[Ru^{III}]=5\times10^{-4}$M, pH 4.5, and $I=0.1$M ($NaClO_4$).

support the operation of an associative interchange (I_a) mechanism. It is worth mentioning here that the reported binding rate of $[Ru^{III}(pac)(H_2O)]$ with such thio-ligands is much lower than the binding rate with AMP. Very recently, kinetic and mechanistic investigations of the reaction of $[Ru^{III}(edta)(SR)]^{2-}$ with 5′-nucleotides (Nu) have been reported (*27*) that looked into the possibility of the binding of the DNA fragments, 5′-nucleotides, to the ruthenium center by removing the coordinated thiolate (RS^-) from $[Ru^{III}(edta)(SR)]^{2-}$.

The first-order rate constants (k_{obs}) were found to be independent of [Nu] under the selected conditions. These results are explicable in terms of the mechanistic proposal outlined in Scheme 7. In the proposed mechanism, aquation of $[Ru^{III}(edta)(SR)]^{2-}$ occurs in a rate-determining step, and subsequently, $[Ru^{III}(edta)(H_2O)]^-$ undergoes rapid aqua substitution by 5′-nucleotides (Nu) to produce $[Ru^{III}(edta)(Nu)]^-$ as the reaction product. The k_{obs} values reported for $[Ru^{III}]=1\times10^{-4}$M, [cysteine]$=1\times0^{-3}$M and $[Nu]=1\times10^{-3}$M are $(5.7\pm0.1)\times10^{-4}s^{-1}$, $(5.4\pm0.1)\times10^{-4}s^{-1}$, $(5.8\pm0.1)\times10^{-4}s^{-1}$, $(5.1\pm0.1)\times10^{-4}s^{-1}$, and $(5.5\pm0.1)\times10^{-4}s^{-1}$ at 25°C and pH 7.2 for Nu=AMP, GMP, IMP, CMP, and UMP, respectively. For all the nucleotides, the rate constant values for the formation of $[Ru^{III}(edta)Nu]^-$ are close to the value ($k_{-1}=5.7\times10^{-4}s^{-1}$ at 25°C) reported for the aquation of $[Ru^{III}(edta)(cys)]^{2-}$ (*24*). A similar observation was also observed for RSH=glutathione. The rate constant values are $(5.0\pm0.1)\times10^{-4}s^{-1}$, $(4.9\pm0.1)\times10^{-4}s^{-1}$, $(4.9\pm0.1)\times10^{-4}s^{-1}$, $(5.0\pm0.1)\times10^{-4}s^{-1}$, and $(4.9\pm0.1)\times10^{-4}s^{-1}$ for Nu=AMP, GMP, IMP, CMP, and UMP, respectively at 25°C and pH 7.2. A very similar observation reported (*3*) in the case of substitution

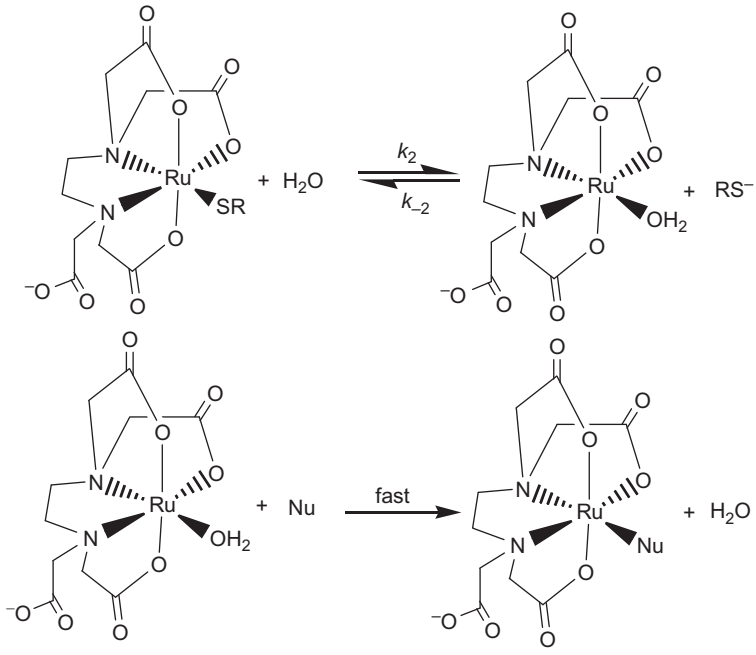

SCHEME 7. Mechanism of the reaction of $[Ru^{III}(edta)(SR)]^{2}$ with 5′-nucleotides (Nu).

of $[Ru^{III}(edta)NCCH_3)]^{-}$ and $[Ru^{III}(edta)(NCS)]^{2-}$ by pyrazine (pz) further validates our mechanistic proposal. The reported results suggest that at a physiological pH of 7.2, the DNA fragments (Nu) can be coordinated to the ruthenium center by replacing coordinated thiols in $[Ru^{III}(edta)(SR)]^{2-}$. The results from the above studies taken together could be of pharmacological significance for such complexes as metallo-drugs.

The reactivity of the Ru-pac complexes toward the binding of the above thio-amino acids (RSH) has been reportedly used to explore the potential role of Ru-pac complexes in the inhibition of the activity of cysteine protease (CP) (*25,26*) and protein tyrosine phosphatase (PTP) (*28*). The Ru-pac complexes were found to inhibit protease activity of the three enzymes bromalien, papain, and ficin, while azo-albumine was used as the substrate (*25,26*). The ability of Ru-pac complexes to inhibit CP activity was attributed to the high affinity of the ruthenium complexes toward binding the SH group in the cysteine residue of the enzymes via a rapid aqua-substitution reaction (Scheme 8).

The results demonstrated the lower efficiency of the Ru-hedtra complex as compared to that of the Ru-edta complex, which is

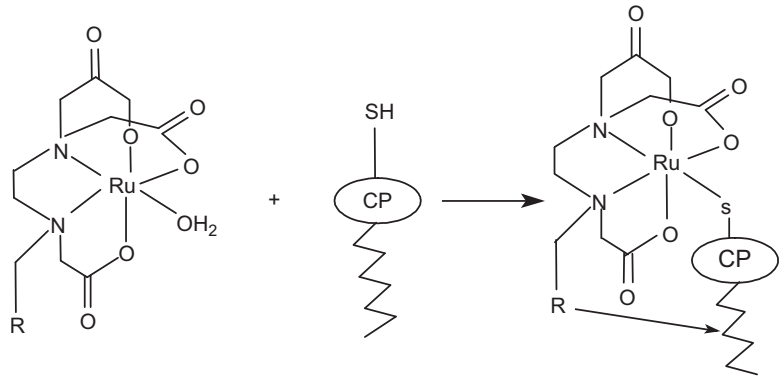

SCHEME 8. Mechanism of cysteine protease (CP) inhibition by Ru-pac complexes. Published in *RSC Journal* (taken from Ref. (*28*)).

TABLE III

RESULTS OF INHIBITION OF A RECOMBINANT *YERSINIA ENTEROCOLITICIA* PTP BY Ru^{III}-EDTA

Run no.	$[Ru^{III}]$ (mM)	[Glutathione] (mM)	% Inhibition
1	0.1	Nil	37±3
2	0.5	Nil	56±5
3	1.0	Nil	67±6
4	1.5	Nil	76±8
5	1.0	10	7±1

Published in *RSC Journal* (taken from Ref. (*28*)).

plausibly associated with the lower affinity of $[Ru^{III}(hedtra)(H_2O)]$ toward the binding of thiols (RSH) (*26*).

The PTPs with cysteine residues in the catalytic domain are critical regulators of signal transduction under normal and pathophysiological conditions (*29*). Defective or inappropriate regulation of PTP activity leads to abnormal tyrosine phosphorylation, which contributes to the development of many human diseases (*30*). The results of PTP inhibition studies by $([Ru^{III}(pac)(OH_2/OH)]$ as typically presented by the data in Table III clearly revealed that $[Ru^{III}(edta)(OH_2/OH)]$ is capable of reducing the hydrolysis of *p*-nitrophenylphosphate by PTP under specified conditions. The $[Ru^{III}(edta)(OH_2)]^-$ complex presumably binds the cysteine residue in the catalytic domain of the PTP through

a rapid aqua-substitution reaction and thus inhibits the protease activity of the enzyme by forming a stable Ru(edta)–enzyme complex. Addition of glutathione to the reaction system substantially reduced the inhibition activity of the Ru^{III}-edta complex (Run 5 in Table III), which further supports the above argument. The observed ability of the Ru^{III}-edta complex toward inhibition of PTP activity is attributed to the high affinity of the $[Ru^{III}(edta)(OH_2)]^-$ complex toward binding the SH group of thio-amino acids. By contrast, $[Ru^{III}(hedtra)(OH)]^-$ ($hedtra^{3-}$ = *N*-hydroxyethlyethylenediaminetriacetate), which is structurally almost identical to $[Ru^{III}(edta)(OH)]^{2-}$, was found to be almost ineffective toward inhibiting the activity of PTP under similar experimental conditions (7% inhibition of PTP activity at $[Ru^{III}(hedtra)(OH)]^- = 1.5\,mM$). Thus, the lower efficiency of the Ru-hedtra complex toward inhibition of PTP as compared to that of the Ru-edta complex is most likely associated with the lower affinity of the Ru-hedtra complex to bind the SH group of the cysteine residue in the catalytic domain of PTP.

It is worth mentioning here that although vanadate and pervanadate (a complex of vanadate and H_2O_2) compounds are well known to modulate insulin metabolic effects by inhibiting PTP activity, vanadate and pervanadate inhibit PTPs by completely different mechanisms (*31*). PTP inhibition by vanadate takes place through an oxidant-independent pathway. By contrast, pervanadate inhibits PTP by irreversibly oxidizing the catalytic cysteine of PTP. In the present case, Ru^{III}-edta inhibits PTP in resemblance to vanadate through an oxidant-independent pathway. However, oxidation of coordinated thio-amino acids in $[Ru^{III}(edta)(SR)]^{2-}$ occurs readily upon addition of H_2O_2 to the solution of $[Ru^{III}(edta)(SR)]^{2-}$ as shown in Fig. 6 by the loss of the spectral features at 510 nm of $[Ru^{III}(edta)(SR)]^{2-}$.

The above results further explore the possibility of a catalytic pathway for the inhibition of PTP by Ru^{III}-edta in the presence of intracellular H_2O_2 through oxidation of the catalytic cysteine residue, as suggested in Scheme 9.

The reactivity of the Ru-pac complexes can provide clues as to possible mechanisms by which the general class of Ru drugs exerts their anticancer activities. Thus, the pac complexes are likely to be better biomimetic models for studies of the *in vivo* activities of Ru complexes in clinical trials than are the parent pro-drugs. Most of the studies on the anticancer properties of the Ru drugs have focused on their interactions with DNA, but since PTP inhibition is known to exert anticancer properties, this may be an important alternative factor in their activities.

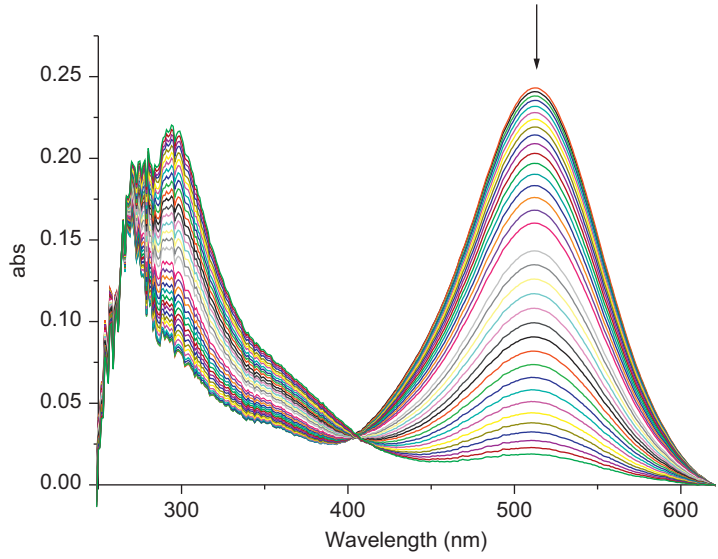

FIG. 6. Spectral changes associated with the oxidation of $[Ru^{III}(edta)(SR)]^{2-}$ by H_2O_2.

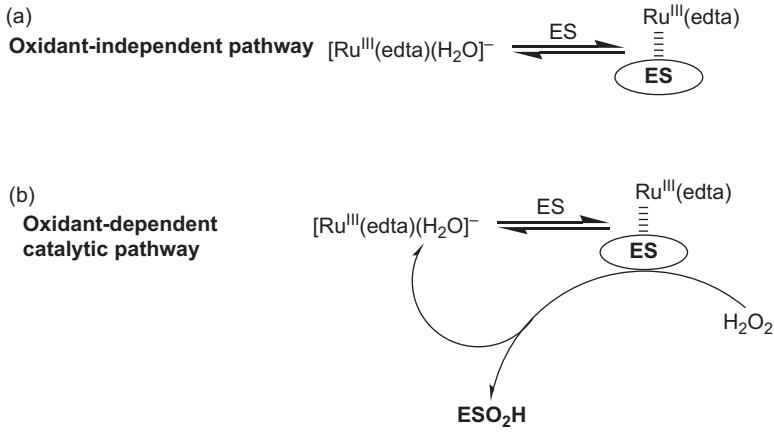

SCHEME 9. Mechanism of PTP inhibition by Ru-pac complexes. Published in *RSC Journal* (taken from Ref. (*28*)).

VI. Reactions of Ru-pac Complexes Involving NO

Nitric oxide (NO) is an important signaling molecule that regulates different biological processes (*22*) including cardiovascular control (*32*), neuronal signaling (*33*) and acts as an agent

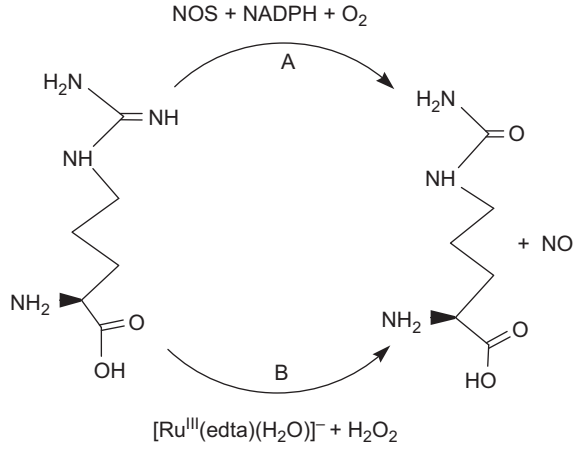

SCHEME 10. Oxidation of L-arginine to No and L-citrulline. Published in *RSC Journal* (taken from Ref. (*41*)).

for defense mechanisms against microorganisms and tumors (*34*). A heme-containing enzyme, nitric oxide synthase (NOS) (*35*), an unusual member of the cytochrome P450 family, catalyzes the oxidation of the guanidine function of L-arginine to NO and citruline using NADPH and O_2 (path A in Scheme 10).

A. NO LIBERATION CATALYZED BY RU-PAC COMPLEXES

In the recent past, Marmion and Nolan have explored (*36*) the potential of the Ru^{III}-edta complex to act as model complex to catalyze the oxidation of L-arginine with H_2O_2 to produce NO and L-citrulline (path B in Scheme 10) in resemblance to NOS activity. Considering the rate of NO production from L-arginine governs the NO levels at specific sites, it is essential to have kinetic and mechanistic information on the $[Ru(edta)(H_2O)]^-$-catalyzed oxidation of L-arginine using H_2O_2 in order to develop the mechanistic understanding of this important biomimetic process. A detailed account of kinetic and spectral data on the $[Ru^{III}(pac)(H_2O)]$ complex acting as model complex to catalyze the oxidation of L-arginine with H_2O_2 to produce NO and L-citrulline (path B in Scheme 10) in resemblance to NOS activity has been reported recently (*37*). The first-order kinetic behavior of the system under turnover conditions supports the occurrence of catalysis (*37*). The kinetic results signifying the catalytic role

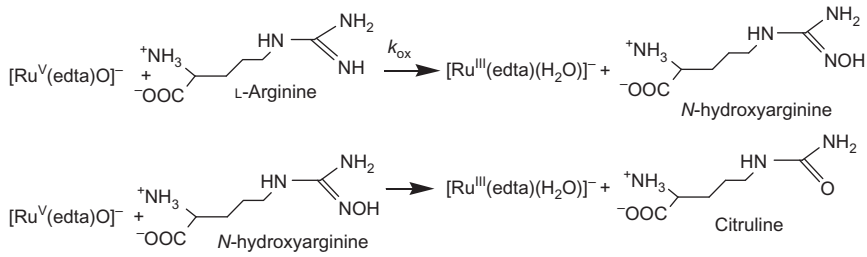

SCHEME 11. Mechanism of Ru-edta catalyzed oxidation of L-arginine. Published in *RSC Journal* (taken from Ref. (*41*)).

of $[Ru^{III}(edta)(OH)]^{2-}$ (at pH 7.0) were reportedly accounted for in terms of the mechanism proposed in Scheme 11.

In the above mechanism, the proposed rate-determining step is the oxidation of L-arginine by $[Ru^{V}(edta)(O)]^{-}$ to produce the *N*-hydroxylated species. In the subsequent step, the so generated *N*-hydroxyarginine undergoes further oxidation by $[Ru^{V}(edta)O]^{-}$ to produce citrulline and NO as reaction products. Measurements with a NO-sensitive electrode confirmed the formation of NO in the reaction system. Most likely, the liberated NO undergoes further oxidation by $[(edta)Ru^{V}(O)]^{-}$ formed in the catalytic cycle under turnover conditions to produce nitrate as final products. Analysis for nitrate using an ion-selective electrode confirmed the presence of nitrate in the resultant mixture at the end of the reaction.

In the preceding section, the possible role of $[Ru^{III}(edta)(H_2O)]^{-}$ for inhibition of PTP in its biological activity has been described in terms of a catalytic oxidation of the cysteine residue in the presence of intracellular H_2O_2 catalyzed by Ru^{III}-pac complexes. On considering NO synthesis to be a prerequisite for proper insulin sensitivity in insulin-target tissues, the results of the present study could be of significance in regard to the enhancement of insulin responsiveness by NO-mediated inactivation of PTP (*38*).

Hydroxyurea (HOU) shows many biological activities and has been considered for treatment of various cancers and sickle cell disease (SCD) (*39*). Sickle cell patients demonstrate *in vivo* NO formation during HOU therapy (*40*). HOU mediates some of its effect via NO production. Recently, it has been explored that Ru^{III}-pac complexes effectively catalyze the oxidation of HOU in the presence of H_2O_2, thus mimicking the action of peroxidase or catalase (Scheme 12) to produce NO in the reaction system (*41*).

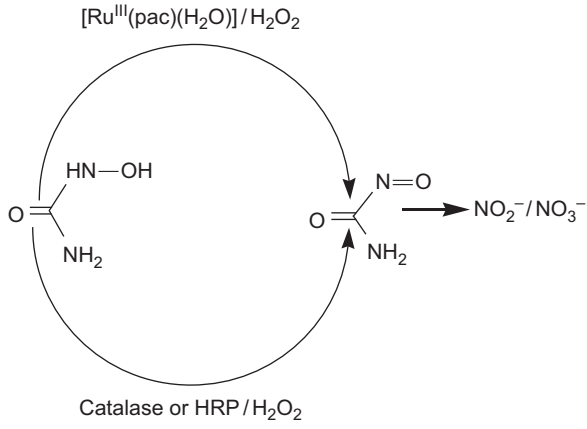

SCHEME 12. Published in *RSC Journal* (taken from Ref. (*41*)).

Measurements with a NO-sensitive electrode confirmed the release of free NO from HOU, though admittedly at a low concentration level. Most probably under the employed conditions, the liberated NO quickly and efficiently undergoes further oxidation by unreacted $[(edta)Ru^{V}(O)]^{-}$ to result in the formation of nitrite and nitrate as final products as detected by further analysis of the resultant mixture using ion chromatography. Formation of CO_2 in the reaction system was also evidenced by using a $Ba(OH)_2$ scrubber. The time course of the HOU oxidation exhibited typical pseudo-zero-order kinetic traces following the induction period (Fig. 7).

The pseudo-zero-order kinetics are consistent with a mechanism (Scheme 13) in which the reaction is initiated via Ru(IV) species formed in the reaction of Ru-pac and H_2O_2.

As suggested in part C of Scheme 13, the apparent concentration of Ru(IV)–OH species remains constant throughout the oxidation process for which depletion of Ru(V)–oxo species ($\lambda_{max}=$ 390 nm) exhibited pseudo-zero-order kinetics. The depletion in $[Ru^{V}(edta)(O)]^{-}$ is much slower in the presence of an excess of H_2O_2 and can be ascribed to the reformation of $[Ru^{V}(edta)(O)]^{-}$ from $[Ru^{III}(edta)(H_2O)]^{-}$ under such conditions. Moreover, the formation of $[Ru^{III}(edta)(OU)]^{2-}$ from the aqua complex is significantly slower than that of $[Ru^{V}(edta)(O)]^{-}$. For that reason, the $[Ru^{V}(edta)(O)]^{-}$ species shows an apparent stability but factually involves redox cycling of Ru between $[Ru^{V}(edta)(O)]^{-}$ and $[Ru^{III}(edta)(H_2O)]^{-}$. The above results point to the possibility of a catalytic pathway for the oxidation of HOU by $[Ru^{III}(edta)$

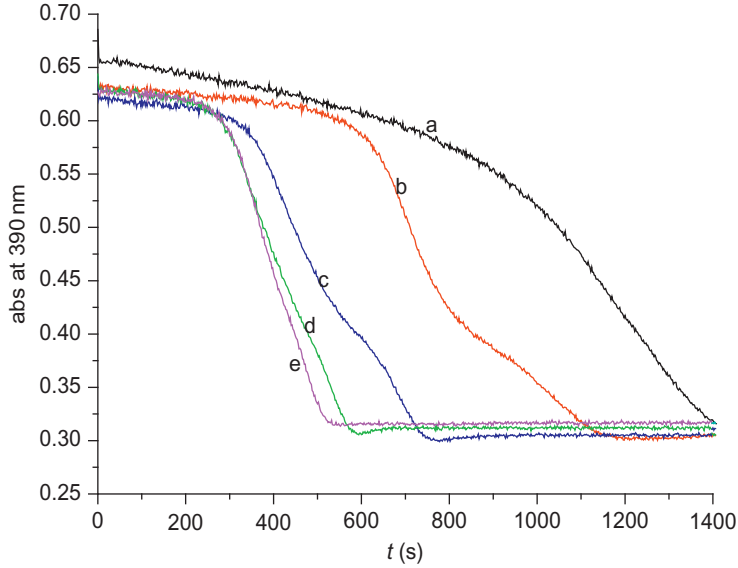

FIG. 7. Absorbance versus time traces at 390 nm for the $[Ru^{III}(edta)(H_2O)]^-$-mediated oxidation of HOU by H_2O_2 at pH 5.0 (acetate buffer), 25 °C, $[Ru^{III}] = 1.0 \times 10^{-4}$ M, $[H_2O_2] = 1.0 \times 10^{-4}$ M and [HOU] = (a) 1×10^{-3} M, (b) 2×10^{-3} M, (c) 4×10^{-3} M, (d) 5×10^{-3} M, and (e) 6×10^{-3} M. Published in *RSC Journal* (taken from Ref. (*41*)).

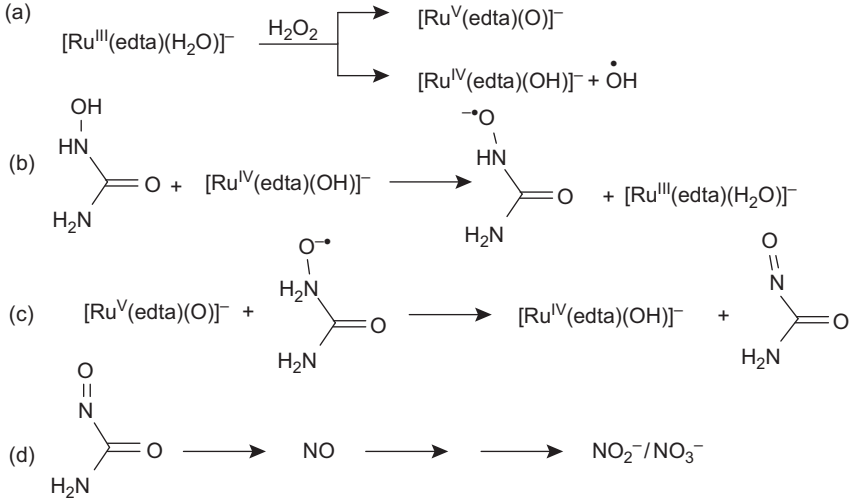

SCHEME 13. Mechanism of Ru-edta catalyzed oxidation of Hydroxyurea (HOU). Published in *RSC Journal* (taken from Ref. (*41*)).

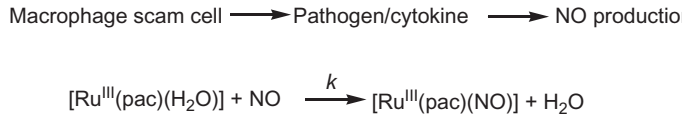

SCHEME 14. No scavenging by Ru-pac complexes.

$H_2O]^-$ in the presence of intracellular H_2O_2, as suggested in Scheme 13. The above results would be of importance not only in understanding its biological activity but may be of more general applicability in understanding the activities of Ru anticancer drugs under oxidative conditions.

B. Ru-pac Complexes as NO Scavenger

In the regulation of nitric oxide in the organism, the excess NO may be absorbed by a metal complex acting as a scavenger. Ru-pac complexes meet the basic requirements for effective NO scavenging: they undergo a rapid substitution reaction and form stable nitrosyl complexes (*42–46*). The Ru–NO bond is reasonably stable and persists through a variety of substitution and redox reactions. This allows the properties of the Ru-pac complexes to be finely tuned, so they can become effective NO scavengers (Scheme 14).

The thermodynamics and kinetics of the interaction of Ru-pac complexes with NO appear to be especially interesting from a medical, catalytic, and kinetic point of view. The Ru-pac complexes scavenge NO rapidly ($k \sim 10^4$–$10^7 M^{-1}s^{-1}$) to form $[Ru^{III}(pac)NO]$ through a straightforward aqua-substitution reaction (Scheme 14). Results of the kinetics of interaction of Ru-edta with NO aimed at understanding the mechanisms of drug action showed that the rate of the aqua substitution of $[Ru^{III}(edta)(H_2O/OH)]^{-/2-}$ with NO is very fast ($1.9–3.3 \times 10^7$ $M^{-1}s^{-1}$ at 7.3°C) in the pH range 6.5–8.0 (*42*). However, at pH 8.0, the higher value for the rate of aqua substitution (3.3×10^7 $M^{-1}s^{-1}$ at 7.3°C) than at pH 6.5 ($2.2 \times 10^7 M^{-1}s^{-1}$ at 7.5°C) does not agree with the pH dependence of the rate constants for the aqua-substitution reaction of the Ru-edta complex with other entering nucleophiles (*15*). This apparently anomalous observation (*42*) could probably be accounted for in terms of the pK_a value for the acid dissociation of coordinated H_2O in $[Ru^{III}(edta)(H_2O)]^-$, which is higher at lower temperature (7.3°C) than the value of 7.6 reported at 25°C (*3*). As a result, the concentration of the most labile $[Ru^{III}(edta)(H_2O)]^-$ species at low temperature (7.3°C) would be even more at pH > 7.6. A

detailed account of the thermodynamics and kinetics of the reaction of Ru-edta complexes with NO was reported by the van Eldik group (*43*). The results of FTIR and ^{15}N NMR spectroscopic studies clearly afforded evidence for the NO^+ character of NO coordinated to the Ru^{III}-edta complex, such that the product can be formulated as $[Ru^{II}(edta)(NO^+)]^-$. The value of the overall equilibrium constant (K_{NO}) determined from UV–Vis spectroscopic and electrochemical methods is $9.1\times10^7 M^{-1}$ at 25°C and pH 5.0. The influence of buffer components (acetate buffer) became clear because the obtained rate constant ($1\times10^5 M^{-1}s^{-1}$ at 8°C and pH 5.0) was two orders of magnitude lower than that reported by Slade *et al*. (*42*) due to the displacement of labile-coordinated water by the more inert acetate ion. An attempt to measure the rate of NO binding directly using laser flash photolysis was unsuccessful although the formation of a di-substituted $[Ru^{II}(edta)(NO^+)(NO_2^-)]^{2-}$ complex was detected by ^{15}N NMR spectroscopy. Laser flash photolysis of this complex was complicated by the number of chemical reaction steps involved.

The preparation, characterization, kinetics, and biochemical activity of various species of Ru-pac complexes (pac=edta; dtpa) have subsequently been reported (*44,45*), reaffirming the NO scavenging ability of Ru-pac complexes and reporting similar rate constant data as Slade *et al*. (*42*) for the Ru-edta complex. However, the binding of NO to Ru-dtpa was significantly slower ($3\times10^5 M^{-1}s^{-1}$ at 20°C and pH 7.4) than that observed for the Ru-edta complex (*42*). Stopped-flow kinetic studies revealed the following reactivity order of Ru-pac complexes for NO: $[Ru^{III}(edta)(H_2O)]^-$ (**1**)$\gg$[[Ru(hedtra)(H_2O)] (**2**)>Ru(medtra)(H_2O)] (**3**) (*46*). The measured second-order rate constants at 15°C and pH 7.2 (phosphate buffer) of 6×10^4 and $3\times10^3 M^{-1}s^{-1}$ for **2** and **3**, respectively, (*46*) are three to four orders of magnitudes lower than that for the reaction between **1** and NO. *In vitro* studies have shown that Ru-edta complexes are successful in scavenging NO in biological systems and suggest that they could play a role in novel therapeutic strategies aimed at alleviating NO-mediated disease states (*47*). However, results from the NO scavenging studies on nitrite production between treated and untreated murine macrophage cells revealed that despite being less kinetically reactive toward NO, the [Ru(medtra)(H_2O)] complex exhibited the highest NO scavenging ability and lowest toxicity of complexes **1**–**3**. It may be envisaged that the lower efficiency observed in NO scavenging for **1** could be associated with its deactivation through the binding of cellular thio molecules, since **1** binds RSH more readily than **2** and **3** (*46*). The role of NO in angiogenesis and tumor progression

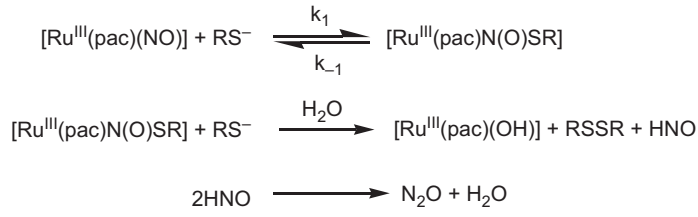

SCHEME 15. Mechanism of the reaction of [Ru(pac)(NO)] complexes with RSH. Published in ACS journal (taken from Ref. (*52*))

was also reported recently (*48–50*). The results of these studies suggest that increased levels of NO correlate with tumor growth and spread in human cancers. Drugs that interfere in the NOS pathway could thus be useful in angiogenesis-dependent tumors, and the Ru^{III}-edta complex was found to be effective in this regard (*50*). The key steps of angiogenesis, endothelial cell proliferation and migration stimulated by vascular endothelial growth factor (VEGF) or NO donor drugs were reportedly blocked by the Ru^{III}-edta complex (*50*).

The reactivity of metal nitrosyl complexes (*51*) with thiols is of particular concern in the mobilization of NO to make it accessible for the vasodilation process. Very recently, it has been reported (*52*) that the S-atom of cysteine reacts to bind the N-atom of the nitrosyl complex of Ru-edta to form a 1:1 intermediate species. Stopped-flow kinetic studies revealed the formation of a transient species, whose rate of formation was found to be first order with respect both [Ru^{III}(pac)(NO)] and RSH. The values of rate constants (k_1) were found to be in the range $(0.2–5)\times 10^4 M^{-1}s^{-1}$ at 25°C. Considering the spectral features and kinetic behavior of various [Ru^{III}(pac)(SR^-)] and [Ru^{III}(pac)NO] species as described in the preceding sections, and analysis for the products of the above reaction (N_2O), the following mechanism (Scheme 15) for the redox reactions involving electron transfer from thiols to coordinated NO, that results in the formation of disulfide (RSSR) and N_2O, has been proposed for the reaction of [Ru^{III}(pac)(NO)] with thiols (RSH).

The above observation is of significance, since it implies the catalytic reduction of NO to N_2O in a biological system. Moreover, the above results imply the catalytic viability of Ru-pac complexes toward NO scavenging. Decomposition of [Ru^{III}(pac)(NO)] in the presence of cellular thio-proteins results in the formation of N_2O and [Ru^{III}(pac)(H_2O)] that returns to the system and reacts again with NO (kinetically preferred over RSH) to reform [Ru^{III}(pac)NO] in the reaction system.

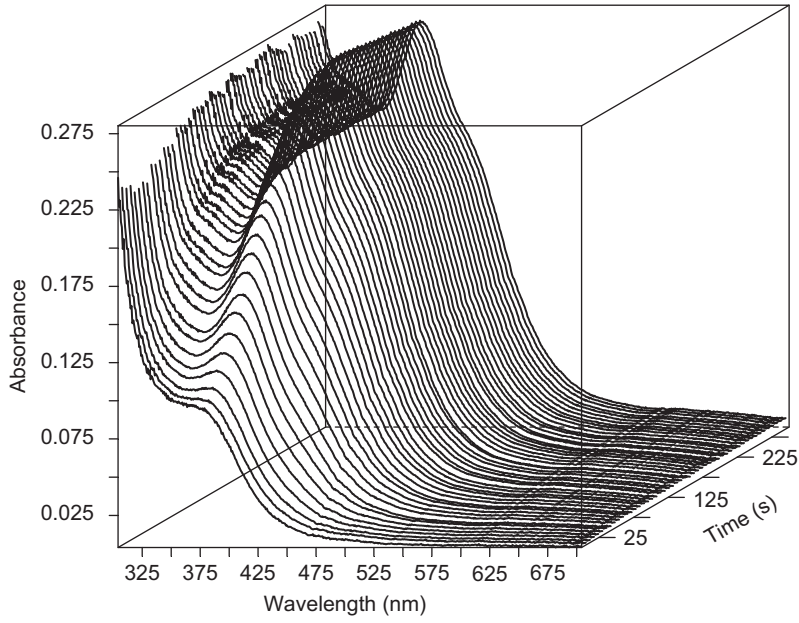

FIG. 8. Spectral changes that occur during the reaction of **1** (1.0×10^{-4}M) with *t*-BuOOH (2.5×10^{-3}M) in water at 25°C and pH 6.2 (0.2M acetate buffer). Published in *RSC Journal* (taken from Ref. (*54*)).

VII. Reaction of Ru^{III}-pac Complexes with Biologically Important Oxidants and Reductants

The reactions of Ru^{III}-pac complexes with biologically important oxidants and reductants are reviewed here to illustrate the most probable mechanism of the interaction between the $[Ru^{III}(pac)H_2O]$ complexes and redox-active cellular species, viz. thio-proteins and H_2O_2. The reactivity of the $[Ru^{III}(edta)(H_2O)]^-$ complex with various oxygen atom donors (ROOH= H_2O_2, ^{t}BuOOH, HSO_5^-) that leads to the formation of the active intermediate $[Ru^{V}(edta)(O)]^-/[Ru^{IV}(edta)OH]^-$ species can be followed kinetically as a function of [ROOH] and temperature at a fixed pH of 5.1 using stopped-flow and rapid scan techniques, as reported recently (*53,54*).

In Fig. 8, the UV–Vis spectral changes that occurred upon mixing aqueous solutions of **1** and H_2O_2 in the chamber of the stopped-flow instrument equipped with a rapid scan spectroscopic attachment are reported as a function of time. The final spectrum of the reaction solution is in good agreement with the spectrum of $[Ru^{V}(edta)O)]^-$ ($\lambda_{max}=391$nm, $\epsilon_{max}=8000\,M^{-1}cm^{-1}$)

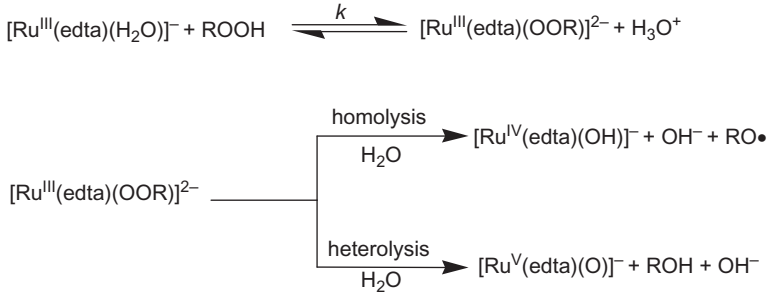

SCHEME 16. Mechanism of the oxidation of Ru-edta complex with ROOH. Published in *RSC Journal* (taken from Ref. (*54*)).

(*55*). The reaction of $[Ru^{III}(edta)(H_2O)]$ with ROOH was found be first order with respect to [Ru^{III}-edta] and [ROOH]. A mechanism (Scheme 16) that involves the rapid formation of a $[Ru^{III}(edta)(OOR)]$ intermediate, followed by homolytic cleavage of the O—O bond leading to the formation of $[Ru^{IV}(edta)(OH)]$ or heterolytic cleavage to form $[Ru^{V}(edta)O]$, is proposed.

Since $[Ru^{V}(edta)(O)]^{-}$ was obtained as predominant product when ROOH=^{t}BuOOH and $KHSO_5$, the common suggested mechanism involves heterolytic cleavage of the O—O bond. The overall second-order rate constants, expressed as kK, that is, the product of the equilibrium constant K for the formation of $[Ru^{III}(edta)(OOR)]^{2-}$ (R=H, ^{t}Bu, and SO_3^{-}) and the rate constant k for the subsequent heterolytic cleavage of the O—O bond to form $[Ru^{V}(edta)(O)]^{-}$, have values that lie in the range 26.5 $M^{-1}s^{-1}$ (for H_2O_2), 1.45 $M^{-1}s^{-1}$ (for ^{t}BuOOH), and 7.0 $M^{-1}s^{-1}$ (for $KHSO_5$) at 25°C. Since the overall reaction is a two step process as outlined in Scheme 16, the ability to form $[Ru^{III}(edta)(OOR)]$ (R=H, ^{t}Bu, and HSO_3^{-}) in the first reaction step through ligand substitution of $[Ru^{III}(edta)(H_2O)]$ by ROOH will partially govern the efficiency of the precursor oxidants (ROOH) to form $[(edta)Ru^{V}(=O)]^{-}$ as the reactive oxidizing species in solution. Based on the pK_a values of the ROOH oxidants, the basicity of the ROOH species is expected to follow the order $HSO_5^{-} < H_2O_2 <$ ^{t}BuOOH, which should also be reflected in the equilibrium constant K for the formation of the $[Ru^{III}(edta)(OOR)]$ intermediates. However, according to the experimental observations, K is much larger for H_2O_2 and $KHSO_5$ than for ^{t}BuOOH, which indicates that the basicity of the ROOH species seems to be less important than the steric hindrance caused by the *tert*-butyl group attached to the hydroperoxide fragment. On the other hand, the formation of $[Ru^{V}(edta)(O)]^{-}$ from $[Ru^{III}(edta)$

$(OOR)]^{2-}$ will depend on the ability of this complex to undergo heterolytic cleavage of the O—O bond expressed by the rate constant k, which in turn should correlate with the reduction potential of the different hydroperoxides under consideration, that is, ^{t}BuOOH ($E^0 = 1.15$V) (*5*) $\ll H_2O_2$ ($E^0 = 1.78$V) $\leq HSO_5^-$ ($E^0 = 1.82$ V) (*6*). From a combination of the separate trends expected for k and K, and a comparison of the trend observed in the values of kK at 25°C, it follows that in addition to the electronic factors considered here, steric hindrance on ^{t}BuOOH and HSO_5^- as compared to H_2O_2 should further account for the fact that kK is significantly smaller for ^{t}BuOOH and HSO_5^- than for H_2O_2.

The findings of this study taken together with those for the reaction of $[Ru^{III}(edta)(H_2O)]$ with H_2O_2 strongly suggest that oxo-transfer from the precursor oxidant ROOH (H_2O_2, ^{t}BuOOH, and $KHSO_5$) to $[Ru^{III}(edta)(H_2O)]$ that results in the formation of the catalytically active $[Ru^{V}(edta)(O)]$ species should proceed through the formation of $[Ru^{III}(edta)(OOR)]$ intermediates (R = H, ^{t}Bu, and SO_3^-) in a rapid pre-equilibrium step, which subsequently undergoes rate-controlling heterolytic cleavage of the O—O bond to produce $[Ru^{V}(edta)(O)]^-$ as a major product (80–90%). However, in the case of $[Ru^{III}(edta)(OOH)]^{2-}$ formed in the reaction of $[Ru^{III}(edta)(H_2O)]$ with H_2O_2, the subsequent reaction involves both parallel heterolytic and homolytic cleavage to produce $[Ru^{V}(edta)(O)]^-$ and $[Ru^{IV}(edta)(OH)]^-$ in the ratio of approximately 1:1. Thus, the ^{t}Bu and SO_3^- substituents in $[Ru^{III}(edta)(OOR)]^{2-}$ cause O—O bond cleavage to clearly favor heterolysis above homolysis. The results of the reported studies demonstrate the capability to tune the fundamental nature of the O—O bond cleavage process and underline the advantage of studying such Ru-pac systems in much detail as reported in this study (*54*). The catalytic ability of Ru-pac complexes toward oxidation of a myriad of organic substrates in the presence of oxygen atom donors (Scheme 17), and the mechanistic aspects of the catalytic process in resemblance of the enzymatic oxidation (cytochrome P450 monoxygenase) were reviewed before (*15*).

The results of the reported studies on Ru-pac complexes seem to be of great significant toward developing Ru-pac-based agents for oxidative cleavage of DNA and artificial nuclease in DNA footprinting experiments. In fact, the DNA cleavage activity of Ru-edta in the presence of primary oxidants, ROOH (H_2O_2, $KHSO_5$), was explored very recently (*56*). DNA cleavage efficiency of Ru-edta was monitored by observing the conversion of supercoiled (SC) plasmid DNA to the circular nicked form, DNA (nicked). Ru-edta showed an appreciable conversion of SC pBluescript (SKþ) DNA to nicked circular DNA (nicked) upon

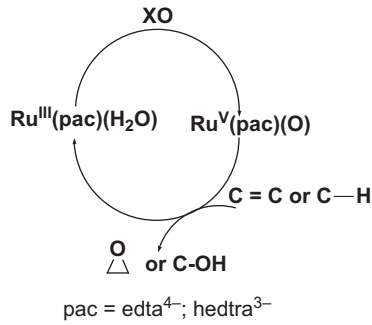

SCHEME 17. Ru-pac complexes catalyzed oxo-functionalization of C = C or C—H bond.

prolonged incubation in the presence of ROOH, and the efficiency of DNA cleavage increases with increasing concentration of PO (*56*). Considering that the oxidation of Ru-edta by ROOH leads to formation of high-valent Ru(V)-oxo species (*54,55*), which are known to oxidize the C—H bond in saturated hydrocarbons (*56*), it has been presumed that a mechanism involving high-valence $[Ru^{V}(edta)(O)]^{-}$ species is operative in the present case. Almost identical cleavage patterns reportedly observed for both Ru-edta/$KHSO_5$ and Ru-edta/H_2O_2 plausibly support the above mechanistic arguments (*56*).

In the presence of biologically significant electron donors, the $[Ru^{III}(edta)(pz)]^{-}$ (pz=pyrazine) complex undergoes reduction through an outer-sphere electron-transfer process, resulting in the formation of the corresponding Ru(II) complex (*57,58*). Electron-transfer reactions of the Ru^{III}-edta complex (*57,58*) resembling to ascorbate oxidase (*59*), catecholase (*60*), and sulfite oxidase (*61*) are reported in the literature. The reduction of $[Ru^{III}(edta)(pz)]^{-}$ with different electron donors D (D=L-ascorbic acid, catechol, sulfite) has been investigated spectrophotometrically and kinetically in aqueous solution. In all cases, the rate of reduction was found to be first order in both the Ru^{III}-edta complex and D, and dehydroascorbic acid (*57*), quinine (*57*), and sulfate (*58*) were the respective reaction products. The following mechanism involving two one-electron-transfer steps has been proposed (Scheme 18) for the reduction of $[Ru^{III}(edta)(pyz)]^{-}$ to $[Ru^{II}(edta)(pyz)]^{2-}$ in the presence of the electron donors, D.

The reported rate data and activation parameters, viz. $k_r=450\ M^{-1}s^{-1}$ at 25°C, pH 6.0, $\Delta H^{\neq}=38\,kJ\,mol^{-1}$, and $\Delta S^{\neq}=-122\,JK^{-1}\,mol^{-1}$ observed for D=ascorbic acid (*57*); $k_r=570\,M^{-1}s^{-1}$ at 30°C, pH 6.0 observed for D=catechol (*57*); and $k_r=23\,M^{-1}s^{-1}$ at 25°C, pH 8.0, $\Delta H^{\neq}=43\,kJ\,mol^{-1}$, and $\Delta S^{\neq}=-73\,JK^{-1}mol^{-1}$

$$[Ru^{III}(edta)(pz)]^- + D \xrightarrow{k_r} [Ru^{II}(edta)(pz)]^{2-} + D^{+\bullet}$$

$$[Ru^{III}(edta)(pz)]^{2-} + D^{+\bullet} \xrightarrow{\text{fast}} [Ru^{II}(edta)(pz)]^{2-} + D^{2+}$$

SCHEME 18. Mechanism of reduction of $[Ru^{III}(edta)(pz)]^-$ with electron donors (D).

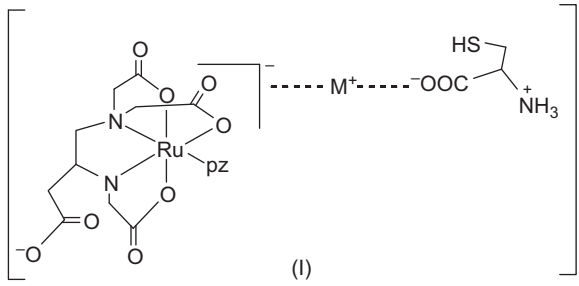

SCHEME 19. Formation of triple-ion intermediate in the reduction of $[Ru^{III}(edta)(pz)]^-$ with RSH. Published in *RSC Journal* (taken from Ref. (*62*)).

observed for D=sulfite (*58*), are consistent with the proposed mechanism for the reduction of $[Ru^{III}(edta)(pz)]^-$ (Scheme 18) involving outer-sphere electron transfer between the reaction partners.

In a very recent paper (*62*), the kinetics of reduction of $[Ru^{III}(edta)pz]^-$ by thio-amino acids (RSH=cysteine, glutathione) resulting in the formation of a red colored $[Ru^{II}(edta)pz]^{2-}$ species (λ_{max}=462nm) and RSSR (oxidation product of RSH) has been reported. The time course of the reaction was followed spectrophotometrically using both conventional mixing and stopped-flow techniques as a function of [RSH], pH, temperature, and pressure. Alkali metal ions were found to have a positive influence ($K^+ > Na^+ > Li^+$) on the reaction rate. The effect of alkali cations has reportedly been attributed to triple-ion formation through an alkali cation bridging between the two negatively charged reactants (Scheme 19), thereby facilitating the electron-transfer process.

It has been assumed that the cation (M^+) acts as a bridge or as a means in bringing the negatively charged $[Ru^{III}(edta)pz]^-$ and zwitterionic RSH (through its $-COO^-$ group) close enough that leads to the formation of **I**, in which electron transfer takes place in an outer-sphere manner. On the basis of the size of the hydrated

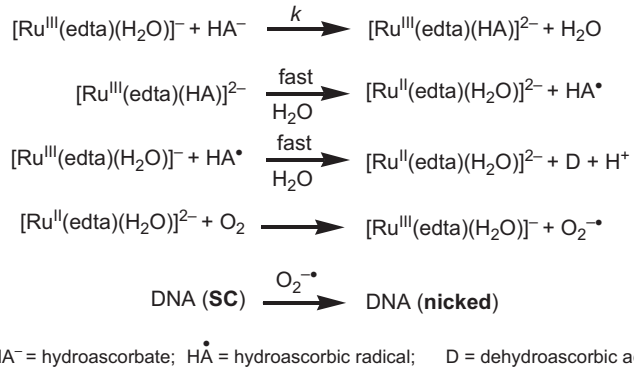

SCHEME 20. Mechanism of DNA cleavage mediated by Ru-edta complex.

cations, which follow the order: $Li^+ > Na^+ > K^+$, the K^+ would be more effective than Na^+ or Li^+ in bringing the reacting species close enough, and thus to facilitate the electron-transfer process. Kinetic data and activation parameters, viz. $k_r = 5.82\,M^{-1}s^{-1}$ at 25°C, pH 5.1, $\Delta H^{\neq} = 56\,kJ\,mol^{-1}$, $\Delta S^{\neq} = -44\,JK^{-1}mol^{-1}$, and $\Delta V^{\neq} = 8.1\,cm^3\,mol^{-1}$ observed for RSH = cysteine (*61*); $k_r = 3.03\,M^{-1}s^{-1}$ at 25°C, pH 5.1, $\Delta H^{\neq} = 55\,kJ\,mol^{-1}$, $\Delta S^{\neq} = -56\,JK^{-1}mol^{-1}$, and $\Delta V^{\neq} = 2.4\,cm^3\,mol^{-1}$ observed for RSH= glutathione (*62*), support the operation of an outer-sphere electron-transfer mechanism in the oxidation of RSH to RSSR by the $[Ru^{III}(edta)pz]^-$ complex. Tumor cell metabolism favors the presence of Ru(II) relative to Ru(III), thus increasing the selective tumor toxicity (*63*). In this context, the chemistry of the thiol–disulfide conversion is of immense importance. Thus, the reported reactions of the biologically active $[Ru^{III}(edta)pz]^-$ complex with different RSHs provide a mechanistic basis for RSH oxidation which could be of significance in understanding the activities of Ru-based antitumor drugs.

The results of the above studies on the reduction of Ru^{III}-edta complexes seem to have direct implications for the results of DNA cleavage studies using Ru^{III}-edta/ascorbate/O_2 system (*56*). The cleavage of SC plasmid DNA to nicked circular DNA (nicked) has reportedly been achieved using the $[Ru^{III}(edta)H_2O]^-$ complex, sodium ascorbate, and molecular oxygen (O_2), and the cleavage efficiency increased with the increasing ascorbate concentration (*56*). The electron-transfer process as proposed in Scheme 20 is possibly operative in the $[Ru^{III}(edta)H_2O]^-$-mediated cleavage of SC plasmid DNA.

The proposed mechanism (Scheme 20) suggested (*56*) for DNA cleavage involves rapid reduction of $[Ru^{III}(edta)H_2O]^-$ by L-

ascorbate (on the stopped-flow timescale) to generate the corresponding Ru(II) complex. The oxidation potential of Ru^{II}-edta complexes lies in the range of −0.29 to −0.15V (vs. SCE) (*15*). Therefore, reoxidation of such Ru(II) species by molecular oxygen (O_2) is thermodynamically favorable and perhaps proceeds in resemblance to Fenton's chemistry as proposed in Scheme 20 involving an inner-sphere oxidation of the metal ion leading to the formation of the corresponding Ru(III) complex and superoxide radical. The superoxide radical ($O_2^{\bullet -}$) though indiscriminative in its nature of oxidative attack presumably causes single strand scission by attacking the deoxyribose unit of DNA to lead to sugar fragmentation, followed by base release and DNA cleavage (*64,65*).

VIII. Concluding Remarks

The purpose of this review was to focus on various intriguing kinetic and mechanistic aspects of Ru-pac complexes concerning their potential in biological applications. The majority of the work discussed here has only appeared in the recent past, and we have primarily reviewed the kinetics and mechanisms of the interaction of Ru-pac complexes with the molecules of biological importance. The ability of Ru-pac complexes to perform oxidative cleavage of DNA appears to be useful for developing Ru-pac-based DNA-cleaving agents. Kinetic evidence for the notion that the high-valent Ru(V)-oxo intermediate in oxidative DNA cleavage is provided by demonstration of its capability to activate O—O bond scission in ROOH by the Ru^{III}-pac complex.

The ability of Ru-pac complexes to bind to DNA constituents at faster rate than to sulfur-containing ligands signifies the possibility of a new family of Ru-pac-based anticancer drugs with low toxicity, but high efficiency. However, experimental testing of this hypothesis is still needed.

The rate of release of NO is important for antihypertensive agents, whereas the rate of NO scavenging is crucial in treating the toxic shock syndrome in which white blood cells generate a dangerously high level of NO in the bloodstream. The [Ru(pac)(NO)] complexes offer a number of features as NO carriers or scavengers. Mechanistic details of Ru^{III}-pac-catalyzed NO production through the oxidation of HOU and L-arginine by H_2O_2 have been illustrated in this review, whereas rapid NO binding to Ru^{III}-pac complexes via straightforward aqua substitution leading to the formation of [Ru(pac)NO] complexes provides a

basis for anti-inflammatory activity. Further, decomposition of [Ru(pac)NO] complexes in the presence of thiols and nitrozation of thiols coordinated to the ruthenium center are other notable findings of immense biochemical importance *per se*. Given that bound NO is very inert toward dissociation in [Ru^{III}(pac)NO], the results of kinetic investigations afforded mechanistic insights into the role of thiolates toward mobilization of NO to the enzymatic targets for triggering the vasodilation process.

The results of kinetic and mechanistic studies of the reaction of [Ru^{III}(pac)(H_2O)] complexes with biomolecules containing a thiol group, leading to the formation of S-coordinated [Ru^{III}(pac)(RS^-)] complexes, and Ru-pac-mediated thiol to disulfide conversion through outer-sphere electron transfer, have afforded mechanistic insight in understanding the role of the activity of Ru^{III}(pac)(H_2O)] complexes in protease (CP and PTP) inhibition. The results could lead to the recognition of Ru-pac complexes as better biomimetic models for studies of the *in vivo* activities of Ru complexes in clinical trials than the parent pro-drugs and find more general applicability.

The reported results taken together, illuminating the mechanistic details of the Ru-pac complex mediated bioinorganic processes, could significantly contribute toward the development of new ruthenium-based metallo-drugs with a lower degree of inactivation and toxic side effects.

Acknowledgments

This work was supported by a research grant (No. SR/S5/BC-15/2006) received from the Department of Science and Technology, Government of India. D. C. is thankful to Prof. Goutam Biswas, Director, CMERI, Durgapur, India, for his encouragement, and to the project members who contributed to the results cited in this review. The authors gratefully acknowledge financial support from the Deutsche Forschungsgemeinschaft and the CSIR-DAAD Exchange Program.

References

1. Matsubara, T.; Creutz, C. *J. Am. Chem. Soc.* **1978,** *100*, 6255–6257.
2. Yoshino, Y.; Uehiro, T.; Saito, M. *Bull. Chem. Soc. Jpn.* **1979,** *52*, 1060–1062.
3. Matsubara, T.; Creutz, C. *Inorg. Chem.* **1979,** *18*, 1956–1966.
4. Shimizu, K.; Matsubara, T.; Sato, G. P. *Bull. Chem. Soc. Jpn.* **1974,** *47*, 1651–1656.

5. Shimizu, K. *Bull. Chem. Soc. Jpn.* **1977,** *50*, 2921–2926.
6. Oyama, N.; Anson, F. C. *J. Electroanal. Interlhcial. Electrochem.* **1978,** *88*, 289–397.
7. Taqui Khan, M. M.; Bajaj, H. C.; Shirin, Z.; Venkatasubramanian, K. *Indian J. Chem. A* **1992,** *31A*, 303–307.
8. Taqui Khan, M. M.; Bajaj, H. C.; Shirin, Z.; Venkatasubramanian, K. *Polyhedron* **1992,** *11*, 1059–1066.
9. Ogino, H.; Shimura, M. *Adv. Inorg. Bioinorg. Mech.* **1986,** *4*, 107–135.
10. Ogino, H.; Katsuyama, T.; Ito, S. *Bull. Chem. Soc. Jpn.* **1990,** *63*, 1370–1373.
11. Bajaj, H. C.; van Eldik, R. *Inorg. Chem.* **1988,** *27*, 4052–4055.
12. Bajaj, H. C.; van Eldik, R. *Inorg. Chem.* **1989,** *28*, 1980–1983.
13. Bajaj, H. C.; van Eldik, R. *Inorg. Chem.* **1990,** *29*, 2855–2858.
14. Chatterjee, D.; Bajaj, H. C. *J. Chem. Soc. Dalton Trans.* **1993,** 1065–1067.
15. Chatterjee, D. *Coord. Chem. Rev.* **1998,** *16*, 273–293 and references cited therein.
16. Vilaplana, S. R.; Basallote, M. G.; Ruiz-Valero, C.; Gutierrez, E.; Gonzalez-Vilchez, F. *J. Chem. Soc. Chem. Commun.* **1991,** 100–101.
17. Vilaplana, R. A.; González-Vílchez, F.; Gutierrez-Puebla, E.; Ruiz-Valero, C. *Inorg. Chim. Acta* **1994,** *224*, 15–18.
18. Gallori, E.; Vettori, C.; Alessio, E.; Gonzalez-Vilchez, F.; Vilapana, R. A.; Orioli, P.; Casini, A.; Messori, L. *Arch. Biochem. Biophys.* **2000,** *376*, 156–162.
19. Chatterjee, D.; Mitra, A.; De, G. S. *Platinum Met. Rev.* **2006,** *50*, 1–12.
20. Chatterjee, D.; Sengupta, A.; Mitra, A.; Basak, S. *Inorg. Chim. Acta* **2005,** *358*, 2954–2959.
21. Chatterjee, D.; Bajaj, H. C.; Das, A. *J. Chem. Soc. Dalton Trans.* **1995,** 2497–2501.
22. Chatterjee, D.; Ward, M. S.; Shepherd, R. E. *Inorg. Chim. Acta* **1999,** *285*, 170–177.
23. Chatterjee, D.; Mitra, A.; Hamza, M. S. A.; van Eldik, R. *J. Chem. Soc. Dalton Trans.* **2002,** 962–965.
24. Povse, V. G.; Olabe, J. A. *Trans. Met. Chem.* **1998,** *23*, 657–662.
25. Chatterjee, D.; Hamza, M. S. A.; Shoukry, M. M.; Mitra, A.; Deshmukh, S.; van Eldik, R. *Dalton Trans.* **2003,** 203–209.
26. Chatterjee, D.; Sengupta, A.; Mitra, A.; Basak, S.; Bhattacharya, R.; Bhattacharyya, D. *Inorg. Chim. Acta* **2005,** *358*, 2960–2965.
27. Chatterjee, D. *Indian J. Chem. A* **2011,** *50A*, 38–40.
28. Chatterjee, D.; Mitra, A.; Levina, A.; Lay, P. A. *Chem. Commun.* **2008,** 2864–2866.
29. Andersen, J. N.; Jansen, P. G.; Echwald, S. M.; Mortensen, O. H.; Fukada, T.; Del Vecchio, R.; Tonks, N. K.; Møller, N. P. *FASEB J.* **2004,** *18*, 8–30.
30. Zhang, Z. Y. *Biochim. Biophys. Acta* **2005,** *1754*, 100–107 and references cited therein.
31. Huyer, G.; Liu, S.; Kelly, J.; Moffat, J.; Payette, P.; Kennedy, B.; Tsaprailis, G.; Gresser, M. J.; Ramachandran, C. *J. Biol. Chem.* **1997,** *272*, 843–851.
32. Calver, A.; Collier, J.; Vallance, P. *Exp. Physiol.* **1993,** *78*, 303–326.
33. Ignarro, L. J. *Hypertension* **1990,** *16*, 477–483.
34. Snyder, S. H.; Bredt, D. S. *Sci. Am.* **1992,** *266*, 68–71.
35. Shibuki, K.; Okada, D. *Nature* **1991,** *349*, 326–328.

36. Marmion, C. J.; Murphy, T.; Nolan, K. B. *Chem. Commun.* **2001,** 1870–1871.
37. Chatterjee, D.; Ghosh, S.; Pal, U. *Dalton Trans.* **2011,** *40*, 683–685.
38. Giroud, C.; Moreau, M.; Mattioli, T. A.; Balland, V.; Boucher, J.-L.; Xu-Li, Y.; Stuehr, D. J.; Santolini, J. *J. Biol. Chem.* **2010,** *285*, 7919–7928.
39. Stevens, M. R. *J. Biol. Regul. Homeost. Agents* **1999,** *13*, 172–175.
40. Nahavandi, M.; Tavakkoli, F.; Wyche, M. Q.; Perlin, E.; Winter, W. P.; Castro, O. *Br. J. Haematol.* **2002,** *119*, 855–857.
41. Chatterjee, D.; Nayak, K. A.; Ember, E.; van Eldik, R. *Dalton Trans.* **2010,** *39*, 1695–1698.
42. Davis, N. A.; Wilson, M. T.; Slade, E.; Fricker, S. P.; Murrer, B. A.; Powell, N. A.; Henderson, G. R. *Chem. Commun.* **1997,** 47–48.
43. Wanat, A.; Schneppensieper, T.; Karocki, A.; Stochel, G.; van Eldik, R. *J. Chem. Soc. Dalton Trans.* **2002,** 941–950.
44. Cameron, B. R.; Darkes, M. G.; Yee, H.; Olsen, M.; Fricker, S. P.; Skerlj, R. T.; Bridger, G. L.; Davis, N. A.; Wilson, M. T.; Rose, D. J.; Zubieta, J. *Inorg. Chem.* **2003,** *42*, 1868–1876.
45. Storr, T.; Cameron, B. R.; Gossage, R. A.; Yee, H.; Skerlj, R. T.; Darkes, M. C.; Fricker, S. P.; Bridger, G. J.; Davis, N. A.; Wilson, M. T.; Maresca, K. P.; Zubieta, J. *Eur. J. Inorg. Chem.* **2005,** 2685–2697.
46. Chatterjee, D.; Mitra, A.; Sengupta, A.; Saha, P.; Chatterjee, M. *Inorg. Chim. Acta* **2006,** *359*, 2285–2290.
47. Fricker, S. P.; Slade, E.; Powell, N. A.; Vaughan, O. J.; Henderson, G. R.; Murrer, B. A.; Megson, I. L.; Bisland, S. K.; Flitney, F. W. *Br. J. Pharmacol.* **1997,** *122*, 1441–1449.
48. Thomsen, L. L.; Miles, D. W. *Cancer Metastasis Rev.* **1998,** *17*, 107–118.
49. Jadeski, L. C.; Hum, K. O.; Chakraborty, C.; Lala, P. K. *Int. J. Cancer* **2000,** *86*, 30–39.
50. Morbidelli, L.; Donnini, S.; Filippi, S.; Messori, L.; Piccioli, F.; Sava, G.; Ziche, M. *Br. J. Cancer* **2003,** *88*, 1484–1491.
51. Wang, G. P.; Xian, M.; Tang, X.; Wen, Z.; Cai, T.; Janczuk, A. J. *Chem. Rev.* **2002,** *102*, 1091–1134.
52. Roncaroli, F.; Olabe, J. A. *Inorg. Chem.* **2005,** *44*, 4719–4727.
53. Chatterjee, D.; Mitra, A.; van Eldik, R. *Dalton Trans.* **2007,** 943–948.
54. Chatterjee, D.; Sikdar, A.; Patnam, V. R.; Theodoridis, A.; van Eldik, R. *Dalton Trans.* **2008,** 3851–3856.
55. Taqui Khan, M. M.; Chatterjee, D.; Merchant, R. R.; Paul, P.; Abdi, S. H. R.; Siddiqui, M. R. H.; Srinivas, D.; Moiz, M. A.; Bhadbhade, M. M.; Venkatasubramaniun, K. *Inorg. Chem.* **1992,** *31*, 2711–2718.
56. Chatterjee, D.; Mitra, A. *J. Coord. Chem.* **2009,** *62*, 1719–1724.
57. Chatterjee, D. *Dalton Trans.* **1996,** 4389–4392.
58. Chatterjee, D. *Trans. Met. Chem.* **1996,** *25*, 227–230.
59. Boyer, P. D., Lardy, H., Myrback, K. (Eds.), The Enzymes, (2nd edn.), Vol. 8. Academic Press: New York, **1963,** pp. 297–311.
60. Wilcox, D. E.; Porras, A. G.; Hwang, Y. T.; Lerch, K.; Winkler, M. E.; Solomon, E. I. *J. Am. Chem. Soc.* **1985,** *107*, 4015–4027.
61. Sullivan, E. P.; Hazzard, J. T.; Jr., Tollin, G.; Enemark, J. H. *J. Am. Chem. Soc.* **1992,** *114*, 9662–9663.
62. Chatterjee, D.; Pal, U.; Ghosh, S.; van Eldik, R. *Dalton Trans.* **2011,** *40*, 1302–1306.

63. Morris, R. E.; Aird, R. E.; Murdoch, P.d.S.; Chen, H.; Cummings, J.; Hughes, N. D.; Parsons, S.; Parkin, A.; Boyd, G.; Jodrell, D. I.; Sadler, P. J. *J. Med. Chem.* **2001,** *44*, 3616–3621.
64. Hertzberg, R. P.; Dervan, P. B. *J. Am. Chem. Soc.* **1982,** *104*, 313–315.
65. Hertzberg, R. P.; Dervan, P. B. *Biochemistry* **1984,** *23*, 3934–3945.

THE CHEMISTRY OF MONOVALENT COPPER IN AQUEOUS SOLUTIONS

ARIELA BURG[a] and DAN MEYERSTEIN[b,c]

[a]Chemical Engineering Department, Sami Shamoon College of Engineering, Beer-Sheva, Israel
[b]Biological Chemistry Department, Ariel University Center of Samaria, Ariel, Israel
[c]Chemistry Department, Ben-Gurion University, Beer-Sheva, Israel

ABSTRACT

Copper complexes are catalysts of a variety of biological and industrial processes, especially redox processes. Cu(I) complexes are key intermediates in most of these processes. This review discusses ligand properties required for the stabilization of Cu(I) in aqueous solutions, obtaining copper complexes with

INORGANIC/BIOINORGANIC REACTION MECHANISMS
VOLUME 64 ISSN 0898-8838 / DOI: 10.1016/B978-0-12-396462-5.00007-6

desired redox potentials, obtaining Cu(I) complexes that are kinetically stabile and have desired chemical reactivity. The factors affecting the effects of ligands on the mechanisms of electron transfer reactions involving Cu(I) complexes are discussed. The role of copper complexes in processes leading to the formation of radicals and the mechanisms of reaction of copper complexes with radicals is analyzed.

Keywords: Copper complexes; Cu(I) complexes; Redox processes; Ligand; Rate constant; Aqueous solutions.

(Gold is for the mistress, Silver for the maid, Copper for the craftsman cunning at his trade.)

Rudyard Kipling

I. Introduction

Copper occurs in four oxidation states, zero, monovalent, divalent, and trivalent (*1*). Its divalent species is the most common and most stable. Copper, particularly copper(I) and its complexes, is a catalyst in many industrial and biological processes. The majority of reactions in which copper is used as a catalyst, usually redox processes, involve monovalent copper as an intermediate and often as the initiator of the catalytic process. The role of copper in biological processes as well as the green chemistry desire to perform catalytic processes in water stresses the importance of Cu(I) in aqueous media.

II. Cu(I) in Aqueous Solutions

A. The Thermodynamics of $Cu^{+}(aq)$

The redox potentials of copper in acidic aqueous solutions are as follows:

$$Cu^{+}(aq) + e^{-} \rightarrow Cu^{o}(s), \qquad E^{o} = 0.521\,V\ (2) \tag{1}$$

$$Cu^{2+}(aq) + e^{-} \rightarrow Cu^{+}(aq), \quad E^{o} = 0.153\,V\ (2) \tag{2}$$

$$Cu^{2+}(aq) + 2e^{-} \rightarrow Cu^{o}(s), \quad E^{o} = 0.342\,V\ (2) \tag{3}$$

From these values, it is clear that $Cu^{+}(aq)$ is unstable and disproportionates in aqueous solutions:

$$2Cu^{+}(aq) \rightleftarrows Cu^{2+}(aq) + Cu^{o}(s), \quad K_{1.4}(3-5) = (1-1.7) \times 10^{6}\,M^{-1} \tag{4}$$

However, if $Cu^{+}(aq)$ is formed in a clean aqueous medium, the disproportionation reaction has often a relatively long induction period as reaction (4a) is endothermic due to the $Cu^{\circ}(s)$ lattice energy.

$$2Cu^{+}(aq) \rightarrow Cu^{2+}(aq) + Cu^{o}(aq) \tag{4a}$$

Furthermore, the concentration of $Cu^{+}(aq)$ in nonacidic aqueous solutions is limited due to the low solubility of $CuOH/Cu_2O$:

$$Cu^{+}(aq) + OH^{-} \rightleftarrows CuOH(s)/Cu_2O(s) \quad K_{SP}(6) = 1 \times 10^{-14}\,M^{-2} \tag{5}$$

Naturally, the concentration of Cu(I) species in aqueous solutions can be increased by adding appropriate ligands (*7–12*).

Thermodynamically, the redox potential equations (1)–(3), that is, ΔG° of these processes are the sum of the following values:

$$\begin{aligned} &\Delta G^{o}(Cu^{n} - Cu^{o})(s)) = \Delta G^{o}(\text{evaporation of } Cu^{o}(s)) \\ &+\Delta G^{o}(\text{ionization}) + \Delta G^{o}(\text{solvation of } Cu^{n}) \end{aligned} \tag{6}$$

In order of using the redox potentials on the SHE scale, a correction for the deviation of this scale from the thermodynamic values has to be introduced to E(absolute) by correcting for the redox potential of the H^{+}/H_2 couple (The redox potential of the H^{+}/H_2 equals thermodynamically to 452.85 kJ $mol^{-1} = -4.706$ V (*13*).). As the lattice energy of $Cu^{\circ}(s)$ equals to -301.4 (*5*) kJ mol^{-1} and the ionization potentials are $IP_I = 745.3$ kJ mol^{-1} (*2*) and $IP_{II} = 1957.3$ kJ mol^{-1} (*2*), one can calculate from these values the solvation energies of Cu^{+} and of Cu^{2+} in water, viz., -1449.47 and -3843.95 kJ mol^{-1}, respectively.

From the lattice energy of copper, the ionization potentials, and the solvation energies, the free energy gain of reaction (4) $\Delta G_{1.4}$ equals -34.41 kJ mol^{-1}. From this gain, $\log K_{1.4} = 6.03$ is calculated. This value is in good agreement with the literature value of $\log K_{1.4} = 6.0$–6.23 (*3–5*).

The calculations described above indicate that the instability of $Cu^{+}(aq)$ stems from the difference between the solvation energies of the two cations and the second ionization potential of copper. This is correct for all transition-metal ions, but as the ionization energies increase along the series faster than the solvation energies, the lower oxidation states become relatively more stable. In order to shift reaction (4) to the left ligands which preferentially bind to Cu(I), must be added to the solution.

B. Cu(I) Complexes

Configurations of copper(I) complexes: Most Cu(I) complexes are tetrahedral as expected for central cations with a d^{10} electronic configuration. However, some of the complexes are linear in accord to the properties of Ag(I) (*1*) and Au(I) (*1*). In aqueous solutions, it is often difficult to determine whether $Cu(I)L_2$ are linear or whether two water molecules act as additional inner-sphere ligands. In the solid state, also trigonal, CuL_3, complexes can be prepared (*1*). Recently (*14*), tripodal ligands were synthesized by attaching thiol groups to nitrilotriacetic acid. These ligands enforce a planar trigonal coordination sphere on the monovalent copper in aqueous solutions via the formation of three Cu—S bonds with a stability constant of $\approx 1 \times 10^{19}\ M^{-3}$.

$Cu(I)L_n$ complexes can be stabilized in aqueous solutions via employing ligands with one or more of the following properties:

1. Ligands that have a lower coordination number with Cu(I) complexes than with Cu(II)complexes; these Cu(I) complexes are stabilized due the entropy gain in reaction (7):

$$Cu(II)L_m + e^- \rightarrow Cu(I)L_n + (m - n)L \qquad (7)$$

2. Ligands that are π acids and therefore prefer Cu(I) over Cu(II) and shift the redox potential of the Cu(II)/Cu(I) couples anodically.
3. Hydrophobic ligands, which often also increase the radius of the complex, decrease the stabilization of Cu(II) by decreasing its solvation energy.
4. Ligands which enforce a tetrahedral coordination sphere, or one which approaches this geometry, on the central cation.
5. Ligands that are soft bases, for example, thiols. Thus, for example, the biological copper-trafficking proteins, the metallochaperone Atx1, and the copper-transporting P-type ATPases have a highly conserved CXXC metal binding motif which binds a single Cu(I) ion via a two-coordinate site consisting of two cysteines (*15*).

All these types of ligands stabilize Cu(I) complexes by shifting the redox potentials of the Cu(II)/Cu°(s) and Cu(I)/Cu°(s) couples and thus shifting the equilibrium constant of reaction (4) to the left (*7–12*). However, ligands might stabilize Cu(I) complexes also kinetically by inhibiting the disproportionation reaction by inhibiting the formation of Cu°(s) via blocking the approach of two copper atoms, this is, for example, the mechanism by which some Cu(I) enzymes are stabilized (*16–21*).

Naturally, all these ligands also increase the solubility of Cu(I) by competing with reaction (5).

B.1. Stabilization of Cu(I)L_n via the entropic effect

The classical examples for this effect are the $[Cu(I)(NR^1R^2R^3)_2]^+$ complexes (R^1, R^2, R^3 = H, alkyl), which are stable toward disproportionation. This is in principle unexpected as these amino ligands are good σ donors and are therefore expected to stabilize the high-valent complex (*22–24*).

The explanation to the unexpected stabilization of the Cu(I) complexes by these ligands is that in reaction (8):

$$\left[Cu(II)\left(NR^1R^2R^3\right)_4\right]^{2+} + e^- \rightarrow \left[Cu(I)\left(NR^1R^2R^3\right)_2\right]^+ + 2NR^1R^2R^3 \quad (8)$$

The number of species on the right-hand side of the equation is larger by 2 than that on the left-hand side. This means that the reaction is driven at least partially, by the resulting entropic gain. Thus, for example, $[Cu(I)(NH_3)_2]^+$ containing solutions can be prepared by adding Cu°(s) to deaerated solutions of $[Cu(NH_3)_4]^{2+}$ (*1,25,26*).

Several other $Cu(I)L_2$ complexes exist, and as all the corresponding Cu(II) complexes are at least tetradentate, the entropic effect clearly is responsible, or at least contributes, to the stabilization of these complexes. Classical examples for such complexes are $CuCl_2^-$, $CuBr_2^-$, and CuI_2^- (*5*). Similar complexes are formed also by the pseudo-halides, for example, CN^-. However for the latter complexes, a contribution of π back-donation clearly contributes to the stabilization. For cyanide, the effect is so large that reaction (9) is exothermic:

$$\left[Cu(II)(CN)_4\right]^{2-} \rightarrow \left[Cu(I)(CN)_2\right]^- + (CN)_2 \quad (9)$$

B.2. Hydrophobic ligands

Hydrophobic ligands, often tertiary amines, decrease the solvation energy (*22–24,27*), inhibit hydrogen bond formation, are weaker σ donors than the analogous hydrophilic ligands, and therefore stabilize low-valent transition-metal complexes, mainly due to the decrease in the solvation energy of the high-valent complexes. The first Cu(I) complex with a tertiary amino ligand was Cu(1,4,5,7,7,8,11,12,14,14-decamethyl-1,4,8,11-tetrraazacyclatetetradecane)$^+$, $[Cu(I)L^1]^+$. The redox

potential of the $[Cu(II/I)L^1]^{2+/+}$ couple is $+0.47$ V versus Ag/AgCl (*27*). The complex $[Cu(I)L^1]^+$ is stable in aqueous solutions and does not react with O_2. The latter observation is probably due to steric hindrance that inhibits the formation of the $L^1Cu^IO_2^+$ complex, see below (Figs. 1 and 2).

The observation that L^1 stabilizes Cu(I), whereas amino ligands including 1,4,8,11-tetraazacyclatetradecane catalyze the disproportionation of Cu(I) (*22,23,27*) suggested that linear tertiary amino ligands, for example, L^2 will also stabilize Cu(I).

Indeed in the presence of L^2 and other tetraazatertiary amines, the comproportionation of $Cu^\circ(s)$ and Cu^{2+} is observed (*22,23*). Tertiary amino ligands also stabilize other low-valent metal complexes, for example, Ni(I) and Cr(II) (*22,23*). The stabilization of low-valent complexes by tertiary amino ligands is attributed to their hydrophobic nature including the inhibition of M—N—H···OH_2 hydrogen bonds. Thus :N—CH_3 are weaker σ donors than :N—H ligands in solutions, though they are better σ donors in the gas phase (*28*).

The combined effect of the absence of M—N—H···OH_2 hydrogen bonds and the increase in the radius of the complexes decreases the solvation energies of the complexes and thus stabilizes the lower-valent complexes, including Cu(I). It is of interest to note that $(CH_3)_2NCH_2CH_2N(CH_3)CH_2CH_2N(CH_3)_2$ and $N(CH_2CH_2N(CH_3)_2)_3$ do not stabilize Cu(I), though they affect the properties of the Cu(II) complexes (*24*).

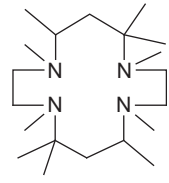

FIG. 1. Lewis structure of L^1 = 1,4,5,7,7,8,11,12,14,14-decamethyl-1,4,8,11-tetrraazacyclatetetradecane.

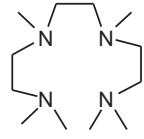

FIG. 2. Lewis structure of L^2 = 2,5,8,11-tetramethyl-2,5,8,11-tetraaza-dodecane.

It should be noted that ligands that contain both hydrophobic groups and other substituents that stabilize Cu(I), for example, alkenes (see, e.g., L^3) have been prepared (*10*) (Fig. 3).

Most ligands that stabilize Cu(I) in aqueous solutions shift as expected the $Cu^{2+/+}(aq)$ redox potential anodically. However, this does not have to be so as can be deduced from the following equations:

$$\begin{aligned} &2[\mathrm{Cu(I)L}_n]^+ \rightleftarrows \left[\mathrm{Cu(II)L}_m\right]^{2+} + \mathrm{Cu}^{\circ} + (2n-m)\mathrm{L}, \\ &K_{1.10} = \left([\mathrm{Cu(II)L}_m][\mathrm{L}]^{2n-m}\right)/[\mathrm{Cu(I)L}_n]^2 = \left(K^{\mathrm{II}}\left[\mathrm{Cu}^{2+}(\mathrm{aq})\right]\right. \\ &\left.[\mathrm{L}]^m[\mathrm{L}]^{2n-m}\right)/\left(K^{\mathrm{I}}\left[\mathrm{Cu}^{+}(\mathrm{aq})\right][\mathrm{L}]^n\right)^2 = K^{\mathrm{II}}\left[\mathrm{Cu}^{2+}(\mathrm{aq})\right]/\left(K^{\mathrm{I}}\right)^2 \\ &\left[\mathrm{Cu}^{+}(\mathrm{aq})\right]^2 = 10^6 K^{\mathrm{II}}/\left(K^{\mathrm{I}}\right)^2 = K_{1.10} \end{aligned} \tag{10}$$

where $K^{\mathrm{II}} = ([\mathrm{Cu(II)L}_m])/([\mathrm{Cu}^{2+}(\mathrm{aq})][\mathrm{L}]^m)$ and $K^{\mathrm{I}} = [\mathrm{Cu^I L}_n]/([\mathrm{Cu}^{+}(\mathrm{aq})][\mathrm{L}]^n)$

Therefore, equilibrium (8) shifts to the left if $(K^{\mathrm{I}})^2 > K^{\mathrm{II}}$, whereas the redox potential of the $\mathrm{Cu^{II}L}_m/\mathrm{Cu^{I}L}_n$ couple is shifted cathodically if $K^{\mathrm{II}} > K^{\mathrm{I}}$ (*10*). Thus, the addition of ligands for which both these criteria are fulfilled to a mixture of $Cu^{2+}(aq)$ and Cu° increases the concentration of the Cu(I) species in the solution and transforms the Cu(I) species into a stronger reducing agents. This is of importance in some catalytic systems where copper ions act as the catalyst and the activity depends on the redox potential of the $[\mathrm{Cu(II)L}_n]/[\mathrm{Cu(I)L}_m]$ couple (*10,25,29,30*).

B.3. π acid ligands

Cu(I) a low-valent cation with a relatively high electron density tends to form complexes with π acids, for example, CO (*1*), CH_3CN (*26,31*), RCN (*31*), RNC (*32*), alkenes (*33*), alkynes (*33*), aromatic compounds (*12*), etc. In principle, these complexes can be divided into two groups (Fig. 4):

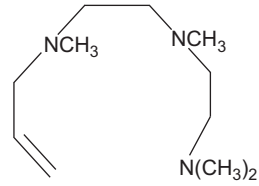

FIG. 3. Lewis structure of L^3 = 2,5,8-trimethyl-2,5,8-triaza-undecane-10-ene.

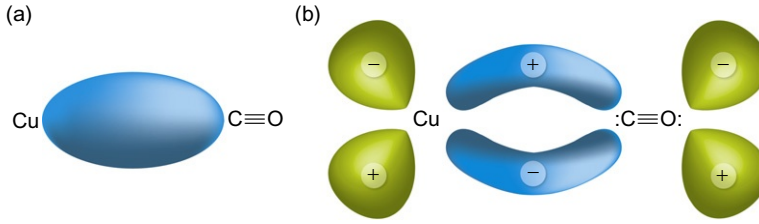

FIG. 4. (a) Formation of σ bond between Cu(I) and CO. (b) Formation of π bond between Cu(I) and CO.

a. Complexes in which the copper ion is linearly bound to the ligand, for example, CO, RCN, etc.
b. Complexes in which the copper is situated perpendicularly to the π bond.

Clearly, these complexes are formed also in nonaqueous media.

The stability constants of complexes of low-valent transition-metal ions with alkenes usually increase when electron-withdrawing substituents, which increase the π acidity, are bound to the alkene. However, this is not observed for Cu(I), see some typical stability constants in Table I.

Clearly, the ethylene complex is more stable than the complexes with maleate and fumarate. However, also methyl substituents, for example, 2-methyl-propene, form weaker complexes than ethylene. These results suggest that for Cu(I), the π acidity and the σ-donating properties of the ligand affect the stability constant of the complexes similarly and that steric hindrance contributes to the stability of these complexes. It is of interest to note that the complex of Cu(I) with acetylene belongs to the first group after the ligand loses a proton—Cu—C≡ CH (*33*)

B.4. Ligands which stabilize Cu(I) via inhibiting kinetically its mechanisms of reaction

Many $[Cu(I)L_n]$ complexes tend to disproportionate (*1*):

$$2Cu(I)L_n \rightarrow Cu^{o}(s) + Cu(II)L_m + (2n - m)L \qquad (11)$$

react with dioxygen (*34,35*):

$$2Cu(I)L_n + O_2 \xrightarrow[-2(n-m)L]{2H^+} 2Cu(II)L_m + H_2O_2 \qquad (12)$$

TABLE I

LOG K VALUES FOR CU(I) COMPLEXES WITH π LIGANDS

The ligand	pK
Benzoic acid[a] (*12*)	3.7
Salicylic acid[a] (*12*)	2.8
3-Bromobenzoic acid[a] (*12*)	3.9
Maleic acid[a] (*9*)	3.9
Fumaric acid[a] (*9*)	4.0
Ethylene (*33*)	5.4
2-Methyl-propene (*33*)	4.4
Allyl alcohol (*33*)	4.7

[a]Log K values for Cu(I) complexes at pH 4.

reduce a substrate, OX, via the inner-sphere mechanism:

$$\mathrm{Cu(I)L}_n + \mathrm{OX} \overset{-\mathrm{L}}{\rightleftarrows} \mathrm{L}_{n-1}\mathrm{Cu(I)OX} \rightarrow \mathrm{Cu(II)L}_m + \mathrm{RED} \qquad (13)$$

The latter two reactions proceed via the inner-sphere mechanism (see below), that is, they require access of the substrate to the central Cu(I) ion. The disproportionation reaction requires the contact of the central copper ion with a surface, preferably a Cu°(s) surface, as the formation of a Cu° atom is extremely endothermic due to the lattice energy of copper, -301.4 kJ mol^{-1} (*5*). Thus ligands that block sterically the approach of a substrate or of a surface to the central copper ion stabilize it (*19*). An extreme example is 1,4,5,7,7,8,11,12,14,14-decamethyl-1,4,8,11-tetraazacyclotetradecane, L^1 (*27*). Thus $[Cu(I)L^1]^+$ is stable even in aerated aqueous solutions (*27*). In analogy, some enzymes with Cu(I) as the active site, for example, CuSOD, inhibit disproportionation or the reaction with O_2 by inhibiting the approach of two Cu(I) central ions to each other which is required for these reactions which are thermodynamically exothermic.

B.5. Ligands which require a tetrahedrally coordinated central ion

Some ligands fit only a tetrahedral coordination sphere, which fits Cu(I), and cannot adopt a planar coordination sphere, which fits Cu(II). These properties shift the redox potential of the Cu(II/I) couple considerably anodically. A typical example for such a ligand is L^4 which forms stable $[Cu(I)L^4{}_2]^+$ complexes (Fig. 5).

This ligand is used for the analytical determination of Cu (I) (*36,37*). The redox potential of the $[CuL^4{}_2]^{2+/+}$ couple is 0.594 V (*38*), whereas the $[Cu(1,10\text{-phenanthroline})_2]^{2+/+}$ couple

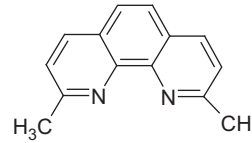

FIG. 5. Lewis structure of $L^4 = 2,9$ dimethylphenanthroline.

is 0.174 V (*38*). The redox potentials of several copper enzymes are similarly affected by the coordination geometry enforced by the enzyme (*17,39,40*).

C. METHOD FOR PREPARATION OF Cu^+(aq)

As stated above, Cu^+(aq) is unstable and disproportionates via reaction (4). However, due to the fact that reaction (4a) is very endothermic as $\Delta G^\circ(Cu^\circ - Cu(s)) = -301.4\ kJ\ mol^{-1}$ (*5*) one can prepare over saturated Cu^+(aq) acidic aqueous solutions. (The acidity is required due to the very low solubility of $CuOH/Cu_2O$ (*6*).). The lifetime of deaerated Cu^+(aq) solutions depends on the purity of the system, that is, on the number of crystallization centers available in the solution or the walls of the container.

Several methods to prepare Cu^+(aq) solutions were developed:

C.1. The ligand exchange method (25,26)

In this procedure, a $Cu(I)L_n$ complex is prepared via the comproportionation method, reaction (10). The solution containing the $Cu(I)L_n$ is removed from the $Cu^\circ(s)$ prior to the removal of the ligand L to form Cu^+(aq). The easiest procedure is to use $L = NH_3$ and remove it by the addition of acid, reactions (14) and (15).

$$\left[Cu(II)(NH_3)_4\right]^{2+} + Cu^o(s) \overset{\text{deaerated}}{\longrightarrow} 2\left[Cu(I)(NH_3)_2\right]^+ \qquad (14)$$

$$\left[Cu(I)(NH_3)_2\right]^+ + 2H^+ \rightarrow Cu^+(aq) + 2NH_4{}^+ \qquad (15)$$

Often the solution of $2[Cu(I)(NH_3)_2]^+$ is injected into an acidic solution containing the substrate the reaction of which with Cu^+(aq) is to be studied (*25,26*).

Alternatively, one could form $[Cu(I)(CO)_n]^+$(aq) or $[Cu(I)(C_2H_4)]^+$(aq) and then by very fast flashing with an inert gas, for example, He or Ar, obtain Cu^+(aq). The problem here is the rate of the flashing that has to be considerably faster than the disproportionation reaction.

C.2. Reaction of Cr^{2+}(aq) (41–43)

A solution of Cu^{2+}(aq) in excess is mixed with acidic Cr^{2+}(aq) solution.

$$\begin{gathered} Cu^{2+}(aq) + Cr^{2+}(aq) \rightarrow Cu^{+}(aq) + Cr^{3+}(aq), \\ k \approx 0.9\,M^{-1}s^{-1}\left(\left[H_3O^{+}\right] = 0.762\,M\right) \end{gathered} \tag{16}$$

The reaction of Cu^{+}(aq) thus prepared can be studied (*41–43*) as long as Cr^{3+}(aq) does not interfere with the study. Naturally, other strong single-electron reducing agents can replace Cr^{2+}, for example, V^{2+}(aq) (*44*).

C.3. Reduction of Cu^{2+}(aq) by radicals applying the pulse radiolysis technique (35,45)

As reaction (16) is relatively slow, one can, if needed, prepare Cu^{+}(aq) *in situ* using the pulse-radiolysis technique. The radiolysis of water is summed up in Eq. (17) where the values in parenthesis are the relative yields of the primary products. CR^1R^2OH, $R^i = H$, CH_3, are strong reducing agents (*46*). The following equations show the production of Cu^{+}(aq) in the presence of methanol, other alcohols can be used, in acidic deaerated aqueous solutions.

$$H_2O \xrightarrow{\gamma, e^-} e^-(aq)(2.65), H(2.65), {}^{\bullet}OH(0.6), H_2(075), H_2O_2(0.45), H^+(2.65)(47) \tag{17}$$

$$e^-(aq) + H^+ \rightarrow H^{\bullet}, \quad k(47) = 2 \times 10^{10}\,M^{-1}s^{-1} \tag{18}$$

$$e^-(aq) + Cu^{2+}(aq) \rightarrow Cu^{+}(aq), \quad k(47) = 3.3 \times 10^{10}\,M^{-1}s^{-1} \tag{19}$$

$${}^{\bullet}OH + CH_3OH \rightarrow {}^{\bullet}CH_2OH + H_2O, \quad k(47) = 4.6 \times 10^{8}\,M^{-1}s^{-1} \tag{20}$$

$$H^{\bullet} + CH_3OH \rightarrow {}^{\bullet}CH_2OH + H_2, \quad k(47) = 1.6 \times 10^{6}\,M^{-1}s^{-1} \tag{21}$$

$$H^{\bullet} + Cu^{2+}(aq) \rightarrow Cu^{+}(aq) + H_3O^{+}, \quad k(47) = 5 \times 10^{8}\,M^{-1}\ s^{-1} \tag{22}$$

$${}^{\bullet}CH_2OH + Cu^{2+}(aq) \rightarrow Cu^{+}(aq) + CH_2O,\ k(47) = 1.1 \times 10^{8}\,M^{-1}s^{-1} \tag{23}$$

One can in principle use only e^-(aq) and $H^\bullet$ as reducing agents and use the $OH^\bullet$ radicals to produce another reagent, for example, the $^\bullet CH_3$ radical, reaction (24), to react with the Cu^+(aq).

$$^\bullet OH + (CH_3)_2SO \rightarrow {}^\bullet CH_3 + CH_3SOOH,\ k(48) = 6.6 \times 10^9\,M^{-1}\,s^{-1} \quad (24)$$

Cu^+(aq) is formed also in the reaction of Cu(II) with "non reducing" radicals, for example, $^\bullet CH_2CO_2^-$ (*49*). However in these reactions, often relatively long-lived intermediates, for example, $(CH_3CO_2)Cu–CH_2CO_2^-$ are formed and might complicate the kinetics of reaction of Cu^+(aq) with the desired substrate.

III. Cu(I)L_n as a Reducing Agent

The coordination sphere of Cu(I) and Cu(II) differs considerably. Thus Cu(II) complexes have commonly an octahedral geometry with a Jahn–Teller distortions (*1*). However, Hodgson *et al.* have recently shown that low molecular weight Cu(II) complexes, for example, $[Cu(II)(H_2O)_5]^{2+}$ and $[Cu(II)(NH_3)_5]^{2+}$ have a square-pyramidal, five-coordinate sphere (*50,51*). On the other hand, Cu(I) complexes have usually a linear or a tetrahedral coordination sphere (*1*). Therefore, the oxidation of Cu(I) complexes or the reduction of Cu(II) complexes involves large geometrical changes. Therefore, the reorganization energies of redox processes involving Cu(II/I) couples are large. As a result, most of these processes proceed via the inner-sphere mechanism.

A. Reactions of Cu^+(aq) with Transition Metal Complexes

Most of the reactions studied with the exception of complexes with ligands with no available electron pair proceed via the inner-sphere mechanism. Thus for example, reaction (25) is considerably faster than reaction (26) (*42*).

$$Cu^+(aq) + Fe(H_2O)_5OH^{2+} \rightarrow Cu^{2+}(aq) + Fe^{2+}(aq),\quad k = 1.6 \times 10^4\,M^{-1}\,s^{-1} \quad (25)$$

$$Cu^+(aq) + Fe^{3+}(aq) \rightarrow Cu^{2+}(aq) + Fe^{2+}(aq),\quad k < 30\,M^{-1}\,s^{-1} \quad (26)$$

and the reduction of $Fe(H_2O)_5F^{2+}$ and $Fe(H_2O)_5N_3{}^{2+}$ are too fast to be measured with $k > 5 \times 10^6$ and $k > 1 \times 10^8\,M^{-1}\,s^{-1}$, respectively (*42*).

Also reaction (27) proceeds via inner-sphere mechanism (*41*).

$$Cu^{+}(aq) + \left[Co(III)(NH_3)_5R\right]^{3+} \rightarrow Cu^{2+}(aq) + \left[Co(II)(NH_3)_5R\right]^{2+} \quad (27)$$

The kinetics of reaction (27) was studied for a variety of R, halides, pseudo-halides, OH^-, and H_2O. The observed rate constants increase along the series of $R = H_2O, CN^-, F^-, NCS^-, OH^-, N_3^-, Cl^-, Br^-$, from 1.0×10^{-3} to $4.5 \times 10^5\ M^{-1}\ s^{-1}$ (*41*) as expected for reactions proceeding via the inner-sphere mechanism. The reduction of $[Co(III)(NH_3)_6]^{3+}$ and $[Co(III)(en)_3]^{3+}$, which are expected to proceed via the outer-sphere mechanism, is too slow to be measured (*41*).

On the other hand, the reduction of a series of $[Ru(III)(NH_3)_5R]^{3+}$ (*52*) (R = pyridine, bipyr) and $[(cyclam)Ni(III)(SO_4)_2]^-$ (*25*) are known to proceed via the outer-sphere mechanism, reactions (28) and (29).

$$Cu^{+}(aq) + \left[Ru(III)(NH_3)_5R\right]^{3+} \rightarrow Cu^{2+}(aq) + \left[Ru(II)(NH_3)_5R\right]^{2+} \quad (28)$$

For this reaction, $\log k_{2.4}$ shows a linear dependence on E° for the different $[Ru(III)(NH_3)_5R]^{3+}$ complexes, $k = (50\text{–}4 \times 10^4)\,M^{-1}s^{-1}$ (*53*).

$$Cu^{+}(aq) + \left[(cyclam)Ni(III)(SO_4)_2\right]^{-} \rightarrow Cu^{2+}(aq) + \left[(cyclam)Ni(II)(SO_4)_2\right]_2^{-}, \quad k = 3.0 \times 10^4\,M^{-1}s^{-1}(25) \quad (29)$$

B. Redox Reaction with NO_2^- as a Model for Copper Nitrite Reductases (CuNIR)

Cu/FeNIR proteins are important enzymes in the dinitrogen cycle (*54*). Dinitrogen is released into the atmosphere by denitrifying bacteria found in soils and sediments (*55*). Nitrate is reduced by nitrate reductase to nitrite. NIR proteins are involved in the one-electron reduction of NO_2^- to NO (*56,57*). NO is reduced to N_2O, which, in turn, is reduced by N_2O reductase to dinitrogen. Some of these enzymes have iron, in the form of FeNIR, in their active site, while others have copper, CuNIR, the latter generally are present in low oxygen environments (*54*). In the presence of oxygen, these enzymes form peroxides, which causes the protein to lose its nitrite reduction function. CuNIR proteins are applicable industrially as biologic sensors of NO_2^-. NIR purified from *Alcaligenes faecalis* S-6 is fixed on a

gold electrode that can then be used as a working electrode for the identification of nitrite (*58*).

CuNIR enzymes are trimers that contain two copper centers, type 1 and type 2, in each monomer (*54,59*). Distinguishable by their spectroscopic properties, type 1 copper centers are usually either intensely blue or green in color depending on the orientation of the amino acid ligands around the copper (*59*). X-ray structures indicate that the ligands around the copper are histidine, cysteine, and methionine, between which hydrogen bonds form. The type 1 copper site has a distorted tetrahedral geometry. In contrast, the type 2 copper centers have no significant visible absorption. The ligands around type 2 centers are histidines with hydrogen bonds between them, and like the type 1 centers, this site also has a tetrahedral geometry (*60*). Type 2 centers contain three histidines and a water molecule (*60*). Studies have shown that nitrite binds to the Cu(II) center displacing the water molecule. Some studies, based on native enzyme or model complexes, assume that the nitrite binds to Cu(II) via the oxygen atoms (*60*), while others assume that the nitrite binds via the nitrogen (*61–64*).

Type 1 serves as an electron absorber (*65*) that rapidly transfers electrons to the type 2 site. In model complexes of the enzyme, the reduction process proceeds via reaction (30) within the type 2 center, the active site of the enzyme:

$$NO_2^- + e^- + 2H^+ \rightarrow NO + H_2O \qquad (30)$$

To proceed, the reduction needs two equivalents of H^+, and a Cu(I)—NO^+ intermediate is formed (*66,67*). The electron transfer from type 1 to type 2 is an essential step of the catalytic cycle (*68*). Pulse radiolysis studies were performed to find the rate constant of the electron transfer between the type 1 and the type 2 centers, reaction (31) (*68–70*).

$$\text{Type 1 Cu}^{\text{I}} - \text{Type 2 Cu}^{\text{II}} \underset{k_b}{\overset{k_f}{\rightleftarrows}} \text{Type 1 Cu}^{\text{II}} - \text{Type 2 Cu}^{\text{I}} \qquad (31)$$

The electron transfer studies used AxNIR and AcNIR (bacterial sources of CuNIR) with either $CO_2^{\bullet -}$ [E° (vs. SHE) = −1.8 V] (*68*) or 1-MNA [E° (vs. SHE) = −1.0 V] as the reductant (*68*). The radicals were formed by irradiating dilute deaerated aqueous solutions containing formate or 1-methylnicotinamide (1-MNA^+) (reactions (32) and (33), respectively):

$$HCO_2^- + OH/H \rightarrow H_2O/H_2 + CO_2^- \qquad (32)$$

$$1\text{–MNA}^{+} + e^{-}(aq) \rightarrow 1\text{–MNA}* \tag{33}$$

The observed rate constants [k_{31}(AxNIR) (*70*)$=(450\pm30)\,s^{-1}$, k_{31}(AcNIR) (*69*)$=(1030\pm80)\,s^{-1}$] are the sums of the forward and backward rate constants. The difference between the rate constants indicates that the internal electron transfer may be the rate-determining step of the catalytic activity. Two factors affect that rate: the ligand exchange at the type 2 center when the substrate NO_2^- binds to the ion center and the reorganization energy of the type 1 center when it transfers its electron.

To better understand CuNIR enzymes, the activities of enzyme models were studied (*60,61,63,64,67,66,71*). Studies on these complexes were performed in either organic or aqueous solvents, depending on the solubility of the complex (in particular, of its ligands) under study. The models that best describe CuNIR activity include complexes with histidines or phenyl groups as ligands (*72*). As these ligands lower the complex solubility in water, the reactions must be studied in organic solvents.

Among the reactions studied was that of $Cu^+(aq)$ with NO_2^- (*61*). The results are consistent with the following mechanism (reactions (34) and (35)), reactions that represent the simplest CuNIR enzyme model (*61*):

$$Cu^+(aq) + NO_2^- \rightleftarrows [Cu^+NO_2^-], \quad K = 140 \pm 25\,M^{-1} \tag{34}$$

$$[Cu^+NO_2^-] + H^+ \rightarrow Cu^{2+} + NO + OH^-, \quad k = 4.6 \times 10^5\,M^{-1}\,s^{-1} \tag{35}$$

The study of reactions (34) and (35) in organic solvents show that H^+ is needed to produce NO (*67,66*).

The value of the stability constant K of $[Cu^+NO_2^-]$, from the study described above, is similar to values reported in the literature for Cu(I) complexes with various ligands in organic solvents (*73,74*). The stability constant of the $[Cu^+NO_2^-]$ complex and other evidence suggest that the nitrite binds to the copper via the nitrogen, as the expected stability constants of Cu(I) complexes with oxo-anions are considerably lower (*60,63,64*). Some models for CuNIR with dinuclear copper complexes show that the nitrite binds to the Cu(II) center via the oxygen atoms and to the Cu(I) center via the nitrogen atom (*60*).

This is expected based on the relative softness of Cu(I). Some studies have shown that the NO formed in the nitrite reduction binds to the copper center as a ligand before its release (*60*). X-ray studies of some complex models supporting the suggestion that a Cu—N bond is formed as a transient (*64*). For some

complexes, there are DFT calculations (*62*) indicating that the low-energy intermediate formed is the one with the Cu—N bond. ESR studies indicate that the product NO is ligated to Cu via a Cu—N bond and there is a spectroscopic evidence for a $[Cu^{I}–NO \leftrightarrow Cu^{II}–NO^{-}]$ intermediate (*75*).

C. Redox Reaction with Dioxygen and Dioxygen as a Ligand

The incentive to study the character and the kinetic behavior of Cu(I) complexes with dioxygen is the same as that behind the study of Cu(I) complexes with nitrite described above. Important enzymes have Cu(I) in their active site and bind dioxygen or activate dioxygen as part of the reactions they are involved in. A few important examples are as follows:

Galactose oxidase (*54,76,77*) is active as a catalyst in two separable reactions, the oxidation of a primary alcohols (reaction (36)) (*77*) and the reduction of dioxygen to hydrogen peroxide (reaction (37)) (*77*):

$$RCH_2OH \rightarrow RCHO + 2e^{-} + 2H^{+} \tag{36}$$

$$O_2 + 2e^{-} + 2H^{+} \rightarrow H_2O_2 \tag{37}$$

The active site of this enzyme in its Cu(II) form contains four amino acids, two tyrosins one of which is a tyrosyl radical, two histidines, and one solvent molecule that together form a five-coordinate metal complex (*54,76*). During the reduction–oxidation reactions, the coordination sphere changes. In the Cu(I) state, only three amino acids are coordinated to the central cation. The unusual two-electron oxidation reaction involves the reduction of the central Cu(II) cation and the tyrosyl radical.

Superoxide dismutase, SOD (*54*), contains copper and zinc in one subunit. The superoxide anion, $O_2^{\bullet -}$, is produced by the reduction of oxygen during respiration in all living species and photosynthesis reactions in plants. This radical anion is toxic probably via the formation of peroxonitrite (*54*) and hydrogen peroxide (*54*). Superoxide dismutase functions as an antioxidant via a catalytic reaction (reaction (38)):

$$2O_2^{\bullet -} + 2H^{+} \rightarrow H_2O_2 + O_2 \tag{38}$$

Each subunit contains Cu(II) and Zn(II). During the catalytic reaction, Cu(II) is reduced to Cu(I) (reaction (39)):

$$Cu(II) + O_2^{\bullet -} \rightarrow Cu(I) + O_2 \tag{39}$$

and reoxidized via

$$\mathrm{Cu(I)} + \mathrm{O_2^{\bullet -}} \xrightarrow{2\mathrm{H^+}} \mathrm{Cu(II)} + \mathrm{H_2O_2} \tag{40}$$

The geometry of the active site around the copper ion changes from square pyramidal in the Cu(II) to trigonal planar for Cu(I).

Soluble water complexes were recently synthesized as mimics of SOD (*78,79*), hopefully for medical use in water. The complexes contain dinuclear Cu(II) and macrocyclic ligands. Comparisons between SOD activity and complex models indicate that the complexes are good models for SOD (*79*).

Based on redox potentials and species concentrations, Goldstein *et al.* (*80*) suggested an alternative mechanism (reactions (41) and (42)) to explain the unique toxicity of $\mathrm{O_2^{\bullet -}}$ compared to other biological reductants like glutathione and vitamin C. In the alternative system, the copper is oxidized rather than reduced as in reaction (36). The active species in this mechanism is trivalent copper.

$$\mathrm{Cu(II)} + \mathrm{O_2^{\bullet -}} + 2\mathrm{H^+} \rightarrow \mathrm{Cu(III)} + \mathrm{H_2O_2} \tag{41}$$

$$\mathrm{Cu(III)} + \mathrm{O_2^{\bullet -}} \rightarrow \mathrm{Cu(II)} + \mathrm{O_2} \tag{42}$$

Cytochrome c oxidase (*54,81*) is part of the mitochondrial respiratory chain (reaction (43)):

$$\mathrm{O_2} + 4\mathrm{e^-} + 4\mathrm{H^+} \rightarrow 2\mathrm{H_2O} \tag{43}$$

A full understanding of the reactions between Cu(I) complexes and oxygen will shed light on the activities and mechanisms of these enzymes. In addition, the enzymes have significant economic importance manifested in the industrial applications of reactions between copper, especially monovalent copper, and oxygen. Finally, the chemistry of these reactions is unique because of the sensitivity of Cu(I) to oxygen.

C.1. Reaction of Cu(I) with dioxygen

$\mathrm{Cu^+(aq)}$ reacts with dioxygen in a radical chain process (*31,34,35,82,83*). The electron transfer reaction is started by the reaction shown below:

$$\mathrm{Cu^+(aq)} + \mathrm{O_2} \rightleftarrows \mathrm{CuO_2^+} \tag{44}$$

All suggested mechanisms (*34,35,83,84*) propose the formation of $\mathrm{CuO_2^+}$, as a necessary intermediate.

$$Cu^{+}(aq) + O_2 \rightleftarrows Cu^{2+}(aq) + O_2^{\bullet -} \quad (45)$$

If the reaction would proceeded via the outer-sphere mechanism, reaction (45), the calculated electron transfer rate constant applying the Marcus cross-relation (*85–87*) would be $1.6 \times 10^{-6}\,M^{-1}\,s^{-1}$ (*35*). However, the measured rate constant is $3.5 \times 10^{4}\,M^{-1}\,s^{-1}$ (*31,88*), which indicates that the reaction proceeds via the inner-sphere mechanism.

In principle, two reaction mechanisms are plausible, single-electron reduction of O_2 to form $O_2^{\bullet -}/H_2O_2$, reactions (2) and (3) in Scheme 1, or a two-electron reduction, involving two $Cu^{+}(aq)$ forming H_2O_2, reaction (4) in Scheme 1. A competition exists between the one-electron and the two-electron reduction mechanisms. Which reaction dominates depends on the reaction conditions, for example, the Cu(II) concentration (*35,89*). The one-electron reduction of O_2 to $O_2^{\bullet -}$ seems to be thermodynamically unfavorable (*89*). The kinetics of reaction (46) obey a rate law for which $Kk = (2.3 \pm 0.4) \times 10^{8}\,M^{-1}\,s^{-1}$ (*35*):

$$Cu^{+}(aq) + O_2 \overset{K}{\rightleftarrows} [CuO_2]^{+} + Cu^{+}(aq) \overset{H^{+},k}{\rightarrow} 2Cu^{2+}(aq) + H_2O_2 \quad (46)$$

Using the pulse radiolysis technique (*7,89*) as an electron source of $[Cu(I)(1,10\text{-phenanthroline})]^{+}$, Goldstein and Czapski found that at low concentrations of Cu(II), the reaction is dominated by the one-electron mechanism (*89*), and at high concentrations of Cu(II), two-electron reduction is favored. Reactions (2) and (3) in Scheme 1 are reversible, and therefore, Cu(II) concentrations affect the reaction direction.

The reaction between dioxygen and $[Cu(I)L^{i}]^{+}$ [L^{i} = imidazole ((1H-imidazol-4-yl)-*N*,*N*-bis((pyridine-2-yl)methyl)methanamine) (*90*), fumarate (*35*), acetonitrile (*31,82*), phenantroline (*89*)] in

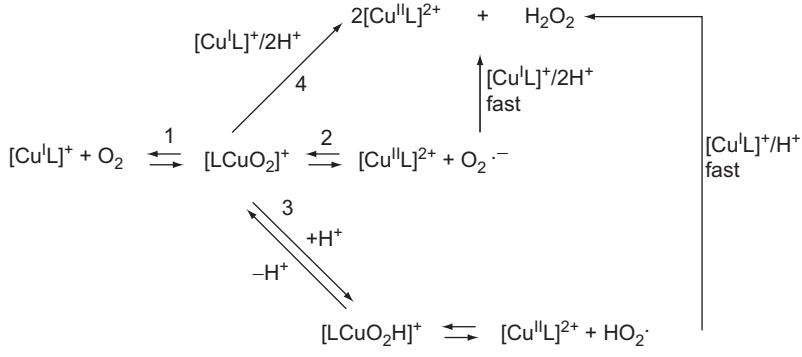

SCHEME 1. Mechanism of reaction of $Cu^{I}L$ with O_2 (*35*).

THF (*90*) or in water (*31,35,89*) was studied. As in the reaction with $Cu^{+}(aq)$, the first step in the reaction is the formation of $[LCu(I)O_2]^{+}$ as the intermediate species. Depending on which ligand is used, the redox potential of the Cu(II/I) couple can shift and steric effects can develop. Thus the reactivity of $[CuI)L]^{+}$ is affected by L. The kinetics of reaction of dioxygen with several $[Cu(I)L]^{+}$ complexes were studied, and the mechanisms of these reactions are summed up in Scheme 1 (*35*):

It was shown that alkenes as ligands (*35*) slow down reactions (2) and (3) in Scheme 1. The effect of alkenes on reaction (4) in Scheme 1 was studied using fumaric acid as an alkene model (*35*). The slow rate of the reaction of [Cu(I)fum] with dioxygen can be attributed to the reaction with $Cu^{+}(aq)$, that is, the reaction with the complex is very slow.

The stability constants of the $LCuO_2$ complexes are also similar. For L = water, phenanthroline, and bipyridyl, which have similar redox potentials, $K \approx 0.2$ M. For L = acetonitrile and fumarate, K is considerably smaller, in accord with the fact that $[Cu(I)CH_3CN]^{+}$ and [Cu(I)fum] are weaker reducing agents. These results indicate that the stability constant is affected by the redox potential.

Some catalytic reactions between Cu(I) complexes or enzymes and O_2 generate interesting intermediates—$Cu^{I}—O—O—R$ and/or the decomposition products of $[Cu^{II}—O^{-\bullet} \leftrightarrow Cu^{III}{=}O^{2-}]^{+}$ (*91,92*). The latter species is not stable and is assumed to be a powerful oxidant, possibly more reactive than $[Fe^{IV}{=}O]^{2+}$ (*92*). Recently, Tolman *et al.* succeeded in trapping these species (*91,92*) using ESI-MS at low temperatures and CH_2Cl_2 using an arene substituent to Cu(I)-α-ketocarboxylate complexes (*91,92*). The reactions described above are one- or two-electron reductions. Biological systems requiring four-electron reduction reactions as in cytochrome *c* oxidase (*54,81*) have a bimetallic active site that includes heme with an Fe ion and a Cu ion. Cytochrome *c* oxidase catalyzes the reduction of dioxygen to water via a four-electron reduction (reaction (43)). Many complexes have been synthesized and studied as models for this enzyme. We choose to focus on the results of a recent study on complexes that incorporate FeCu porphyrins (*93*). These complexes reduce O_2 to water via two routes, two- and four-electron reductions. Coutsolelos *et al.* (*93*) have shown in electrochemical studies that complexes that include copper, such as FeCu, increase the catalytic activity of the four-electron reduction over that of the corresponding Fe complexes. Using a copper complex, an intermediate species, Fe—O—O—Cu, is formed which induces the reduction of the O—O bond (*18*).

Model complexes for four-electron reduction enzymes are not only of biological importance, but they also have technological

potential as catalysts in fuel cells (*18,94–96,81*). For example, the electrocatalytic activity of different $[(L)Fe^{II}Cu^{I}]^{+}$ complexes (L = a binucleating ligand having a heme and covalently tethered tris(2-pyridyl)methylamine which binds copper as a tetradentate ligand) was studied by Karlin *et al.* as a model for cytochrome *c* oxidase (*18*). The results indicate that the reduction of O_2 is indeed a four-electron reduction. During the reduction, $Fe^{III}—(O_2{}^{2-})—Cu^{II}$ and $Fe^{III}—O_2$ intermediates are formed.

Although as noted above that monovalent copper complexes are sensitive to O_2 and their reactions with O_2 are fast, some Cu(I) complexes are stable in the presence of O_2 (*36,97,98*). Thus $[CuL^1]^+$ does not react with O_2 (*27*), and [Cu(I)fumarate] reacts only via dissociation to $Cu^+(aq)$ as noted above (*35*). Another ligand which inhibits the reaction with O_2 is 2,9-methyl-phenanthroline (*89*) ($E_{1/2}$(oxidation) = 0.67 V in CH_2Cl_2). All these ligands shift the redox potential of the Cu(II/I) couple anodically, thus decreasing the stability of the $LCuO_2$ complexes and/or sterically inhibiting their formation.

D. Fenton-Like Reaction

The Fenton reaction is the Fe(III/II)-catalyzed oxidation of organic substrates, RH, by H_2O_2 (*99,100*) (reactions (47) and (48)):

$$Fe^{2+}(aq) + H_2O_2 \rightleftarrows Fe^{2+}H_2O_2 \rightarrow Fe^{3+}(aq) + OH^- + OH^\bullet \quad (47)$$

$$RH + OH^\bullet \rightarrow R^\bullet + H_2O \quad (48)$$

Under some conditions, the active oxidant is Fe(IV)=O and not the hydroxyl radical (*101*). Reactions entailing other low-valent transition-metal complexes that react like iron are called Fenton-like reactions (*100,102,103*). Fenton-like reactions were studied with $Cu^+(aq)$ and its complexes, such as $[Cu(I)(phenanthroline)_2]^+$ (*102*). The results of these studies indicate that transient complexes, Cu(I)-H_2O_2, are formed. However, $OH^\bullet$ is not formed directly as proposed in reaction (47) (*103*).

The rate constant of reaction (49) was determined (*103*).

$$2Cu^+(aq) + H_2O_2 + 2H^+ \rightarrow 2Cu^{2+}(aq) + 2H_2O, \quad k = (4.1 \pm 0.4) \times 10^3\,M^{-1}\,s^{-1} \quad (49)$$

The rate constant determined in the presence of 1 M *tert*-butyl alcohol is slower than that observed in the absence of the alcohol, $k = (3.8 \pm 0.2) \times 10^3\,M^{-1}\,s^{-1}$ (*103*). The decrease in the reaction rate constant could not be explained by the reaction between

Cu^{+}(aq) with *tert*-butyl alcohol radical, which is very fast (*104*), $k = 2.6 \times 10^{10}\ M^{-1}\ s^{-1}$. Masarwa (*103*) explained this result as indicating that the transient $(H_2O)_nCu^{+\bullet}O_2H^{-}$ reacts with the organic substrate, thus changing the mechanism occurring in the absence of an organic substrate (*103*).

The study of Fenton-like reactions is significant for biological systems. Csapski *et al*. studied the Fenton reaction in the presence of $[Cu(I)(phenanthroline)_2]^{+}$ and DNA (*102*). They showed that the Cu(I) complex binds to DNA, the double helical structure of which was degraded by either the $^{\bullet}OH$ radical or $[Cu(III)(phenanthroline)_2]^{3+}$, which is formed via the oxidation of $[Cu(I)(phenanthroline)_2]^{+}$ by H_2O_2.

E. Ligand Effects on the Chemical Activity of Copper(I) Complexes

Ligands are expected to affect the kinetics of reaction of a central cation differently for reactions that proceed via the outer-sphere mechanism than for those which proceed via the inner-sphere mechanism:

a. The effect of ligands on the kinetics of outer-sphere reactions is expected to be due to two factors: the effect of the ligands on the redox potential of the central cation and on the rate constant of the electron self-exchange reaction.
b. The effect of ligands on the kinetics of inner-sphere reactions is expected to be due to several factors:
   1. The effect of the ligand on the redox potential of the central cation.
   2. Steric hindrance that might inhibit the formation of the transient complex.
   3. The rate constant of ligand exchange that affects the rate of formation of the complex.
   4. The stability constant of the transient complex as discussed above for reaction of Cu(I) with O_2.

Therefore, the effect of some ligands on the kinetics of reactions which proceed via the two mechanisms was studied: reaction (50) was chosen as an example of a reaction which proceeds via the outer-sphere mechanism (*105*) and reactions (51)–(53) were chosen as examples of reactions which proceed via the inner-sphere mechanism (*25,29,41,61*).

$$[(cyclam)Ni(III)(SO_4)_2]^{-} + [Cu(I)L]^{+} \rightarrow [(cyclam)Ni(II)(SO_4)_2]^{2-} + [Cu(II)L]^{2+} \qquad (50)$$

$$\left[(NH_3)_5CoIII\right)Cl]^{2+} + [Cu(I)L]^{+} \rightarrow \text{Products} \quad (51)$$

$$NO_2^{-} + [Cu(I)L]^{+} \rightarrow \text{Products} \quad (52)$$

$$Cl_3CCOO^{-} + [Cu(I)L]^{+} \rightarrow \text{Products} \quad (53)$$

The ligands studied were L^2 and L^6, Fig. 6, which shift the redox potential of the complex cathodically, acetonitrile and fumaric acid (fum), which shift the redox potential anodically. The latter two ligands slow down the rate constants of all the reactions studied, Table II, as expected due to their effect on the redox potential of Cu(I).

On the other hand, $[Cu(I)L^2]^{+}$ (*10,24*), a stronger reducing agent than Cu^{+}(aq), affects the rate constants of the reduction reactions in a more complex way. The rate constant of the outer-sphere reduction is nearly not affected, that is, the decrease in the rate constant of the electron self-exchange reaction compensates the increase in the redox potential. For the inner-sphere reactions, L^2 slows down the reaction with Cl_3CCOO^{-} probably due to steric hindrance. On the other hand, L^2 accelerates considerably the reduction of NO_2^{-} probably by stabilizing the transient complex $L^2Cu(I)NO_2$ and has only a minor effect on the rate of reduction of $[Co(III)(NH_3)_5Cl]^{2+}$.

F. Electron Self-exchange Rate Constant

The rate constants, k_{12}, of redox reactions proceeding via the outer-sphere mechanism, for example, reaction (50) (*105*), depend, according to the Marcus theory (*85–87*) (Eqs. 54 and 55), on the equilibrium constant of the cross-reaction, K_{12}, and on the electron self-exchange rate constants, k_{11} and k_{22}, of the redox couples.

$$k_{12} = (k_{11}k_{22}K_{12}\, f_{12})^{1/2} W_{12}{}^{1-3}, \quad (W_{12} \text{ is the work function and } \Delta G^{o} = -RT\ln K_{12}) \quad (54)$$

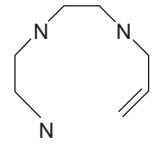

Fig. 6. Lewis structure of L = 1,4,7-triaza-decane-9-ene.

TABLE II

RATE CONSTANTS FOR ELECTRON TRANSFER REACTIONS (50)–(53)

$[Cu(I)L]^+$	$k_{2.26}$ ($M^{-1}\,s^{-1}$) (25)	$k_{2.27}$ ($M^{-1}\,s^{-1}$) (25)	$k_{2.28}$ ($M^{-1}\,s^{-1}$) (61)	$k_{2.29}$ ($M^{-1}\,s^{-1}$) (29)	E^{o}[b]
Cu^+(aq)	3.0×10^4	5.4×10^4	5.0 At pH 4.9	6.0	0.15 (5)
$[Cu(I)L^2]^+$ (for reactions (50)–(52)	2.3×10^4	2.4×10^4	35 ± 10 At pH 5	0.14	0.08 (for L^2) (24)
$[Cu(I)L^6]^+$ (for reaction (53)[a]					-0.035 (for L^6) (10)
$[Cu(I)fum]^+$	$\leq3.0\times10^1$	1.0×10^2	Not studied	<0.015	0.38
$[Cu(I)(CH_3CN)]^+$	$\approx8.5\times10^2$	2.2×10^2	Ac decreases the		0.35
$[Cu(I)(CH_3CN)_n]^+$	$\approx5.0\times10^1$	9.3	rate	$n=2$ 0.075	0.41

[a] Reaction (53) was studied with L^6.

[b] E° is the redox potential for the $[Cu(II/I)L]^{2+/+}$ couple with respect to NHE.

$$\ln f_{12} = \frac{\ln K_{12}}{4\ln(k_{11}k_{22}/Z^2)} \tag{55}$$

Several electron self-exchange rate constants of the $Cu(II/I)_{aq}$ couple, reaction (56), were derived applying the Marcus cross-relation (Table III).

$$^{*}Cu^{2+}(aq) + Cu^{+}(aq) \overset{k_{11}}{\rightleftarrows} {}^{*}Cu^{+}(aq) + Cu^{2+}(aq) \tag{56}$$

The discrepancy between the results seems to be beyond experimental error, though three of the four systems yield k_{11} within reasonable experimental error. If the results derived from the reactions with $[Co(II)Sep]^{2+}$ and $[Co(III)(en)_3]^{3+}$ are not experimental errors, then one has to conclude that in the other systems vibrationally excited products are formed in the cross-reaction and that $k_{11}(Cu^{2+/+}(aq) \leq 1 \times 10^{-9}\ M^{-1}\ s^{-1}$ (*109*).

k_{11} was evaluated applying the Marcus cross-relation also for a variety of copper complexes. The results point out that ligands affect considerably the electron self-exchange rate constants. In Tables IV and V are listed few examples of electron self-exchange rate constants of blue copper proteins and copper complexes, respectively.

The electron self-exchange rate constants of proteins are considerably larger than those of the inorganic copper complexes (Tables IV and V) (*11,25,106,111*). This is attributed to the large changes in the coordination sphere structures of the Cu(II) and Cu(I) inorganic complexes in comparison to the relative rigid active sites of the proteins.

Similarly, the ligands in the complex $[CuL^{10}{}_2]^{2+/+}$ (*11*) enforce a tetrahedral, or a distorted tetrahedral, coordination sphere, and therefore, a relatively large k_{11} is observed for this complex (Fig. 7).

The k_{11} values for the other $[CuL^{i}]^{2+/+}$ couples are all relatively slow. As they were all derived applying the Marcus cross-relation, the question whether in the reactions studied the products are not vibrationally excited has to be analyzed.

For several other ligands, for example, L^9, the electron transfer reactions were shown to proceed via the "gated mechanism," that is, via the formation of unstable transients with the coordination configuration of the reactant (*11*) (Scheme 2).

G. Reaction of $Cu^{+}(aq)$ with Hydrogen Atoms

$Cu^{2+}(aq)$ catalyzes, though slowly, hydrogenation reactions (*112*). It was proposed that the key intermediate in this process is $Cu^{II}H^{+}(aq)$ formed via (*112*):

TABLE III

K_{11} REPORTED IN THE LITERATURE FOR THE $Cu(II/I)_{aq}$ COUPLE

k_{11} ($M^{-1}\,s^{-1}$) for reaction (56)	Redox reaction studied[a]	ΔE° (V)[a]
1.0×10^{-4} (*106*)	$[Ni(I)decamethylcyclam]^{+}+Cu^{2+}(aq)\rightleftarrows[Ni(II)$ decamethylcyclam$]^{2+}+Cu^{+}(aq)$	1.049 (*107*)
2.6×10^{-4} (*25*)	$[Ni(III)Cyclam(SO_4^{2-})_2]^{-}+Cu^{+}(aq)\rightleftarrows[Ni(II)Cyclam(SO_4^{2-})_2]^{2-}+Cu^{2+}(aq)$	0.637 (*25*)
5.0×10^{-7} (*108*)	$[Co(II)Sep]^{2+}+Cu^{2+}(aq)\rightleftarrows[Co(II)Sep]^{3+}+Cu^{+}(aq)$	0.413 (*108*)
$\leq1\times10^{-9}$ (*109*)	$[Co(III)(en)_3]^{3+}+Cu^{+}(aq)\rightleftarrows[Co(II)(en)_3]^{2+}+Cu^{2+}(aq)$	0.41 (*109*)
2.0×10^{-4} (*52*)	$[Ru(III)L]+Cu^{+}(aq)\rightleftarrows[Ru(II)L]+Cu^{2+}(aq)$	(0.267–0.547) (*53*)

[a] E° $(Cu^{+}(aq)+e^{-}\rightarrow Cu^{+}(aq))=0.153$ V.

TABLE IV

ELECTRON SELF-EXCHANGE RATE CONSTANTS OF BLUE COPPER PROTEINS

Blue copper protein	k_{11} ($M^{-1}\,s^{-1}$)
A.v. plastocyanin (*39*)	$(1.50 \pm 0.13) \times 10^5$
Stellacyanin (*40*)	1.2×10^5
Azurin (*17*)	$(2.4 \pm 1.0) \times 10^6$

TABLE V

ELECTRON SELF-EXCHANGE RATES CONSTANTS FOR [CUII/I)L]

$[CuL]^{2+/+}$	k'_{11} ($M^{-1}\,s^{-1}$)
$[CuFum]^{II/I}$ (*25*)	$\leq 3.0 \times 10^{-7}$
$[CuCH_3CN]^{II/I}$ (*25*)	$\sim 9.7 \times 10^{-5}$
$[Cu(CH_3CN)_2]^{II/I}$ (*25*)	$\sim 2.2 \times 10^{-6}$
$[CuL^2]^{II/I}$ (*25*)	1.4×10^{-5}
$[CuL^7]^{II/I}$ (*11*)	0.4
$[CuL^8]^{II/I}$ (*11*)	4×10^{-4}–0.015[a]
$[CuL^9]^{II/I}$ (*11*)	0.01
$[CuL^{10}]^{II/I}$ (*11*)	0.71–427[a]
$[CuL^{11}]^{II/I}$ (*110*)	10^3

[a] k_{12} for those complexes were studied with several oxidation reagents. There is a range for the same k_{11}. The reason for this range is the same for the range which was formed to k_{11} of the $Cu^{2+/+}$(aq) couple.

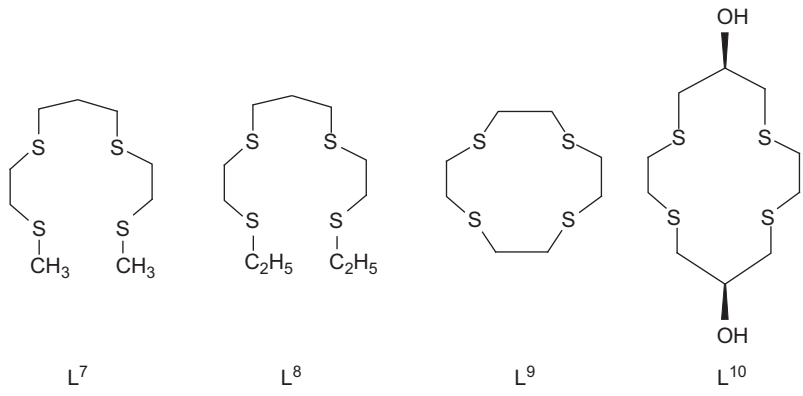

FIG. 7. Lewis structures for L^7 = 2,5,9,12-tetrathiatridecane; L^8 = 3,6,10,13-tetrathiapentadecane; L^9 = 1,4,7,10-tetrathiacyclododecane; L^{10} = *syn*-3,6,10,13-tetrathiacyclotetradecane-1,8-diol.

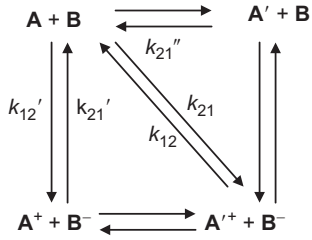

SCHEME 2. The square mechanism (*11*).

$$Cu^{2+}(aq) + H_2 \leftrightarrows Cu^{II}H^+(aq) + H^+(aq) \tag{57}$$

It seemed therefore of interest to measure the properties of $Cu^{II}H^+(aq)$. This was done by the following reaction:

$$H^\bullet + Cu^+(aq) \rightarrow Cu^{II}H^+(aq) \tag{58}$$

using the pulse radiolysis technique (*113*).

The intermediate $Cu^{II}H^+(aq)$ is formed via reaction (56) that has a rate constant of $(5 \times 10^9 \leq k \leq 2 \times 10^{10}) M^{-1} s^{-1}$ (*113*). $Cu^{II}H^+(aq)$ decomposes with a rate constant of $(4.0 \pm 1.5) \times 10^3\ s^{-1}$ (*113*) a process which is attributed to reaction (59):

$$Cu - H^+(aq) + H_2O \rightarrow Cu^{2+}(aq) + H_2 + OH^-(aq) \tag{59}$$

a heterolytic decomposition of the Cu^{II}—H bond (*113*).

H. REACTION OF CU(I) WITH CARBON-CENTERED ALKYL RADICALS

Copper complexes are catalysts in a variety of processes which involve as transients compounds with Cu—C σ bonds (*114,115*). These, or analogous, transients can be formed via the reactions:

$$Cu(I) + {}^\bullet R \rightarrow Cu^{II} - R \tag{60}$$

$$Cu(II) + {}^\bullet R \rightarrow Cu^{III} - R \tag{61}$$

Reaction (58) is always considerably faster than reaction (61) (*49,116*).

It has been proposed that the transient species formed in reactions (60) and (61) are key intermediates in catalytic processes or simple model compounds to these intermediates.

The rate constant of all reactions or alkyl radicals with $Cu^+(aq)$, reaction (61a)

$$Cu^{+}(aq) + {}^{\bullet}R \rightarrow Cu^{II} - R(aq), \quad k > 10^{8}\,M^{-1}\,s^{-1}\,(121) \qquad (61a)$$

approach the diffusion-controlled limit (*116*). However, the analogous reactions of $[Cu(I)L^{2}]^{+}$ are considerably slower (*49*).

The simplest transient formed in reaction (61a) is Cu^{II}—$CH_3(aq)$ (*117*). This transient decomposes via

$$2Cu^{II} - CH_3(aq) \rightarrow 2Cu^{+}(aq) + C_2H_6, \quad k(49) = 1.5 \times 10^{8}\,M^{-1}\,s^{-1} \qquad (62)$$

without the involvement of ${}^{\bullet}CH_3$ radicals. The analogous decomposition reaction of $L^{2}Cu^{II}$–$CH_3{}^{+}(aq)$ proceeds via the same mechanism, though with a lower rate constant (*49*). Also Cu^{II}–$CH_2CH_2CO_2{}^{-}$ decomposes via an analogous mechanism (*49*). However, $L^{2}Cu$–$CH_2CH_2CO_2{}^{-}$ decomposes via homolysis (*49*) of the Cu^{II}—C bond a result suggesting that L^{2}, due to steric hindrance, weakens the Cu^{II}—C bond. The only carbon-centered radicals which are known to react with $Cu^{+}(aq)$ to form intermediates which decomposes via homolysis are the ${}^{\bullet}CR^{1}R^{2}OH$ radicals which are strong reducing agents:

$$Cu^{+}(aq) + {}^{\bullet}CR^{1}R^{2}OH \rightleftarrows Cu - CR^{1}R^{2}OH, \quad K \qquad (63)$$

For the ${}^{\bullet}CH_2OH$ radical, $K = 5 \times 10^{3}\,M^{-1}$ (*116*). For ${}^{\bullet}C(CH_3)_2OH$ and ${}^{\bullet}CH(CH_3)OH$, K is too small to be measured. Cu^{II}–$CHRCO_2{}^{-}$, $R = H, CH_3$, and $L^{2}Cu^{II}$–$CHRCO_2{}^{-}$, decomposes heterolytically, L^{2} slows down this process (*49*).

Transient complexes of the type Cu^{II}–$CR^{1}R^{2}CR^{3}R^{4}X$, where $X = OH$ (*118*), $NH_3{}^{+}$ (*118–120*), $OPO_3{}^{2-}$, decompose via β elimination of X^{-}.

$$Cu^{II} - CR^{1}R^{2}CR^{3}R^{4}X \rightarrow Cu^{2+}(aq) + R^{1}R^{2}C = CR^{3}R^{4} + X^{-} \qquad (64)$$

For $(phen)_2Cu^{II}$—$CR^{1}R^{2}CR^{3}R^{4}X$, this reaction is slowed down considerably (*121*).

When methyl radicals react with $Cu(CO)_n(aq)$, $n = 1$–4, the following reactions occur (*122*):

$$Cu(CO)_n(aq) + {}^{\bullet}CH_3 \rightarrow (CO)_nCu^{II} - CH_3 \qquad (65)$$

$$(CO)_nCu^{II} - CH_3 \rightarrow (CO)_{n-1} - Cu^{II} - C(CH_3) = O \rightarrow Cu^{2+}(aq) + CH_3CHO \qquad (66)$$

Finally, it should be pointed out that none of the transients LCu^{II}–$CR^{1}R^{2}R^{3}$ or Cu^{II}–$H^{+}(aq)$ decompose via reduction of the copper ion. This is attributed to the observation that all these

reactions, including the reaction (67), are endothermic due to the lattice energy of $Cu^{\circ}(s)$.

$$Cu^{II} - H^{+}(aq) \rightarrow Cu^{o}(aq) + H^{+}(aq) \tag{67}$$

I. Ligand Exchange Reactions

The kinetics of the reaction

$$Cu(H_2O)_n^{+} + H_2O^{*} \rightleftarrows Cu(H_2O)_{n-1}H_2O^{*+} + H_2O \tag{68}$$

were not measured. However, the observation that the rate constants of the reactions

$$\begin{gathered} Cu^{+}(aq) + cis/trans\, HO_2CCH = CHCO_2H \rightarrow \\ [Cu(I)cis/trans\, HO_2CCH = CHCO_2H]^{+} \end{gathered} \tag{69}$$

approach the diffusion-controlled limit $k \approx 2 \times 10^9\ M^{-1}\ s^{-1}$ suggests that the $k_{2.42} \geq 10^9\ s^{-1}$ (7). Furthermore, the same conclusion is derived from the observation that the rate constants of all the reactions

$$Cu^{+}(aq) + H^{\bullet}/{}^{\bullet}CR^1R^2R^3 \rightarrow Cu^{II} - H/CR^1R^2R^3 \tag{70}$$

are higher than $10^9\ M^{-1}\ s^{-1}$. This conclusion is based on the assumption that $Cu^{+}(aq)$ is not the linear $[Cu(I)(H_2O)_2]^{+}$ complex which would allow approach of $^{\bullet}R$ or the alkene without the displacement of an aquo ligand.

When the $[Cu(II)L^{12-15}]^{2+}$ are reduced via a fast reaction, the following reactions are observed (*116,123*) (Fig. 8).

$$\left[Cu(II)L^{12-15}\right]^{2+}(planar) + CO_2^{\bullet -} \rightarrow \left[Cu(I)L^{12-15}\right]^{+}(planar) + CO_2 \tag{71}$$

$$\left[Cu(I)L^{12-15}\right]^{+}(planar) + H_3O^{+}/H_2O \rightleftarrows \left[Cu(III)L^{12-15} - H\right]^{2+} + H_2O/OH^{-} \tag{72}$$

$$\left[Cu(I)L^{12-15}\right]^{+}(planar) + CO_2^{\bullet -} \rightarrow \left[Cu(I)L^{12-15}\right]^{+}(tetrahedral) \tag{73}$$

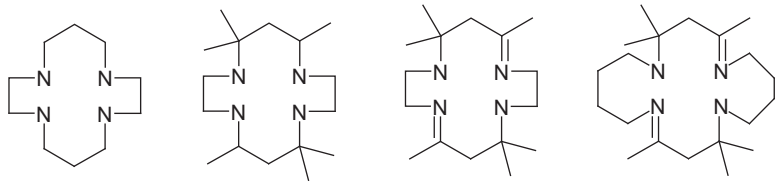

FIG. 8. Lewis structures for L^{12} = 1,4,8,11-tetraazacyclotetradecane; L^{13} = c-racemic 5,7,7,12,14,14-hexamethyl-1,4,8,11-tetraazacyclotetradecane; L^{14} = 5,7,7,12,14,14-hexamethyl-1,4,8,11-tetraazacyclo-tetradeca-4,11-diene; L^{15} = 2,2,4,11,11,13-hexamethyl-1,5,10,14-tetraazacyclo-octadeca-4,13-diene.

$$\left[\mathrm{Cu(III)L^{12-15}-H}\right]^{2+} \rightleftarrows \left[\mathrm{Cu(I)L^{12-15}}\right]^{+}(\text{tetrahedral}) \tag{74}$$

$$\left[\mathrm{Cu(III)L^{12-15}}\right]^{2+} \text{or} \left[\mathrm{Cu(I)L^{12-15}}\right]^{+}(\text{tetrahedral}) + \mathrm{H_3O^+} \rightarrow \mathrm{Cu^+(aq)} + \left(\mathrm{H_2L^{12-15}}\right)^{2+} \tag{75}$$

A comparison of the rate constants of the isomerization reaction, to form the tetrahedral complex, and the ligand loss reaction, reaction (75), points out the following (*123,124*):

1. The rate constants for L^{12} are considerably higher than for L^{13}, that is, the steric bulkiness added by the methyl substituents slows down considerably the ligand exchange.
2. The rate constants for L^{13} and L^{14} are similar, that is, the unsaturation of the ligand has little effect on the kinetics.
3. The rate constant for L^{15} is higher than that for the other ligands, that is, the flexibility of the ligand affects, as expected, the kinetics of the ligand exchange reactions.
4. $[Cu(I)L^{14}]^+$ is stable at $pH \geq 7$.
5. $[Cu(I)L^{15}]^+$ disproportionation, that is, the two central copper ions can approach each other.

IV. Catalysis

Copper complexes are known to catalyze a variety of processes (*30,125–132*). Most of these processes are redox processes. The choice of copper complexes as catalysts for these processes is due too:

1. The redox potential of these complexes transforms Cu(I) complexes to be reasonably good single-electron reducing

agents and the corresponding Cu(II) complexes reasonably good oxidizing agents.
2. The ligand exchange rate constants of both Cu(I) and Cu(II) complexes are very fast, a property which is essential as the electron self-exchange rates of the Cu(II/I)(aq) couple and many Cu(II/I)L_m complexes are relatively slow, and therefore, most redox processes proceed via the inner-sphere mechanism (*25,30,61,132*).
3. The tendency of both Cu(I) and Cu(II) complexes to react with alkyl and aryl radicals, $R^{\bullet}$, to form transient complexes of the type Cu(II)—R or Cu(III)—R is essential in a large variety of catalytic processes, though mainly in aprotic solvents (*49,116,133*).
4. The tendency of Cu(I) to form $d \rightarrow \pi$ complexes with alkenes and aromatic compounds (*12,33*).

A. Catalysis of Redox Reactions in Aqueous Solutions

Copper ions catalyze a variety of inorganic redox reactions. The kinetics and mechanisms of some of these reactions were analyzed in detail. Thus, the reduction of V(IV) by Sn(II) and Ge(II) is catalyzed by Cu ions in the presence of high concentrations of Cl^-. The mechanism involves the reduction of Cu(II) by Sn(II) or by Ge(II) followed by the reduction of V(IV) by Cu(I) (*134*). These reactions proceed via the inner-sphere mechanism (*134*). Also the copper-catalyzed reduction of peroxonitrite by sulfite (*135*), the copper-catalyzed reduction of a Ni(IV) complex by thiols (*136*), and the reduction of superoxide bound to binuclear cobalt(III) complexes by thiols (*137*) and by ascorbate (*138*) follow analogous inner-sphere mechanisms. Copper ions also catalyze the reduction of peroxide-bound Cr(IV) by ascorbate(*139*).

A mechanism involving the polarization of the ascorbate ligand by a Cu(II) central ion was proposed (*138*), though the involvement of Cu(I) cannot be ruled out (*139*). All these reactions proceed via the inner-sphere mechanism; however, the copper-catalyzed reduction of superoxide bound to a binuclear cobalt(III) complex by 2-aminoethanethiol proceeds via the outer-sphere mechanism (*140*). This is attributed to the effect of 2-aminoethanethiol as a ligand on the rate constant of the Cu(II/I) electron self-exchange reaction which is suggested to proceed via the "gated" mechanism.

When copper ions are added to the Fenton reaction, the mechanism changes from

$$Fe(H_2O)_6^{2+} + H_2O_2 \rightarrow Fe(H_2O)_6^{3+} + {}^{\bullet}OH + OH^- \quad (76)$$

$$RH + {}^{\bullet}OH \rightarrow R^{\bullet} + H_2O \quad (77)$$

$$2R^{\bullet} \rightarrow R_2/(R - H + RH) \quad (78)$$

$$R^{\bullet} + Fe(H_2O)_6^{3+} \rightarrow R^+ + Fe(H_2O)_6^{2+} \quad (79)$$

to

$$R^{\bullet} + Cu(H_2O)_n^{2+} \rightarrow Cu^{III} - R(aq) \quad (80)$$

$$Cu^{III} - R(aq) \rightarrow Cu(I)(aq) + ROH/R_{-H} \quad (81)$$

$$Cu(I)(aq) + Fe(H_2O)_6^{3+} \rightarrow Cu(H_2O)_n^{2+} + Fe(H_2O)_6^{2+} \quad (82)$$

This shift in mechanism is due to the fact that reaction (79) is considerably slower than reaction (80) (*115,141*). These reactions have naturally to be considered also in the Cu(I)-catalyzed Fenton-like reactions where $R^{\bullet}$ radicals are formed. These processes are of special importance in biological systems in which copper complexes are known to induce oxidative stress (*142–147*). The Cu(I) species are formed in biological systems by reduction of Cu(II) by ascorbate, thiols, etc.

B. Copper Catalysis in Synthetic and Industrial Processes

Copper is commonly used as a catalyst for a variety of organic reactions applying organometallic intermediates (*114,115, 148–150*). These processes include the Ullmann reaction, the Sandmeyer reaction, the Meerwein reaction, the Click reaction, a variety of atom transfer processes including polymerizations, etc. Many of these processes involve radicals and redox processes initiated by the copper species. All these processes are usually carried out in aprotic solvents and are therefore beyond the scope of this review. However, the mechanism of some of them was studied in aqueous solutions with the hope to perform them in this medium and in order of determining their detailed mechanisms.

B.1. The Ullmann reaction

In general, the Ullmann reaction is the transformation of a halide, X, with a hydroxide (*12,30,151,152*) or with an OR reaction (83):

$$ArX + OR^- \xrightarrow{Cu^o/Cu^{II}} ArOR + X^-(R = H; alkyl; aryl) \qquad (83)$$

Like other processes catalyzed by Cu(I), it is slow. It has been shown, however, that certain ligands can stabilize the monovalent copper, thus facilitating an increase in its concentration, which, in turn, augments the rate of the reaction (*30,151*).

This reaction was studied in the presence of acetonitrile, NH_3 or L^2 as ligands to monovalent copper in aqueous solutions (*30,151*). Each ligand has a unique effect on the redox potential of the Cu(I) complex and stabilizes Cu(I) in a different way as was mentioned in Section II. The addition of a ligand increases the Cu(I) concentration in the solution, but it also influences the reactivity of the Cu(I) as a catalyst (*30,151*).

The catalytic formation of salicylic acid from *o*-bromo-benzoic acid was chosen as a model for studying the Ullmann reaction in aqueous solution (reaction (84)) (*30,151*):

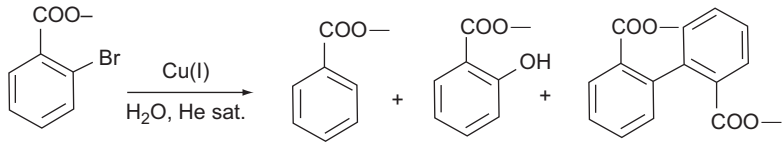

(84)

The Cu(I) has two roles in this process, the first is binding to the aromatic ring, thus weakening the C—Br bond. This is followed by debromination and formation of a transient with a Cu(II)—C σ bond (species **1**, Fig. 9). The formation of benzoic acid is faster under acidic conditions than under alkaline conditions. This could be because the reaction of species **1** with H_2O is slower than the reaction of species **1** with H_3O^+ (*30*).

To decrease the yield of the reaction by-product, benzoic acid, the pH should be kept above 8. Using the ligand L^2 as a buffer and as a ligand of Cu(I), the reaction is markedly accelerated. Furthermore, L^2 inhibits the formation of diphenoic acid (*30*), possibly due to the steric hindrance induced by the ligand. Thus $[Cu(I)L^2]^+$ is a very good catalyst for this reaction in slightly alkaline aqueous solutions (*30*).

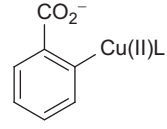

FIG. 9. Species **1**.

B.2. The Sandmeyer reaction

In the Sandmeyer reaction, a diazonium ion, ArN_2^+, is decomposed and a halogen, X, is substituted by Cu(I) as catalyst (*127,129,130*), reaction (85):

$$ArN_2^+ + X^- \xrightarrow{Cu^{o/CuII}} ArX + N_2 \quad (X = \text{halogen}, Ar = \text{aryl}) \qquad (85)$$

The proposed mechanism for this reaction is presented in reactions (86)–(88):

The first step is the release of N_2 from ArN_2^+ and the formation of the aryl radical, $Ar^\bullet$, and divalent copper salt, reaction (86):

$$ArN_2^+ + Cu^{I}Cl_2^- \rightarrow Ar^\bullet + N_2 + Cu^{II}Cl_2 \qquad (86)$$

The second step is the formation of a σ bond between the aryl radical and the halogen, X (reaction (87)), and the reduction of Cu(II) to Cu(I).

$$Ar^\bullet + Cu^{II}Cl \rightarrow ArCl + Cu^{I}Cl \qquad (87)$$

The last step is reaction (88), the formation of the monovalent Cu complex.

$$Cl^- + Cu^{I}Cl \rightarrow Cu^{I}Cl_2^- \qquad (88)$$

If the reaction is run in aqueous solutions, OH^- from the water can replace the halide as the aryl substituent, thus forming phenols (*129*). The reaction of the 2-benzoylphenyl radical to form the corresponding phenol is slower than the reaction forming the halo-aryl. The hydroxylation rate constant equals $(1.47 \pm 0.17) \times 10^6\ M^{-1}\ s^{-1}$ (*129*), and the chlorination rate constant equals $8.8 \times 10^6\ M^{-1}\ s^{-1}$ (*129*).

B.3. The Meerwein reaction

The Meerwein reaction, reaction (89), is carried out with alkenes (*127,132,153*), which are known Cu(I) ligands.

$$ArN_2^+ + H_2C{=}CHR \xrightarrow{CuCl/\ -\ N_2} ArCH_2CHClR + Cu^+ \quad (Ar = \text{aryl}) \qquad (89)$$

This reaction is a useful tool for the synthesis of molecules such as indols (*154*), quinolinones (*155*), and benzothiophenes (*156*), all of which play important roles in the pharmaceutical industry. Despite the economic importance of this reaction and the many studies done in this field, its mechanism is still not fully

elucidated. Schrauzer *et al*. (*157*) suggested that the first step in the mechanism is reaction (90), in which Cu(I) activates the ethene double bond.

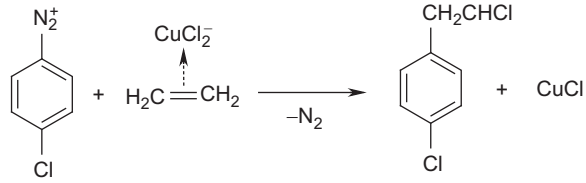

(90)

Vogel *et al*. (*158,159*) suggested a mechanism involving cupric chloride, $CuCl_3^-$ (reaction (91)), in which the active species is Cu(II):

$$p\text{–}ClC_6H_4N_2{}^+Cl^- + CH_2{=}\,CH_2CuCl_3{}^- \underset{-N_2}{\rightarrow} p\text{–}ClC_6H_4CH_2CH_2Cl + CuCl_3{}^- \qquad (91)$$

Recently, Wolfer *et al*. (*160*) proposed that the first step in the mechanism is the formation of a complex between Cu(I) and the aryl-diazonium, displayed in Fig. 10. Next the nitrogen is released and an aryl radical forms. The active species is Cu(I), which activates the aromatic ring and initiates the reaction; as mentioned above (*12*) Cu(I) binds aromatic compounds as ligands.

B.4. The Click reactions

Click reactions are a variety of condensation reactions in which Cu(I) is used as a catalyst for the synthesis of oligomers or polymers. The starting reactants are typically alkyne-azides (*125*), but thiol-enes (TEC) and other alkenes (Diels–Alder) are also used (*128*). Several of their properties—selectivity, high yield, mild conditions, for example, room temperature, and fast reactions that proceed via minimal steps—make them desirable for use in green chemistry, a relatively new field that has undergone explosive development in recent years (*125,126,128,161*).

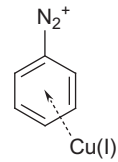

FIG. 10. Species **2**.

Because of these features, they are also popular in the synthesis of biologically important molecules.

The suggested mechanisms of the various catalytic Click reactions involve the formation of dinuclear or tetranuclear copper complexes (*162,163*) as the catalyst (Fig. 11) and the creation of a Cu—C bond or a Cu═C bond in the intermediate species (*49,121,122,162–166*). DFT calculations were used to ascertain the relative stabilities of such complexes (*163*), showing that the mononuclear complex was more stable than the polynuclear complex.

Finn *et al.* (*162*) studied the kinetics of the reaction between benzyl-azide and phenylacetylene in a DMSO/H_2O solution (reaction (92)):

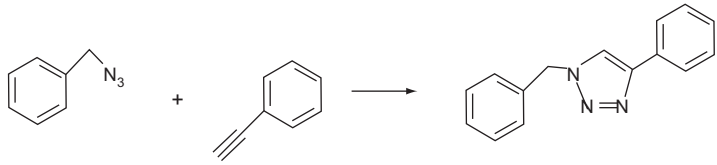

(92)

Under the experimental conditions, with Cu(I) in excess, the rate law is

$$\text{rate} = k[\text{alkyne}]^{1.3\pm0.2}[\text{azide}]^{1\pm0.2}[\text{Cu(I)}]^{0} \qquad (93)$$

Under catalytic conditions, the reaction was independent of the alkyne concentration and second order with respect to Cu(I) (*163*). The first step in the suggested mechanism is the formation of a dinuclear copper complex, an intermediate species that reacts with the azide.

B.5. Heterogeneous catalysis

Copper complexes adsorbed (*167–169*) and covalently (*170*) bound to electrode surfaces were shown to be good electrocatalysts for the four-electron reduction of dioxygen. The results indicate that a $Cu_2O_2L_2$ (L = phenantroline) intermediate is formed during the reduction.

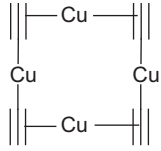

FIG. 11. Tetranuclear copper.

In principle, binding a copper catalyst to a surface requires that during the catalytic cycle the copper ions will not be released into the solvent. Recently, it was shown that this is even the case for $Cu(OH)_xAl_2O_3$ which contains ca. 10% water as a catalyst for the catalytic synthesis of *N*,*N*-bicyclic pyrazolidinone in organic solvents, a process which involves Cu(I) as the reactive intermediate (*171*).

V. Summary

This review summarizes a variety of important processes in which Cu(I) is involved as a reducing agent and as a catalyst. We addressed the factors that affect its stability in aqueous solutions, focusing on the rate of the electron transfer and on the mechanism of those processes. Although a wide variety of studies were reviewed here, they all point out that the ligands have major effects on the reaction rates and mechanisms. We hope that this review will shed light on the importance of, and complications involved in, reactions in aqueous solutions and as such contribute to the development of processes that utilize water as a solvent.

Abbreviations

AxNIR, AcNIR	bacterial sources of CuNIR
CuNIR	copper nitrite reductases
cyclam	1,4,8,11-tetraazacyclotetradecane
en	ethylenediamine
FeNIR	iron nitrite reductases
fum	fumaric acid
L^1	1,4,5,7,7,8,11,12,14,14-decamethyl-1,4,8,11-tetrraazacyclatetetradecane
L^{10}	*syn*-3,6,10,13-tetrathiacyclotetradecane-1,8-diol
L^{11}	dmp = 2,9-dimethyl-1,10-phenanthroline
L^{12}	1,4,8,11-tetraazacyclotetradecane
L^{13}	c-racemic 5,7,7,12,14,14-hexamethyl-1,4,8,11-tetraazacyclotetradecane
L^{14}	5,7,7,12,14,14-hexamethyl-1,4,8,11-tetraazacyclo-tetradeca-4,11-diene
L^{15}	2,2,4,11,11,13-hexamethyl-1,5,10,14-tetraazacyclo-octadeca-4,13-diene
L^2	2,5,8,11-tetramethyl-2,5,8,11-tetraaza-dodecane
L^3	2,5,8-trimethyl-2,5,8-triaza-undecane-10-ene
L^4	2,9 dimethylphenanthroline
L^5	a binucleating ligand having a heme and covalently tethered copper binding tris(2-pyridyl)methylamine tetradentate
L^6	1,4,7-triaza-decane-9-ene

L^7	2,5,9,12-tetrathiatridecane
L^8	3,6,10,13-tetrathiapentadecane
L^9	1,4,7,10-tetrathiacyclododecane
Sep	sepulchrate
SOD	superoxide dismutase enzyme
THF	tetrahydrofuran

References

1. Cotton, F. A.; Wilkinson, G. *Advanced Inorganic Chemistry* (3rd edn.). Interscience Publishers: New York, **1972**.
2. Weast, R. C. *CRC Handbook of Chemistry and Physics.* CRC: Boca Raton, FL, **1987**.
3. Endicott, J. F.; Taube, H. *Inorg. Chem.* **1965,** *4*, 437.
4. Altermatt, J. A.; Manahan, S. E. *Inorg. Nucl. Chem. Lett.* **1968,** *4*, 1.
5. Latimer, W. M. *Oxidation Potentials.* Prentice-Hall: New York, **1961**.
6. Dean, J. A. *Lange's Handbook of Chemistry.* McGraw-Hill: New York, **1992**.
7. Meyerstein, D. *Inorg. Chem.* **1975,** *1716–1717*, 1716.
8. Rorabacher, D. B.; Meagher, N. E.; Juntunen, K. L.; Robandt, P. V.; Leggett, G. H.; Salhi, C. A.; Dunn, B. C.; Schroeder, R. R.; Ochrymowycz, L. A. *Pure Appl. Chem.* **1993,** *65*, 573.
9. Navon, N.; Masarwa, A.; Cohen, H.; Meyerstein, D. *Inorg. Chim. Acta* **1997,** *261*, 29.
10. Navon, N.; Golub, G.; Cohen, H.; Paoletti, P.; Valtancoli, B.; Bencini, A.; Meyerstein, D. *Inorg. Chem.* **1999,** *38*, 3484.
11. Rorabacher, D. B. *Chem. Rev.* **2004,** *104*, 651.
12. Saphier, M.; Burg, A.; Sheps, S.; Cohen, H.; Meyerstein, D. *Dalton Trans.* **1999,** *11*, 1845.
13. Phillips, C. S. G.; Williams, R. J. P. *Inorganic Chemistry* **,** (Vol. 2). Oxford University Press: Oxford, **1966**.
14. Pujol, A. M.; Gateau, C.; Lebrun, C.; Delangle, P. *Chem. Eur. J.* **2011,** *17*, 4418.
15. Badarau, A.; Dennison, C. *J. Am. Chem. Soc.* **2011,** *133*, 2983.
16. Gray, H. B.; Malmstrom, B. G.; Williams, R. J. P. *J. Biol. Inorg. Chem.* **2000,** *5*, 551.
17. Groeneveld, C. M.; Dahlin, S.; Reinhammar, B.; Canters, G. W. *J. Am. Chem. Soc.* **1987,** *109*, 3247.
18. Halime, Z. K.-E.; Matthew, T.; Qayyum, M. F.; Mondal, B.; Gandhi, T.; Puiu, S. C.; Chufan, E. E.; Sarjeant, A. A. N.; Hodgson, K. O.; Hedman, B.; Solomon, E. I.; Karlin, K. D. *Inorg. Chem.* **2010,** *49*, 3629.
19. Le Poul, N.; Campion, M.; Douziech, B.; Rondelez, Y.; Le Clainche, L.; Reinaud, O.; Le Mest, Y. *J. Am. Chem. Soc.* **2007,** *129*, 8801.
20. Savelieff, M. G.; Lu, Y. *J. Biol. Inorg. Chem.* **2010,** *15*, 461.
21. Torres, J.; Wilson, M. T. *Biochim. Biophys. Acta Bioenerg.* **1999,** *1411*, 310.
22. Golub, G.; Zilbermann, I.; Cohen, H.; Meyerstein, D. *Supramol. Chem.* **1996,** *6*, 275.
23. Golub, G.; Cohen, H.; Meyerstein, D. *Chem. Commun.* **1992,** *5*, 397.
24. Golub, G.; Cohen, H.; Paoletti, P.; Bencini, A.; Messori, L.; Bertini, I.; Meyerstein, D. *J. Am. Chem. Soc.* **1995,** *117*, 8353.
25. Burg, A.; Maimon, E.; Cohen, H.; Meyerstein, D. *Eur. J. Inorg. Chem.* **2007,** *4*, 530.

26. Parker, A. J. *Search* **1973,** *4*, 426.
27. Jubran, N.; Cohen, H.; Koresh, Y.; Meyerstein, D. *Chem. Commun.* **1984,** *24*, 1683.
28. Clark, T.; Hennemann, M.; van Eldik, R.; Meyerstein, D. *Inorg. Chem.* **2002,** *41*, 2927.
29. Navon, N.; Burg, A.; Cohen, H.; Van Eldik, R.; Meyerstein, D. *Eur. J. Inorg. Chem.* **2002,** *2*, 423.
30. Rusonik, I.; Cohen, H.; Meyerstein, D. *Dalton Trans.* **2003,** *10*, 2024.
31. Zuberbuehler, A. *Helv. Chim. Acta* **1970,** *53*, 473.
32. Green, O.; Gandhi, B. A.; Burstyn, J. N. *Inorg. Chem.* **2009,** *48*, 5704.
33. Buxton, G. V.; Green, J. C.; Sellers, R. M. *J. Chem. Soc. Dalton Trans.* **1976,** *21*, 2160.
34. Zuberbuehler, A. D. *Stud. Surf. Sci. Catal.* **1991,** *66*, 249.
35. Navon, N.; Cohen, H.; Van Eldik, R.; Meyerstein, D. *Dalton Trans.* **1998,** *21*, 3663.
36. Jahng, Y.; Hazelrigg, J.; Kimball, D.; Riesgo, E.; Wu, R.; Thummel, R. P. *Inorg. Chem.* **1997,** *36*, 5390.
37. Dunbar, W. E.; Schilt, A. A. *Talanta* **1972,** *19*, 1025.
38. James, B. R.; Williams, R. J. P. *J. Chem. Soc.* **1961,** 2007.
39. Jensen, M. R.; Hansen, D. F.; Led, J. J. *J. Am. Chem. Soc.* **2002,** *124*, 4093.
40. Dahlin, S.; Reinhammar, B.; Wilson, M. T. *Biochem. J.* **1984,** *218*, 609.
41. Parker, O. J.; Espenson, J. H. *J. Am. Chem. Soc.* **1969,** *91*, 1968.
42. Parker, O. J.; Espenson, J. H. *Inorg. Chem.* **1969,** *8*, 1523.
43. Shaw, K.; Espenson, J. H. *Inorg. Chem.* **1968,** *7*, 1619.
44. Parker, O. J.; Espenson, J. H. *Inorg. Chem.* **1969,** *8*, 185.
45. Gogolev, A. V.; Shilov, V. P.; Pikaev, A. K. *High Energy Chem. (Transl. Khim. Vys. Energ.)* **1997,** *31*, 71.
46. Wardman, P. *J. Phys. Chem. Ref. Data* **1989,** *18*, 1637.
47. Buxton, G. V.; Greenstock, C. L.; Helman, W. P.; Ross, A. B. *J. Phys. Chem. Ref. Data* **1988,** *17*, 513.
48. Veltwisch, D.; Janata, E.; Asmus, K. D. *Perkin Trans. 2* **1980,** *1*, 146.
49. Navon, N.; Golub, G.; Cohen, H.; Meyerstein, D. *Organometallics* **1995,** *14*, 5670.
50. Frank, P.; Benfatto, M.; Szilagyi, R. K.; D'Angelo, P.; Della Longa, S.; Hodgson, K. O. *Inorg. Chem.* **2005,** *44*, 1922.
51. Frank, P.; Benfatto, M.; Hedman, B.; Hodgson, K. O. *Inorg. Chem.* **2008,** *47*, 4126.
52. Davies, K. M. *Inorg. Chem.* **1983,** *22*, 615.
53. Taube, H.; Gaunder, R. G. *Inorg. Chem.* **1970,** *9*, 2627.
54. Albrecht, M.; Robert, H.; Thomas, P.; Karl, W. *Handbook of Metalloproteins.* Wiley: New York, **2001**.
55. Cowan, J. A. *Inorganic Biochemistry: An Introduction.* VCH: New York, **1993**. p. 204.
56. Berks, B. C.; Ferguson, S. J.; Moir, J. W. B.; Richardson, D. J. *Biochim. Biophys. Acta Bioenerg.* **1995,** *1232*, 97.
57. Wasser, I. M.; de Vries, S.; Moeenne-Loccoz, P.; Schroeder, I.; Karlin, K. D. *Chem. Rev.* **2002,** *102*, 1201.
58. Sasaki, S.; Karube, I.; Hirota, N.; Arikawa, Y.; Nishiyama, M.; Kukimoto, M.; Horinouchi, S.; Beppu, T. *Biosens. Bioelectron.* **1998,** *13*, 1.
59. Lucas, H. R.; Karlin, K. D. *Metal Ions Life Sci.* **2009,** *6*, 295.
60. Sundararajan, M.; Hillier, I. H.; Burton, N. A. *J. Phys. Chem. B* **2007,** *111*, 5511.
61. Burg, A.; Lozinsky, E.; Cohen, H.; Meyerstein, D. *Eur. J. Inorg. Chem.* **2004,** *18*, 3675.
62. Silaghi-Dumitrescu, R. *J. Inorg. Biochem.* **2006,** *100*, 396.

63. Kujime, M.; Fujii, H. *Angew. Chem.* **2006,** *45*, 1089.
64. Yokoyama, H.; Yamaguchi, K.; Sugimoto, M.; Suzuki, S. *Eur. J. Inorg. Chem.* **2005,** *8*, 1435.
65. Zumft, W. G. *Microbiol. Mol. Biol. Rev.* **1997,** *61*, 533.
66. Chen, C.-S.; Yeh, W.-Y. *Chem. Commun.* **2010,** *46*, 3098.
67. Chuang, W.-J.; Lin, I.-J.; Chen, H.-Y.; Chang, Y.-L.; Hsu, S. C. N. *Inorg. Chem.* **2010,** *49*, 5377.
68. Farver, O.; Pecht, I. *Progr. Inorg. Chem.* **2007,** *55*, 1.
69. Farver, O.; Eady, R. R.; Pecht, I. *J. Phys. Chem. A* **2004,** *108*, 9005.
70. Farver, O.; Eady, R. R.; Abraham, H. L.; Pecht, I. *FEBS Lett.* **1998,** *436*, 239.
71. Mahapatra, S.; Halfen, J. A.; Tolman, W. B. *Chem. Commun.* **1994,** *14*, 1625.
72. Heather, R. L.; Karlin, K. D. *Metals Ions Life Sci.* **2009,** *6*, 295.
73. Beretta, M.; Bouwman, E.; Casella, L.; Douziech, B.; Driessen, W. L.; Gutierrez-Soto, L.; Monzani, E.; Reedijk, J. *Inorg. Chim. Acta* **2000,** *310*, 41.
74. Monzani, E.; Koolhaas, G J A A; Spandre, A.; Leggieri, E.; Casella, L.; Gullotti, M.; Nardin, G.; Randaccio, L.; Fontani, M.; Zanello, P.; Reedijk, J. *J. Biol. Inorg. Chem.* **2000,** *5*, 251.
75. Sarma, M.; Mondal, B. *Inorg. Chem.* **2011,** *50*, 3206.
76. Whittaker, J. W. *Chem. Rev.* **2003,** *103*, 2347.
77. Arends, I W C E; Gamez, P.; Sheldon, R. A. *Adv. Inorg. Chem.* **2006,** *58*, 235.
78. Qi, Z.-P.; Cai, K.; Yuan, Q.; Okamura, T.-A.; Bai, Z.-S.; Sun, W.-Y.; Ueyama, N. *Inorg. Chem. Commun.* **2010,** *13*, 847.
79. Huang, Q.; Li, S. R.; Peng, Z.; Zhou, H.; Zhiquan, P.; Hu, X. *Inorg. Chem. Commun.* **2010,** *13*, 867.
80. Goldstein, S.; Czapski, G.; Meyerstein, D. *J. Am. Chem. Soc.* **1990,** *112*, 6489.
81. Shin, H.; Lee, D.-H.; Kang, C.; Karlin, K. D. *Electrochim. Acta* **2003,** *48*, 4077.
82. Mi, L.; Zuberbuehler, A. D. *Helv. Chim. Acta* **1991,** *74*, 1679.
83. Karlin, K. D.; Tyeklar, Z. *Bioinorganic Chemistry of Copper.* Chapman and Hall: New York, **1993**.
84. Solomon, E. I.; Ginsbach, J. W.; Heppner, D. E.; Kieber-Emmons, M. T.; Kjaergaard, C. H.; Smeets, P. J.; Tian, L.; Woertink, J. S. *Faraday Discuss.* **2011,** *148*, 11.
85. Marcus, R. A. *J. Electroanal. Chem.* **2000,** *483*, 2.
86. Marcus, R. A. *Angew. Chem.* **1993,** *105*, 1161.
87. Marcus, R. A. *Rev. Mod. Phys.* **1993,** *65*, 599.
88. Bakac, A. *Progr. Inorg. Chem.* **1995,** *43*, 267.
89. Goldstein, S.; Czapski, G.; Van Eldik, R.; Cohen, H.; Meyerstein, D. *J. Phys. Chem.* **1991,** *95*, 1282.
90. Lee, Y.; Park, G.-Y.; Lucas, H. R.; Vajda, P. L.; Kamaraj, K.; Vance, M. A.; Milligan, A. E.; Woertink, J. S.; Siegler, M. A.; Narducci Sarjeant, A. A.; Zakharov, L. N.; Rheingold, A. L.; Solomon, E. I.; Karlin, K. D. *Inorg. Chem.* **2009,** *48*, 11297.
91. Hong, S.; Huber, S. M.; Gagliardi, L.; Cramer, C. C.; Tolman, W. B. *J. Am. Chem. Soc.* **2007,** *129*, 14190.
92. Gupta, A. K.; Tolman, W. B. *Inorg. Chem.* **2010,** *49*, 3531.
93. Ladomenou, K.; Charalambidis, G.; Coutsolelos, A. G. *Inorg. Chim. Acta* **2010,** *363*, 2201.

94. Mirica, L. M.; Ottenwaelder, X.; Stack, T. D. P. *Chem. Rev.* **2004,** *104*, 1013.
95. Cracknell, J. A.; Vincent, K. A.; Armstrong, F. A. *Chem. Rev.* **2008,** *108*, 2439.
96. Fukuzumi, S.; Kotani, H.; Lucas, H. R.; Doi, K.; Suenobu, T.; Peterson, R. L.; Karlin, K. D. *J. Am. Chem. Soc.* **2010,** *132*, 6874.
97. Nabeshima, T.; Inaba, T.; Furukawa, N.; Ohshima, S.; Hosoya, T.; Yano, Y. *Tetrahedron Lett.* **1990,** *31*, 6543.
98. Yang, P.; Yang, X.-J.; Wu, B. *Eur. J. Inorg. Chem.* **2009,** *20*, 2951.
99. Fenton, H. J. H. *J. Chem. Soc. Trans.* **1894,** *65*, 899.
100. Czapski, G.; Samuni, A.; Meisel, D. *J. Phys. Chem.* **1971,** *75*, 3271.
101. Rachmilovich-Calis, S.; Masarwa, A.; Meyerstein, N.; Meyerstein, D.; van Eldik, R. *Chem. Eur. J.* **2009,** *15*, 8303.
102. Goldstein, S.; Czapski, G. *J. Free Radic. Biol. Med.* **1985,** *1*, 373.
103. Masarwa, M.; Cohen, H.; Meyerstein, D.; Hickman, D. L.; Bakac, A.; Espenson, J. H. *J. Am. Chem. Soc.* **1988,** *110*, 4293.
104. Burns, W. G.; May, R.; Buxton, G. V.; Tough, G. S. *Faraday Discuss. Chem. Soc.* **1977,** *63*, 47.
105. Lappin, A. G.; McAuley, A. *Adv. Inorg. Chem.* **1988,** *32*, 241.
106. Burg, A.; Meyerstein, D. *Inorg. Chim. Acta* **2010,** *363*, 737.
107. Jubran, N.; Ginzburg, G.; Cohen, H.; Koresh, Y.; Meyerstein, D. *Inorg. Chem.* **1985,** *24*, 251.
108. Sisley, M. J.; Jordan, R. B. *Inorg. Chem.* **1992,** *31*, 2880.
109. Pillai, G. C.; Ghosh, S. K.; Gould, E. S. *Inorg. Chem.* **1988,** *27*, 1868.
110. Itoh, S.; Noda, K.; Yamane, R.; Kishikawa, N.; Takagi, H. D. *Inorg. Chem.* **2007,** *64*, 1419.
111. Chaka, G.; Sonnenberg, J. L.; Schlegel, H. B.; Heeg, M. J.; Jaeger, G.; Nelson, T. J.; Ochrymowycz, L. A.; Rorabacher, D. B. *J. Am. Chem. Soc.* **2007,** *129*, 5217.
112. Halpern, J.; MacGregor, E. R.; Peters, E. *J. Phys. Chem.* **1956,** *60*, 1455.
113. Mulac, W. A.; Meyerstein, D. *Inorg. Chem.* **1982,** *21*, 1782.
114. Cornils, B.; Herrmann, W. A. *Applied Homogeneous Catalysis with Organometallic Compounds: A Comprehensive Handbook in Two Volumes* **,** (Vol. 2). Wiley VCH: **1996**.
115. Kochi, J. K. *Free Radicals in Organometallic Chemistry and in Organic Reactions Catalyzed by Metal Complexes* **,** (Vol. 278). Academic Press: New York, **1978**.
116. Freiberg, M.; Mulac, W. A.; Schmidt, K. H.; Meyerstein, D. *Faraday Trans. 1* **1980,** *76*, 1838.
117. Cohen, H.; Meyerstein, D. *Inorg. Chem.* **1986,** *25*, 1505.
118. Goldstein, S.; Czapski, G.; Cohen, H.; Meyerstein, D.; Cho, J. K.; Shaik, S. S. *Inorg. Chem.* **1992,** *31*, 798.
119. Goldstein, S.; Czapski, G.; Cohen, H.; Meyerstein, D. *Inorg. Chem.* **1992,** *31*, 2439.
120. Goldstein, S.; Czapski, G.; Cohen, H.; Meyerstein, D. *Inorg. Chim. Acta* **1992,** *192*, 87.
121. Goldstein, S.; Czapski, G.; Cohen, H.; Meyerstein, D. *Inorg. Chem.* **1988,** *27*, 4130.
122. Szulc, A.; Meyerstein, D.; Cohen, H. *Inorg. Chim. Acta* **1998,** *270*, 440.
123. Freiberg, M.; Lilie, J.; Meyerstein, D. *Inorg. Chem.* **1980,** *19*, 1908.
124. Freiberg, M.; Meyerstein, D.; Yamamoto, Y. *Dalton Trans.* **1982,** *6*, 1137.
125. Best, M. D. *Biochemistry* **2009,** *48*, 6571.

126. Constable, E. C.; Housecroft, C. E.; Price, J. R.; Schweighauser, L.; Zampese, J. A. *Inorg. Chem. Commun.* **2010,** *13*, 495.
127. Dickerman, S. C.; DeSouza, D. J.; Jacobson, N. *J. Org. Chem.* **1969,** *34*, 710.
128. Franc, G.; Kakkar, A. K. *Chem. Soc. Rev.* **2010,** *39*, 1536.
129. Hanson, P.; Hammond, R. C.; Gilbert, B. C.; Timms, A. *Perkin Trans. 2* **1995,** *12*, 2195.
130. Hanson, P.; Rowell, S. C.; Walton, P. H.; Timms, A. W. *Org. Biomol. Chem.* **2004,** *2*, 1838.
131. Kolb, H. C.; Finn, M. G.; Sharpless, K. B. *Angew. Chem.* **2001,** *40*, 2004.
132. Rondestvedt, C. S.Jr., *Org. React.* **1976,** *24*, 225.
133. Freiberg, M.; Meyerstein, D. *Faraday Trans. 1* **1980,** *76*, 1825.
134. Yang, Z.; Gould, E. S. *Dalton Trans.* **2003,** *20*, 3963.
135. Al-Ajlouni, A. M.; Gould, E. S. *Inorg. Chem.* **1997,** *36*, 362.
136. Mandal, S.; Bose, R. N.; Reed, J. W.; Gould, E. S. *Inorg. Chem.* **1996,** *35*, 3159.
137. Ghosh, S. K.; Saha, S. K.; Ghosh, M. C.; Bose, R. N.; Reed, J. W.; Gould, E. S. *Inorg. Chem.* **1992,** *31*, 3358.
138. Saha, S. K.; Ghosh, M. C.; Gould, E. S. *Inorg. Chem.* **1992,** *31*, 5439.
139. Ghosh, S. K.; Gould, E. S. *Inorg. Chem.* **1989,** *28*, 1948.
140. Ghosh, S. P.; Saha, S. K.; Bose, R. N.; Reed, J. W.; Ghosh, M. C.; Gould, E. S. *Inorg. Chem.* **1993,** *32*, 2261.
141. Walling, C. *Acc. Chem. Res.* **1975,** *8*, 125.
142. Perron, N. R.; Garcia, C. R.; Pinzon, J. R.; Chaur, M. N.; Brumaghim, J. L. *J. Inorg. Biochem.* **2011,** *105*, 745.
143. Qiao, X.; Ma, Z.-Y.; Xie, C.-Z.; Xue, F.; Zhang, Y.-W.; Xu, J.-Y.; Qiang, Z.-Y.; Lou, J.-S.; Chen, G.-J.; Yan, S.-P. *J. Inorg. Biochem.* **2011,** *105*, 728.
144. Jomova, K.; Valko, M. *Toxicology* **2011,** *283*, 65.
145. Murakami, K.; Shimizu, T.; Irie, K. *J. Amino Acids* **2011,** 654207.
146. Lin, C.-J.; Huang, H.-C.; Jiang, Z.-F. *Brain Res. Bull.* **2010,** *85*, 235.
147. Ying, W.; Xiong, Z.-G. *Curr. Med. Chem.* **2010,** *17*, 2152.
148. Poli, R. *Eur. J. Inorg. Chem.* **2011,** *10*, 1513.
149. Eckenhoff, W. T.; Pintauer, T. *Dalton Trans.* **2011,** *40*, 4909.
150. Surry, D. S.; Buchwald, S. L. *Chem. Sci.* **2010,** *1*, 13.
151. Saphier, M.; Masarwa, A.; Cohen, H.; Meyerstein, D. *Eur. J. Inorg. Chem.* **2002,** *5*, 1226.
152. Cohen, T.; Cristea, I. *J. Am. Chem. Soc.* **1976,** *98*, 748.
153. Mastrorilli, P.; Nobile, C. F.; Taccardi, N. *Tetrahedron Lett.* **2006,** *47*, 4759.
154. Raucher, S.; Koolpe, G. A. *J. Org. Chem.* **1983,** *48*, 2066.
155. Theodoridis, G.; Malamas, P. *J. Heterocycl. Chem.* **1991,** *28*, 849.
156. Obushak, N. D.; Matiichuk, V. S.; Martyak, R. L. *Chem. Heterocycl. Compd.* **2003,** *39*, 878.
157. Fritz, H. P.; Schrauzer, G. N. *Chem. Ber.* **1961,** *94*, 650.
158. Rondestvedt, C. S.; Jr., Vogel, O. *J. Am. Chem. Soc.* **1955,** *77*, 3401.
159. Rondestvedt, C. S.; Jr., Vogel, O. *J. Am. Chem. Soc.* **1955,** *77*, 2313.
160. Wolfer, Y. *The effect of 2,5,8,11-tetramethyl-2,5,8,11-tetraazadodecane as a ligand on the catalytic properties of Cu(I).* Ben-Gurion University: Beer-Sheva, **2010**.
161. Golas, P. L.; Matyjaszewski, K. *Chem. Soc. Rev.* **2010,** *39*, 1338.
162. Rodionov, V. O.; Fokin, V. V.; Finn, M. G. *Angew. Chem.* **2005,** *44*, 2210.
163. Straub, B. F. *Chem. Commun.* **2007,** *37*, 3868.
164. Mulac, W. A.; Meyerstein, D. *Chem. Commun.* **1979,** *20*, 893.

165. Masarwa, M.; Cohen, H.; Meyerstein, D. *Inorg. Chem.* **1986,** *25*, 4897.
166. Masarwa, M.; Cohen, H.; Meyerstein, D. *Inorg. Chem.* **1991,** *30*, 1849.
167. Lei, Y.; Anson, F. C. *Inorg. Chem.* **1994,** *33*, 5003.
168. Thorum, M. S.; Yadav, J.; Gewirth, A. A. *Angew. Chem.* **2009,** *48*, 165.
169. McCrory, C. C. L.; Ottenwaelder, X.; Stack, T. D. P.; Chidsey, C. E. D. *J. Phys. Chem. A* **2007,** *111*, 12641.
170. McCrory, C. C. L.; Devadoss, A.; Ottenwaelder, X.; Lowe, R. D.; Stack, T. D. P.; Chidsey, C. E. D. *J. Am. Chem. Soc.* **2011,** *133*, 3696.
171. Yoshimura, K.; Oishi, T.; Yamaguchi, K.; Mizuno, N. *Chem. Eur. J.* **2011,** *17*, 3827.

HYPOTHIOCYANITE

MICHAEL T. ASHBY

Department of Chemistry and Biochemistry, University of Oklahoma,
Norman, Oklahoma, USA

Abstract

Thiocyanate (SCN^-) is the usual substrate for the human defensive peroxidases (components of human innate defense that include lactoperoxidase, salivary peroxidase, myeloperoxidase, and eosinophil peroxidase). The initial product of the peroxidase-catalyzed oxidation of SCN^- by hydrogen peroxide is the antimicrobial agent hypothiocyanite ($OSCN^-$). Stoichiometric methods of preparing $OSCN^-$ are also known. This review addresses the synthesis and chemistry of $OSCN^-$ and its derivatives in general, with particular attention paid to reactions that may be biologically relevant and to the evidence for putative biological intermediates. As SCN^- is considered to be a pseudohalide in several aspects of reactivity, the inorganic chemistry of $OSCN^-$ is, not surprisingly, related to the corresponding hypohalites, albeit complicated by reactions of the cyano moiety of $OSCN^-$.

INORGANIC/BIOINORGANIC REACTION MECHANISMS
VOLUME 64 ISSN 0898-8838 / DOI: 10.1016/B978-0-12-396462-5.00008-8

Keywords: Hypothiocyanite; Thiocyanate; Pseudohalide; Peroxidase; Lactoperoxidase; Myeloperoxidase; Antimicrobial; Kinetics; Mechanism.

I. Introduction

The earliest report of hypothiocyanite was in 1918 by Bjerrum and Kirschner (as the proton-conjugate hypothiocyanous acid, a.k.a. hyporhodanous acid, and formulated as HCNSO) (*1,2*). The relevance of hypothiocyanite—now formulated as $OSCN^-$—to human health would become evident much later (*vide infra*) (*3*). However, Treviranus discovered the biological significance of the thiocyanate ion (SCN^-), the chemical precursor of $OSCN^-$, a century earlier (1814) when a substance in saliva was found to produce a blood-red color upon addition of ferric ion (*4,5*). This review focuses on the chemical characterization and possible biological relevance of chemical reactions of $OSCN^-$ and products derived therefrom.

Thiocyanate is produced endogenously as a detoxification product of the reaction between cyanide (CN^-) and thiosulfate ($S_2O_3^{2-}$) in the liver (*6*). There are many endogenous and exogenous sources of CN^-, including the metabolism of vitamin B_{12} and certain foods containing cyanogenic glucosides, for example, nuts (especially almonds) and cruciferous vegetables (e.g., the *Brassica*) (*7*). Nonmetabolic sources of cyanide in humans include tobacco and occupationally derived smoke (HCN, e.g., $>200\,\mu g$/cigarette) (*8*), chlorination of glycine by human myeloperoxidase (MPO) during inflammation (*9*), and cyanogenesis (the biochemical production of CN^-) by *Pseudomonas aeruginosa* (an opportunistic pathogen that infects wounds and the lungs of immune-compromised individuals) (*10–14*). Finally, in the absence of other reaction partners, $OSCN^-$ is known to decompose to give CN^- (*15,16*), among other products. Thiocyanate is abundant in all physiologic fluids and especially in those that are derived from the mucosae (e.g., saliva, lachrymal fluids, breast milk, and the mucosal layer of the lung), where the concentration of SCN^- is one or two orders of magnitude larger than in blood plasma as a consequence of its active transport (*17*). The concentration of SCN^- in physiologic fluids varies widely depending on diet and smoking habits. Normal nonsmokers have saliva SCN^- concentrations of 0.5–2 mM, while some smokers may have concentrations as high as 6 mM (*18*). Hence, a high saliva SCN^- concentration can be a biomarker for exposure to tobacco or occupational smoke. Unlike many other inorganic ions, such as Ca^{2+}

(biological messenger and structural component of bone), K^+ (osmotic regulator), CO_3^{2-} (pH buffering), and PO_4^{2-} (ATP, DNA, etc.), SCN^- is not generally considered to be a biologically functional ion. However, in addition to being a product of detoxification of CN^-, the SCN^- ion plays an important role as a substrate for human defensive peroxidases (components of the human innate defense stratagem that include lactoperoxidase (LPO), salivary peroxidase (SPO), myeloperoxidase (MPO), and eosinophil peroxidase (EPO)). The product of oxidation of SCN^- by the defensive peroxidases is hypothiocyanite ($OSCN^-$), the central focus of this review.

There are approximately 200 references in the primary literature that explicitly mention HOSCN and/or $OSCN^-$. Roughly one-quarter of the publications are in the dental literature (e.g., *Caries Research*, *Journal of Dental Research*, etc.), one-quarter are in the food literature (e.g., *Journal of Dairy Research*, *Journal of Applied Microbiology*, etc.), one-quarter are in the medical literature (e.g., *Blood, Infection and Immunity*, etc.), and the remainder are in the chemical literature. There are a very large number of additional publications that certainly concern $OSCN^-$; however, the compound is not explicitly mentioned. For example, there are over 6000 papers that involve the enzyme LPO, for which thiocyanate is known to be the substrate *in vivo*, and $OSCN^-$ the product. Interestingly, many of the publications in the dental and dairy literature predate most of the chemical studies. Indeed, much of the current interest in $OSCN^-$ is derived from its relevance in food science and medicine. There appears to be a regrettable lack of communication between these disciplines; consequently, many inconsistencies exist in the literature, particularly concerning the chemistry. In addition, the primary conclusions of many of these studies have been rendered suspect due to relatively recent advances in our understanding of the chemistry of $OSCN^-$. Recent kinetic measurements suggest that $OSCN^-$ should not exist under the conditions that were employed in some of the studies. As we learn more about the chemistry of $OSCN^-$, there is a need to constantly reevaluate the earlier literature.

The chemistry and biochemistry of thiocyanate was last thoroughly reviewed in a 1975 monograph (*19*). The biological chemistry of $OSCN^-$ (in the context of the LPO system) was reviewed in a 1985 monograph (*3*), which was brought up to date in a 2009 review article (*20*). While the latter review focused on the biological relevance of $OSCN^-$, the present review addresses the chemistry of $OSCN^-$ and its derivatives in general, with particular attention paid to the evidence for putative biological intermediates.

II. Molecular Structure, Properties, and Synthesis

A. Molecular Structure

Hypothiocyanite is a highly reactive chemical species that has never been isolated in a pure form; however, it has been the subject of extensive theoretical (*21–23*) and spectroscopic (*24–30*) investigation. Early molecular orbital calculations by Pyykko and Runeberg predicted that the relative thermodynamic stabilities of the isomers of hypothiocyanite (in the gas phase) are $OCNS^- > ONCS^- > OSCN^-$ (*21*). However, it was subsequently concluded by Sundholm that the computed relative thermodynamic stabilities (in the gas phase) of the isomers are $OCNS^- > OSCN^- > ONCS^-$ (*22*). A subsequent theoretical study by Dua *et al*. included additional isomers: $OCNS^- > SOCN^- > OSCN^- > ONCS^- > OSNC^-$ (*23*). The ultraviolet (UV) spectrum of hypothiocyanite in aqueous solution has been measured under various conditions (*24,29*), but the electronic spectrum does not differentiate between the possible isomers. In an effort to distinguish between alternative formulations for hypothiocyanite, nuclear magnetic resonance (NMR) (*25–28,30*) and mass spectra (*23,27*) have been collected and analyzed. Chronologically, ^{15}N NMR spectra were collected first by Modi *et al*. (*26,30*), and a subsequent theoretical study was performed by Sundholm in an effort to analyze the observed ^{15}N NMR chemical shift (*22*). The latter theoretical study by Sundholm also yielded computed magnetic shielding constants for ^{13}C, but they were not compared with ^{13}C NMR chemical shifts that had been previously measured experimentally (*28*). Several ^{13}C NMR studies of hypothiocyanite have also appeared in the interim (*25,27*), but these studies did not refer to the earlier computational study by Sundholm. Sundholm concluded that his computed ^{15}N shielding constants were most consistent with a formulation of $OSCN^-$ (or possibly $ONCS^-$), but his conclusion was based upon experimental ^{15}N NMR spectra that were subsequently disputed (*31*). In addition to the aforementioned studies of the spectroscopic properties of hypothiocyanite in solution, there have been two gas-phase studies by mass spectrometry (*23,27*). Arlandson *et al*. have employed negative ion electrospray ionization mass spectrometry (ESI-MS) to identify the major stable products of the EPO-catalyzed oxidation of SCN^- by H_2O_2 (*27*). In addition to several unidentified contaminate ions, an ion with *m/z* 74 was observed that could correspond to hypothiocyanite, but this observation did not distinguish between the different possible isomers. A more recent study by

Dua *et al*. employed collision-induced dissociation (CID) mass spectra to produce molecular precursors that were selected to yield $OSCN^-$, $ONCS^-$, and $OCNS^-$ (*23*). When combined with the aforementioned theoretical calculations, the CID spectra provided evidence that $OSCN^-$ is a product of the oxidation of SCN^- by H_2O_2, but it was suggested that some of the other ions that were observed by Arlandson *et al*. were possibly due to $ONCS^-$ (or other isomers). In addition to conflicting conclusions that arise when comparing the aforementioned theoretical and spectroscopic studies, it is noted that many of the experimental results that have been previously reported appear to be inconsistent with the estimated lifetimes of hypothiocyanite under the conditions of the experiments (*vide infra*).

In an effort to reconcile these inconsistencies, the UV, the ^{13}C NMR, and the ^{15}N NMR spectra that result when hypothiocyanite is synthesized by various solution methods (*vide infra*) were reinvestigated (*31*). Importantly, in contrast to earlier investigations, the latter study employed kinetic methods to evidence the correlations between the spectroscopic signatures that were attributed to hypothiocyanite. All of the available synthetic methods (*vide infra*) produced essentially the same initial UV, ^{13}C NMR, and ^{15}N NMR spectra. The UV spectrum reveals a λ_{max} of 376 nm (ϵ_{376}=26.5 $M^{-1}cm^{-1}$), which was a previously unreported distinguishing feature (Fig. 1). The ^{13}C NMR spectrum that was observed (δ=127.8 ppm at pH 13 vs. dioxane at 66.6 ppm) (*31*) is comparable to those that have been previously reported for $OSCN^-$ (although in some cases different assignments were made). However, the ^{15}N NMR spectrum (δ=−80.6 ppm at pH 13 vs. NO_3^- at δ=0) contrasts with previous reports. It was concluded that all of the available synthetic methods produce the same species, and that the spectra were self-consistent with the formulation $OSCN^-$ (*31*). Perhaps the most significant contribution of the latter study was the report of the unique spectral signature (Fig. 1, λ_{max} of 376 nm) that has facilitated the unambiguous identification of $OSCN^-$ in subsequent mechanistic studies (*vide infra*).

B. Properties of Hypothiocyanite and Its Derivatives

Thiocyanate is a pseudohalide in that it resembles a halide in its charge and reactivity (*32–36*). Table I summarizes the known inorganic derivatives of thiocyanate, and when appropriate, also lists examples of corresponding halide analogues. Note that since sulfur and the halides belong to Groups 16 and 17, respectively, the oxidation numbers of analogous compounds differ by one.

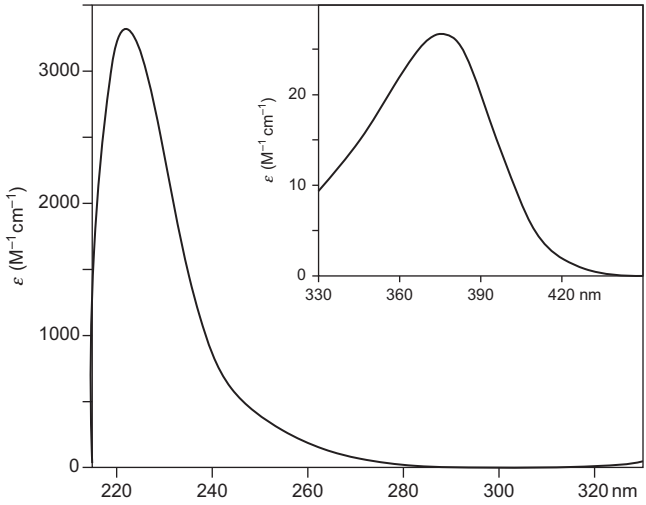

FIG. 1. UV spectrum of $OSCN^-$ at pH 13. Thiocyanogen (0.5 ml of 11.5 mM $(SCN)_2$ in CCl_4) was extracted into NaOH (10 ml of 0.1 M) solution to produce $OSCN^-$ (575 μM final concentration). The spectrum in this figure was obtained by subtraction of the spectrum of SCN^-. Inset: UV–vis spectrum observed when SCN^- (1 M) is reacted with OCl^- (1.28 mM) using a stopped-flow apparatus.

TABLE I

THIOCYANATE AND OXIDOTHIOCYANATE DERIVATIVES AND HALIDE ANALOGUES

Thiocyanate Derivatives		Halide Analogues
HSCN	Thiocyanic acid	HCl, HBr, HI
SCNH	Isothiocyanic acid	Ditto
SCN^-	Thiocyanate	Cl^-, Br^-, I^-
$(SCN)_2$	Thiocyanogen	Cl_2, Br_2, I_2
$(SCN)_3^-$	Trithiocyanite	Cl_3^-, Br_3^-, I_3^-
NCSCN	Dicyanosulfide	ClCN, BrCN, ICN
$S_3C_2N_2H_2$	Xanthane hydride	–
Oxidothiocyano Derivatives		**Halide Analogues**
HOSCN	Hypothiocyanous acid	HOCl, HOBr, HOI
$OSCN^-$	Hypothiocyanite	OCl^-, OBr^-, OI^-
HO_2SCN	Cyanosulfurous acid	$HClO_2$, $HBrO_2$, HIO_2
O_2SCN^-	Cyanosulfite	ClO_2^-, BrO_2^-, IO_2^-
HO_3SCN	Cyanosulfuric acid	$HClO_3$, $HBrO_3$, HIO_3
O_3SCN^-	Cyanosulfate	ClO_3^-, BrO_3^-, IO_3^-
$H_2NC(=O)SOH$	Thiocarbamic acid S-oxide	–
$H_2NC(=O)SO^-$	Thiocarbamate-S-oxide	–

For example, the formal oxidation numbers for the elements in HSCN are H(+1), S(−2), C(+4), and N(−3), whereas for HCl they are H(+1) and Cl(−1). For $(SCN)_2$, they are S(−1), C(+4), and N (−3), whereas for Cl_2 they are Cl(0). The oxidation numbers for Cl in Cl^-, OCl^-, ClO_2^-, ClO_3^-, and ClO_4^- are −1, +1, +3, +5, and +7. The corresponding oxidation numbers for S in SCN^-, $OSCN^-$, O_2SCN^-, and O_3SCN^- are −2, 0, +2, and +4 (the oxidation numbers for C and N do not change). By analogy to the highest oxidation number that is observed for the halogens (+7; e.g., ClO_4^-), completely oxidized SCN^- yields sulfate:

$$SCN^- + 5O^{2-} \rightarrow SO_4^{2-} + OCN^- + 8e^- \quad (1)$$

Note that the oxidation numbers of the elements of the reactants are S(−2), C(+4), N(−3), and O(−2), whereas the oxidation numbers for the products are S(+6), C(+4), N(−3), and O(−2); thus it is the sulfur center that has formally undergone an eight electron oxidation (cf. the aforementioned Cl(−1) to Cl(+7), which is also an eight electron oxidation).

B.1. Acid/base properties of thiocyanate derivatives

Many of the physical and chemical properties of the oxoacids of the halides exhibit trends that are related to the sizes and electronegativities of the central atoms. Thus, the known acid dissociation constants for thiocyanic acid (HSCN) (*37*) and hypothiocyanous acid (HOSCN), pK_a=−1.4 and 5.3, respectively, can be understood in the context of trends observed for hydrohalic and hypohalous acids. Hydrohalic acids (e.g., HCl, HBr, and HI) are fully ionized in water, as is HSCN. The pK_a of an oxo acid $XO_y(OH)_z$ can be estimated using the empirical formula (Pauling's rule): pK_{a1}=8.5–5.7y. Thus, the electron-withdrawing, charge-stabilizing capacity of each additional oxo group decreases the acid dissociation constant by about 10^5. Accordingly, the expected pK_a values for HOX, $HOXO$, $HOXO_2$, and $HOXO_3$ are 8.5, 2.8, −2.9, and −8.6, respectively. The measured acid dissociation constants of oxo acids without oxo groups (i.e., the hydroxides of nonmetals for which y=0) are 8.5±2 (i.e., in the range 6.5–10.5). The actual pK_a values for HOCl and HOClO are 7.5 and 2.0, respectively (a typical difference of 5.5). As expected, $HOClO_2$ and $HOClO_3$ are strong acids. The effect of the central atom is reflected in the pK_a trends for HOX for X=Cl, Br, and I (7.5, 8.6, and 10.6, respectively). Thus, more electronegative central atoms inductively stabilize the negative charge of the oxoanion, thereby facilitating ionization. Not

unexpectedly, the pK_a of HOSCN is 5.3, substantially more acidic than the hypohalous acids of Group 17. The exceptional acidity of HOSCN reflects the resonance stabilization that is anticipated for the conjugate base $OSCN^-$. Based upon the aforementioned trends, we anticipate HO_2SCN and HO_3SCN would be strong acids in water (fully ionized), although their acid dissociation constants are unknown.

B.2. Redox properties of thiocyanate derivatives

The oxidation potential of the 2 $SCN^- = (SCN)_2$ couple falls between those of the corresponding couples for Br^- and I^- (Table II) (*38–40*). The $SCN^- = OSCN^-$ couple is comparable to the corresponding I^- couple (*41*). The oxidation potential of SCN^- relative to the halides explains the oxidation of SCN^- by Cl_2 (*42*) and Br_2 (*43*) and the oxidation of I^- by $(SCN)_2$. The latter reaction is one that can be used to quantify $(SCN)_2$ (*44*). The relative oxidation potentials also facilitate the definition of inter (pseudo)halogens like $I^{\delta+}$-$SCN^{\delta-}$ (iodine thiocyanate) (*45,46*) versus $Cl^{\delta-}$-$SCN^{\delta+}$ (thiocyanogen chloride) (*47*) and $Br^{\delta-}$-$SCN^{\delta+}$ (thiocyanogen bromide), which react accordingly.

TABLE II

TWO-ELECTRON REDOX COUPLES FOR X^- (VS. SHE)

Couple (pH 0 and 14)	E° (V)
$2I^- = I_2 + 2e^-$	−0.536
$2SCN^- = (SCN)_2 + 2e^-$	−0.77
$2Br^- = Br_2 + 2e^-$	−1.065
$2Cl^- = Cl_2 + 2e^-$	−1.360
$2F^- = F_2 + 2e^-$	−2.65
Couple (pH 0)	**E° (V)**
$I^- + H_2O = HOI + H^+ + 2e^-$	−0.987
$SCN^- + H_2O = HOSCN + H^+ + 2e^-$	
$Br^- + H_2O = HOBr + H^+ + 2e^-$	−1.331
$Cl^- + H_2O = HOCl + H^+ + 2e^-$	−1.484
Couple (pH 14)	**E° (V)**
$I^- + 2OH^- = OI^- + H_2O + 2e^-$	−0.485
$SCN^- + 2OH^- = OSCN^- + H_2O + 2e^-$	−0.44 to 0.39[a]
$Br^- + 2OH^- = OBr^- + H_2O + 2e^-$	−0.761
$Cl^- + 2OH^- = OCl^- + H_2O + 2e^-$	−0.841

[a] pH 6.5.

It is apparent that the halogens (X_2) are less powerful oxidants than the corresponding hypohalous acids (HOX). For example, the oxidation potentials of Cl_2 and HOCl are +1.36 and +1.48V, respectively (Table II). As expected, the hypohalous acids are more powerful oxidants than their conjugate hypohalites (OX^-) (cf. the one volt difference in potentials of HOCl and OCl^-). Accordingly, the rates of reactions of $OSCN^-$ (vis-à-vis HOSCN) are pH dependent (*vide infra*).

C. Synthetic Methods Used to Prepare Hypothiocyanite

There exist three fundamental ways to prepare $OSCN^-$: (1) hydrolysis of thiocyanogen, $(SCN)_2$ in aqueous base; (2) enzyme-catalyzed oxidation of SCN^- by H_2O_2; and (3) oxidation of SCN^- by electrophilic halogenating agents. The advantages and disadvantages of each of these methods will be discussed next.

C.1. Preparation by hydrolysis of thiocyanogen under alkaline conditions

A standard method of preparing $OSCN^-$ is the hydrolysis of $(SCN)_2$ at pH 13, which is accomplished by first synthesizing and quantifying $(SCN)_2$ in an organic solvent and subsequently hydrolyzing/extracting with aqueous base. The properties of $(SCN)_2$ will be described first, then the peculiar requirements for the hydrolysis will be described.

By analogy to halogens, thiocyanogen $(SCN)_2$ is moderately stable. It can be prepared as colorless crystals by suspending AgSCN in SO_2 at $-20°C$ and oxidizing the coordinated SCN^- with Br_2 or I_2 (*48*):

$$2Ag(SCN) + Br_2 \rightarrow 2AgBr + (SCN)_2 \qquad (2)$$

Crystalline $(SCN)_2$ melts to give a yellow liquid before spontaneously polymerizing to give polythiocyanogen, $(SCN)_x$, an amorphous brick-red solid. In addition to the chemical means of oxidizing SCN^-, electrolysis of concentrated aqueous solutions of alkali metal and ammonium salts of SCN^- in acid evolve $(SCN)_2$ (*49*). More practically, $(SCN)_2$ can be synthesized *in situ* by oxidizing a suspension of $Pb(SCN)_2$ in CCl_4 with Br_2 (*44*). Wet CCl_4 works more effectively than dry, purified solvent (unpublished results). Other solvents such as $CHCl_3$, CS_2, Et_2O, AcOH, and CH_3NO_2 can be used as well, but not as effectively as CCl_4 (unpublished results). After filtering the precipitated $Pb(SCN)_2$, colorless solutions of $(SCN)_2$ can be used for subsequent preparation of $OSCN^-$ (*vide infra*). The

concentration of $(SCN)_2$ in CCl_4 can be confirmed spectrophotometrically (ϵ_{296nm}=140$M^{-1}cm^{-1}$). Thiocyanogen exhibits a single ^{13}C NMR ($CDCl_3$) resonance at 107–108 ppm (*48,50*) and a resonance at 286.6 ppm in the ^{14}N NMR ($CDCl_3$) spectrum (*48*). The IR spectrum of $(SCN)_2$ exhibits a strong ν(C≡N) band at 2161 cm^{-1}, a ν(C—S) band at 669 cm^{-1}, a ν(S—S) band at 492 cm^{-1}, and two ν(S—C≡N) bands at 404 and 372 (*48,50–52*). The Raman spectrum shows bands at 2158, 668, 494, and 397 cm^{-1} (*48*). The X-ray crystal structure has been determined (*48*).

Dropwise addition of CCl_4 solutions of $(SCN)_2$ into 0.1 M NaOH produces quantitative yields of $OSCN^-$, provided the concentration of $OSCN^-$ does not exceed about 1 mM (*16,53*), as determined spectrophotometrically (Fig. 1) (*31*). Higher concentrations of $OSCN^-$, up to about 5 mM, can be achieved with reduced chemical yield. Importantly, no $OSCN^-$ is produced when $(SCN)_2$ is hydrolyzed near neutral pH, as evidenced by the absence of the characteristic spectrum in Fig. 1 (unpublished results). This is true for $(SCN)_2$ that is generated in CCl_4 and extracted into neutral water, as well as for $(SCN)_2$ produced by oxidation of SCN^- at low pH (e.g., by using Cl_2) followed by pH neutralization (unpublished results). The concentration of $OSCN^-$ can be determined spectrophotometrically using its characteristic absorption at λ_{max}=376 nm. Unfortunately, the low molar absorptivity (ϵ_{376}=26.5$M^{-1}cm^{-1}$) makes this method generally practical only for millimolar concentrations of $OSCN^-$ using a cuvette with a 10-cm pathlength (*31*). However, effective pathlengths of 1 m can be achieved with fiber optic cells which permit the spectrophotometric quantification of low micromolar concentrations of $OSCN^-$ (*31*). A more routine, albeit less selective, quantification of $OSCN^-$ can be achieved with 5-thio-2-nitrobenzoic acid (TNB, λ_{max}=412 nm, ϵ_{412nm}=14,150$M^{-1}cm^{-1}$), which is oxidized to colorless 5,5′-dithiobis-(2-nitrobenzoic acid) (DTNB, Ellman's reagent) in a TNB:$OSCN^-$ ratio of 2:1 (*16*). Although the oxidation of TNB is not specific to $OSCN^-$, confirmation that $OSCN^-$ is the oxidant can be achieved using a kinetic methodology (*54*).

C.2. Enzyme-catalyzed oxidation of SCN^- by H_2O_2

The uncatalyzed oxidation of SCN^- by H_2O_2 is an exceedingly slow reaction at neutral pH (*55*), and the intermediate $OSCN^-$ decomposes before substantial amounts can accumulate (*56*). The reaction can be proton catalyzed, but even at very low pH, the reaction is too slow to be a practical method of synthesizing $OSCN^-$ (*57,58*). Many enzymes catalyze the oxidation of SCN^- by H_2O_2, including the human defensive peroxidases LPO (*3*),

EPO (*59*), and MPO (*60*). Human SPO, which is closely related to LPO, but not identical, uses SCN^- exclusively *in vivo* (*61*). For all of the human defensive peroxidases, SCN^- is usually the major endogenous substrate (although under some circumstances MPO and EPO also use Cl^- and Br^-, respectively). The resulting hypo(pseudo)halites are employed in host defense as antimicrobials. Thyroid peroxidase is a human enzyme that liberates iodine for addition to tyrosine residues on thyroglobulin for the production of thyroxine (T4) or triiodothyronine (T3), which are thyroid hormones, but it also oxidizes SCN^-, which explains the deleterious effect of excess SCN^- on thyroid function when it competes for I^- (*62*). Vanadium bromoperoxidase from marine algae (*25*) and *Euphorbia* peroxidase from the latex of a perennial Mediterranean shrub (*63*) are also known to catalyze the reaction of SCN^- and H_2O_2, but SCN^- is not considered to be a natural substrate for these enzymes. Note that plant horseradish peroxidase is capable of catalyzing the oxidation of SCN^- by H_2O_2, but the product appears to be the $SCN^{\cdot}$ radical, and the resulting chemistry is different than that expected for $OSCN^-$ (*64,65*). One would expect the radicals to couple to give $(SCN)_2$, and as noted before, $(SCN)_2$ does not hydrolyze near neutral pH to give $OSCN^-$.

Commercially available and inexpensive bovine LPO is the most convenient enzyme for the laboratory production of $OSCN^-$; however, there are limitations in using enzymes to produce $OSCN^-$. The optimal pH for the LPO system (LPOS, which comprises LPO, SCN^-, and H_2O_2) is between 5 and 7.5, depending on the concentrations of both SCN^- and H_2O_2 (*66*). In general, the efficiency of the LPOS drops off markedly above pH 7. Since HOSCN is relatively unstable (pK_a=5.3), for synthetic purposes, the useful pH range is 6–8 when using the LPOS to produce $OSCN^-$, but after enzyme production of $OSCN^-$, the pH can be adjusted. At SCN^- to H_2O_2 ratios of 2 or more and H_2O_2 concentrations of about 500 μM or less, quantitative reaction of SCN^- and H_2O_2 are observed to produce $OSCN^-$. Under acidic conditions, but not at neutral pH, SCN^- inhibits the LPOS at low micromolar concentrations (*67*). However, concentrations of $OSCN^-$ as high as 3–4 mM can be achieved while employing 10 mM SCN^- and 5 mM H_2O_2 near neutral pH (unpublished results). Importantly, to avoid oxidative inactivation of the enzyme, H_2O_2 must be added to solutions of LPO only in the presence of SCN^-. In addition to inactivation of the LPOS by high concentrations of SCN^- and H_2O_2, there is some evidence that $OSCN^-$ itself may inactivate LPO (unpublished results).

C.3. Electrophilic halogenating agents

Given their relative oxidizing potentials (*vide supra*), it is not unexpected that Cl_2 (*58*), Br_2 (unpublished results), HOCl (*42*), and HOBr (*43*) are capable of oxidizing SCN^- to produce $(SCN)_2$ under acidic conditions (*58*) and to produce $OSCN^-$ under basic conditions (*31*). Chlorine dioxide (ClO_2) also oxidizes SCN^- in acid, probably to produce $(SCN)_2$, but it is not as effective as the halogens and hypohalous acids (*68*). However, inorganic chloramine (NH_2Cl) and organic chloramines (e.g., taurine chloramine and dichloramine) produce $OSCN^-$ under neutral and basic conditions (*54*).

Because of the rapid reactions of SCN^- with electrophilic halogenating agents and the propensity of $OSCN^-$ to react with similar rates with the oxidants (*vide infra*), overoxidation of SCN^- is a significant problem with this method unless an excess of SCN^- is employed and measures are taken to slow the reaction down, such as by employing alkaline conditions for the hypohalites (the hypohalous acids are the reactive species) or less reactive organic chloramines. For example, a 400-fold molar excess of SCN^- over OCl^- is required for stoichiometric production of $OSCN^-$ at pH 13 using a hand mixer comprised of two Hamilton syringes and a T-mixer (*31*). However, millimolar concentrations of $OSCN^-$ can be produced using a 10-fold excess of SCN^- at pH 13 employing a vortex mixer while adding OCl^- dropwise (*69*). The overoxidation products have not been found to interfere with the mechanisms of most chemical reactions (unpublished results).

N-Thiocyanatosuccinimide (NTS) is an electrophilic thiocyanating agent (*70–72*) that is isolated as a pale yellow solid after reaction of *N*-bromosuccinimide with NaSCN in CH_2Cl_2 under Finkelstein conditions (*73*):

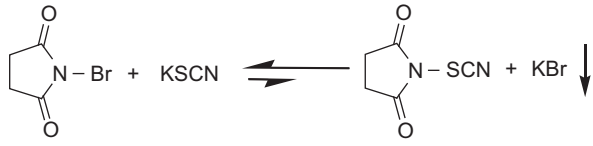

(3)

The synthesis of NTS may be compared with the aforementioned reaction of HOBr with SCN^-, which presumably proceeds through an unobserved BrSCN intermediate that is subsequently hydrolyzed. The reaction of NBS with SCN^- appears to be a nucleophillic substitution of Br^- in CH_2Cl_2, whereas the reaction of HOBr with SCN^- proceeds via electrophilic transfer of Br^+ to SCN^- (which is once more serving the role of nucleophile). NTS exhibits reaction properties under acidic conditions that are consistent with the production of $(SCN)_2$ (*42*). However, the intermediate involvement of $(SCN)_2$ and/or HOSCN for

reactions of NTS has not been demonstrated. While other *N*-SCN derivatives may be potential sources of $OSCN^-$ or a reaction surrogate, they are generally less stable and more difficult to work with than NTS (unpublished results).

III. Reaction Mechanisms

A. General Reaction Properties

Hypothiocyanite reacts as an electrophilic thiocyanating agent. Thus, HOSCN is more reactive than $OSCN^-$. While no reactions of $OSCN^-$ have been documented (except for its reaction with $(SCN)_2$, *vide infra*), it is noteworthy that hypohalous acids are typically four to eight orders of magnitude more reactive than hypohalites. For example, the rates of reaction of HOCl and OCl^- with cysteine differ by about four (*74*), and with SCN^- differ by seven (*42*), orders of magnitude. Accordingly, it is not expected that $OSCN^-$ plays a significant role in any reactions below pH 10 for which it is serving as an electrophile. As an electrophile, HOSCN reacts most effectively with good nucleophiles that have relatively low oxidation potentials. Since the $S^{\delta+}$ reaction center of HOSCN is categorized as a soft acid by Pearson's Hard–Soft Acid–Base (HSAB) Theory (*75,76*), it follows that the most effective nucleophile partners are soft bases. The only reaction partners for HOSCN in a neutral pH aqueous environment that have been definitively demonstrated (e.g., by mechanistic studies) are thiolates (RS^-, R=alkyl and aryl) (*77,78*) and cyanide (CN^-) (*79*) anions, both of which are considered to be soft bases (*75,76*). However, we have observed the reaction of HOSCN with I^- and other soft bases that are likely reaction partners for HOSCN (unpublished results). Also, the reaction of HOSCN with SCN^- apparently plays a role in the decomposition mechanism of $OSCN^-$ near neutral pH (vis-à-vis $HO(SCN)_2^-$, *vide infra*). Under acidic conditions, HOSCN reacts with RS^- to produce sulfenyl thiocyanates (RSSCN) (*80*) and with the soft SCN^- anion to produce $(SCN)_2$ (*81*). Although the question of whether HOSCN or $(SCN)_2$ (via comproportionation) is the reaction partner with RSH to produce RSSCN in acid has not been investigated, there is evidence that the hydrolysis of RSSCN produces the corresponding sulfenic acid RSOH and SCN^- (not RSH and HOSCN) (*82*). Under alkaline conditions, the hard base OH^- reacts with HOSCN, but nucleophilic attack is on the C≡N bond, not the S center (*83,84*). It has been recently reported that oxidation of tryptophan residues is observed on reaction of HOSCN with proteins, but not free tryptophan, or tryptophan-containing

peptides (*85*). The reaction of HOSCN with tryptophan, which appears to be inconsistent with the general reaction properties of HOSCN, will be discussed later.

The investigations of the inorganic and organic chemistry of SCN derivatives (including $OSCN^-$) in aqueous medium are beginning to reveal general reactivity trends. Two of the patterns can be summarized by the following generic reaction pathways that are based upon the HSAB principle. Hard nucleophiles (e.g., X^-=OH^-) tend to react at the C-center of the SCN group:

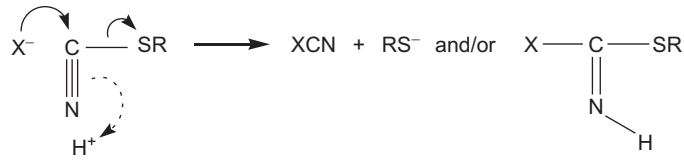

(4)

Metathesis products (XCN+RSH) tend to be favored in anhydrous organic solvents, whereas addition products tend to be favored in aqueous medium. Examples of such reactions include the hydrolysis of HOSCN to give thiocarbamate-*S*-oxide (*84*):

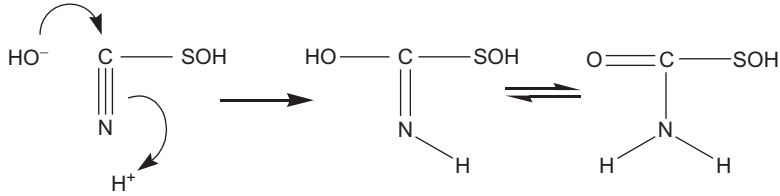

(5)

The corresponding hydrolysis of dicyanosulfide (NCSCN) is also an example of such a reaction (*79*):

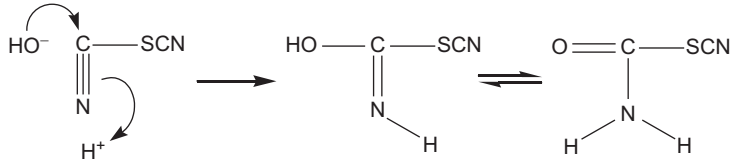

(6)

In contrast, soft nucleophiles (e.g., RS^-) tend to react at the sulfur center. For example, glutathione (GSH) reacts with HOSCN to produce sulfenyl thiocyanate intermediates (*80*):

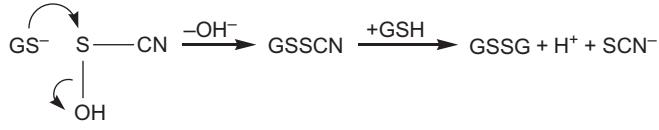

(7)

An analogous reaction occurs for NCSCN (*79*):

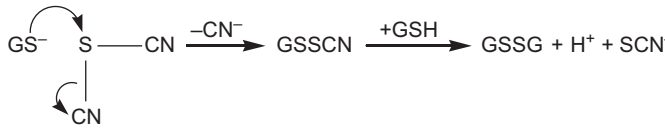

(8)

These and other reactions of $OSCN^-$ that have been investigated mechanistically are summarized in Fig. 2. Some details of these investigations will be discussed next.

B. Inorganic Reactions

B.1. Hydrolysis of $(SCN)_2$ to produce HOSCN under acidic conditions

The inorganic reactions of $OSCN^-$ in general follow the principles that have already been outlined; it acts like a pseudo-hypohalite. By analogy to the hydrolysis of halogens to produce hypohalites, early studies of the inorganic chemistry of $OSCN^-$ have included the hydrolysis of $(SCN)_2$, a reaction that is usually initiated by the heterogeneous extraction of $(SCN)_2$ from organic solvents into acidic or alkaline aqueous solutions, a technique that is not conducive to studying fast reactions (note that extraction into neutral solution does not produce $OSCN^-$).

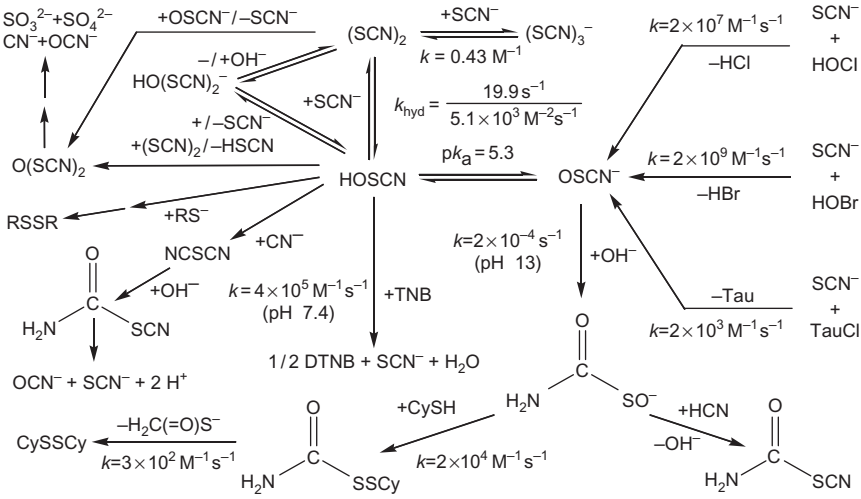

Fig. 2. Examples of reactions of hypothiocyanite that have been investigated mechanistically.

Stanbury investigated the aqueous chemistry of $(SCN)_2$, which was generated under very acidic conditions by oxidation of SCN^- (*58,68,86,87*). Stanbury's first studies of the oxidation of SCN^- by ClO_2 and H_2O_2 were hampered by the sluggish kinetics of the oxidation reactions and a subsequent decomposition of $(SCN)_2$ that competed with its formation (*58,68*). This problem was overcome by employing Cl_2/HOCl as an oxidant mixture, which apparently produces $(SCN)_2$ within the mixing time of a stopped-flow experiment (*86*). Stanbury's investigations have provided evidence that $(SCN)_2$, in the presence of excess SCN^-, is in rapid equilibrium with trithiocyanate $(SCN)_3^-$ (cf. the corresponding equilibrium between I_2 and I_3^-) (*87*):

$$(SCN)_2 + SCN^- \rightleftharpoons (SCN)_3^-, \quad K_9 = 0.43\,M^{-1} \tag{9}$$

The decomposition of $(SCN)_2$ under acidic conditions has also been investigated by Stanbury (*86*). These studies yielded an equilibrium constant (K_{10}) for the hydrolysis of $(SCN)_2$ to give HOSCN and SCN^-, as well as a rate constant for the disproportionation of HOSCN (k_{11}):

$$(SCN)_2 + H_2O \rightleftharpoons HOSCN + SCN^- + H^+,$$
$$K_{10} = \frac{k_{10}}{k_{-10}} = \frac{k_{hyd}^{SCN}}{k_{comp}^{SCN}} = 5.7 \times 10^{-4}\,M^2 \tag{10}$$

$$2HOSCN \rightarrow O_2SCN^- + SCN^- + 2H^{+-},$$
$$k_{11} = 6.9 \times 10^4\,M^{-1}\,s^{-1} \tag{11}$$

In deriving a rate law for the hydrolysis of $(SCN)_2$ that accounted for their observed second-order kinetics, Stanbury *et al.* assumed HOSCN, $(SCN)_2$, and $(SCN)_3^-$ are in rapid equilibrium (*86*). Through $[SCN^-]$-jump stopped-flow experiments, Ashby *et al.* have subsequently shown that the equilibrium between $(SCN)_2$ and $(SCN)_3^-$ occurs within the mixing time (unpublished results). However, first-order kinetics that were subsequently observed by Ashby at low $[H^+]$ and $[SCN^-]$ suggest that hydrolysis can become rate limiting under certain circumstances (*81*). In addition to the mechanism that was previously proposed by Stanbury *et al.* (mechanism I of Scheme 1, excluding the rapid equilibrium between $(SCN)_2$ and $(SCN)_3^-$ that will be taken into consideration later) (*86*), a second mechanism was proposed by Ashby *et al.* (mechanism II of Scheme 1) (*81*). The two mechanisms differ in the third step, namely disproportionation of HO_2SCN in the former mechanism and oxidation of HO_2SCN

Mechanism I:

$$3\{(SCN)_2 + H_2O = HOSCN + SCN^- + H^+\}$$
$$2\{2\,HOSCN \rightarrow HO_2SCN + SCN^- + H^+\}$$
$$2\,HO_2SCN \rightarrow O_3SCN^- + HOSCN + H^+$$
$$O_3SCN^- + H_2O \rightarrow SO_4^{2-} + HCN + H^+$$
$$3\,(SCN)_2 + 4\,H_2O \rightarrow SO_4^{2-} + 5\,SCN^- + HCN + 7\,H^+$$

Mechanism II:

$$3\{(SCN)_2 + H_2O = HOSCN + SCN\_ + H^+\}$$
$$2\,HOSCN \rightarrow HO_2SCN + SCN^- + H^+$$
$$HO_2SCN + HOSCN \rightarrow O_3SCN^- + SCN^- + 2\,H^+$$
$$O_3SCN^- + H_2O \rightarrow SO_4^{2-} + HCN + H^+$$
$$3(SCN)_2 + 4\,H_2O \rightarrow SO_4^{2-} + 5\,SCN^- + HCN + 7\,H^+$$

SCHEME 1. Overall stoichiometries of the hydrolysis and disproportionation of $(SCN)_2$ for two proposed mechanisms.

by HOSCN in the latter mechanism. A common rate law has been derived for the two mechanisms that differs only in a proportionality constant ($k_{11}'=P\cdot k_{11}$, where $P=3/2$ and 3 for mechanisms I and II, respectively) (*81*):

$$\frac{-\mathrm{d}[(SCN)_2]}{\mathrm{d}t} = k_{11}'\left[\frac{2k_{10}[(SCN)_2]}{k_{-10}[H^+][SCN^-]\left(\sqrt{1+\frac{4k_{10}k_{11}'}{k_{-10}^2[H^+]^2[SCN^-]^2}[(SCN)_2]}+1\right)}\right]^2 \qquad (12)$$

$$\alpha = \frac{4E_{10}k_{11}'}{k_{-10}^2[H^+]^2[SCN^-]^2} \qquad (13)$$

Equation (12) is useful for describing limiting extremes. If $1 \ll \alpha[(SCN)_2]$ (which is expected to occur for high pH and low $[SCN^-]$), the k_{10} step becomes rate limiting, and first-order kinetics are expected. In contrast, if $1 \gg \alpha[(SCN)_2]$ (which can be expected for low pH and high $[SCN^-]$), the k_{11} step becomes rate limiting, and second-order kinetics can be expected. Much of the data that were analyzed by Stanbury *et al.* exhibit clean second-order kinetics (*86*). In contrast, Ashby *et al.* focused on the regime of $[H^+]$ and $[SCN^-]$, where the observed kinetics are essentially first order (*81*). In contrast to the previously reported second-order kinetic data that were based upon changes in absorbance which had to

be converted to molar pseudo-second-order rate constants by applying a conversion factor (*86*), k_{10} (the first-order rate constant for hydrolysis of $(SCN)_2$) could be obtained directly from the spectral kinetic traces that were measured (*81*). The observed first-order rate constants (k_{obs}) approach a pH-independent value of ca. $20\,s^{-1}$, which corresponds to the hydrolysis of $(SCN)_2$ by H_2O (Eq. 10). This reaction can be considered to be a nucleophilic attack of H_2O on $(SCN)_2$. A seven-order-of-magnitude difference exists between the second-order rate constants for nucleophilic attack of H_2O versus OH^- on I_2 (*88*), so it is conceivable that the gradual increase of k_{obs} with increasing pH that was observed is due to an increasing contribution of OH^-, even under the very acidic conditions of the aforementioned measurements.

Stanbury *et al*. have taken two approaches to evaluating K_{10}. In the first approach, the initial absorptions were fit to an equation that was derived using the assumption that the resulting absorption is the composite of the equilibria of Eqs. (9) and (10) (*87*). Subsequently, beginning with an equilibrium mixture of $(SCN)_2$ and $(SCN)_3^-$, Stanbury *et al*. have investigated the reaction sequence of Eqs. (9)–(11) (*86*). Their pseudo-second-order kinetic traces were fit to the rate law (where P was assigned a value of 3/2 by Stanbury *et al*.):

$$k_{obs}' = P\left(\frac{K_{10}{}^2 k_{11}}{[H^+]^2[SCN^-]^2}\right)\left(1 + K_9[SCN^-] + \frac{K_{10}}{[SCN^-][H^+]}\right)^{-2} \quad (14)$$

The complexity of Eq. (14) stems from the fact that for constant $[SCN^-]$ and $[H^+]$, the observed rate data are pseudo-second-order (k_{obs}'). Since homogeneous second-order kinetics depend upon the initial concentration of the reactant, k_{obs}' must be written in terms of the partitioning between $(SCN)_2$ and $(SCN)_3^-$ (i.e., by taking into account K_9). In fitting their data to Eq. (14), K_9 was held constant ($0.43\,M^{-1}$), and thus two parameters were obtained: $K_{10}{}^2 k_{11}$ and K_{10}. The value for K_{10} that was obtained using initial absorptions ($K_{10}=5.4(\pm1.9)\times10^{-4}M^2$) and the value that was obtained using Eq. (14) ($K_{10}=5.7(\pm0.8)\times10^{-4}M^2$) were self-consistent. By comparison, Ashby obtained a value of $K_{10}=[HOSCN][SCN^-][H^+]/[(SCN)_2]=k_{10}/k_{-10}=k_{hyd}{}^{SCN}/k_{comp}{}^{SCN}=19.8(\pm0.7)s^{-1}/5.14(\pm0.07)\times10^{-3}M^{-2}s^{-1}=3.8\times10^{-3}M^2$, which differs from the values that were determined by Stanbury *et al*. by roughly an order of magnitude (*81*). However, given the potential sources of error (including a large estimated error for $K_9=0.4(\pm0.3)M^{-1}$ and the likelihood that at least part of the data that were analyzed by Stanbury *et al*. were probably in the regime where Eq. (12) for $1 \ll \alpha[(SCN)_2]$ was more appropriate), the values of K_{10} are comparable.

TABLE III

RATE CONSTANTS FOR THE HYDROLYSIS OF X_2 (X_2+H_2O), RATE CONSTANTS FOR COMPROPORTIONATION OF HOX AND X^- ($HOX+X^-+H^+$) AND THE CORRESPONDING EQUILIBRIUM CONSTANTS

X	k_{hyd}^X (s^{-1})	k_{comp}^X ($M^{-2}s^{-1}$)	$K_{hyd}^X = \frac{k_{hyd}^X}{k_{comp}^X}$ (M^2)	References
Cl	15	1.8×10^4	8.3×10^{-4}	(89)[a]
Br	98	1.6×10^{10}	6.1×10^{-9}	(90)[b]
I	1.1×10^8	2.0×10^{20}	5.4×10^{-13}	(88)[c]
SCN	20	5.1×10^3	3.9×10^{-3}	(81)[d]

[a]These data were determined at 20°C and μ=0.5M. For comparison, $K_{hyd}^{Cl}=8.3\times10^{-4}$ M^2 at 25°C and μ=0.1M.
[b]These data were determined at 25°C and μ=0.5M. For comparison, $K_{hyd}^{Br}=6.2\times10^{-9}$ M^2 at 25°C and μ=1.0M.
[c]Consult the discussion of Eqs. (15) and (16) herein and reference (88) for an explanation of the origin of these rate constants.
[d]These data were determined at 18°C, μ=1.0M.

The rate constants for hydrolysis of the halogens (k_{hyd}^X) are compared with the rate constant for hydrolysis of $(SCN)_2$ (i.e., k_{10}) in Table III. It is remarkable how similar k_{hyd}^X is for X=Cl, Br, and SCN (i.e., ca. 10–100 s^{-1}). In sharp contrast, k_{hyd}^X for I_2 is five orders of magnitude larger than the other (pseudo)halogens. Table III also summarizes the rate constants for comproportionation of HOX and X^- (k_{comp}^X), as well as the equilibrium constants that are derived from the ratio of the two rate constants, $K_{hyd}^X=k_{hyd}^X/k_{comp}^X$. Despite the fact that the redox potential of SCN^- lies somewhere between that of Br^- and I^- (40), the equilibrium constant for $(SCN)_2$ is more similar to Cl_2 than to either Br_2 or I_2. Given that k_{hyd} is very similar for X=Cl, Br, and SCN, the similarity of K for X=Cl and SCN is due to their closely matched values of k_{comp}^X, which at ca. $10^4M^{-2}s^{-1}$ are substantially smaller than the corresponding values that have been determined for Br and I. Before continuing this discussion, it is important to note that the aqueous chemistry of I_2 and HOI is substantially more complicated than the corresponding chemistry for X=Cl and Br (cf. Section III.B.3). At high pH (above ca. pH 7), the major pathway of I_2 hydrolysis proceeds through nucleophilic attack that produces the intermediate I_2OH^-. However, in the pH regime of this study (below pH 2), the major hydrolysis pathway for I_2 is via addition of H_2O and the intermediate H_2OI^+. Thus, the equilibrium and rate constants for X=I in Table III are given by ($K_{hyd}^I=K_{15}K_{16}$) (88,91,92):

$$I_2 + H_2O \rightleftharpoons H_2OI^+ + I^-, \quad K_{15} = k_{15}/k_{-15} = 0.12\,s^{-1}/1 \times 10^{10}\,M^{-1}s^{-1} = 1.2 \times 10^{-11}\,M \tag{15}$$

$$H_2OI^+ \rightleftharpoons HOI + H^+, \quad K_{16} = k_{16}/k_{-16} = 9 \times 10^8\,s^{-1}/2 \times 10^{10}\,M^{-1}s^{-1} = 4.5 \times 10^{-2}\,M \tag{16}$$

Accordingly, the hydrolysis of I_2 is not an elementary reaction.

The hydrolysis of I_2 aside, it is apparent that the rates of hydrolysis of X_2 for X=Cl, Br, and SCN under acidic conditions are comparable, and that the differences between the positions of the equilibria lie in the relative rates of comproportionation. From a thermodynamic perspective, since HX are fully ionized, HOX are completely unionized, and the values of k_{hyd}^X are comparable, the trend of $k_{comp}^{SCN} < k_{comp}^{Cl} << k_{comp}^{Br}$ must relate to the relative stabilities of X_2 versus HOX and X^-. These relative stabilities are the result of a combination of bond enthalpies (e.g., X—X vs. O—X) and solvation effects. Solvation energies are expected to be particularly important for the anions and for the species that can form strong hydrogen bonds. From a kinetic perspective, the trend that is observed for k_{hyd}^X must reflect the relative nucleophilicity (*93*) of X^- versus the electrophilicity of $HO^{\delta-}X^{\delta+}$. Regarding the nucleophilicity, we note that SCN^- is an ambidentate ligand, and that it is known to produce products that are the result of both S and N nucleophilic attack (*94*). This naturally raises the question of whether the reactions involve HOSCN and/or HONCS. As noted earlier, the structure of the initial product that is produced by the reaction of HOBr and SCN^-, the reaction that was employed to produce "HOSCN" for the study, is indeed HOSCN and not HONCS (*31*). Thus, the rate of nucleophilic attack on HOSCN was measured. Regarding the attacking nucleophile, the simplest mechanisms would be nucleophilic attack by the S of SCN^-. Since the Swain-Scott parameters suggest that Br^- and SCN^- are comparable nucleophiles and that both are better nucleophiles than Cl^- (n=2.99, 4.02, and 4.93 for Cl^-, Br^-, and SCN^-, respectively) (*95*), the origin of the trend in k_{hyd}^X may be due to the relative electrophilicities of HOX. It is noteworthy that HOBr generally reacts several orders of magnitude faster with nucleophiles than HOCl does (*42,43,96,97*). Thus, HOBr appears to be the better electrophile. The second-order rate constants for the reaction of HOX with SCN^- are 2.3×10^7 (*42*), 2.3×10^9 (*43*), and 5.1×10^3 (*81*)M^{-1} s^{-1} for X=Cl, Br, and SCN, respectively. Since these reactions involve a common reactant, it was concluded that the relative electrophilicities are HOBr>HOCl≫HOSCN, at least with respect

to the nucleophile SCN^- (*81*). The relative reactivities of HOCl and HOBr toward nucleophiles are largely independent of the nature of the nucleophile (*96,97*), and this may be the case for HOSCN as well. For example, the rates of oxidation of CN^- by HOCl, HOBr, and HOSCN are 1.2×10^9 (*98*), 4.2×10^9 (*99*), and $7.5\times10^7\,M^{-1}s^{-1}$ (*79*), respectively. Importantly, as the reactions approach the diffusion limit (10^9–$10^{10}\,M^{-1}s^{-1}$), the aforementioned trend may become obscured. It would appear likely that HOSCN is generally a relatively poor electrophile. Accordingly, it is not surprising that the only reaction partners that have been found for HOSCN are strong, soft nucleophiles (SCN^-, CN^-, I^-, and thiolates).

B.2. Oxidation of SCN^- to produce HOSCN

Ashby *et al.* have investigated the kinetics of the reactions of hypochlorite (OCl^-) (*42*) and hypobromite (OBr^-) (*43*) with SCN^- under alkaline conditions. The mechanisms involve fast reactions between the corresponding hypohalous acids and SCN^-, and with near diffusion-controlled kinetics in the case of HOBr:

$$\begin{aligned} &HOX \rightleftharpoons OX^- + H^+, \\ &pK_a(HOCl) = 7.4 \;\text{ and }\; pK_a(HOBr) = 8.6 \end{aligned} \tag{17}$$

$$\begin{aligned} &HOX + SCN^- \rightarrow OSCN^- + X^- + H^+, \\ &k(X = Cl) = 2.3\times10^7\,M^{-1}s^{-1} \\ &\text{and }\; k(X = Br) = 2.3\times10^9\,M^{-1}s^{-1} \end{aligned} \tag{18}$$

In contrast to OCl^-, OBr^- also reacts with SCN^- with a measurable rate, albeit with a rate constant ($3.8\times10^4\,M^{-1}s^{-1}$) that is five orders of magnitude smaller than that of its conjugate acid (*43*). Through the comparison of time-resolved electronic spectra, time-resolved ^{13}C NMR spectra, and time-resolved ^{15}N NMR spectra, it was concluded that the enzyme system (LPO/H_2O_2/SCN^-), hydrolysis of $(SCN)_2$ at high pH, and oxidation of SCN^- by HOX (X=Cl, Br) all yield the same initial species (*31*). The development of a facile *in situ* synthesis of $OSCN^-$ by oxidation of SCN^- with OX^- (X=Cl, Br) (*42,43*) created opportunities to investigate some of the fast chemical reactions of $OSCN^-$ and its derivatives, including the comproportionation of HOSCN with SCN^- ($k_{-10}=k_{comp}^{SCN}$, the reverse of Eq. 10) and a reinvestigation of the hydrolysis of $(SCN)_2$ that yields a direct measurement of the rate constant for Eq. (10) ($k_{10}=k_{hyd}^{SCN}$).

*B.3. Decomposition of $OSCN^-$ at neutral pH**

Until recently, there have been no methodical investigations of the kinetics and mechanisms of the decomposition of $OSCN^-$ near physiologically relevant neutral pH conditions. However, anecdotal reports indicated that the decomposition of $OSCN^-$ is faster at low pH and with high concentrations of SCN^-. Considering the observation that $(SCN)_2$ does not yield $OSCN^-$ when it is hydrolyzed at neutral pH (*16,86,100,101*), one might conclude that the comproportionation of HOSCN and SCN^- to give $(SCN)_2$ is involved in the decomposition mechanism of $OSCN^-$ near neutral pH. However, isotopic exchange of the C atoms of $OSCN^-$ and SCN^- is not observed near neutral pH, as might be expected for a reversible comproportionation (*102*):

$$HOSCN + S^{14}CN^- + H^+ \rightarrow NCS - S^{14}CN + H_2O \quad (19)$$

$$NCS - S^{14}CN + H_2O \rightarrow HOS^{14}CN + SCN^- + H^+ \quad (20)$$

It is furthermore noteworthy that $(SCN)_2$ accelerates the decomposition of $OSCN^-$ (i.e., $OSCN^-$ and $(SCN)_2$ react at neutral pH before the latter species decomposes, unpublished results). When HOSCN is reacted with $^{35}SCN^-$, the SO_4^{2-} that is obtained does not contain the label. While the ^{14}C and ^{35}S tracer studies do not preclude the involvement of NCSCN, O_2SCN^-, O_3SCN^-, and other possible intermediates, they suggest that the reversible equilibrium between $OSCN^-$ and $(SCN)_2$ in the presence of SCN^- (Eqs. 19 and 20) is not involved in the decomposition mechanism. The eventual decomposition products of $OSCN^-$ are CN^-, OCN^-, SO_3^{2-}, and SO_4^{2-}, depending on the specific reaction conditions. These products may be accounted for by the following atom/electron balance (which does not necessarily reflect the intimate mechanism or the intermediates that are involved):

$$2HOSCN \rightarrow HO_2SCN + HSCN \quad (21)$$

$$HO_2SCN + HOSCN \rightarrow HO_3SCN + HSCN \quad (22)$$

$$HO_3SCN + H_2O \rightarrow H_2SO_3 + HOCN \text{ and/or } H_2SO_4 + HCN \quad (23)$$

Eqs. (21)–(23) yield the net reaction Eq. (24):

*The uncited results that are described in B.3 have been recently published: Kalmar, J.; Woldegiorgis, K. L.; Biri, B.; Ashby, M. T. *J. Am. Chem. Soc.*, **2011**, *133*, 19911–19921.

$$3\mathrm{HOSCN} + \mathrm{H_2O} \rightarrow (\mathrm{H_2SO_3} + \mathrm{HOCN\ and/or\ H_2SO_4} + \mathrm{HCN}) + 2\mathrm{HSCN} \quad (24)$$

It has been previously suggested that the mechanism involves dismutation of HOSCN (Eq. 21) because second-order kinetics have been observed under pH conditions where $OSCN^-$+HOSCN predominate (*16,103*). However, others have reported first-order kinetics for the decomposition of $OSCN^-$ (*102*). The mechanism of Eqs. (21)–(23) has been proposed to produce H_2SO_4+HCN (*103*), but CN^- is not produced quantitatively, presumably because it reacts with HOSCN to produce NCSCN, which subsequently hydrolyzes to produce a 1:1 mixture of SCN^- and OCN^- (*79*). Importantly, although there is no experimental evidence for the intermediates of Eqs. (21)–(23) that have been proposed to be involved in the decomposition of $OSCN^-$, cyanosulfite, O_2SCN^- (*104,105*), and cyanosulfate, O_3SCN^- (*106*), have been observed in nonaqueous media (but not in water). However, many other potential intermediates are possible, including the unknown anhydride (cf. thiosulfinate esters, the anhydrides of sulfenic acids):

$$2\mathrm{HOSCN} = \mathrm{NCSS(=O)CN} + \mathrm{H_2O} \quad (25)$$

In the presence of excess SCN^-, the decomposition of HOSCN and $(SCN)_2$ around pH 4.0 in acetate buffer and the decomposition of $OSCN^-$ around pH 7.0 in phosphate buffer have been recently investigated in detail, and it was shown that the observed mechanisms are relevant to the stability of $OSCN^-$ at physiological pH (unpublished results). As SCN^- is considered to be a pseudohalide in several aspects of reactivity (*32–34*), some of the interpretation was based upon analogous hydrolysis chemistry of the halogens (*88,107,108*). The proposed mechanism of decomposition of HOSCN/$OSCN^-$ is illustrated in Eqs. (26)–(35):

$$\mathrm{HOSCN} = \mathrm{OSCN^-} + \mathrm{H^+}, \quad K_{26}\ \text{fast equilibrium} \quad (26)$$

$$\mathrm{HOSCN} + \mathrm{SCN^-} = \mathrm{HO(SCN)_2^-}, \quad k_{27}\ \text{and}\ k_{-27}\ (K_{27} = k_{27}/k_{-27}) \quad (27)$$

$$\mathrm{HO(SCN)_2^-} = (\mathrm{SCN})_2 + \mathrm{H_2O}, \quad k_{28}\ \text{and}\ k_{-28}\ (K_{28} = k_{28}/k_{-28}) \quad (28)$$

$$\mathrm{HO(SCN)_2^-} + \mathrm{H^+} = (\mathrm{SCN})_2 + \mathrm{H_2O}, \quad k_{29}\ \text{and}\ k_{-29}\ (K_{29} = k_{29}/k_{-29}) \quad (29)$$

$$(\mathrm{SCN})_2 + \mathrm{SCN^-} = \mathrm{(SCN)_3^-}, \quad K_{30}\ \text{fast equilibrium} \quad (30)$$

$$OSCN^- + (SCN)_2 \rightarrow O(SCN)_2 + SCN^-, \quad k_{31}, \text{RDS} \tag{31}$$

$$O(SCN)_2 + H_2O \rightarrow O_2SCN^- + SCN^- + 2H^+ \tag{32}$$

$$O_2SCN^- + HOSCN \rightarrow O_3SCN^- + SCN^- + H^+ \tag{33}$$

$$O_3SCN^- + H_2O \rightarrow {SO_4}^{2-} + HCN + H^+ \tag{34}$$

$$O_3SCN^- + H_2O \rightarrow {SO_3}^{2-} + OCN^- + 2H^+ \tag{35}$$

Giving the net equation:

$$\begin{aligned} 3HOSCN + H_2O \rightarrow X{SO_4}^{2-} + XHCN + (1-X){SO_3}^{2-} \\ +(1-X)OCN^- + 2SCN^- + (5-X)H^+ \end{aligned} \tag{36}$$

As no second-order behavior was observed during the decomposition of $OSCN^-$, the reaction of two HOSCN and/or $OSCN^-$ molecules cannot be a major pathway under the conditions that were employed (*81,86*). The reactive species was found to be HOSCN, both at lower (~4) and at higher (~7) pH. SCN^- is regarded as a pseudohalide and $(SCN)_2$ as a pseudo-halogen based on their chemical reactivity (*43,58,68,81,86,87*). The role of I_2OH^- in the hydrolysis chemistry of I_2 has been previously described in detail (*88,107,108*). Accordingly, equilibria (27)–(29) were proposed to account for the observed kinetics during the decomposition of HOSCN. The dissociation of $HO(SCN)_2^-$ to $(SCN)_2$ (Eq. 28) is assumed, which can be proton catalyzed at lower pH (Eq. 29). The general rate law is given by:

$$v = k_{31}\left[(SCN)_2\right][OSCN^-] \tag{37}$$

Using the steady-state approximation for $[HO(SCN)_2^-]$ and $[(SCN)_2]$,

$$\begin{aligned} v &= \frac{\alpha(1-\alpha)k_{27}k_{30}(k_{28}+k_{29}[H^+])[H^+][SCN^-][HOSCN]_T^2}{k_{-27}(k_{-28}[OH^-]+k_{-29})+(1-\alpha)k_{31}(k_{-27}+k_{28}+k_{29}[H^+])[HOSCN]_T} \\ \alpha &= \frac{[H^+]}{K_{26}+[H^+]} \\ [HOSCN]_T &= [HOSCN]+[OSCN^-] \end{aligned} \tag{38}$$

Considering that

$$\begin{aligned} k_{-27}\left(K_{26}+\left[H^+\right]\right)(k_{-28}[OH^-]+k_{-29}) \ll K_{26}k_{31}(k_{-27} \\ +k_{28}+k_{29}[H^+])[HOSCN]_T \end{aligned} \tag{39}$$

which is valid under the applied conditions, leads to the rate law:

$$v = \frac{k_{27}(k_{28} + k_{29}[H^+])[H^+][SCN^-][HOSCN]_T}{(k_{-27} + k_{28} + k_{29}[H^+])(K_{26} + [H^+]} \quad (40)$$

And, at pH 7 assuming that $k_{29}[H^+] \ll k_{28}$ and $[H^+] \ll K_{26}$:

$$v = \frac{k_{27}k_{28}[H^+][SCN^-][HOSCN]_T}{K_{26}(k_{-27} + k_{28})} \quad (41)$$

The experimentally determined and the deduced limiting rate laws agree at both pH 4 and 7. However, the proposed mechanism does not account for all the observed kinetic phenomena, which clearly indicate the presence of an alternative mechanism at pH≥7 and $[SCN^-]_0 \leq [HOSCN]_{T,0}$. The disproportionation of HOSCN/$OSCN^-$ in a bimolecular reaction can be a feasible explanation (*81,86*). However, at pH>11, $OSCN^-$ is known to hydrolyze to thiocarbamate-S-oxide (*84*).

A global data fit to the proposed model was carried out, which gave good fit, and the resulting calculated rate and equilibrium constants are given in Table IV.

To complement the study of the mechanism of decomposition of $OSCN^-$ around pH 4 and 7, the mechanism of the decomposition of $(SCN)_2$ around pH 4 with large SCN^- excess was also studied (unpublished results). The initial spectrum of the generated $(SCN)_2$ solution around pH 4 was found to be pH dependent as a result of the equilibria of Eqs. (28) and (29), which are

TABLE IV

CONSTANTS RESULTING FROM GLOBAL FIT OF THE KINETIC DATA FOR THE DECOMPOSITION OF $(SCN)_2$ AND HOSCN/$OSCN^-$ IN THE pH REGION FROM 4 TO 7

K_{26}	$(1.17\pm0.4)\times10^{-5}$M[a]
k_{27}	$50.0\pm0.9\,M^{-1}s^{-1}$
k_{-27}	$(2.07\pm0.09)\times10^{3}s^{-1}$
K_{27}	$2.4\times10^{-2}\,M^{-1}$[b]
k_{28}	$137\pm23\,s^{-1}$
k_{-28}[c]	*$3.6\times10^{11}M^{-1}s^{-1}$*[b]
K_{28}	$(2.65\pm0.3)\times10^{9}M^{-1}$
k_{29}	$61\,M^{-1}s^{-1}$[b]
k_{-29}	$(1.29\pm0.07)\times10^{8}M^{-1}s^{-1}$
K_{29}	4.8×10^{-7}[b]
K_{30}	$0.54\pm0.1\,M^{-1}$[a]
k_{31}	$(4.01\pm0.3)\times10^{6}M^{-1}s^{-1}$

[a] May be compared with the values of $K_{26}=1.41\times10^{-5}$M and $K_{30}=0.43\,M^{-1}$ that have been previously reported (*77,86,87*).

[b] Deduced from other constants.

[c] The value of k_{-28} (italic) is overestimated; the limiting rate of diffusion is ca. 10^{10} $M^{-1}s^{-1}$ in water.

considered fast under the applied conditions and competitive with the formation of $(SCN)_3^-$ in Eq. (30). It was suggested that $HOSCN/OSCN^-$ is produced in the dissociation of $OH(SCN)_2^-$ in reverse of Eq. (27) and that it subsequently reacts with $(SCN)_2$ in the rate-limiting step (Eq. 31). The protonation state of the reacting species in Eq. (27) could not be determined based on the kinetic experiments. In deriving the general rate law, equilibrium K_{29} was omitted because $K_{29}=K_{28}K_w[H_2O]^{-1}$ and $OSCN^-$ is assumed to react with $(SCN)_2$ (Eq. 31) (*vide infra*). Using the steady-state approximation for $[HOSCN]_T$ and starting with Eq. (37):

$$\begin{aligned} v &= \frac{(1-\alpha)k_{-27}k_{31}K_{28}[OH^-][(SCN)_2]_T^2}{\left(\alpha k_{27}[SCN^-] + \dfrac{(1-\alpha)k_{31}[(SCN)_2]_T}{1+K_{28}[OH^-]+K_{30}[SCN^-]}\right)\left(1+K_{28}[OH^-]+K_{30}[SCN^-]^2\right)}\alpha \\ \alpha &= \frac{[H^+]}{K_{26}+[H^+]} \\ [(SCN)_2]_T &= [(SCN)_2] + [(SCN)_3^-] + [HO(SCN)_3^-] \end{aligned} \tag{42}$$

For high $[(SCN)_2]_T$

$$K_{27}(1+K_{28}[OH^-]+K_{30}[SCN^-][H^+][SCN^-] \ll k_{31}K_{26}[(SCN)_2]_T \tag{43}$$

and the limiting rate law is

$$v = \frac{k_{-27}k_{28}[H^+][OH^-][(SCN)_2]_T}{1+K_{28}[OH^-]+K_{30}[SCN^-]} \tag{44}$$

Thus, reaction corresponding to k_{-27} is rate limiting when $[(SCN)_2]_T$ is high. A global data analysis was performed, and the parameter k_{31} was approximated. The proposed kinetic model fits well to the experimental data set and the obtained constants are listed in Table IV. In spite of the high quality of the fit, the limiting rate laws (and therefore the obtained parameters) can be regarded only as approximations, as seen, for example, in the value of k_{-28} which exceeds $10^{10}M^{-1}s^{-1}$. Although taking into consideration that numerous independently recorded data sets were analyzed simultaneously without considering the error of the independent parameters (i.e., initial concentrations and pH), the results are satisfactory.

Importantly, the rate laws and the mechanisms for the decomposition of HOSCN and $(SCN)_2$ are consistent with the aforementioned anecdotal information concerning their properties near neutral pH.

B.4. Reaction of HOSCN with CN^-

As discussed previously, the chief sources of CN^- in humans are metabolism of cyanogenic food, tobacco and occupationally derived smoke, inflammation, and microbial cyanogenesis. As $OSCN^-$ and CN^- may be associated in a biological setting, it is noteworthy that $OSCN^-$ and CN^- react with pH-dependent kinetics to produce SCN^- and cyanate (OCN^-) via dicyanosulfide (NCSCN), with the maximum rate occurring near neutral, physiological pH (*79*). In the presence of excess CN^-, pseudo-first-order kinetics were observed at pH 6.7 and 11.0, and a first-order dependency on the $[CN^-]_0$ was found. The effect of pH on the rate of reaction of $OSCN^-$ with CN^- was investigated from pH 4.0 to 11.3. Below pH 9.0 and above pH 9.5, only one reaction was observed. However, in the very narrow region of pH from 9.0 to 9.5, biphasic kinetics behavior was observed. A plot of pH versus k_{obs} for the pH regions where first-order kinetics were observed produces a bell-shaped curve, which is expected when a conjugate acid reacts with a conjugate base. These data could in principle be equally well described by the reactions of HOSCN+CN^- and $OSCN^-$+HCN; however, given that HOSCN is a better electrophile than its conjugate base $OSCN^-$, and given that CN^- is a better nucleophile than cyanous acid (HCN), the mechanism of Eqs. (46)–(51) was proposed. The bell-shaped pH dependency of k_{obs} is described by the following equation:

$$k_{obs} = \frac{k_{38}K_a^{HCN}[H^+][OSCN]_T}{[H^+]^2 + [H^+]K_a^{HCN} + [H^+]K_a^{HOSCN} + K_a^{HOSCN}K_a^{HCN}} \quad (45)$$

Equation (45) is derived assuming that the proton equilibria (corresponding to $K_a{}^{HOSCN}$ and $K_a{}^{HCN}$) are fast, and that k_{48} is irreversible (which appears to be a valid assumption at lower pH, *vide infra*). From Eq. (45), the computed pK_a for HOSCN of 4.8 for I=1.0 is comparable to the value of 5.1 that was previously determined at I=0.015 (*24*). The computed pK_a for HCN of 9.4 for I=1.0 is comparable to the value of 9.0 that was previously determined under the same conditions (*109*). The comparable values for the pK_as for HOSCN and HCN that were obtained for the fits of the kinetic data and the values that have been measured independently evidence the proposed mechanism of the reaction of HOSCN with CN^- (the k_{48} step below):

$$HOSCN \rightleftharpoons H^+ + OSCN^-, \quad pK_a{}^{HOSCN} = 4.8 \quad (46)$$

$$HCN \rightleftharpoons H^+ + CN^-, \quad pK_a^{HCN} = 9.4 \quad (47)$$

$$\mathrm{HOSCN} + \mathrm{CN^-} \rightarrow \mathrm{NCSCN} + \mathrm{OH^-}, \quad k_{48} = 7.5 \times 10^7\,\mathrm{M^{-1}\,s^{-1}} \tag{48}$$

$$\mathrm{NCSCN} + \mathrm{OH^-} \overset{\mathrm{rds}}{\rightarrow} \mathrm{OCN^-} + \mathrm{SCN^-} + \mathrm{H^+}, \quad k_{49} < 100\,\mathrm{M^{-1}\,s^{-1}}(\mathrm{pH} < 7) \tag{49}$$

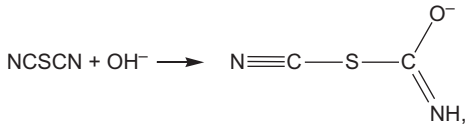

k_{50} = 26 s^{-1}(pH 9.3 and 20 mM CN$^-$) (50)

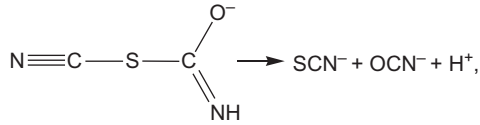

k_{51} = 0.5 s^{-1}(pH 9.3 and 20 mM CN$^-$) (51)

The mechanism of the reaction of $OSCN^-$ with CN^- becomes more complicated above pH 9. On the supposition that the added complexity was due to the reaction steps that follow the initial reaction of HOSCN with CN^-, NCSCN was independently synthesized and the kinetics of its hydrolysis above pH 9 were investigated (*79*). The kinetics of hydrolysis of NCSCN had been previously studied, albeit only below pH 7 (*110*). Whereas single exponential kinetics are observed for the hydrolysis of NCSCN below pH 7, biphasic kinetics are observed at pH 9.3 (*79*). The first reaction corresponds to the build-up of an intermediate that subsequently decays at the same rate as the second exponential that was observed during the reaction of HOSCN with CN^- at pH 9.3. The chemical nature of the intermediate that is formed during the hydrolysis of NCSCN remains unresolved. Since the eventual products of the reaction of HOSCN+CN^- and the hydrolysis of NCSCN (OCN^- and SCN^-) are stable at pH 9.3, and since the intermediate is only observed during the alkaline hydrolysis of NCSCN, it was suggested that the intermediate is produced by nucleophilic attack of OH^- on one of the unsaturated C≡N bonds (Eq. 6), by analogy to a similar reaction that was observed for the hydrolysis of $OSCN^-$ at high pH to give $H_2NC(=O)SO^-$ (Eq. 5), and it was proposed that the intermediate may be carbamoyl thiocyanate ($H_2NC(=O)SCN$) (*79*).

C. Organic Reactions

The only organic reaction for which involvement of $OSCN^-$ has been unambiguously demonstrated by detailed mechanistic

studies is its reaction with thiols (*77,78*) to give disulfides vis-à-vis sulfenyl thiocyanate intermediates (*80,111*). The mechanism of such reactions will be discussed in detail. However, it has been recently suggested that HOSCN may react with tryptophan residues in proteins, but not with free tryptophan, or with tryptophan-containing peptides (*85*). The limited mechanistic information that is available for the latter reaction will also be discussed.

C.1. Oxidation of thiolates by HOSCN

The kinetics and mechanism of the reaction of HOSCN/$OSCN^-$ with 5-thio-2-nitrobenzoic acid (TNB) have been investigated as a function of pH (*77*). The reaction is first order with respect to [$OSCN^-$] and first order with respect to [TNB]. The observed bell-shaped profile in the 2.5<pH<8 region once more suggests the reaction of a conjugate acid with a conjugate base. Assuming that the acid/base equilibria are rapid, the mechanism of Eqs. (52)–(55) was proposed (where TNB^- is the carboxylate anion, TNB^{2-} includes deprotonation of the thiol, and DTNB is the disulfide):

$$\mathrm{HOSCN} = \mathrm{H^+} + \mathrm{OSCN^-}, \quad \mathrm{p}K_\mathrm{a}^{\mathrm{HOSCN}} = 4.8 \tag{52}$$

$$\mathrm{TNB^-} = \mathrm{H^+} + \mathrm{TNB^{2-}}, \quad \mathrm{p}K_{\mathrm{a}2}^{\mathrm{TNB}} = 4.4 \tag{53}$$

$$\mathrm{HOSCN} + \mathrm{TNB^{2-}} \rightarrow \mathrm{TNBSCN^-} + \mathrm{OH^-}, \quad k_{39} = 1.3 \times 10^8\,\mathrm{M^{-1}\,s^{-1}} \tag{54}$$

$$\mathrm{TNBSCN^-} + \mathrm{TNB^{2-}} \rightarrow \mathrm{DTNB^{2-}} + \mathrm{SCN^-}, \quad k_{40} = \text{fast} \tag{55}$$

The mechanism of Eqs. (52)–(55) yields the following rate law:

$$k_\mathrm{obs} = \frac{k_{53}K_{\mathrm{a}2}^{\mathrm{TNB}}[\mathrm{H^+}][\mathrm{OSCN}]_T[\mathrm{TNB}]_T}{[\mathrm{H^+}]^2 + [\mathrm{H^+}]K_{\mathrm{a}2}^{\mathrm{TNB}} + [\mathrm{H^+}]K_\mathrm{a}^{\mathrm{HOSCN}} + K_\mathrm{a}^{\mathrm{HOSCN}}K_{\mathrm{a}2}^{\mathrm{TNB}}} \tag{56}$$

Fitting the observed rate constants to Eq. (56) while fixing $\mathrm{p}K_{\mathrm{a}2}{}^{\mathrm{TNB}}$ to its measured value of 4.4 yielded $\mathrm{p}K_\mathrm{a}{}^{\mathrm{HOSCN}}$=4.8 (comparable to values measured independently) and k_{39}=1.3×10^8 $\mathrm{M^{-1}s^{-1}}$. Including a possible reaction between HOSCN and TNB^- (the thiol) did not improve a fit of the data, suggesting that only the thiolate is reactive toward HOSCN. The sulfenyl thiocyanate intermediate (TNBSCN) was not observed. Sulfenyl thiocyanates are reactive molecules that are subject to hydrolysis to give free SCN^- and the corresponding sulfenic acid (RSOH) (*112,113*) or its corresponding thiosulfenate ester (RS(=O)SR)

(*74,82*). Accordingly, a mathematically equivalent expression would result for a mechanism, whereby Eq. (55) is replaced with Eqs. (57) and (58) (where TNBOH is the sulfenic acid):

$$TNBSCN^- + OH^- \rightarrow TNBOH^- + SCN^-, \quad k_{42} = \text{fast} \qquad (57)$$

$$TNBOH^- + TNB^{2-} \rightarrow DTNB^{2-} + OH^-, \quad k_{43} = \text{fast} \qquad (58)$$

Although not observed in the 2.5<pH<8 region, sulfenyl thiocyanates are observed under more acidic conditions (e.g., pH 0), where hydrolysis to the sulfenic acid is slowed (*80,82,111*). Furthermore, RSSCN moieties have been detected in proteins, where they are presumably protected in hydrophobic environments (*114*) (*vide infra*).

C.2. Reaction of HOSCN with aromatic residues in proteins

There is no direct evidence that HOSCN reacts with aromatic compounds. However, if the LPOS is activated by addition of H_2O_2 in the presence of tyrosine, tryptophan, or histidine, chemical modification of these free amino acids is observed (*114*). The same modifications are observed when $(SCN)_2$ in CCl_4 is added to aqueous solutions of these aromatic amino acids (*114*). In contrast, when the LPOS is activated or $(SCN)_2$ in CCl_4 is added to aqueous solutions, and the aromatic compounds are subsequently introduced, little or no modification of the compounds is observed (*114*). The fact that $OSCN^-$ is not produced when $(SCN)_2$ decomposes near neutral pH strongly suggest that $(SCN)_2$ (or a derivative thereof), and not HOSCN, is involved in the reactions. Indeed, $(SCN)_2$ has been used in organic solvents to effect displacement of hydrogens of unsaturated hydrocarbons by a thiocyano group (*44*).

IV. Biological Relevance

A. Sources of Hypothiocyanite *In Vivo*

Based upon the existing information, only the enzyme-catalyzed oxidation of SCN^- by H_2O_2 and oxidation of SCN^- by electrophilic halogenating agents are expected to be important pathways for the production of $OSCN^-$ *in vivo*. Hydrolysis of $(SCN)_2$ (e.g., by the one-electron oxidation of SCN^- and coupling of the resulting radicals) is not expected to produce significant amounts of $OSCN^-$ between pH 4 and 10, although production

of $(SCN)_2$ may be relevant during the oxidation of SCN^- in hydrophobic environments (cf. Sections III.C.2 and IV.B).

A.1. Enzyme production of $OSCN^-$

The mechanism of oxidation by human defensive enzymes appears to be similar: reaction of the ferriheme enzyme with H_2O_2 to form Compound I (which contains two oxidizing equivalents more than the resting enzyme), followed by direct reaction of the halide with Compound I in a two-electron O-atom-transfer process to produce the hypohalite. Under conditions whereby an excess of substrate (Cl^-, Br^-, I^-, and/or SCN^-) exists with respect to the oxidant (H_2O_2), hypohalite product distributions during the enzyme-catalyzed oxidation of (pseudo)halides depends upon three factors: (1) the redox potential of the enzyme, (2) the rate of reaction of the active form of the enzyme (Complex I) with the substrate (which is in part related to the redox potential of the enzyme) (*115*), (3) and the relative concentrations of the substrates. Under conditions of limiting oxidant (excess halide), the product distributions are given by

$$[OCl^-] : [OBr^-] : [OI^-] : [OSCN^-] = k_{Cl}[Cl^-] : k_{Br}[Br^-] : k_I[I^-] : k_{SCN}[SCN^-] \quad (59)$$

The relative redox potentials of Compound I are LPO∼SPO<EPO<MPO. Whereas LPO and SPO can only oxidize SCN^- and I^- with appreciable rates, EPO can also oxidize Br^-, and MPO can oxidize all of the halide substrates. Table V summarizes the expected products for MPO in two diverse

TABLE V

TWO-ELECTRON REDOX COUPLES FOR X^- (E_o', pH 7 VS. SHE), APPARENT RATE CONSTANTS (k_x) OF MPO COMPOUND I ($\times 10^4 M^{-1}s^{-1}$) WITH X^-, REFERENCE RANGE VALUES OF X^- IN PHYSIOLOGIC FLUIDS (μM OR mM), AND SPECIFICITIES (S)[a] FOR OXIDATION OF X^- BY MPO

X^-	E° (V)	k_x ($\times 10^{-4}$)	RRV inplasma	Plasma S	RRV in saliva	Saliva S
Cl^-	1.08	2.5	**100–120 mM**	**344 (80%)**	20–30 mM	3 (3%)
Br^-	0.93	110	20–100 μM	8 (2%)	40–200 μM	0.6 (<1%)
I^-	0.57	720	0.6–1.8 μM	1 (0%)	10–50 μM	1 (1%)
SCN^-	0.77	960	20–120 μM	78 (18%)	**1–3 mM**	**89 (95%)**

Consensus substrates in bold.

[a]The mean RRV was used to compute $S = k_x[X^-]/k_I[I^-]$. The expected percentage is given in parentheses.

physiological environments. MPO has the highest redox potential of all known human defensive peroxidases, and it is the only mammalian enzyme that has a sufficient oxidation potential to oxidize Cl^- at an appreciable rate. In addition to the nature of the enzyme, it is clear that the anticipated product distribution also depends upon the availability of the substrates. Overoxidation becomes an issue as the halides are consumed by oxidation (i.e., when H_2O_2 is no longer the limiting chemical reagent). This subject will be broached next.

A.2. Production of $OSCN^-$ by oxidation of SCN^-

As discussed earlier, HOCl and HOBr are capable of oxidizing SCN^- in uncatalyzed reactions that can approach diffusion reaction limits (*42,43*). Note that the diffusion limit *in vivo* can be quite different than under conditions of turbulent mixing in a stopped-flow instrument (*vide infra*). It has been suggested that SCN^- may compete with other cellular targets (e.g., GSH), thereby limiting cellular damage that might be caused by the more powerful oxidants (*42,43*). However, even for cases where SCN^- is not kinetically competent to react with HOCl before chlorination of cellular components, it has been shown that SCN^- can subsequently react with some of the oxidized cellular components. Small molecule, macromolecular, and cellular chloramines react with SCN^- to produce $OSCN^-$ (*54*), and we have recently shown that such reactions can resuscitate otherwise mortally oxidized mammalian cells (unpublished results). Importantly, $OSCN^-$ reacts with HOX (X=Cl and Br) at rates that are comparable to SCN^- (unpublished results), so overoxidation is possible unless SCN^- is in large excess. While HOSCN regenerates SCN^- upon its reaction with reductants (e.g., Eq. 7), overoxidation of SCN^- can lead to its depletion.

B. Thiocyanate-Derived Species Found *In Vivo*

It would certainly be a mistake to conclude on the basis of known chemical mechanisms alone, what roles *in vivo* SCN^--derived species are likely to play. Some case studies of unexpected results will be discussed next.

B.1. Production of $(SCN)_2$

Many unexpected reactions that are observed *in vivo* can be rationalized by the fact that model reactions are largely

investigated under homogeneous conditions, whereas most reactions that occur in cells take place in heterogeneous environments (cf. Section IV.C). For example, previous studies have suggested that $(SCN)_2$ should not exist in water at neutral pH, and yet electrophilic aromatic substitution reactions are apparently observed in proteins (*85*). In some cases, such reactions could be explained by the fact that human defensive peroxidases are cationic proteins that associate with negatively charged surfaces, such as the outer membranes of bacteria (*116–118*), eukaryotes (*119,120*), DNA (*121*), and some proteins (*122*). Such associations could result in delivery of SCN^--derived oxidants via relatively nonpolar pathways.

B.2. Thiocarbamate-S-oxide

The reaction of $OSCN^-$ with OH^- at neutral pH is too slow to account for the observation of thiocarbamate-S-oxide at neutral pH (unpublished results). However, we have observed thiocarbamate-S-oxide during the decomposition of $(SCN)_2$ under certain conditions neutral pH (unpublished results), which suggests that unexplored alternative mechanisms may exist for the production of SCN^--derived species.

B.3. Significance of chloramines and their reactions with SCN^-

A large number of cellular targets are expected to be more kinetically competent than amines *in vivo*, yet a significant percentage of extracellular HOCl produces chloramine moieties (*123,124*), and we have shown that under certain time-dependent circumstances, reduction of those chloramines back to amines with SCN^- is sufficient to resuscitate otherwise mortally damaged cells (unpublished results).

B.4. The higher oxidation states of SCN^-

We note that little research effort has thus far focused on characterizing the higher oxidation products of $OSCN^-$ that must certainly exist on the way to the SO_4^- and OCN^- that is eventually observed. The fact that OCN^- is observed when $OSCN^-$ decomposes *in vivo* (*27*) and the hypothesis that OCN^- may play a pathogenic role (*125*) suggest that the higher oxidation states that must be transiently produced during the decomposition of $OSCN^-$ to give OCN^- should be given more attention.

C. Biologically Relevant Reactions

There have been many efforts to predict the fate *in vivo* of peroxidase-derived oxidants (*97,123,124,126–129*). For example, armed with rate constants for model reactions and estimates for the concentrations of potential reactants, Pattison *et al*. have concluded that proteins are the major target of HOCl in plasma (*124*). Notwithstanding the challenges associated with modeling the relatively homogeneous (albeit complicated) environment of plasma, predicting the reaction pathways of the hypohalites, including $OSCN^-$, in tissues is a daunting task. For example, the rate constants for many of the reactions of hypo(pseudo) halous acids approach the diffusion limit, 10^9–$10^{10} M^{-1}s^{-1}$ in relatively nonviscous media. However, what constitutes "diffusion-controlled" *in vivo* is certainly very different than the homogeneous turbulently mixed conditions found in a stopped-flow instrument. Within a cell, such issues as excluded space, sequestration, electrostatics, viscosity, and diffusivity must be taken into consideration. For example, diffusion coefficients decrease approximately exponentially with the volume fraction that is occupied by the solute, and the total mass density of protein and nucleic acids within the cytoplasm is $\sim 200 mg ml^{-1}$ (20–30% of the cytoplasmic volume (*130*)). In addition, diffusion rates are inversely dependent upon viscosity, and the viscosity of the cytoplasm is 8–10 times that of pure water. Finally, the rates of diffusion also depend upon the sizes of the reacting molecules (cf. small molecules and large proteins).

Interesting conclusions are reached if the perturbations on reaction rates that are described in the previous paragraph are treated more quantitatively. The rate constant for a reaction can be ideally described by the Arrhenius equation. Since a reaction occurs for every collision between molecules in a diffusion-controlled reaction, the rate constant for such a reaction is given by the pre-exponential term A (i.e., the activation barrier is zero), which can be approximated by the following equation:

$$k = A_{\text{diff}} = 4\pi(r_x + r_y)(D_x + D_y)N_o/1000 \qquad (60)$$

where r is the radius (in cm), D is the diffusion coefficient (in $cm^2 s^{-1}$), and N_o is Avagadro's number. The diffusion coefficient of a small molecule in water is $\sim 10^{-5} cm^{-2}s^{-1}$, whereas the value for a small protein in water is $\sim 10^{-6} cm^{-2}s^{-1}$. Larger proteins may have diffusion coefficients as high as $\sim 10^{-8} cm^{-2}s^{-1}$ in water. The effect of viscosity (η) on D is given by the Stokes–Einstein relationship

$$D = \frac{k_B T}{6\pi\eta r} \tag{61}$$

where k_B is the Bolzmann's constant and T is the absolute temperature. The effects of molecular crowding within a cell have been approximated by the relationship $\eta=\eta_o(1+2.5\varphi)$, where η_o is the viscosity of the fluid phase of the solvent ($\eta_o=1$ for water), 2.5 is the frictional coefficient for the solute considered as a spherical particle, and φ is an obstruction factor that represents molecular crowding or the fractional volume of solution occupied by cosolutes (*131*). Interestingly, the values of φ vary markedly, depending upon the solute (e.g., φ for cytosolic imidazol-1-ylacetic acid and lactic acid, two molecules of similar size, were found to be 0.99 and 2.19) and the environment (e.g., φ for water in the cytosol and mitochondria were found to be 0.89 and 1.59) (*131*). The variability of φ of highlights the importance of solute-specific interactions *in vivo*. Even more interesting is the fact that the macromolecules are more significantly influenced by the crowding that is present *in vivo*. The difference between the diffusion coefficients of the smallest molecules and the largest proteins is only a factor of 10–100 in water, but the difference is 10^3–10^5 in the cytosol, membranes, organelle, and intercellular space of tissue. Thus, D for lactate (a representative small molecule) in water is about $2\times10^{-5}\,\mathrm{cm^{-2}s^{-1}}$ (*132*) and its "diffusion-controlled" limit (with respect to itself) is given by

$$k = 4\pi\left(2\times\left(2\times10^{-5}\,\mathrm{cm}\right)\right)\left(2\times\left(10^{-9}\,\mathrm{cm^{-2}\,s^{-1}}\right)\right)N_o/1000 \approx 10^9\,\mathrm{M^{-1}s^{-1}} \tag{62}$$

In contrast, D for lactate in the cytoplasm of *Escherichia coli* is about $10^{-9}\mathrm{cm^{-2}s^{-1}}$ (*131*), and its "diffusion-controlled" limit (with respect to itself) is computed to be $10^6\mathrm{M^{-1}s^{-1}}$. Thus, the diffusion limit is three orders of magnitude smaller for this small molecule within the cell as compared to water. The first important conclusion of this analysis is that bimolecular reactions between small molecules are slowed considerably in the crowded conditions of a cell. Consequently, unimolecular reaction mechanisms that might not be kinetically competent (or even observed) in the laboratory could be feasible in the confines of a cell. Consider now a protein within the cytoplasm. For example, D for maltose-binding protein (72kDa) is 10^{-12} in the cytoplasm and 10^{-14} in the periplasm of *E. coli*. (*133*). Within the periplasm, the diffusion-limited rate constant between two maltose-binding proteins is approximated by

$$k = 4\pi\left(2 \times \left(2.5 \times 10^{-7}\,\mathrm{cm}\right)\right)\left(2 \times \left(10^{-14}\,\mathrm{cm^{-2}\,s^{-1}}\right)\right)$$
$$N_o/1000 \approx 10^2\,\mathrm{M^{-1}\,s^{-1}} \tag{63}$$

A 10,000-fold difference is expected to exist within the confines of a cell between the diffusion limits of two small molecules (Eq. 62) and two large macromolecules (Eq. 63). The second important conclusion of this analysis is that large molecules are essentially spatially immobilized when exogenous highly reactive small molecules enter the cell. For prokaryotes, reaction is therefore expected to occur from the outside inward (like the layers of an onion) with damage occurring sequentially to the outer membrane, the periplasmic space, the cytoplasmic membrane, and finally the cytoplasm. Even within the cytoplasm, reactions are not expected to be uniform. For example, proteins that are closely associated with the cytoplasmic membrane might be more susceptible to reaction than those proteins that are associated with the genome. For eukaryotes, damage could be expected to cytosolic proteins before damage occurs to the organelle (*131*). This analysis presupposes that the reactive molecules are produced extracellularly. Naturally, reactive species that are produced within the cell can be expected to react at the site of generation (*121*).

V. Conclusions and Outlook

The biological relevance of $OSCN^-$ has motivated a thorough investigation of its chemistry. Considerable effort has focused on understanding the mechanisms by which $OSCN^-$ is formed, as well as the mechanisms of its comproportionation, disproportionation, and hydrolysis reactions. These studies have uncovered new chemical species, including $(SCN)_3^-$ (cf. I_3^-) (*38,81,86,87*), $H_2NC(=O)SO^-$ (*83,84*) and $HO(SCN)_2^-$ (cf. HOI_2^-) (unpublished results). The biological significance of these species is unknown, as is the relevance of other as-yet-uncharacterized SCN^--derived species that are certainly produced during the redox cascade that eventually results in the destruction of $OSCN^-$. The reaction chemistry of $OSCN^-$ and its derivatives with organic compounds has also received considerable attention. These studies have yielded a meager set of co-reactants (Section III.C). It seems certain that other moieties are reactive toward $OSCN^-$ *in vivo*. For example, the iron–sulfur proteins that are prevalent in the respiratory chain may be a target of $OSCN^-$ in prokaryotes (*134–136*). Further study will be required to fully understand the reaction chemistry of

$OSCN^-$, for its own sake and in the context of biology. However, these studies must continue with the caveat that reactions *in vivo* may not be relevant to the chemistry *in vitro*, and indeed, it may not be feasible to study the latter reactions in a laboratory setting (Section IV.C).

Acknowledgments

The author is indebted of the efforts of his colleagues and coworkers who have contributed to our understanding of $OSCN^-$. Also, this "accounts"-like review emphasizes our research, but the important contributions by pioneers of the field must be given due credit, including Edwin Thomas, Kenneth Pruitt, and Jorma Tenovuo. The generous financial support that has been provided by the National Science Foundation, National Institutes of Health, American Heart Association, Petroleum Research Fund, and Oklahoma Center for the Advancement of Science and Technology has been appreciated.

References

1. Bjerrum, N.; Kirschner, A. *Kgl. Danske Videnskabernes Selskab.* **1918,** *8*, 76.
2. Lecher, H.; Wittwer, M.; Speer, W. *Ber. Dtsch. Chem. Ges. B* **1923,** *56B*, 1104.
3. Pruitt, K. M.; Tenovuo, J. O. "The Lactoperoxidase System: Chemistry and Biological Significance"; In: *Immunology Series,* (Vol. 27), Dekker: New York, **1985** 257pp.
4. Below, J. F.; Jr., Connick, R. E.; Coppel, C. P. *J. Am. Chem. Soc.* **1958,** *80*, 2961.
5. Clark, C. R. *J. Chem. Educ.* **1997,** *74*, 1214.
6. Wrobel, M.; Jurkowska, H.; Sliwa, L.; Srebro, Z. *Toxicol. Mech. Methods* **2004,** *14*, 331.
7. Weuffen, W.; Franzke, C.; Thuerkow, B. *Nahrung* **1984,** *28*, 341.
8. Moir, D.; Rickert, W. S.; Levasseur, G.; Larose, Y.; Maertens, R.; White, P.; Desjardins, S. *Chem. Res. Toxicol.* **2008,** *21*, 494.
9. Zgliczynski, J. M.; Stelmaszynska, T. *Biochim. Biophys. Acta Enzymol.* **1979,** *567*, 309.
10. Conner, G. E.; Wijkstrom-Frei, C.; Randell, S. H.; Fernandez, V. E.; Salathe, M. *FEBS Lett.* **2007,** *581*, 271.
11. Ryall, B.; Davies, J. C.; Wilson, R.; Shoemark, A.; Williams, H. D. *Eur. Respir. J.* **2008,** *32*, 740.
12. Broderick, K. E.; Chan, A.; Balasubramanian, M.; Feala, J.; Reed, S. L.; Panda, M.; Sharma, V. S.; Pilz, R. B.; Bigby, T. D.; Boss, G. R. *J. Infect. Dis.* **2007,** *197*, 457.
13. Askeland, R. A.; Morrison, S. M. *Appl. Environ. Microbiol.* **1983,** *45*, 1802.
14. Pessi, G.; Haas, D. *J. Bacteriol.* **2000,** *182*, 6940.

15. Chung, J.; Wood, J. I. *Arch. Biochem. Biophys.* **1970,** *141*, 73.
16. Aune, T. M.; Thomas, E. L. *Eur. J. Biochem.* **1977,** *80*, 209.
17. Fragoso, M. A.; Fernandez, V.; Forteza, R.; Randell, S. H.; Salathe, M.; Conner, G. E. *J. Physiol.* **2004,** *561*, 183.
18. Valdes, M. G.; Diaz-Garcia, M. E. *Crit. Rev. Anal. Chem.* **2004,** *34*, 9.
19. Newman, A. A. *Chemistry and Biochemistry of Thiocyanic Acid and its Derivatives* **,** Academic Press: London, England, **1975,** p. 351.
20. Hawkins, C. L. *Free Radic. Res.* **2009,** *43*, 1147.
21. Pyykko, P.; Runeberg, N. *J. Chem. Soc. Chem. Commun.* **1991,** 547.
22. Sundholm, D. *J. Am. Chem. Soc.* **1995,** *117*, 11523.
23. Dua, S.; Maclean, M. J.; Fitzgerald, M.; McAnoy, A. M.; Bowie, J. H. *J. Phys. Chem. A* **2006,** *110*, 4930.
24. Hogg, D. M.; Jago, G. R. *Biochem. J.* **1970,** *117*, 779.
25. Walker, J. V.; Butler, A. *Inorg. Chim. Acta* **1996,** *243*, 201.
26. Modi, S.; Deodhar, S. S.; Behere, D. V.; Mitra, S. *Biochemistry* **1991,** *30*, 118.
27. Arlandson, M.; Decker, T.; Roongta, V. A.; Bonilla, L.; Mayo, K. H.; MacPherson, J. C.; Hazen, S. L.; Slungaard, A. *J. Biol. Chem.* **2001,** *276*, 215.
28. Pollock, J. R.; Goff, H. M. *Biochim. Biophys. Acta* **1992,** *1159*, 279.
29. Pruitt, K. M.; Tenovuo, J. *Biochim. Biophys. Acta* **1982,** *704*, 204.
30. Modi, S.; Behere, D. V.; Mitra, S. *Biochim. Biophys. Acta* **1991,** *1080*, 45.
31. Nagy, P.; Alguindigue, S. S.; Ashby, M. T. *Biochemistry* **2006,** *45*, 12610.
32. Boehland, H.; Golub, A. M.; Koehler, H.; Lisko, T. P.; Samoilenko, V. M.; Skopenko, V. V.; Cincadze, G. V. *Chemistry of Pseudohalides.* Dr. Alfred Huethig Verlag: Heidelberg, **1979,** p. 440.
33. Okulik, N. B.; Jubert, A. H.; Castro, E. A. *Adv. Quantum Chem. Bond. Struct.* **2008,** 119.
34. Okulik, N. B.; Jubert, A. H.; Castro, E. A. *J. Struct. Chem.* **2008,** *49*, 922.
35. Patai, S., Rappoport, Z. *Chemistry of Halides, Pseudo-Halides and Azides, Part 2* **,** Wiley: Chichester, **1995,** p. 916.
36. Patai, S., Rappoport, Z. *Chemistry of Halides, Pseudo-Halides and Azides, Part I* **,** Wiley: Chichester, **1995,** p. 860.
37. Morgan, T. D. B.; Stedman, G.; Whincup, P. A. E. *J. Chem. Soc.* **1965,** *4813*, .
38. Krishnan, P. *J. Solid State Electrochem.* **2007,** *11*, 1327.
39. Loucka, T.; Janos, P. *Electrochim. Acta* **1996,** *41*, 405.
40. Hughes, M. N. "General Chemistry [of Thiocyanic Acid and its Derivatives]" In: "*Chem. Biochem. Thiocyanic Acid Deriv.*"; Ed. Newman, A. A.; Academic Press: New York, **1975** pp. 1–67.
41. Pruitt, K. M.; Tenovuo, J.; Andrews, R. W.; McKane, T. *Biochemistry* **1982,** *21*, 562.
42. Ashby, M. T.; Carlson, A. C.; Scott, M. J. *J. Am. Chem. Soc.* **2004,** *126*, 15976.
43. Nagy, P.; Beal, J. L.; Ashby, M. T. *Chem. Res. Toxicol.* **2006,** *19*, 587.
44. Wood, J. L. *Org. React. (N. Y.)* **1946,** 240.
45. Zeng, Y.; Zheng, S.; Meng, L. *Inorg. Chem.* **2004,** *43*, 5311.
46. Li, Y.; Qiao, Z.; Qiao, S.; Zhao, J.; Li, H.; Wang, D. *Inorg. Chem.* **2003,** *42*, 8446.
47. Guy, R. G.; Pearson, I. *J. Chem. Soc. Perkin Trans. 1* **1973,** 281.
48. Burchell, C. J.; Kilian, P.; Slawin, A. M. Z.; Woollins, J. D.; Tersago, K.; Van Alsenoy, C.; Blockhuys, F. *Inorg. Chem.* **2006,** *45*, 710.
49. Krishnan, P.; Gurjar, V. G. *J. Appl. Electrochem.* **1995,** *25*, 792.
50. Cataldo, F. *Polyhedron* **2000,** *19*, 681.

51. Nelson, M. J.; Pullin, A. D. E. *J. Chem. Soc.* **1960,** *604*.
52. Bacon, R. G. R.; Irwin, R. S. *J. Chem. Soc.* **1958,** 778.
53. Hoogendoorn, H.; Piessens, J. P.; Scholtes, W.; Stoddard, L. A. *Caries Res.* **1977,** *11*, 77.
54. Xulu, B. A.; Ashby, M. T. *Biochemistry* **2010,** *49*, 2068.
55. Wilson, I. R.; Harris, G. M. *J. Am. Chem. Soc.* **1960,** *82*, 4515.
56. Christy, A. A.; Egeberg, P. K. *Talanta* **2000,** *51*, 1049.
57. Wilson, I. R.; Harris, G. M. *J. Am. Chem. Soc.* **1961,** *83*, 286.
58. Figlar, J. N.; Stanbury, D. M. *Inorg. Chem.* **2000,** *39*, 5089.
59. Slungaard, A.; Mahoney, J. R.Jr., *J. Biol. Chem.* **1991,** *266*, 4903.
60. van Dalen, C. J.; Whitehouse, M. W.; Winterbourn, C. C.; Kettle, A. J. *Biochem. J.* **1997,** *327*, 487.
61. Ashby, M. T. *J. Dent. Res.* **2008,** *87*, 900.
62. Michot, J. L.; Osty, J.; Nunez, J. *Eur. J. Biochem.* **1980,** *107*, 297.
63. Pintus, F.; Spano, D.; Bellelli, A.; Angelucci, F.; Scorciapino, A. M.; Anedda, R.; Medda, R.; Floris, G. *Biochemistry* **2010,** *49*, 8739.
64. Wojciechowski, G.; Huang, L.; Ortiz de Montellano, P. R. *J. Am. Chem. Soc.* **2005,** *127*, 15871.
65. Adak, S.; Mazumdar, A.; Banerjee, R. K. *J. Biol. Chem.* **1997,** *272*, 11049.
66. Wever, R.; Kast, W. M.; Kasinoedin, J. H.; Boelens, R. *Biochim. Biophys. Acta* **1982,** *709*, 212.
67. Pruitt, K. M.; Mansson-Rahemtulla, B.; Baldone, D. C.; Rahemtulla, F. *Biochemistry* **1988,** *27*, 240.
68. Figlar, J. N.; Stanbury, D. M. *J. Phys. Chem. A* **1999,** *103*, 5732.
69. M. T. Ashby, Synthesis and Use of Hypothiocyanite, US Patent 7238334, The Board of Regents of the University of Oklahoma, USA, 2006, 10pp.
70. Mokhtari, B.; Azadi, R.; Rahmani-Nezhad, S. *Tetrahedron Lett.* **2009,** *50*, 6588.
71. Falck, J. R.; Gao, S.; Prasad, R. N.; Koduru, S. R. *Bioorg. Med. Chem. Lett.* **2008,** *18*, 1768.
72. Toste, F. D.; De Stefano, V.; Still, I. W. J. *Synth. Commun.* **1995,** *25*, 1277.
73. Ashby, M.; Aneetha, H.; Carlson, A.; Scott, M.; Beal, J. *Phosphorus Sulfur Silicon Relat. Elem.* **2005,** *180*, 1369.
74. Nagy, P.; Ashby, M. T. *J. Am. Chem. Soc.* **2007,** *129*, 14082.
75. Pearson, R. G. *J. Chem. Educ.* **1968,** *45*, 643.
76. Pearson, R. G. *J. Chem. Educ.* **1968,** *45*, 581.
77. Nagy, P.; Jameson, G. N. L.; Winterbourn, C. C. *Chem. Res. Toxicol.* **2009,** *22*, 1833.
78. Skaff, O.; Pattison, D. I.; Davies, M. J. *Biochem. J.* **2009,** *422*, 111.
79. Lemma, K.; Ashby, M. T. *Chem. Res. Toxicol.* **2009,** *22*, 1622.
80. Ashby, M. T.; Aneetha, H. *J. Am. Chem. Soc.* **2004,** *126*, 10216.
81. Nagy, P.; Lemma, K.; Ashby, M. T. *Inorg. Chem.* **2007,** *46*, 285.
82. Lemma, K.; Ashby, M. T. *J. Org. Chem.* **2008,** *73*, 3017.
83. Wang, X.; Ashby, M. T. *Chem. Res. Toxicol.* **2008,** *21*, 2120.
84. Nagy, P.; Wang, X.; Lemma, K.; Ashby, M. T. *J. Am. Chem. Soc.* **2007,** *129*, 15756.
85. Hawkins, C. L.; Pattison, D. I.; Stanley, N. R.; Davies, M. J. *Biochem. J.* **2008,** *416*, 441.
86. Barnett, J. J.; McKee, M. L.; Stanbury, D. M. *Inorg. Chem.* **2004,** *43*, 5021.
87. Barnett, J. J.; Stanbury, D. M. *Inorg. Chem.* **2002,** *41*, 164.
88. Lengyel, I.; Epstein, I. R.; Kustin, K. *Inorg. Chem.* **1993,** *32*, 5880.

89. Wang, T. X.; Margerum, D. W. *Inorg. Chem.* **1994,** *33*, 1050.
90. Beckwith, R. C.; Wang, T. X.; Margerum, D. W. *Inorg. Chem.* **1996,** *35*, 995.
91. Sebok-Nagy, K.; Koertvelyesi, T. *Int. J. Chem. Kinet.* **2004,** *36*, 596.
92. Schmitz, G. *Int. J. Chem. Kinet.* **2004,** *36*, 480.
93. Phan, T. B.; Breugst, M.; Mayr, H. *Angew. Chem. Int. Ed.* **2006,** *45*, 3869.
94. Loos, R.; Kobayashi, S.; Mayr, H. *J. Am. Chem. Soc.* **2003,** *125*, 14126.
95. Koskikallio, J. *Acta Chem. Scand.* **1969,** *23*, 1477.
96. Pattison, D. I.; Davies, M. J. *Biochemistry* **2004,** *43*, 4799.
97. Pattison, D. I.; Davies, M. J. *Chem. Res. Toxicol.* **2001,** *14*, 1453.
98. Gerritsen, C. M.; Margerum, D. W. *Inorg. Chem.* **1990,** *29*, 2757.
99. Gerritsen, C. M.; Gazda, M.; Margerum, D. W. *Inorg. Chem.* **1993,** *32*, 5739.
100. Rayson, M. S.; Mackie, J. C.; Kennedy, E. M.; Dlugogorski, B. Z. *Inorg. Chem.* **2011,** *50*, 7440.
101. Mamman, S.; Iyun, J. F. *Int. J. Pure Appl. Chem.* **2007,** *2*, 429.
102. Thomas, E. L. *Biochemistry* **1981,** *20*, 3273.
103. Walden, P.; Audrieth, L. F. *Chem. Rev.* **1928,** *5*, 339.
104. Kornath, A.; Blecher, O.; Ludwig, R. *J. Am. Chem. Soc.* **1999,** *121*, 4019.
105. Kornath, A.; Blecher, O. *Z. Anorg. Allg. Chem.* **2002,** *628*, 625.
106. Jander, G.; Gruttner, B.; Scholz, G. *Chem. Ber.* **1947,** *80*, 279.
107. Palmer, D. A.; Van Eldik, R. *Inorg. Chem.* **1986,** *25*, 928.
108. Truesdale, V. W.; Luther, G. W.; Greenwood, J. E. *Phys. Chem. Chem. Phys.* **2003,** *5*, 3428.
109. Martell, A. E.; Smith, R. M. In "*Critical Stability Constants*"; Plenum Press: New York, **1976**.
110. Kitching, W.; Smith, R. H.; Wilson, I. R. *Aust. J. Chem.* **1962,** *15*, 211.
111. Nimmo, S. L. A.; Lemma, K.; Ashby, M. T. *Heteroatom. Chem.* **2007,** *18*, 467.
112. Kettenhofen, N. J.; Wood, M. J. *Chem. Res. Toxicol.* **2010,** *23*, 1633.
113. Rehder, D. S.; Borges, C. R. *Biochemistry* **2010,** *49*, 7748.
114. Aune, T. M.; Thomas, E. L.; Morrison, M. *Biochemistry* **1977,** *16*, 4611.
115. Furtmuller, P. G.; Burner, U.; Obinger, C. *Biochemistry* **1998,** *37*, 17923.
116. Miyasaki, K. T. *J. Dent. Res.* **1990,** *69*, 1780.
117. Miyasaki, K. T.; Zambon, J. J.; Jones, C. A.; Wilson, M. E. *Infect. Immun.* **1987,** *55*, 1029.
118. Britigan, B. E.; Ratcliffe, H. R.; Buettner, G. R.; Rosen, G. M. *Biochim. Biophys. Acta Gen. Subj.* **1996,** *1290*, 231.
119. Wright, C. D.; Nelson, R. D. *Biochem. Biophys. Res. Commun.* **1988,** *154*, 809.
120. Henderson, W. R.; Jong, E. C.; Klebanoff, S. J. *J. Immunol.* **1980,** *124*, 1383.
121. Gomez-Mejiba, S. E.; Zhai, Z.; Gimenez, M. S.; Ashby, M. T.; Chilakapati, J.; Kitchin, K.; Mason, R. P.; Ramirez, D. C. *J. Biol. Chem.* **2010,** *285*, 20062.
122. Hoogendoorn, H. *Protides Biol. Fluids* **1985,** *32*, 133.
123. Pattison, D. I.; Hawkins, C. L.; Davies, M. J. *Biochemistry* **2007,** *46*, 9853.
124. Pattison, D. I.; Hawkins, C. L.; Davies, M. J. *Chem. Res. Toxicol.* **2009,** *22*, 807.
125. Wang, Z.; Nicholls, S. J.; Rodriguez, E. R.; Kummu, O.; Hoerkkoe, S.; Barnard, J.; Reynolds, W. F.; Topol, E. J.; DiDonato, J. A.; Hazen, S. L. *Nat. Med.* **2007,** *13*, 1176.

126. Pattison, D. I.; Hawkins, C. L.; Davies, M. J. *Chem. Res. Toxicol.* **2003,** *16*, 439.
127. Hawkins, C. L.; Pattison, D. I.; Davies, M. J. *Amino Acids* **2003,** *25*, 259.
128. Nagy, P.; Ashby, M. T. *Chem. Res. Toxicol.* **2007,** *20*, 79.
129. Winterbourn, C. C.; Hampton, M. B.; Livesey, J. H.; Kettle, A. J. *J. Biol. Chem.* **2006,** *281*, 39860.
130. Cayley, S.; Record, M. T.Jr., *Biochemistry* **2003,** *42*, 12596.
131. Garcia-Perez, A. I.; Lopez-Beltran, E. A.; Kluner, P.; Luque, J.; Ballesteros, P.; Cerdan, S. *Arch. Biochem. Biophys.* **1999,** *362*, 329.
132. Ribeiro, A. C. F.; Lobo, V. M. M.; Leaist, D. G.; Natividade, J. J. S.; Verissimo, L. P.; Barros, M. C. F.; Cabral, A M T DP.V. *J. Solut. Chem.* **2005,** *34*, 1009.
133. Konopka, M. C.; Shkel, I. A.; Cayley, S.; Record, M. T.; Weisshaar, J. C. *J. Bacteriol.* **2006,** *188*, 6115.
134. Shin, K.; Hayasawa, H.; Lonnerdal, B. *J. Appl. Microbiol.* **2001,** *90*, 489.
135. Hurst, J. K.; Barrette, W. C.; Jr., Michel, B. R.; Rosen, H. *Eur. J. Biochem.* **1991,** *202*, 1275.
136. Sermon, J.; Vanoirbeek, K.; De Spiegeleer, P.; Van Houdt, R.; Aertsen, A.; Michiels, C. W. *Res. Microbiol.* **2005,** *156*, 225.

INDEX

Note: Page numbers followed by "*f*" indicate figures, and "*t*" indicate tables.

CONTENTS OF PREVIOUS VOLUMES

VOLUME 45

VOLUME 46

VOLUME 47

VOLUME 52

VOLUME 53

VOLUME 54

VOLUME 55

VOLUME 56

VOLUME 57

VOLUME 58

VOLUME 59

VOLUME 60

VOLUME 61

VOLUME 62

VOLUME 63